

2006

Fluvial geomorphology and late quaternary geochronology of the Gwydir fan-plain

Timothy J. Pietsch
University of Wollongong

Recommended Citation

Pietsch, Timothy J, Fluvial geomorphology and late quaternary geochronology of the Gwydir fan-plain, PhD thesis, School of Earth and Environmental Sciences, University of Wollongong, 2006. <http://ro.uow.edu.au/theses/492>

Research Online is the open access institutional repository for the University of Wollongong. For further information contact the UOW Library: research-pubs@uow.edu.au

NOTE

This online version of the thesis may have different page formatting and pagination from the paper copy held in the University of Wollongong Library.

UNIVERSITY OF WOLLONGONG

COPYRIGHT WARNING

You may print or download ONE copy of this document for the purpose of your own research or study. The University does not authorise you to copy, communicate or otherwise make available electronically to any other person any copyright material contained on this site. You are reminded of the following:

Copyright owners are entitled to take legal action against persons who infringe their copyright. A reproduction of material that is protected by copyright may be a copyright infringement. A court may impose penalties and award damages in relation to offences and infringements relating to copyright material. Higher penalties may apply, and higher damages may be awarded, for offences and infringements involving the conversion of material into digital or electronic form.

FLUVIAL GEOMORPHOLOGY AND LATE QUATERNARY GEOCHRONOLOGY
OF THE GWYDIR FAN-PLAIN

A thesis submitted in fulfillment of the requirements for the award of the degree

DOCTOR OF PHILOSOPHY

from

The University of Wollongong

by

Timothy J. Pietsch

BAppSci (Env.Sci.) (Hons.) (Charles Sturt University)

School of Earth and Environmental Sciences

II

I, Timothy J. Pietsch, declare that this thesis, submitted in fulfilment of the requirements for the award of Doctor of Philosophy, in the School of Earth and Environmental Sciences, University of Wollongong, is wholly my own work unless otherwise referenced or acknowledged. The document has not been submitted for qualifications at any other academic institution.

Timothy J. Pietsch

15/12/2005

Abstract

This study examines the downstream changes in the character of the Gwydir distributary system which flows across the Gwydir fan-plain, a large (~ 7500 km²) low gradient alluvial surface which forms part of the Darling Riverine Plains of southeastern Australia. The Late Quaternary history of the distributary system is evaluated by investigating the chronology and probable discharges of palaeochannels at or near the surface of the fan-plain.

Channels of the contemporary distributary system are characterized by downstream *declining* discharges, in part a result of the interaction of the modern system with remnants of the preceding palaeochannel systems. The hydraulic geometry of the contemporary channels revealed that these distributaries do not have a uniform response to declining discharge, with differences in heights of off-takes leading to differences in sedimentology, hydrology and channel morphology. Of the four distributaries, the Gwydir River is the bedload transporting trunk stream, hence its hydraulic geometry is fundamentally influenced by the need to maintain bedload conveyance as discharge declines downstream. It maintains a relatively deep channel facilitated in part by adoption of an anabranching habit in its lower reaches, and by relatively continuous flow that keeps its bed free of vegetation. Hence it has a relatively low W/D ratio. Contrary to an expectation for clay dominated bedload-free channels with banks of high material strength, depth in the Mehi, Moomin and Carole declines relatively rapidly downstream with little or no change in width. This results in large increases in W/D ratio downstream. It appears that long intervals of no flow in these three distributaries with their elevated off-takes encourage the growth of dense sturdy vegetation on their beds, directing flow energy to the banks during flood events.

Planform analyses show that bend radius of curvature and meander wavelength are strongly correlated with discharge, channel depth and flow velocity, but are poorly correlated with width. Width appears to be responding to conditions other than discharge, probably the presence of within-channel vegetation. The negative correlation between sinuosity and unit stream power, and between sinuosity and apparent bank

strength, indicate that an increase in channel width allows or indeed requires a decrease in gradient through meandering.

Analyses of the palaeochannels of the Gwydir fan-plain revealed that alluvial quartz grains here are unsuitable for traditional thermoluminescence analysis, as it is invariably heavily contaminated with inclusions of feldspar which causes severe age underestimation. An alternative single-grain optically stimulated luminescence (OSL) method shows that downstream fluvial transport of quartz in contemporary channels increases its luminescence sensitivity due to repeated cycles of burial and exposure. Three potential applications of this finding are; a) sediment tracing, b) river hydrology description and c) palaeochannel connectivity analysis

Application of the revised OSL technique reveals that the palaeochannels on the surface of the Gwydir fan-plain date from at least 70 ka. The oldest, the Challicum, dates to Oxygen Isotope Stage 4 (OIS 4) and shows limited surface preservation so no reliable palaeohydrological estimates could be made. The largest preserved palaeochannel system, the Coocalla unit with a palaeodischarge of $\sim 2550 \text{ m}^3\text{s}^{-1}$, dates to mid OIS 3 ($\sim 45 - 35 \text{ ka}$), a time of enhanced fluvial activity across the Murray-Darling basin and nearby coastal systems. Two more well preserved palaeochannels, the Kookabunna and Kamilaroi, were both active during OIS 2 ($\sim 20 - 15 \text{ ka}$) with discharges of $\sim 1240 \text{ m}^3\text{s}^{-1}$ and $\sim 1310 \text{ m}^3\text{s}^{-1}$, respectively. A period of enhanced aeolian activity has been identified at $\sim 4 \text{ ka}$, followed by the establishment of the contemporary system, with a total *combined* channel capacity mid-fan of $\sim 200 \text{ m}^3\text{s}^{-1}$. The Gwydir fan-plain reveals a Late Quaternary history of flow regime decline by approximately an order of magnitude. The present system of greatly reduced flow competence responds to a marked downstream reduction in discharge with a set of spatial hydraulic geometry and planform changes that are clearly not simply the inverse of more usual systems where discharge increases downstream.

Acknowledgements

Throughout the course of this study I have received advice, support and encouragement from a number of people to whom I would like to express my sincere thanks.

I would like to thank my supervisor Professor Gerald Nanson for his unstinting support and good-natured encouragement throughout my extended candidature. I am especially grateful for the freedom and resources given me to pursue ideas as they arose, and for the Job-like patience demonstrated in correcting my many drafts and my many misconceptions.

My co-supervisor, Professor Jon Olley, I would like to thank for generous provision of time, energy and encouragement to pursue excellence in OSL dating. Special thanks are due for the protective wing beneath which I have had space to play scientist.

Financial support for this thesis was provided by APA and CSIRO Scholarships, ARC grants to Gerald Nanson and ongoing support from my parents. Tim Cohen, Ben Ackerman, Gerald Nanson, Hugo Bomen, Nicole Pietsch, Bruce Pietsch and Cameron Pietsch all provided much needed field assistance. Lively discussions with fellow post-grads Tim Cohen, Maria Coleman, Martine Coupel and Simon Fagan were always enjoyable.

Thanks are due to my family. My Mum and Dad have always supported me with boundless love and wise counsel, more so in these last few years. To my sons Lachlan and James, I extend my thanks for your patience if not your understanding, and for games and fun. Finally, to Nicole whose love sustains me I thank for many sacrifices, for support in too many ways to count, for patience tested to breaking, for kindness and love. Thankyou for caring for me and for our boys.

Table of Contents

Abstract	III
Acknowledgements	V
Table of Contents	VI
Index of Figures	X
Index of Tables.....	XIII
List of Symbols and Abbreviations.....	XIV
Chapter 1 Thesis Background and Objectives.....	1
Chapter 2 Study Area and River Characteristics	5
2.1 Introduction.....	5
2.1.1 Naming Conventions	6
2.2 Geographical Setting	10
2.3 Geological Setting	18
2.4 Fluvial System.....	23
2.4.1 Gwydir River.....	27
2.4.2 Mehi River.....	33
2.4.3 Carole Creek.....	35
2.4.4 Moomin Creek.....	36
2.4.5 Big Leather and Gingham Watercourses	37
2.5 Palaeochannel Systems.....	39
2.6 Summary and Questions Arising.....	44
Chapter 3 Hydraulic Geometry	49
3.1 Bivariate Hydraulic Geometry	49
3.1.1 Introduction	49
3.1.2 Data Collection	57
3.1.3 Bivariate Hydraulic Geometry of the Gwydir, Mehi, Carole & Moomin ..	60
3.1.4 The Hydrology / Vegetation / Bank-Strength Hypothesis	77
3.1.5 Supporting Evidence	82
3.1.6 Summary of Bivariate Hydraulic Geometry	86
3.2 Multivariate Hydraulic Geometry	87
3.2.1 Introduction	87
3.2.2 The Huang and Co-Workers Model of Multivariate Hydraulic Geometry	88
3.2.3 Multivariate Hydraulic Geometry of the Gwydir, Mehi, Carole & Moomin	91
3.2.4. Comparison with Previously Examined Channels	95
3.2.5 Implications for Future Channel Evolution.....	97

3.3 Summary of Multivariate Hydraulic Geometry	98
Chapter 4 Channel Planform Characteristics	101
4.1 Introduction.....	101
4.2 Data	103
4.3 Techniques	103
4.3.1 Standard Planform Measures	103
4.3.2 Series Analysis Planform Measures	104
4.4 Verification of Series Analysis Techniques	109
4.4.1 Modelled Meander Traces	111
4.4.2 Expected Results	111
4.4.2.1 Radius of Curvature	111
4.4.2.2 Wavelength.....	113
4.4.2.3 Direction Variance.....	113
4.4.3 Results of Series Analysis of $\theta = \alpha \sin kx$ Models	114
4.5 Results	117
4.5.1 Downstream Variation in Planform.....	117
4.5.2 Planform – Hydraulic Geometry Relations.....	122
4.5.3 Planform – Discharge Relations and Palaeohydrology	127
4.6 Summary of Channel Planform.....	130
Chapter 5 Geochronological Methods	133
5.1 Introduction.....	133
5.2 Existing Geochronological Data for the Lower Gwydir	133
5.3 Sample Collection	135
5.4 Luminescence Dating of Sediments.....	136
5.5 TL Dating.....	137
5.5.1 Introduction	137
5.5.2 Sample Preparation Procedures.....	141
5.5.3 Sample Analysis	141
5.5.4 TL Results	143
5.6 OSL Dating	144
5.6.1 Introduction	144
5.6.2 Sample Preparation.....	145
5.7 TL/OSL Comparison	146
5.8 Development of an Improved OSL Method	150
5.9 Application of Olley <i>et al.</i> (2004a) Method to Gwydir Samples.....	154
5.9.1 OSL Data Analysis	155
5.9.2 Dose Rate Determination.....	156
5.10 Initial Results	157
5.10.1 Dose Rates and Disequilibrium Investigation.....	157
5.10.2 D_e Distributions	158
5.11 Summary	163
Chapter 6 A Non-Geochronometric Application for OSL	165
6.1 Introduction.....	165
6.2 Quartz Sensitivity.....	165
6.3 Methodology	171

6.3.1 Experiment 1	171
6.3.2 Experiment 2	174
6.4 Initial Results	174
6.4.1 A Note on Units and Uncertainties	176
6.5 Applications	177
6.5.1 Sediment Sources for the Gwydir River	178
6.5.2 River Description for the lower Gwydir	182
6.5.3 Palaeochannel Connectivity Analysis.....	184
6.6 Summary and Discussion.....	186
Chapter 7 Gwydir Fan-Plain Chronology.....	189
7.1 Well-Defined Channels and Palaeochannels	189
7.2 Surficially Undefined Palaeochannels.....	191
7.3 Palaeochannel Remnants and Aeolian Dunes.....	197
7.4 Age Estimates.....	199
7.5 Summary	201
Chapter 8 The Late Quaternary Evolution of the Gwydir Fan-Plain	205
8.1 Introduction.....	205
8.2 Quaternary Australia.....	208
8.3 Lacustrine History of the Murray-Darling Basin and Surrounds.....	209
8.4 Late Quaternary Fluvial Records	211
8.5 Episodes of Enhanced Fluvial Activity	213
8.5.1 The Murrumbidgee Throughout the Last Glacial Cycle.....	213
8.5.2 Other Murray-Darling Basin Fluvial Records.....	216
8.5.3 Discussion of Murray-Darling Basin Fluvial History.....	218
8.6 The Gwydir Fan Plain Record.....	222
8.7 Suggested Mechanism	224
8.8 Summary	229
Chapter 9 Summary and Final Remarks	235
References	245
Appendix A: DIPNR survey plans referred to in text.	267
Appendix B: Hydraulic geometry data.....	291
Appendix C: Hydraulic geometry bivariate plots.	296
Appendix D: Planform section centrelines.....	299
Appendix E: OSL D_e radial plots.	303
Appendix F: Published ages for fluvial deposits of the Murray-Darling basin.	307

Appendix G: Lake George case study.	309
---	------------

Index of Figures

Figure	Description	Pg
2.1	The Gwydir River catchment.	8-9
2.2	Moree 1: 250 000 Airborne radiometry data.	13
2.3	Climatic data for the Gwydir catchment.	15
2.4	Examples of palaeochannel remnants on the fan surface.	16
2.5	Gingham Watercourse, Bunnoor Swamp and unnamed palaeochannel.	17
2.6	Schematic representation of downstream decline in channel capacity.	18
2.7	Geology of the Gwydir catchment, upstream of Moree.	19
2.8	Airborne radiometry data showing two palaeochannels.	21
2.9	Geology and radiometry of part of the Terry Hie Hie catchment.	22
2.10	Partial duration series for Gwydir River at Gravesend.	24
2.11	Flood map of the February 2001 flood.	25
2.12	'Valley' and stream gradients for the Gwydir fan-plain.	28
2.13	Gwydir River at The Raft.	29
2.14	Example of flood hydrograph for the Gwydir River.	31
2.15	Architecture of the Gwydir fan-plain contemporary fluvial system.	32
2.16	LANDSAT / SPOT image of Mehi River above Mallowa Ck off-take.	34
2.17	1974 Air photo of the Gwydir River – Carole Creek bifurcation.	36
2.18	Flow along Big Leather Watercourse impeded by a 'biological dam'.	38
2.19	LANDSAT / SPOT image of Gwydir River near Wandoona Waterhole.	39
2.20	Bullarah quarry from the air and quarry face.	40
2.21	Challicum Pit, ~20 km west of Moree.	41
2.22	Saturated soil on the property 'Gingham'.	41
2.23	Airborne radiometry data showing palaeochannels.	42
2.24	Topography and borehole data of 'Tara Loop'.	43
2.25	Palaeochannel map of the Gwydir fan-plain.	47
3.1	Frequency distributions of downstream hydraulic geometry exponents.	55
3.2	Cross-sections and sediment sampling site locations.	58
3.3	Gwydir River: downstream variation in W.D, W, D, W/D, Q_{bf} and ω .	61
3.4	Mehi River: downstream variation in W.D, W, D, W/D, Q_{bf} and ω .	62
3.5	Moomin Creek: downstream variation in W.D, W, D, W/D, Q_{bf} and ω .	63
3.6	Carole Creek: downstream variation in W.D, W, D, W/D, Q_{bf} and ω .	64
3.7	Combined hydraulic geometry exponents for all study streams.	66
3.8	Slope vs. Distance Downstream for all study streams.	68
3.9	W/D ratio vs. Slope for all study streams.	70
3.10	Bedform existence field of Simons and Richardson (1966).	71
3.11	Plot of number of channels of the Gwydir River against approximate 'valley' distance from Pallamallawa.	73
3.12	Downstream development in channel boundary sediments.	75
3.13	Schematic representation of the architectural arrangement of off-takes.	78-79
3.14	Relationship between Schumms' M and W/D ratio for all streams.	80
3.15	Air photo extracts of the Gwydir distributary system, showing density of in-channel vegetation.	84
3.16	Air photograph of section of the Moomin Creek showing effects of flow disruption.	85

Figure	Description	Pg
3.17	Downstream hydraulic geometry relationships for all sites.	88
3.18	The relationship between W/D ratio and the ratio of shear stress acting on the walls (τ_w) to channel two-dimensional shear stress ($\rho g D S$).	90
3.19	Representation of the use of an invariant power function in place of Equation 3.1.	91
3.20	Derivation of C_W values for channels of the lower Gwydir.	93
3.21	The effect on C_W of using different estimates of Manning's n .	94
3.22	Development in channel shape at Moomin Plains.	98
4.1	Channel reaches for planform analysis.	102
4.2	Measurement of meander wavelength (λ).	105
4.3	Calculation of R_C .	106
4.4	Inflection point location and sinuosity determination.	109
4.5	Examples of sine generated curves used to test automated series analysis techniques.	112
4.6	Comparisons of measured $\overline{R_C}$, $\overline{\lambda_{series}}$ and P_{series} values with expected values.	115
4.7	Comparison of section of Mehi River (near Cross-Section 20) with sine generated curve of approximately equal scale and angularity.	116
4.8	Comparisons between manually measured λ and P and the equivalent series analyses.	119
4.9	Downstream planform development in the Gwydir distributary system.	120
4.10	Linear relationships between planform scale (λ or R_C) and the product of W and S for all study streams.	124
4.11	Relationship between sinuosity (P) and stream power (ω) for all study streams.	126
4.12	Relationship between sinuosity (P) and bank strength (C_W) for the Mehi, Carole and Moomin.	126
4.13	Relationship between channel planform scale (λ or R_C) and bankfull discharge.	128
5.1	Location of adjacent valleys with geochronologies for fluvial features.	135
5.2	Energy-level representation of luminescence.	138
5.3	Elements of a TL glow curve.	139
5.4	Location and calculated ages (in ka) of TL samples.	140
5.5	Plot of ratio of Natural to Regenerated TL output.	142
5.6	Age comparisons for 53 sites from numerous published sources.	144
5.7	Comparison of the IRSL output from 2 subsamples of GF-OSL/TL_4.	148
5.8	Comparison of D_e populations when using standard SAR protocol and modified SAR protocol.	152
5.9	Comparisons of single-grain optical ages determined using the minimum age model with independent age estimates for 12 Holocene samples.	153
5.10	Comparison between D_r as determined using HR γ S against D_R as determined using NAA or TS α C.	160
5.11	Examples of Radial Plots.	160
5.12	Comparison of errors associated with D_e s derived from the linear vs. the non-linear regions of the growth curve for different grains.	161
5.13	Indications of unlikelihood of dose rate heterogeneity.	162

Figure	Description	Pg
6.1	Energy band model of the competition between R-centres and L-centres for free charge.	167
6.2	OSL response to the test dose throughout a standard SAR protocol.	170
6.3	Geology and sampling points of the Castlereagh River.	172
6.4	Increases in sensitivity with distance downstream and number of cycles.	175
6.5	Sensitivity values, in arbitrary units, of quartz samples collected within the upper Gwydir Catchment.	179
6.6	Downstream trend in sensitivity for quartz sampled from the Gwydir River.	181
6.7	Sensitivity values in arbitrary units of quartz samples collected within the Gwydir distributary system	182
6.8	Differential sensitivity increase in arbitrary units (a.u.) for streams of the Gwydir distributary system.	183
6.9	Sensitivity values and ages for samples from the Kookabunna Palaeochannel compared to Bullarah Pit (GF-22) and Browns Ck (GF-12).	185
7.1	Palaeochannel age map of the Gwydir fan-plain.	190
7.2	Kamilaroi palaeochannel, showing sampling location and borelog data.	191
7.3	Kookabunna palaeochannel, showing sampling locations and borelog data.	192
7.4	Mia Mia palaeochannel, showing sampling location and borelog data.	193
7.5	Coocalla palaeochannel, showing sampling locations and borelog data.	194
7.6	Region near sampling location on Browns Creek (GF-12) showing Bullarah quarry (GF-22), Kookabunna palaeochannel and borelog data.	195
7.7	Borelog data from isolated gravel pits.	196
7.8	Borelog data from palaeochannel remnants.	198
7.9	Borelog data from suspected aeolian dunes.	199
7.10	Plot of Depth vs. Age for floodplain samples at Yarraman.	200
7.11	Age / Rank plot for OSL ages collected from the Gwydir fan-plain.	202
8.1	Map of southeastern Australia showing locations of sites discussed in Chapter 8.	207
8.2	Water level curves for Willandra Lakes, Lake George and Lakes Urana and Cullival.	211
8.3	Migrational / Aggradational sedimentological model of Page and Nanson (1996).	215
8.4	Phases of enhanced fluvial activity in valleys of the Murray-Darling basin.	221
8.5	Fluvial activity in the Murray-Darling basin throughout the last glacial cycle.	222
8.6	Daily runoff event exceedence for four catchments in the Murray-Darling basin.	228
8.7	Schematic diagram of the age and form of the major depositional features on the Gwydir fan-plain.	232

Index of Tables

Table	Description	Pg
3.1	Downstream hydraulic geometry exponents for the lower Gwydir channels.	67
3.2	Results of particle size analysis for 25 sites in the Gwydir distributary system.	74
3.3	Direct and indirect derivation of C_W for the study streams.	95
3.4	Gross ranges of variation in C_W for various bank types. (After Huang and Nanson, 1998).	96
4.1	Planform analysis results of all study reaches of the Gwydir distributary system.	118
4.2	Additional data describing radius of curvature and meander λ distributions.	121
4.3	Equation parameters for all study streams for linear functions of the form: $\lambda = M(W \text{ or } D \text{ or } V \text{ etc}) + B$ and $R_C = M(W \text{ or } D \text{ or } V \text{ etc}) + B.$	123
4.4	Equation parameters for exponential functions of slope and stream power against sinuosity for all study streams.	124
4.5	Palaeochannel discharge estimates from planform analyses.	128
5.1	Results of Cooper Creek TL / OSL analysis (Fagan 2001).	142
5.2	Details of samples taken for TL.	143
5.3	Comparison of D_e produced on large (3 mm) aliquots of quartz using OSL vs. TL.	147
5.4	Comparison of the Standard and Modified SAR protocols, after Olley et al. (2004a).	151
5.5	Radionuclide data for 4 samples from the lower Gwydir, as determined using HR γ S.	158
5.6	Radionuclide data for all samples (except GF-29) from the lower Gwydir, as determined using NAA.	159
6.1	Sensitivity values for all Gwydir Catchment samples.	180-181
6.2	Sensitivity Values for ancient deposits of the lower Gwydir Valley.	186
7.1	D_e estimate, over dispersion parameter, D_R and calculated OSL age for all samples.	203

List of Symbols and Abbreviations

a	Coefficient in width-discharge relationship
A'	Channel area parameter
b	Exponent in width-discharge relationship
c	Coefficient in depth-discharge relationship
C_A	Coefficient of channel area related to bank strength
C_D	Coefficient of channel depth related to bank strength
C_W	Coefficient of channel width related to bank strength
D	Channel depth
D_e	Equivalent natural dose
D'	Channel depth parameter
D_r	Dose rate
f	Exponent in depth-discharge relationship
g	Gravitational acceleration
$IRSL$	Infra-red stimulated luminescence
k	Coefficient in velocity-discharge relationship; Meander pathlength parameter
m	Exponent in velocity-discharge relationship
M	Schumm's weighted silt index
OSL	Optically stimulated luminescence
P	Sinuosity
P_{series}	Sinuosity as determined using series analysis
Q	Discharge
Q_{bf}	Bankfull discharge
R	Hydraulic radius
$\overline{R_C}$	Mean radius of curvature
S	Channel slope
TL	Thermoluminescence
V	Flow velocity; variance
W	Channel width
W'	Channel width parameter
α	Maximum deviation angle of sine generated curve
λ	Meander wavelength
$\overline{\lambda}$	Mean wavelength
$\overline{\lambda}_{series}$	Mean wavelength as determined using series analysis
λ^*	Meander pathlength
θ	Channel direction
ρ	Water density
σ_d	Overdispersion parameter

Chapter 1 Thesis Background and Objectives

The Gwydir fan-plain is a large alluvial surface emerging from the foothills of the Great Dividing Range in northern New South Wales (NSW), upon which a variety of channel forms are displayed. Formed in unconsolidated sediments, with self-deformable boundaries, these channels are arranged as a distributary system with downstream *declining* discharges. Their variety of form indicates a diverse range of controlling variables, a topic of investigation that, in fluvial channels generally, has been a central theme of geomorphology since the early twentieth century. However, few such investigations have examined distributary streams with downstream declining discharges, consequently the Gwydir fan-plain provides an opportunity to investigate the controls on channel form under unusual circumstances.

Leopold and Maddock's (1953) pioneering research into the statistical interrelationships amongst natural channel variables allowed new insight into controls on channel form, thus providing a radical departure from descriptive geomorphology based on the Davisian erosion model. Their hydraulic geometry approach epitomized a new and emerging *quantitative* geomorphology that was closely related to the independently developed so-called 'regime theory' approach developed from engineering studies of stable irrigation canals (Lindley, 1919; Lacey, 1929-1930, 1946; Lane, 1937, 1953; Blench, 1952, 1957). With quantitative descriptions of channel form came a new appreciation of the balance, or equilibrium, between contemporary forms and processes, with the current channel form shown to be largely unrelated to antecedent conditions. In other words, rivers develop a time-independent morphology that is sustained for as long as their independent variables remain relatively constant. Furthermore, change in independent variables will result in channel morphology shifting to a new equilibrium condition.

The tripartite division of time by Schumm and Lichty (1965) into cyclic (geologic), graded (modern) and steady (present), provides a framework within which to place geomorphic change, and recognizes that independent variables controlling channel form are not constant at all spatial and temporal scales. Furthermore, the distinction between cause and effect depends on the spatial and temporal scale of observation, with channel

forms in particular illustrating the tendency for dependencies to be reversed when the temporal limits of observation are narrowed. For example, over graded time (the last 1000 years or so) channel morphology is a dependent variable, being a function of some average of water and sediment discharge, however, for time periods classed as steady (< 1 year) channel morphology is an independent variable, with bankfull discharge for any single event largely determined by the inherited form of the channel established through graded time. Thus the historical perspective should not be overlooked when channel form is investigated. In an Australian context the evolutionary development of river channels is perhaps of greater interest than in European and North American systems, as here rates of geomorphic process are low and the landscape-rejuvenating effects of periodic glaciations are generally absent.

The objective of this study is to describe, measure, and posit explanations for, the variety of channel forms occurring on the Gwydir fan-plain. Traditional methods of river channel analysis, in cross-section, planform or through time, are not wholly appropriate to the study of the Gwydir fan-plain channels. A major theme running through this thesis is, therefore, a consideration of the importance of choosing appropriate techniques for channel analysis. Several factors particular to the study area militate against the simple application of standard techniques. Firstly, rivers with downstream declining discharges have unusual relationships between the direction of change in discharge, and the direction of change in independent variables (e.g. valley slope). Secondly, techniques for the objective measurement of channel planform are, as yet, under-developed such that quantitative analysis of the planform of long lengths of channel is impractical using traditional means. Thirdly, on the Gwydir fan-plain environmental variables have been altered to some extent by human intervention, therefore some level of reconstruction of prior conditions is required to explain present channel forms. Lastly, understanding of channel change through geological time requires good chronological control, which remains a particular challenge in fluvial environments.

Though this thesis is concerned primarily with the channels of the Gwydir fan-plain, two other field areas are included, investigations of which have been undertaken to complement and further explore the themes raised by the principal study. The first is the upper Gwydir catchment: it is of obvious interest as the source of sediment and water

discharge, with channel changes on the fan-plain reflecting changes in the upper catchment. The second is the nearby Castlereagh catchment which has been selected, for its simpler geology, to test a novel method of sediment tracing based on the effects on quartz of fluvial transport. The sediment tracing method is subsequently applied in the Gwydir catchment.

In summary, the specific objectives of this thesis are:

- To comprehensively describe the contemporary and late Quaternary fluvial systems of the Gwydir fan-plain, with particular focus on the interactions between the two.
- To investigate the nature of the contemporary hydraulic geometry and planform developments associated with the downstream decline in discharge on the Gwydir fan-plain.
- To characterise geochronologically the sediments of the Gwydir fan-plain, using state of the art luminescence techniques.
- To compare the landscape evolution of the Gwydir fan-plain with other geomorphic developments in the Murray-Darling basin to enable inferences to be made regarding possible climatic drivers of this change.

This investigation provides one of the first detailed analyses of hydraulic geometry and planform changes in a system with downstream declining discharges. Furthermore, the chronology of the antecedent environmental conditions which contribute to the downstream declining discharge and which relate to Quaternary climate change are investigated using recently developed luminescence techniques.

Chapter 2 Study Area and River Characteristics

Chapter Two provides an introduction, by way of geographical description, to the principal study area. The description provided is not intended to be exhaustive, and is necessarily selective in the choice of which geographical features or aspects are included. In addition to developing the contextual setting, such description serves to highlight the inspirations for this study. Sections 2.2 and 2.3 provide land-use, climatological, geomorphological and geological data relevant to the thesis, while Sections 2.4 and 2.5 provide more specific information on the contemporary and relict fluvial systems of the Gwydir fan-plain. On the basis of the information presented in Sections 2.2-2.5, Section 2.6 sets out the questions that present themselves as of specific relevance to the thesis topic with an introduction to the approaches employed for the investigation.

2.1 Introduction

Providing an accurate description of the ‘natural’ river system of the Gwydir fan-plain is complicated by a post-settlement history of channel modification. An attempt has therefore been made to reconstruct the form and function of the fluvial system prior to European settlement. Although anthropogenic influences on channel form prior to European settlement cannot be discounted, they are assumed to be diffuse and therefore slight. The reconstruction of the pre-European form of the lower Gwydir channels is based on the detailed record of channel alterations kept by the NSW Department of Infrastructure, Planning and Natural Resources (DIPNR, formerly the Department of Land and Water Conservation – DLWC, and prior to that the Department of Water Resources - DWR).

Significant channel alteration works have been undertaken in the study area since European settlement was initiated in the 1860s (or earlier by some reports e.g. Haworth *et al.*, 1999; Gale and Haworth, 2002). Since the 1890s, and especially around the time of the establishment of Copeton Dam and its associated irrigation system (1960s-1970s), many of the channels in the study area were surveyed in plan, cross-section and

long-section, preparatory to channel alteration. These surveys form the basis for channel description in the study area. Many reaches were surveyed multiple times and, unless stated, the descriptions provided in the following sections, and in Chapters 3 and 4, refer to the earliest survey. Surveys are cited as “Plan (series)/(number)”, as held by the Custodian of Plans DIPNR. Cited plans are included as Appendix A.

Descriptions of the palaeochannel systems of the Gwydir fan-plain, as provided in this chapter, are based principally on interpretation of remotely sensed imagery, and are presented in the form of a palaeochannel map in Section 2.5. Additional sedimentological and topographical field data were also obtained by the author for the purpose of palaeochannel description, and a sample of this data is presented along with the above map. Further sedimentological description is provided in Chapter Seven.

2.1.1 Naming Conventions

Locally used geographical place names and spellings are, with one exception, adopted for this thesis. This, however, may create confusion for those not familiar with the study area, as many of the place names use geographical terms that have conventional meanings different from those implied by their use in the study area. For example, the lower Gwydir Valley is not technically a valley, the Goonal Ana Branch is not technically an anabranch, and ‘watercourse’, when used nominally, is reserved for describing a specific fluvial form, rather than used as a general term. Some clarification of terms is therefore warranted.

The one exception to using local terminology is in describing the study area. Rather than use ‘lower Gwydir Valley’, or ‘Gwydir fan’, the term ‘Gwydir fan-plain’ has been adopted. Nanson and Gibling (2003) have reviewed the use of terms describing low gradient sediment cones, describing a number of schemes which distinguish sediment bodies on the basis of their surface gradient. However, none of these approaches accurately describes the study area. The area below Pallamallawa is distinctly fan shaped in its upper reaches; however it is of too low slope to be considered a true alluvial fan, *sensu* Blair and McPherson (1994). In the scheme of Stanistreet and McCarthy (1993), the study area would be classified a *braided fluvial fan* placing it in

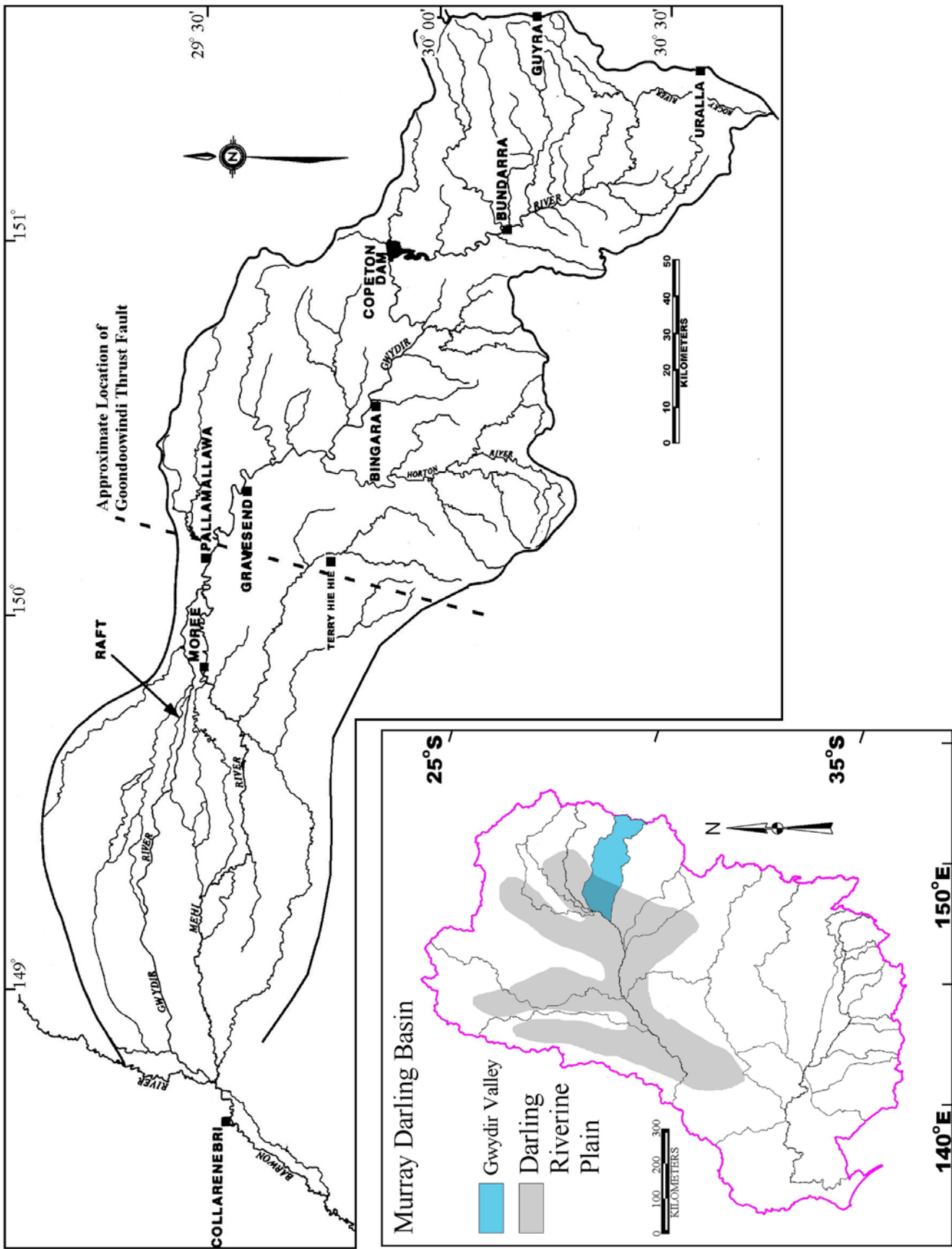
the same class as the Kosi system emerging from the Himalaya, to which the study area bears little resemblance. The Gwydir channels are certainly not braiding, rather the Gwydir is closer in appearance to the second of Stanistreet and McCarthy's fluvial fan classes, *low sinuosity / meandering fluvial fans*, to which the Okavango system belongs. However, this class description too is inadequate for the Gwydir system, as north-south (transverse) convexity is not maintained across the study area, but rather grades to a planar surface in the lower reaches. Hence the term *fan-plain* has been adopted to describe that part of the Gwydir system below Pallamallawa (Figure 2.1) characterized by distributary channel development. The term Gwydir fan-plain is therefore both a general description of the study area, as well as a specific term for the main geographic feature of the study area.

The Gwydir fan-plain is part of the coalescing floodplains of the northern part of the Murray-Darling basin known collectively as the Darling Riverine Plains. The north and south boundaries of the Gwydir fan-plain are arbitrarily rather than physically defined, as occasional inter-basin transfer of floodwaters occurs from the adjoining Macintyre and Namoi River systems.

In the study area, the term *watercourse* is not a general term for a stream, but rather has a more specific meaning. While nowhere succinctly stated, a definition for the term *watercourse* as used by locals could be expressed as:

A generally linear arrangement of floodplain elements (e.g. wetlands, waterholes, palaeochannels, sand dunes) along which predominantly non-channelised shallow flow is regularly transmitted.

In the study area the Big Leather and Gingham Watercourses provide 'type' examples of such features, but numerous smaller, mostly un-named, examples exist on the fan-plain.



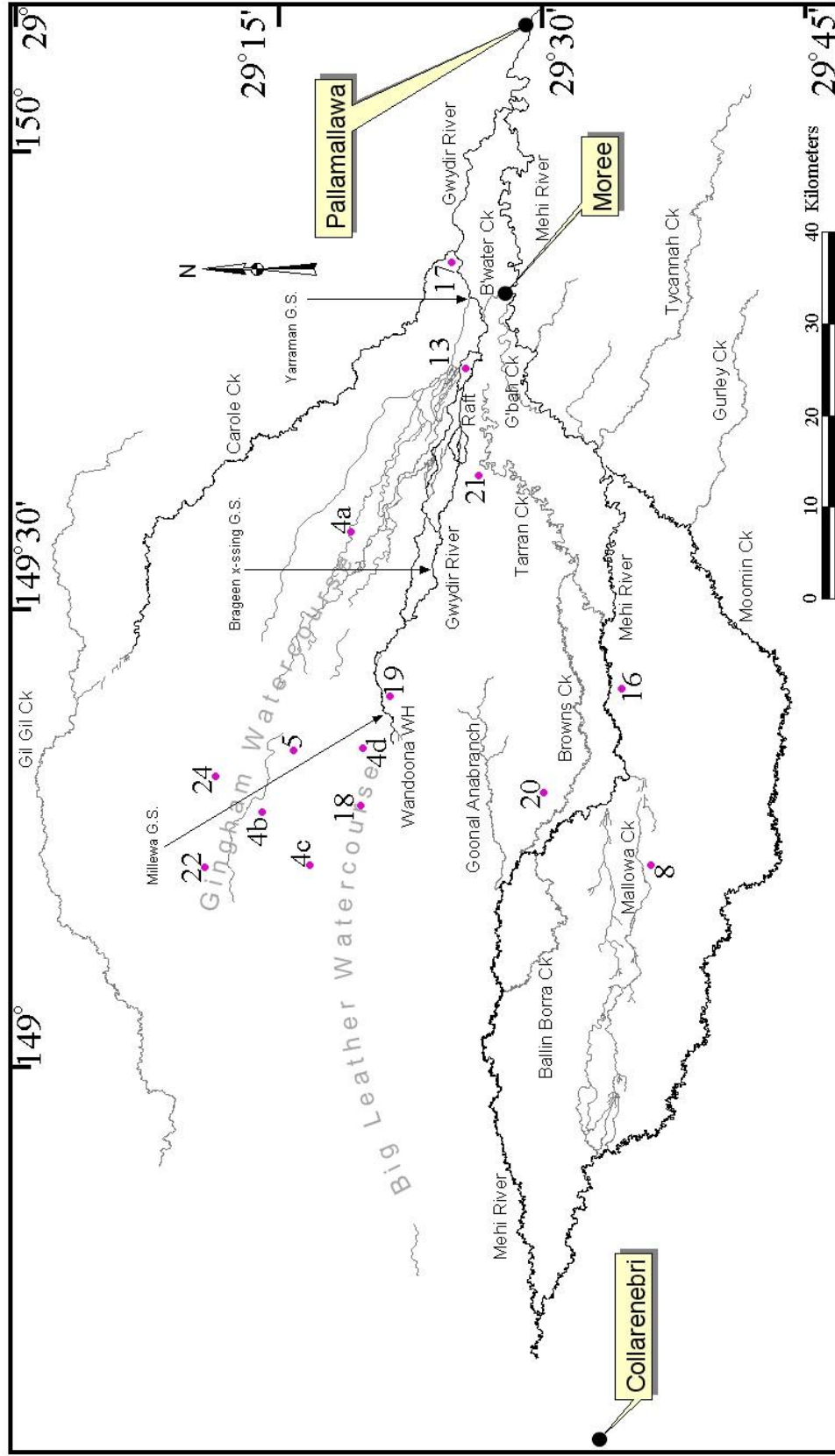


Figure 2.1: (Opposite Page) The Gwydir River catchment. Inset shows location of Darling Riverine Plains and Gwydir catchment within Murray-Darling Basin. (This Page) Streams of the Gwydir distributary system. Major streams shown in bold. Numbered symbols indicate location of subsequent figures in Chapter 2.

Although not strictly grammatically correct, a flexible approach to the use of the definite article has been adopted when listing several named channels, as some are rivers and some are creeks. While, by convention, *the* Gwydir River, is acceptable, *the* Carole Creek is not. Thus (especially in Chapter 3) rather than referring to “*the Gwydir and Mehi Rivers, and Moomin and Carole Creeks*”, a less cumbersome shorthand will be used: “*the Gwydir and Mehi*” or “*the Mehi, Moomin and Carole*” as examples.

Throughout this thesis reference is made to distinct palaeochannel assemblages. Names for these units have been assigned based on the parish where they are most prominent. The following parish names have been adopted for different palaeochannel units which are described in subsequent Chapters: *Challicum*, *Colmlee*, *Kamilaroi*, *Kookabunna* and *Mia Mia*.

2.2 Geographical Setting

The Gwydir fan-plain forms part of the Darling Riverine Plain, a system of extensive alluvial plains in the northern half of the Murray-Darling basin. Approximately 7 500 km² in extent, the fan-plain is bounded to the east by the Goondiwindi Thrust Fault, which separates the uplifted New England Fold-Belt from the fore-land Gunnedah-Bowen and Surat Basins (Tadros, 1993). Upstream of the Goondiwindi Thrust, the Gwydir River drains a ~12 300 km² montane region consisting of large areas of plateau and hilly country and smaller areas of ruggedly mountainous country. The fan-plain surface is crossed by numerous palaeochannels radiating out from a point near the fan head. These palaeochannels are considerably dissected and most are heavily obscured by younger floodplain accretion. However, some palaeochannels, though dissected, stand above the surrounding subdued topography. As in other parts of the Murray-Darling basin, for example the Goulburn, (Bowler, 1978); the Murray (Pels, 1964b; Page *et al.*, 1991; Ogden *et al.*, 2001); the Murrumbidgee, (Butler, 1950; 1958; Schumm, 1968; Page and Nanson, 1996; Page *et al.*, 1996); the Lachlan (Kemp, 2001); and the Namoi (Young *et al.*, 2002) palaeochannel remnants on the fan-plain appear to record episodes of fluvial activity greatly enhanced in comparison to the present hydrological regime.

Recently available radiometric data for the study area provides a clear illustration of the fan-plain structure (Figure 2.2), including the presence of a minor fan, referred to here as the Terry Hie Hie fan. It is on the south eastern shoulder of the major fan, and has distorted its symmetrical development. Riley and Taylor (1978), using Landsat imagery (Band 5), differentiated on the major fan the '*most recent fan deposits*' from '*areas of older(?) fan deposits (displaying) numerous palaeochannels, lakes and dunes(?)*' (punctuation is that of Riley and Taylor). The '*most recent fan deposits*' appear to coincide with the contemporary system of predominantly fine-grain floodplain deposits that have formed around, between, and on areas of palaeochannel deposits.

The Gwydir River embouchure is at an approximate elevation of 235 m at Pallamallawa and falls to 150 m near Collarenabri over a distance of 135 km. The area between Pallamallawa and Moree forms a 'panhandle', being constrained laterally by colluvium covered bedrock to the north and south (Figure 2.2, Sections A & B). Near Moree the influence of sub-cropping bedrock diminishes and the full fan structure is able to develop, though in part constrained to the south by the presence of the Terry Hie Hie fan. Fifty percent of the catchment above Pallamallawa has an elevation greater than 600 m, with the highest point in the catchment being Mount Lindsay at 1450 m. The Terry Hie Hie fan has a catchment of approximately 645 km², most of which is occupied by the Nandewar Volcanics and Rocky Creek Formation.

The Gwydir River catchment experiences an east-west climatic gradient, with annual rainfall averaging 800 mm in the eastern mountain headwaters, falling to 500 mm at the western toe of the fan-plain. Conversely, annual evaporation potential ranges from less than 1250 mm in the east, to 1750 mm in the west (NSW DWR, 1993). The Gwydir fan-plain is subject to very warm summers, with maximum daily temperatures having their highest monthly means, 33.4°C in Moree and 35.6°C in Collarenabri, in January (Figure 2.3). Accompanying this summer peak in temperatures is a peak in rainfall and discharge. Almost the entire runoff for the catchment is generated above Pallamallawa, with the area of the Gwydir fan-plain contributing almost no runoff. On the surface of the fan-plain, run-off is restricted by low slopes, absorbent soil conditions and high moisture deficits. Comparison of stream flow records with records from newly established rain gauges on the fan-plain, indicate that localized storm events have little

direct effect on even local stream flows. Thus it is the rainfall conditions in the upper catchment that determine the trunk stream flow.

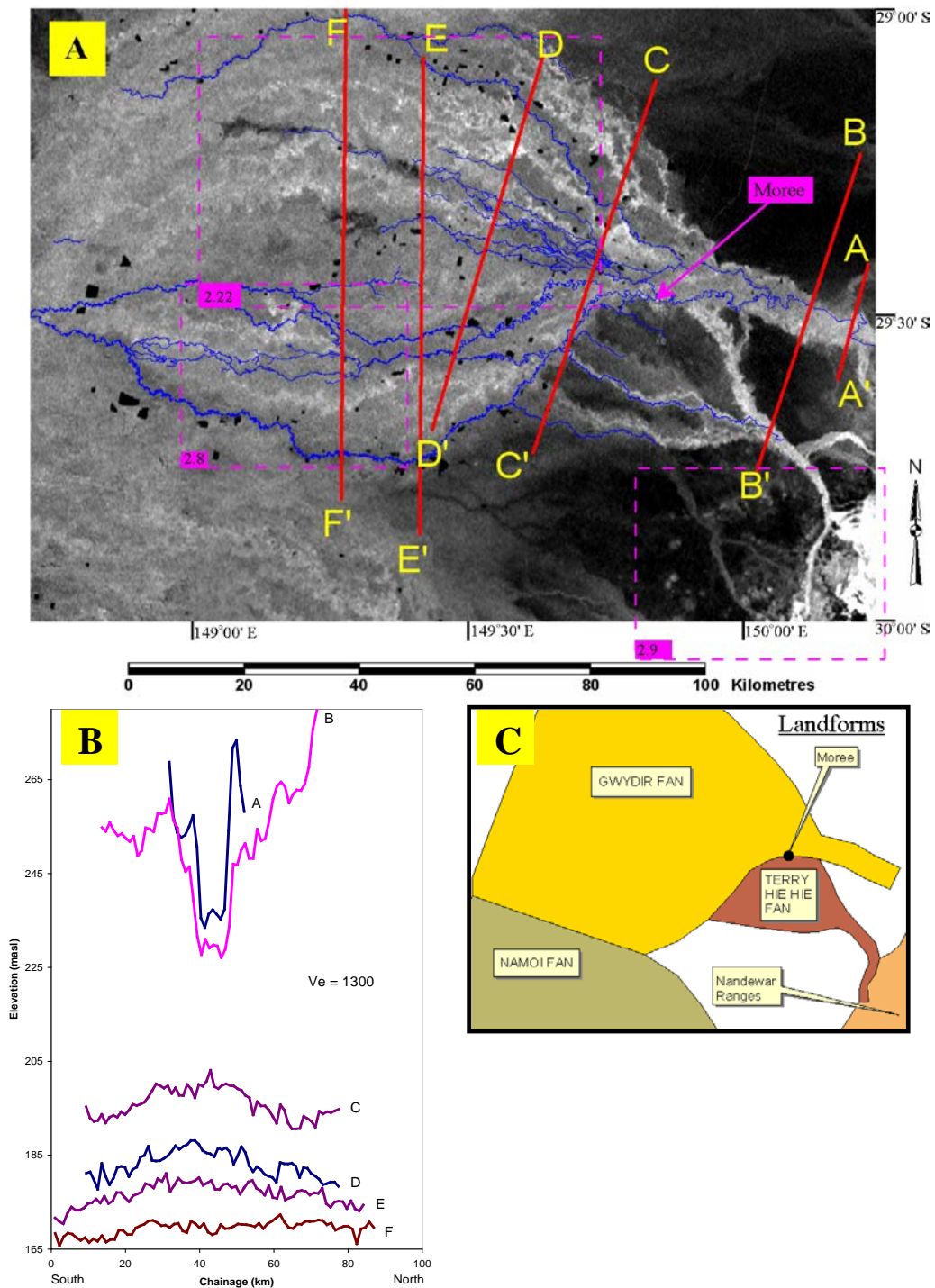
In numerous places on the fan-plain surface disjointed remnants of palaeochannels form waterholes and natural-levee-bound wetlands, many of which provide significant habitat (Figure 2.4). Series of circular depressions and raised sand bodies concordant with former meander traces also provide evidence of the importance of former fluvial features in shaping the present landscape. This palimpsest of relict channels adds considerably to the geomorphic complexity of the fan-plain surface, thereby affecting flood-routing and contributing to the downstream discharge distribution and reduction outlined below.

Upon debouching from the Great Dividing Range onto the fan-plain, the contemporary Gwydir River develops a distributary pattern with at least six synchronously operating channels, as well as numerous poorly defined floodways, some of which have formed where raised palaeochannel deposits restrict lateral flow (Figure 2.5).

Average annual flow in the Gwydir River as it enters the fan is approximately $800 \times 10^6 \text{ m}^3$ ($\sim 25 \text{ m}^3 \text{ s}^{-1}$) (median: $520 \times 10^6 \text{ m}^3$ per year). However, variation is high with annual discharges ranging from zero to over four times the average annual discharge. Only in exceptional flow events does the Gwydir River maintain a course to the Barwon River (Figure 2.1), the regional base-level. Only minor amounts of flow, representing about 6 % of the average annual discharge passing Pallamallawa, are carried across the fan-plain to the Barwon by the two largest distributaries, the Mehi River and Carole - Gil Gil Creek. Accompanying this diminution of flow is a commensurate reduction in channel capacity (Figure 2.6). Whether this flow diminution is cause or consequence of channel capacity reduction, or both, remains problematic.

The main industry in the study area is agriculture, with irrigated cotton being the most financially significant sector ($\sim \$200$ million a^{-1}). Irrigated agriculture relies on water released from Copeton Dam, which has a capacity of 1 364 000 ML. This is almost twice the natural average annual flow on to the fan-plain, as gauged at Pallamallawa, and almost three times the natural median annual flow. Completed in 1973, Copeton Dam,

Figure 2.2: (A) Moree 1: 250 000 Airborne radiometry data, showing % K and (B) elevation data (NSW Bureau of Mineral Resources, 2002) and (C) landform interpretation. Note high % K values (light colour) in the south east corner apparently corresponding with rhyolitic tuff units of the Rocky Creek Formation as well as trachyte units of the Nandewar Volcanics. Coarse grain palaeochannels on the fan have distinctly higher % K values (lighter colour) than the adjacent fine grain floodplains. Low % K regions in north-east, south and extreme north-west are colluvium-covered bedrock. Location of transects chosen arbitrarily to reveal fan structure. Insets show locations of subsequent figures. Contemporary streams traced in blue.



and the associated weirs and diversion works, are currently used to facilitate an average yearly extraction of about 200 000 MI (NSW DLWC, no date). However, in just the ten year period following the 1990/91 growing season, the extraction has ranged from below 50 000 MI to nearly 400 000 MI (NSW DLWC, no date). Irrigation also results in minor extractions amounting to between 10 000 and 15 000 MI a⁻¹ from shallow aquifers below the surface of the fan-plain. However, as these aquifers are recharged directly from regulated streams, the distinction between shallow groundwater and surface water is somewhat artificial. In addition to the shallow groundwater sources, aquifers associated with the Great Artesian Basin are tapped at a depth of over 1000 m. This water, however, is not suitable for irrigation, and its use is restricted to 'stock and domestic' purposes, as well as filling public and private swimming pools in Moree. As this latter use requires a constant flow to maintain the water's temperature (~39°C), it creates a significant source of thermal and solute pollution directed into the Mehi River at Moree.

Recharge to shallow aquifers is estimated to be 38 000 MI a⁻¹ (NSW DLWC, no date), and therefore is a significant contributor to downstream discharge diminution. Though difficult to calculate the volumes involved, ample opportunities for floodplain storage created by natural geomorphic elements (often in combination with vast reed beds) exist on the fan-plain. The storage capacity on the fan-plain surface would appear to greatly exceed the quantity stored in readily accessible shallow aquifers, and thus would have a correspondingly greater impact on downstream hydrograph attenuation. While recent broad-acre land-forming has seen a reduction in the geomorphic complexity of the fan-plain and a likely decrease in the opportunities for natural floodplain storage, these changes have been more than compensated for by built storages on the fan-plain. In addition to Copeton Dam in the upper catchment, these private on-farm storages on the fan-plain, (appearing as polygonal black areas in Figure 2.2), have an estimated total capacity of 350 000 MI (NSW DWR, 1993). These structures are built to make use of so called off-allocation flows, whereby rainfall events occurring below Copeton Dam (especially in the sub-catchment of the Horton River) cause river discharges to be in excess of immediate demand. The harvesting of off-allocation flows is a major factor in reducing the penetration of flow events along (usually) terminal distributaries towards the distal reaches of the fan-plain, and has been a major cause of wetland contraction. Recent changes to the water supply arrangements for the Gwydir distributary system

(outlined in *Water Sharing Plan for the Gwydir Regulated River Water Source* (2003), a statutory document produced for the NSW Minister for Land and Water Conservation in accordance with the *Water Management Act 2000*) have sought to prevent wetland contraction through strategic protection of off-allocation flows that follow prolonged dry periods, allowing for the refilling of critical waterholes.

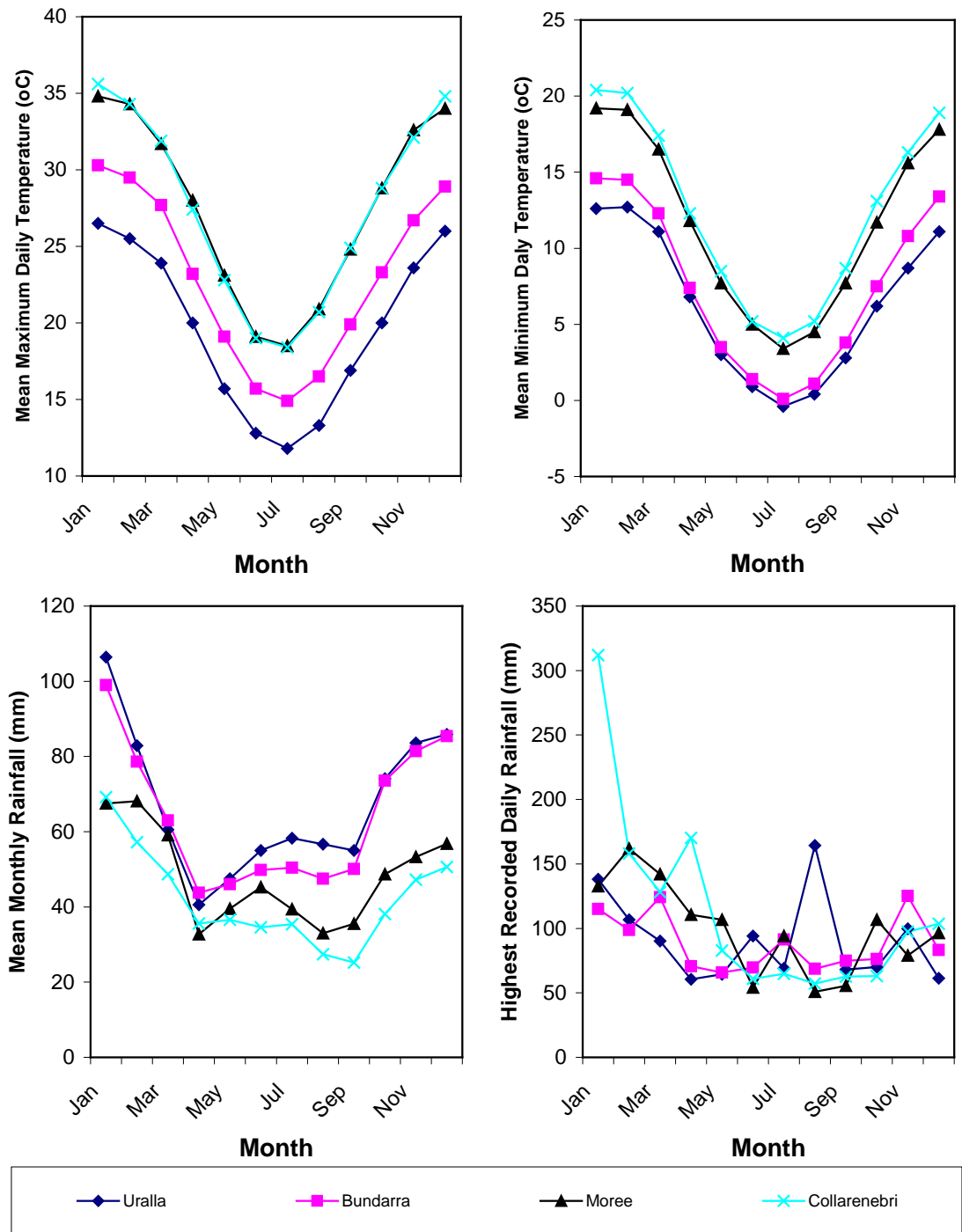


Figure 2.3: Climatic Data for the Gwydir Catchment (see Figure 2.1 for locations of towns) (Data retrieved 01/06/2002 www.bom.gov.au).



Figure 2.4 (opposite page): Examples of palaeochannel remnants on the fan surface. (a) Floodwaters occupying a former channel. (b) Pear Paddock Lagoon, a circular depression formed where (presumably) a fine grain point bar has been deflated (note adjacent incipient version to the immediate right). (c) Floodwaters banking up against raised palaeochannel. (d) Meander belt components that in places obstruct flow (middle-ground) while elsewhere (fore-ground and back-ground) forming pools. Latitudes and Longitudes omitted for clarity; see Figure 2.1 for locations. All photos: Moree DIPNR.



Figure 2.5: Gingham Watercourse (narrow blue strip in background), Bunnoor Swamp (left middleground) and unnamed palaeochannel (right foreground). Flow in watercourse and palaeochannel to the left. See Figure 2.1 for location of approximate middle ground. (Photo: Moree DIPNR).

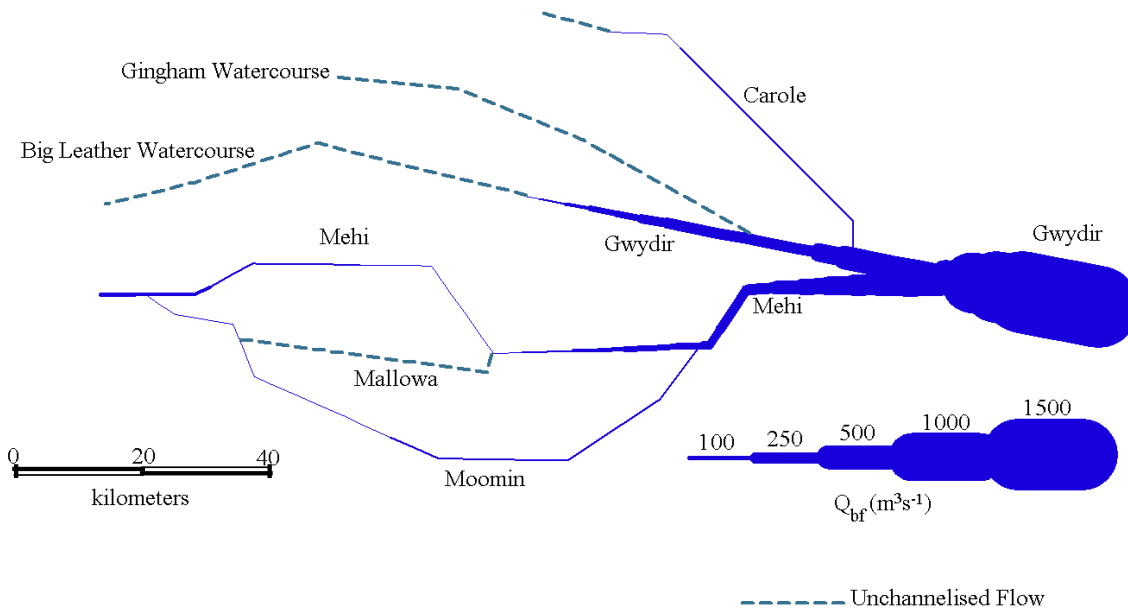


Figure 2.6: Schematic representation of downstream decline in channel capacity (Calculated from NSW DLWC Hydrological Data).

2.3 Geological Setting

With its headwaters in the New England Fold-Belt and Nandewar Volcanics (Figure 2.7), the Gwydir River drains an area of considerable geological diversity. Granites and granodiorites of the New England Batholith, heavily folded Devonian glacio-fluvial complexes including tuffs and pyroclastics and Miocene trachytes and basalts all contribute to a lithologically mixed sediment load. A large area of Jurassic sandstone, an extension of the Pilliga Sandstone which is discussed later in Chapter 6, extends to the north of the Gwydir River, providing a particularly productive source of coarse quartz sand.

Cretaceous and Jurassic confining layers of the Surat Basin form the basement rock for the Gwydir fan-plain. An infilled early-Cainozoic valley cut into the basement rock runs to the north of Moree then swings southwards to eventually join the palaeo-valley of the Namoi. Alluvium of the Gwydir fan-plain has been accumulating since the mid Miocene (Martin 1980), with a complex three-dimensional array of inter-bedded gravels, sands, silts and clays evident in drilling logs. Some minor basalt flows are

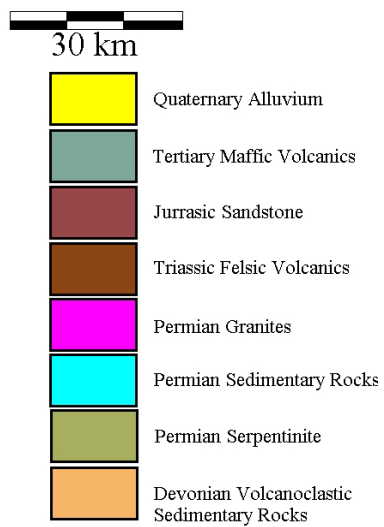
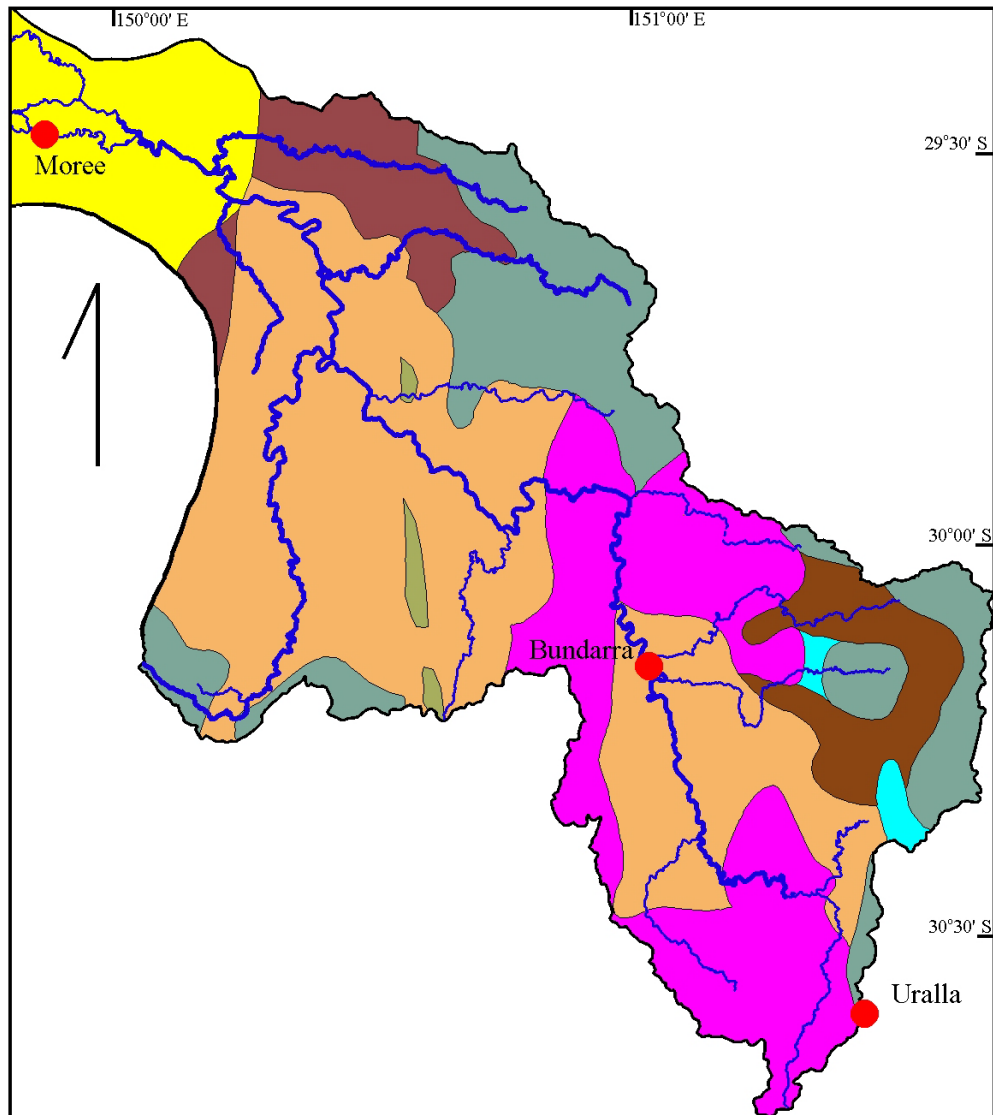


Figure 2.7: *Geology of the Gwydir catchment, upstream of Moree (National Geoscience Database 1 : 2 000 000). Towns shown are those for which meteorological data is presented in Figure 2.3.*

located high in the sequence to the north of Moree. The depth of relatively unconsolidated alluvium increases towards the west, with maximum depths being about 80 m. Most of the region has a surficial cover 40-60 m thick over 'bedrock'.

The 1968 Moree 1:250 000 geological map is striking in its uniformity, with over 93% of the mapped area, including all of the main study area, assigned '*Riverine plain deposits of black and red clayey silt, sand and coarse gravel*' (NSW Geological Survey, 1968). The questionable usefulness of such a general classification has led to the development of more appropriate mapping procedures, with the collection of the radiometric data presented in Figure 2.2 being part of a NSW Bureau of Mineral Resources (BMR) project aimed at achieving this goal. This data set can also be put to more immediate use in the delineation of palaeochannels.

In radiometric tracings of the drainage paths out onto the fan-plain surface, it can be clearly seen that it is the coarse grain palaeochannels that have the highest potassium (K) signature, while the fine grain floodplain sediments associated with the contemporary channel system are consistently low in K (Figure 2.8). There appears to have been a change in the character of the sediment deposited between the time of palaeochannel activity and establishment of the contemporary system, possibly due to a change in provenance.

An examination of high resolution geological maps of the upper catchment revealed that there are several candidate rock types that could be the source of the highly potassic 'stringers' of alluvium evident in Figure 2.2 (and Figure 2.8). Unfortunately the radiometric data set does not extend east into the upper catchment of the Gwydir, thus radiometric description of the source rocks is not directly possible. However, the south-east corner of the data set overlaps with areas of exposed bedrock in the sub-catchment of the Terry Hie Hie fan (Figure 2.9). In this area, three main rock units have been identified: the Rocky Creek Conglomerate (part of the Volcanoclastic Sedimentary Rocks unit in Figure 2.7), the Pilliga Sandstone and Tertiary Basalts. Of these, the Rocky Creek Conglomerate seems to be the main source for potassic materials moving down the main drainage paths. The Pilliga Sandstone also appears bright, though this may in part be due to the surficial admixture of material from the adjacent (i.e. up slope) Rocky Creek Conglomerate. The lobe of the Pilliga Sandstone almost completely

surrounded by alluvium in the south-west corner of Figure 2.9 does not appear nearly as bright as its equivalent unit 10 km to the east, which would suggest that, in its pure form, the Pilliga Sandstone is not a significant potassium source. The Cretaceous Rolling Downs Group appears in a small area in the north, however in this location it is largely obscured by Quaternary residual and colluvial deposits and therefore its signature is somewhat indistinct. The Tertiary basalts, while predominantly regions of low K, have isolated pockets of highly potassic rock, which are here assumed to be trachyte plugs.

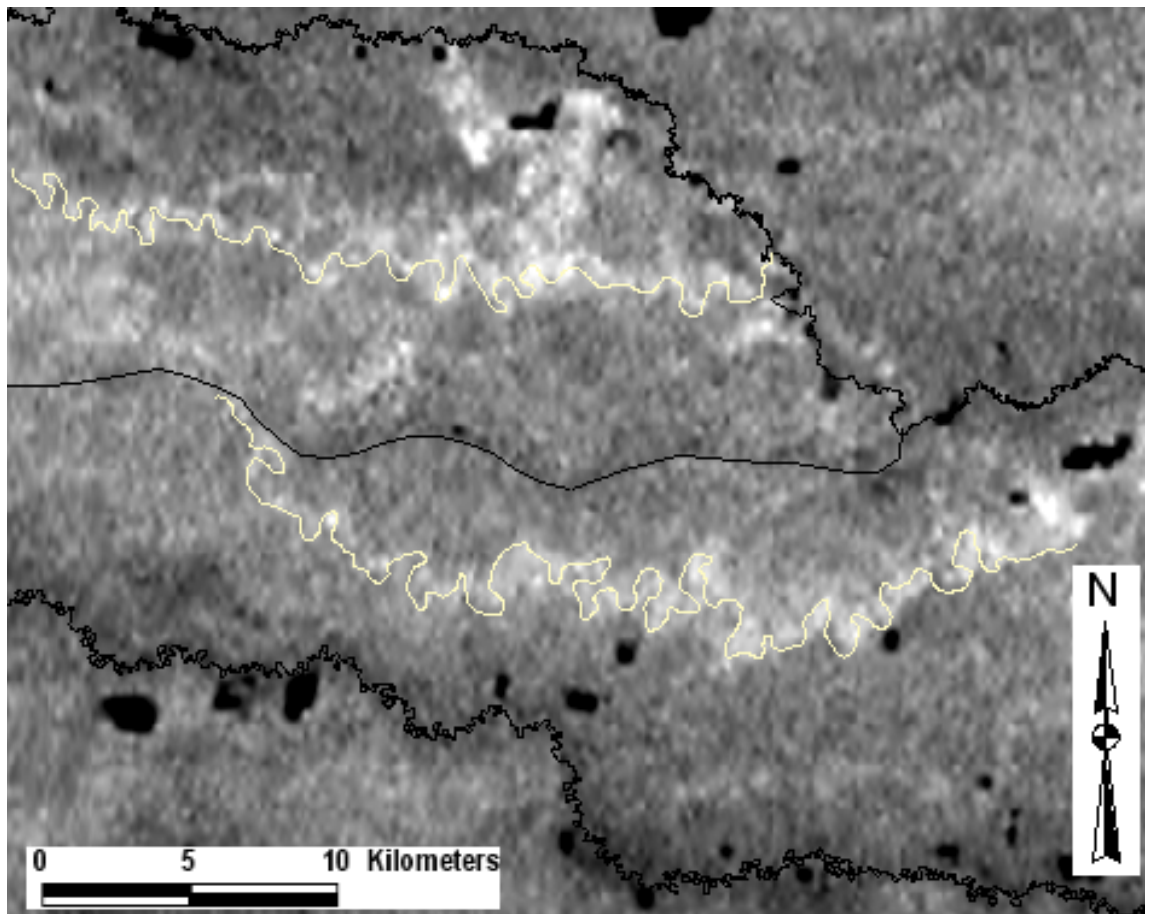


Figure 2.8: Airborne radiometry data showing bands of high K % (light colour) associated with two palaeochannels (yellow), with contemporary streams (black) flanked by low K % floodplains (Radiometric Data: NSW Bureau of Mineral Resources, 2002). Note the contemporary streams shown are the Mehi River (top), Mallowa Creek (middle) and Moomin Creek (bottom). See Figures 2.1 and 2.2 for location.

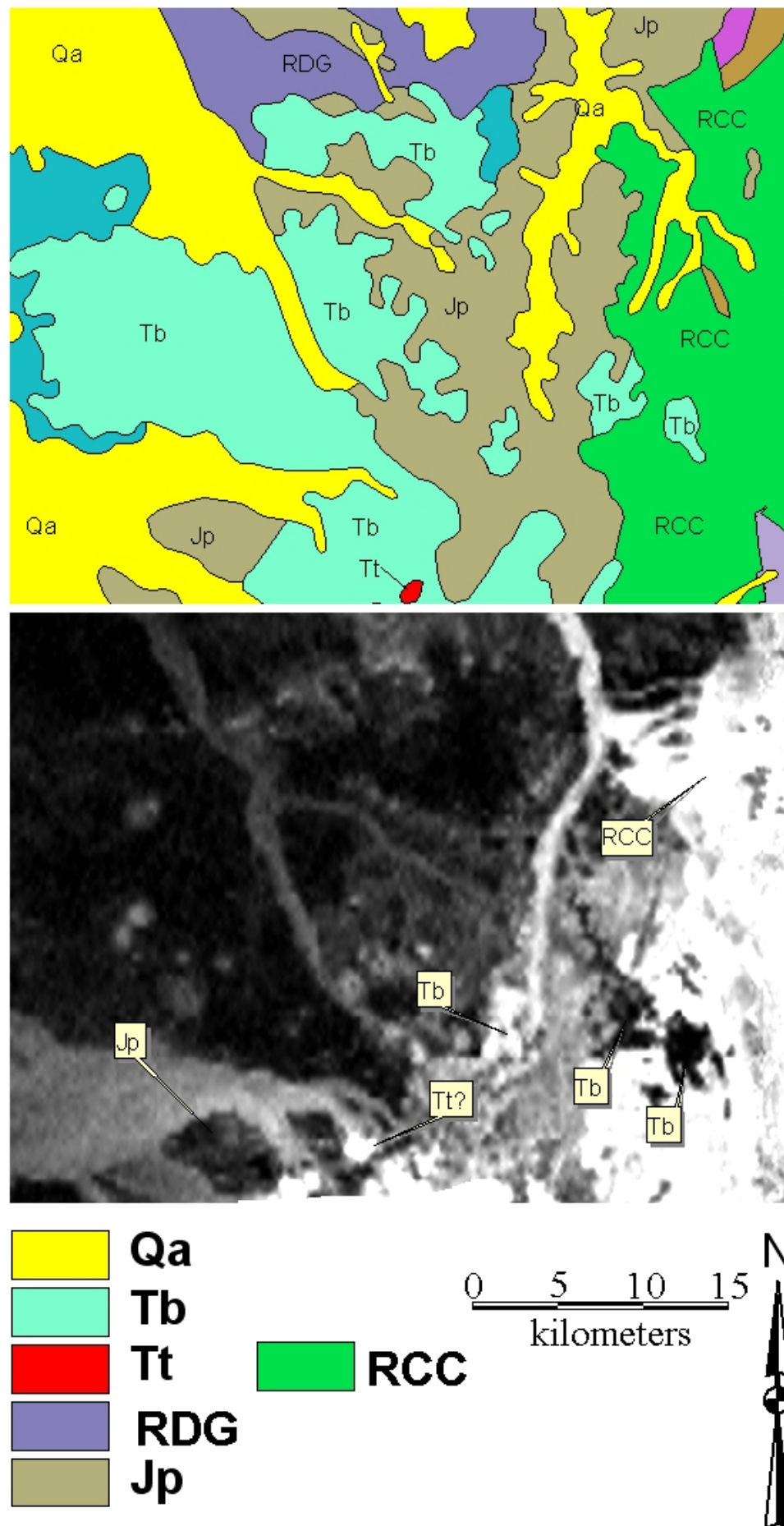


Figure 2.9 (opposite page): *Geology (from NSW 1: 1 000 000 Geology Series) and radiometry (K %) of part of the Terry Hie Hie catchment. Qa: Quaternary Alluvium. Tb: Tertiary Basalt. Tt: Tertiary Trachyte. RCC: Rocky Creek Conglomerate. Jp: Pilliga Sandstone. RDG: Rolling Downs Group. Note that Rocky Creek Conglomerate is always bright, whereas the Tertiary basalt is highly variable in its K signature. The localized bright spots within the basalt are assumed to be unmapped trachyte plugs. See Figure 2.2 for location.*

2.4 Fluvial System

Within-channel flow across the Gwydir fan-plain is carried by four main streams; the Gwydir River, the Mehi River, Moomin Creek and Carole Creek. In addition to within-channel flow it is normal for water to move over floodplains along so-called watercourses. Named watercourses such as the Gingham Watercourse and the Big Leather Watercourse (Figure 2.1) are shown on survey plans of the early part of the twentieth century as being mostly series of swamps which, for the present purposes, are taken as being wetlands without open water that connect occasional waterholes (wetlands which have open water), and exhibiting only rare stretches of formed channel. Shallow channels have been artificially cut along both the Gingham Watercourse and the Big Leather Watercourse and are currently maintained to allow greater penetration of low-flow ‘stock and domestic’ diversions. This though, has come at the cost of dewatering of previously prime, naturally irrigated, pastureland.

The distributary system of the Gwydir fan-plain is highly prone to flooding. Except for isolated pockets of high ground associated with sand dunes and palaeochannel remnants, the entire study area is subject to prolonged periods of inundation. However, in most cases, floods spill along a particular floodway rather than inundating the entire fan-plain. The total channel capacity of the Gwydir distributary system is insufficient to accommodate the flow capable of being carried within the banks of the Gwydir River upstream of Pallamallawa. Thus, even a small (within banks) rise of flow in the Gwydir River upstream of the embouchure results in out-of-channel flow downstream. An approximate indication of the periodicity of this process can be given by plotting the total combined channel capacity of the Gwydir distributary channels (say, in all streams

crossing transect D, on Figure 2.2) onto the partial flood series for the Gwydir River at Gravesend gauging station (located above the embouchure – see Figure 2.1) (Figure 2.10).

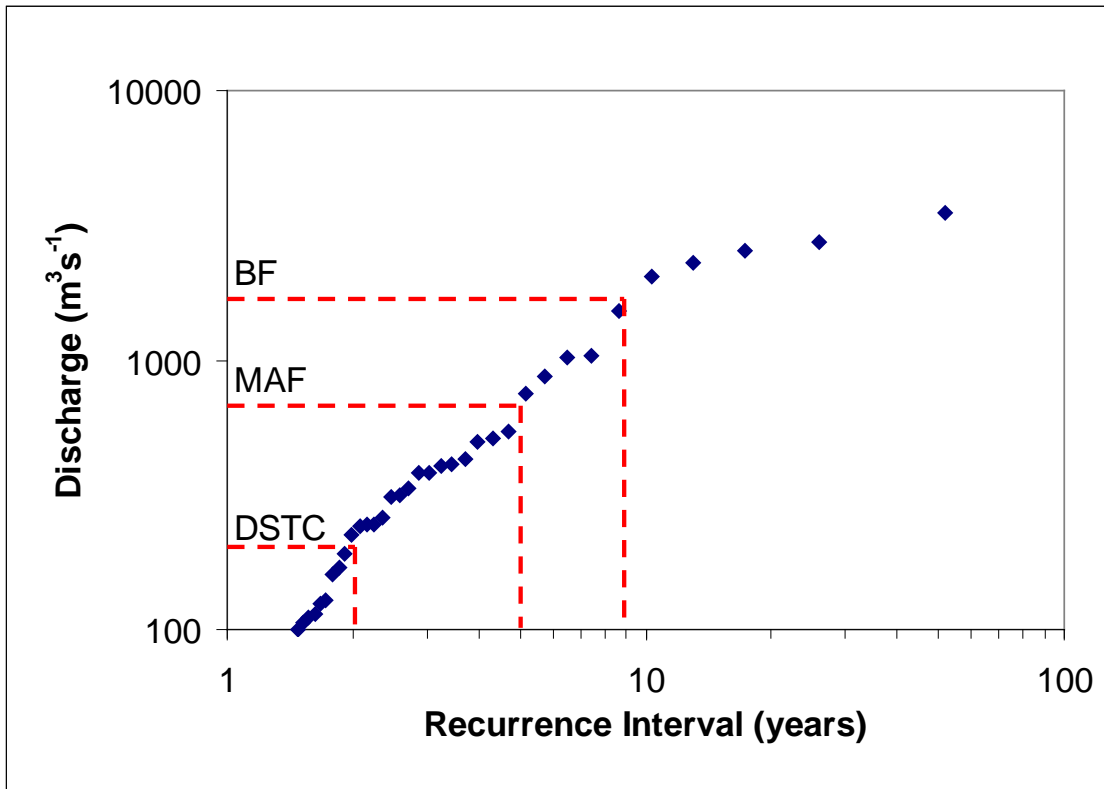


Figure 2.10: Partial duration series for Gwydir River at Gravesend, with total capacity of all channels mid-fan plotted. Channel capacities estimated from data presented in Chapter 3. Gravesend data is from 1950 to 2000. BF = Bankfull discharge at Gravesend. MAF = Mean Annual Flood at Gravesend. DSTC = Downstream Total Capacity.

Figure 2.11 (opposite page): Flood map of the February 2001 flood. Note the approximately linear stretches of floodwater, constrained laterally by raised palaeochannels (plotted in subsequent figures), and in some places, the contemporary channels. Data retrieved 01/01/02 www.dartmouth.edu/~floods/

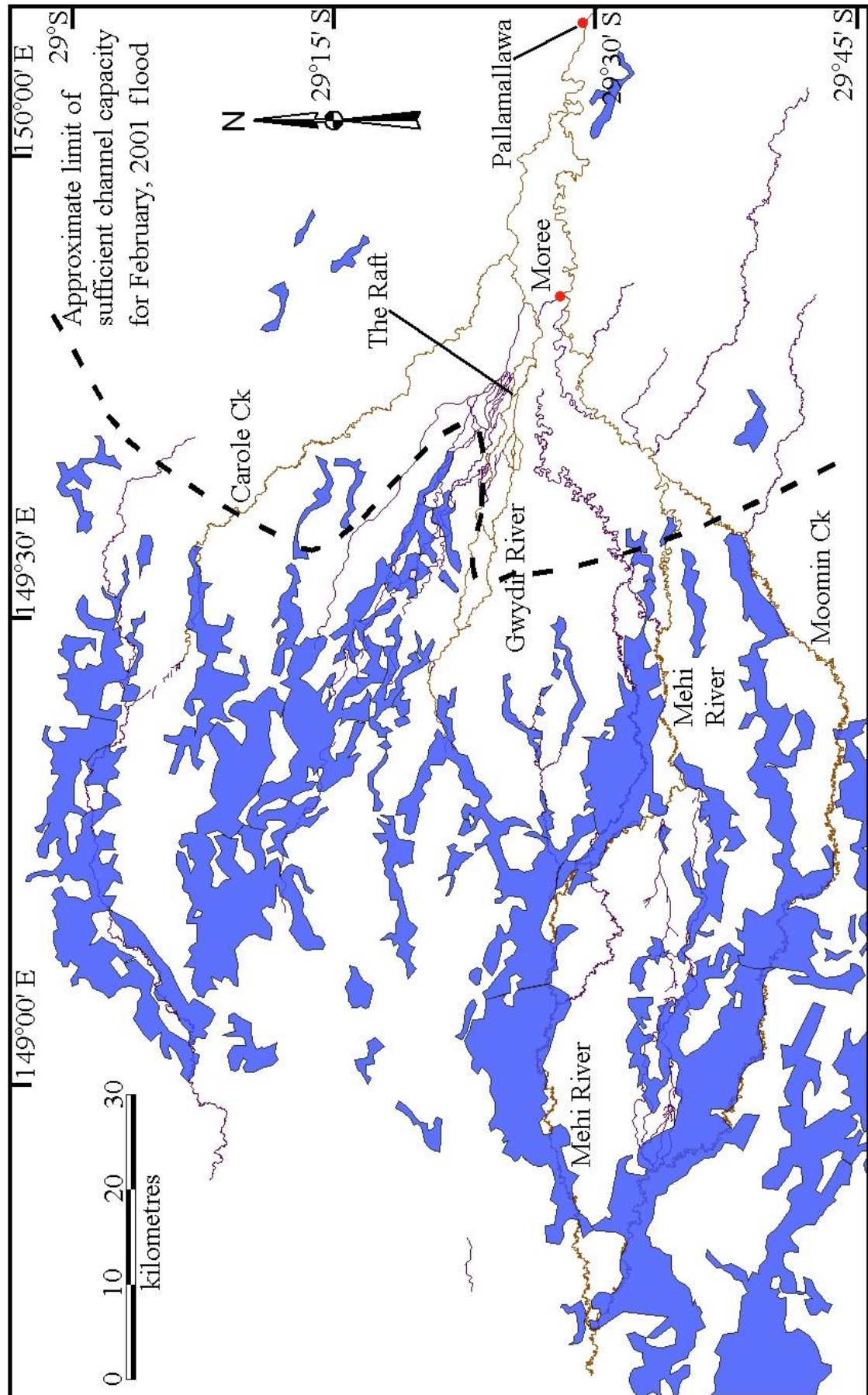


Figure 2.10 shows that water in excess of the total capacity of the channels of the fan-plain will be delivered from upstream with a recurrence interval of approximately two years. Though this may indicate that over-bank flow on the fan should be expected, on average, once every two years, 'flooding' actually occurs more frequently than this. This is because, as can be seen from Figure 2.5, many channels deliver their (usually within-banks) flow to un-channelised watercourses via floodouts, where the water body can shallow and broaden, resembling an over-bank flood. Furthermore, under pre-regulation conditions, it would be unlikely for a fully equitable distribution of floodwaters amongst all channels to occur. It is far more likely that moderate flows would be accommodated (initially at least) principally by one or two channels which, having less than the total combined channel capacity, would therefore spill at more frequent intervals.

Though flooding (perhaps an inappropriate term where overbank flow, or at least non-channelised flow, is the norm) is a regular occurrence, it is not necessarily a predictable one. Mahaffey (1985) describes a bewildering array of flood behaviour that serves to describe the dynamism of the system. Apart from obvious examples (one being the large woody debris dam known locally as the Raft, see below), predicting flood response to system changes is not straightforward.

Vegetation in channels and watercourses is one cause of changes in flood behaviour and this, along with minor geomorphic changes, is as much a function of previous flows as of the present circumstance. Thus, flood prediction requires consideration of the effects of preceding flows on the vegetation status of channels. Recent flooding along the Moomin Creek (February, 2001) saw inundation of areas that local landholders understood to have been dry since settlement, even though the causative storm event was not in itself unusual (Figure 2.11). Unraveling the conjunction of factors that brought about this situation is beyond the scope of the present investigation, though it does provide an example of the challenges faced by landholders and those charged with management of the water resource.

2.4.1 Gwydir River

The Gwydir River flows out of the foothills of the Great Dividing Range approximately 7 km south east of Pallamallawa. From there it runs by Pallamallawa, then north of Moree, extending approximately 90 km from the embouchure, before losing definition in the vicinity of Wandoona Waterhole (Figure 2.1). Over this distance valley slope is maintained at approximately 0.0007 with channel slopes between 0.0005 and 0.00055 (Figure 2.12). Downstream of Wandoona Waterhole, flows follow barely defined waterways interspersed with occasional waterholes, a reach formerly known as the Big Leather Watercourse. Although a gradual decline in slope is detectable west of Wandoona Waterhole, disruption of channelised flow does not appear to be directly related to any major break in slope. Rather, it would seem that the absence of channelised flow below Wandoona Waterhole is just the end point of a trend, observable below Pallamallawa, of a progressively declining channel with declining stream power. Where stream power reaches the minimum threshold for channel maintenance, overland flow results; the reciprocal of the situation proposed in the classic Horton (1945) model of overland flow.

As the trunk stream from which distributaries take off, the Gwydir River carries most of the bedload delivered to the fan-plain. Large gravel-cobble bars can be found in the Gwydir River near Moree, with sand bars and splays found further downstream. Of the four channels studied, the Gwydir River is the least sinuous, perhaps due to its relatively coarse bedload.

Of the four main streams, the Gwydir River has the greatest contraction in size and discharge downstream, due in part to the natural diversion of high flows along effluent streams (i.e. the Mehi River and Carole Creek) and watercourses. A striking feature of the Gwydir River is the Raft (Figures 2.1 and 2.13), a large woody debris dam that, since at least the 1870s, has been gradually accreting upstream towards Moree from a point about 7 km upstream of Brageen Crossing (Mahaffey, 1985). It is now over 15 km long. Given the high sedimentation rates in the vicinity of the Raft, much of this length is now buried and the course of the former channel mostly obscured. The head of the Raft is now stabilized about 20 km west of Moree, where it partly dams the Gwydir River, creating the Gwydir Pool.

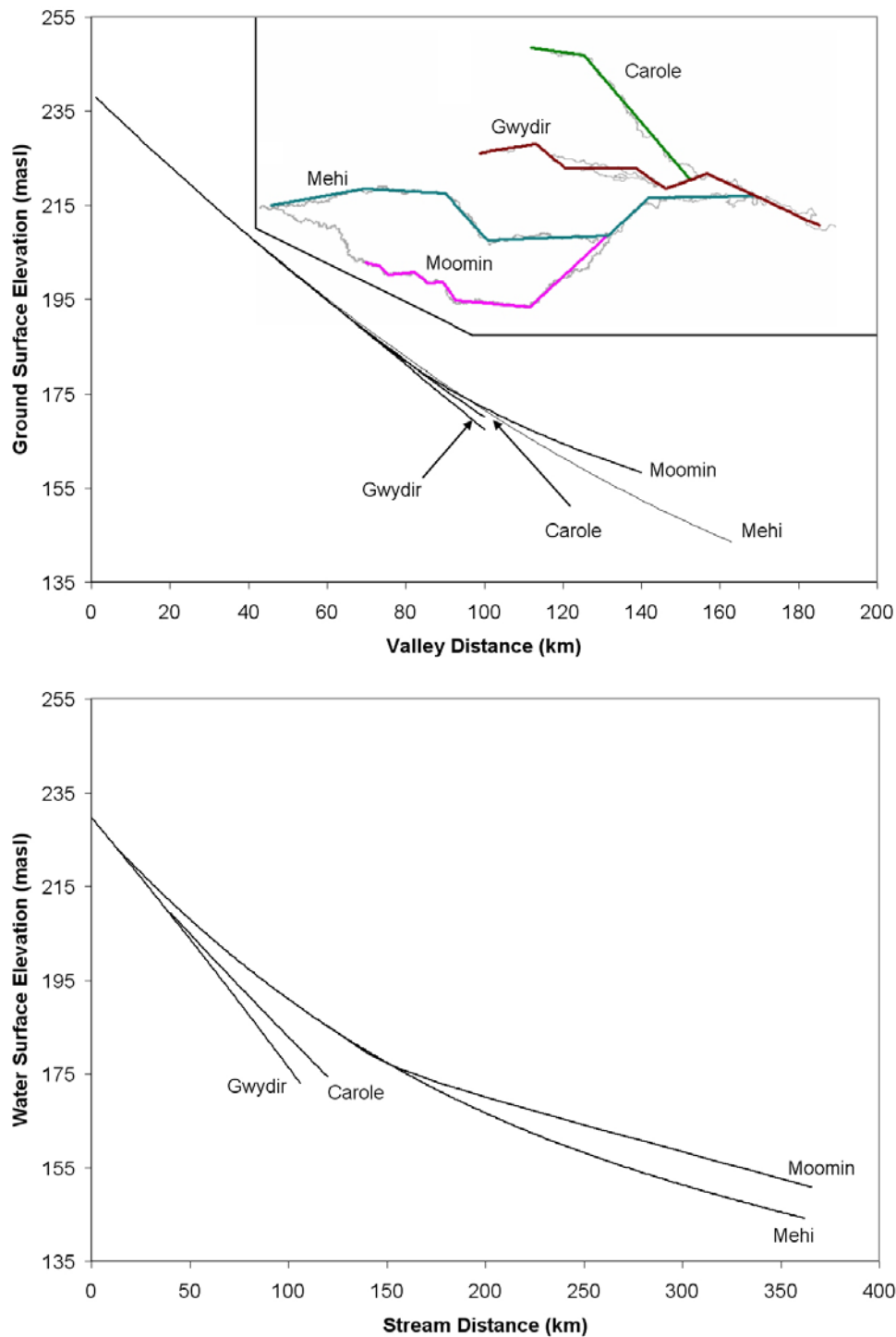


Figure 2.12: ‘Valley’ (Top) and stream (Below) gradients for the Gwydir fan-plain. Note that lines shown are lines of best fit to survey data, all with R values > 0.99 . River distances refer to stream distance from Pallamallawa Gauging Station, including length of trunk stream(s) in the case of distributaries. Inset shows chosen ‘valley’ lines for each stream.

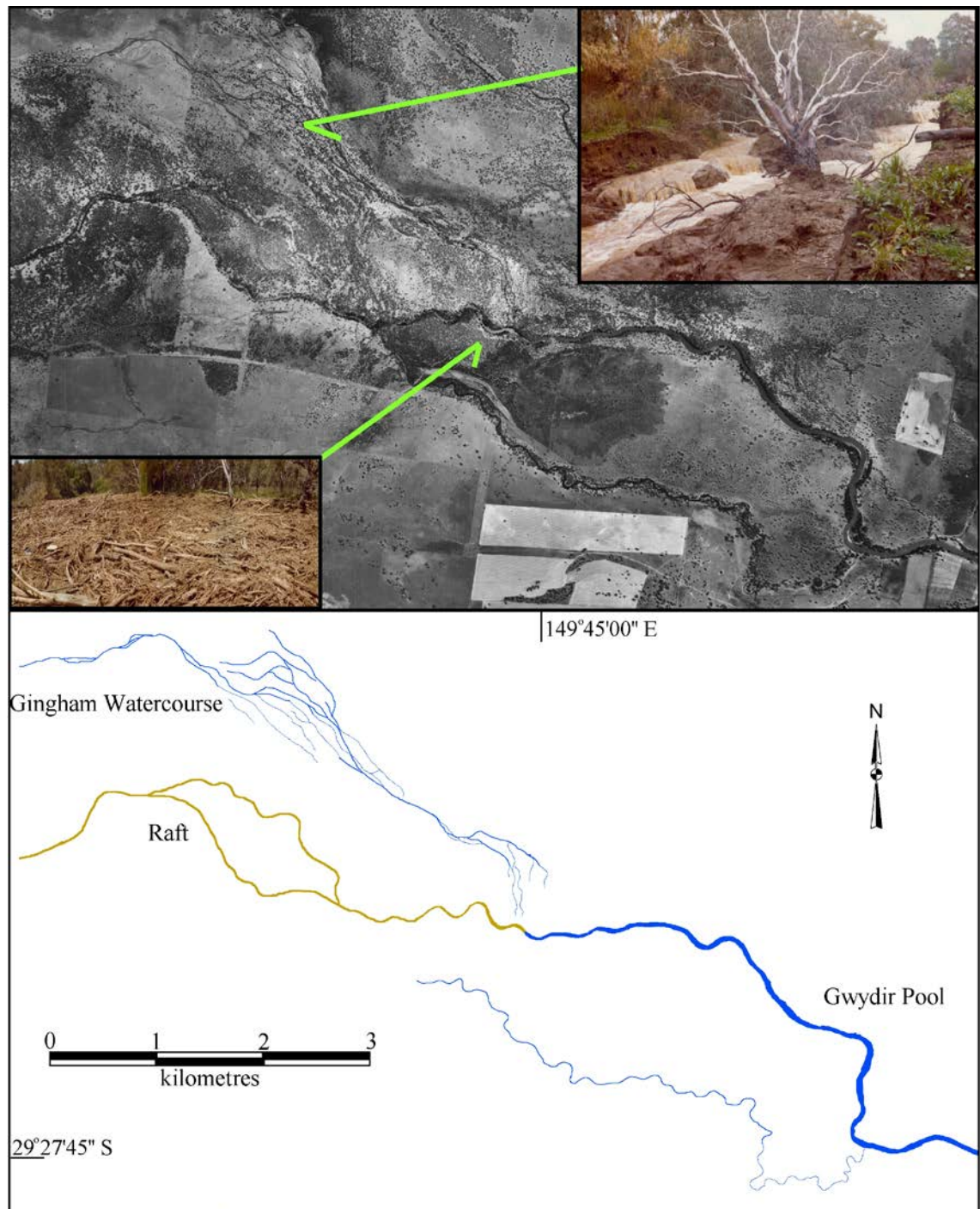


Figure 2.13: Gwydir River at the Raft. Top shows 1967 air photograph of the Raft, with schematic diagram shown below. Left bottom photo inset shows close up of woody debris, with right top photo inset showing one of many freshly cut channels at the head of Gingham Watercourse. (Inset Photos: DIPNR).

Prior to the turn of the twentieth century it appears that most of the flow in the Gwydir River below Brageen Crossing was divided between the Big Leather Watercourse (now known as the Gwydir River, see Figure 2.1) and the Goonal Anabranh (Figure 2.1), through which it would flow eventually into the Mehi River downstream of Browns Creek (e.g. Plans 36/25; 36/27; 36/45). Early plans (e.g. Plan 36/28) have the Mehi River labeled as “the Gwydir or Meei (*sic*) River”, with the presently named Gwydir River labeled “the Goonal or Great Ana Branch (*sic*) of Gwydir River”. Plans dated 1908 show the Big Leather Watercourse originating in a swamp bordering the (presently named) Goonal Anabranh, with a channel line surveyed and constructed to bypass the lower reaches of the Goonal Anabranh (Plan 36/18). This artificial channel was apparently designed to greatly increase the proportion of flows going into the Big Leather Watercourse compared to the Goonal Anabranh, although it probably had little effect on the distribution of large floods. By 1936 (Plan 36/60; 36/88) the upper reaches of the Goonal Anabranh appear to have completely silted up, with most flow directed down the Big Leather Watercourse. Prior to 1936, the Gingham Watercourse, which takes off upstream of the present day Raft (see Figure 2.13), ran with less frequency than either the Big Leather Watercourse or the Goonal Anabranh, and was therefore considered as less desirable for grazing purposes (Mahaffey, 1985). With the progression of the Raft upstream creating the Gwydir Pool (i.e. raising general water levels), the Gingham Watercourse began to run more frequently than, at first, the Goonal Anabranh, and eventually, more frequently than the Big Leather Watercourse. By 1976 the Raft was so emplaced that most moderate flows went to the north along the Gingham Watercourse, a situation that was in part rectified by the 1985 construction of the Tyreel regulator which allowed water to be directed back into the Big Leather Watercourse (now termed the Gwydir River (Figure 2.1B)). Prior to 1985, the area to the north of the Raft was a relatively dynamic part of the floodplain, with multiple channels cut by spills from the Gwydir Pool (Figure 2.13 right top photo inset).

At present flow transmission in the Gwydir River is greatly affected by both the contraction in channel capacity and natural and artificial diversions of water. Figure 2.14 illustrates the combined effects of these two processes on the hydrograph of a moderate flood. Between Yarraman and Brageen gauging stations is the Raft, which, by diverting water along the Gingham Watercourse, results in much of the difference between the two hydrographs. Additionally, between Yarraman and Brageen, and

between Brageen and Millewa, there is a considerable contraction in channel capacity. A greater proportion of the flow is thus moving along outside the channel and is therefore not gauged. Returning to Figure 2.11, it can be seen that, for the 2001 flood at least, the Raft diverted a large proportion of the flow in the Gwydir River north-north-west along the Gingham Watercourse where there was extensive flooding.

The Gwydir River is linked to the second major stream considered in this thesis, the Mehi River, by three minor streams: Broadwater, Tarran-Browns and Greenbah Creeks, as well as the now mostly silted up Goonal Anabranh. Broadwater Creek runs through Moree, between the two rivers, and will flow in either direction, depending on which river is highest (Plan 36/55). Greenbah Creek and Tarran-Browns Creek carry overland flow, spilt from the Gwydir, south into the Mehi. Similarly, the lower reaches of the Goonal Anabranh, having not silted up, still capture some overland flow spilling from the Gwydir. Figure 2.15 illustrates schematically the channel cross-section forms and topographic relationships between the main streams of the Gwydir fan-plain, showing the downstream morphological development of each channel.

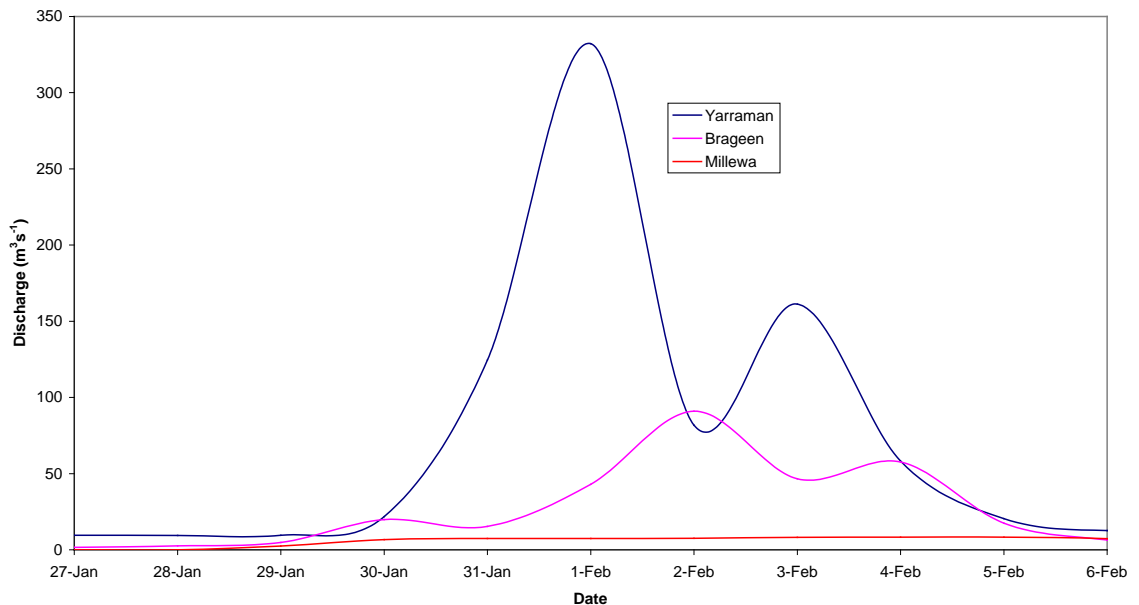


Figure 2.14: Example of flood hydrographs (February 1997) for the Gwydir River. (NSW DLWC Hydrological Data (Pineena 7)). Note that Yarraman gauging station is upstream of the Raft, while Brageen and Millewa gauging stations are downstream. Millewa gauging station is immediately upstream of Wandoona Waterhole (Figure 2.1), below which channelised flow in the Gwydir River ceases.

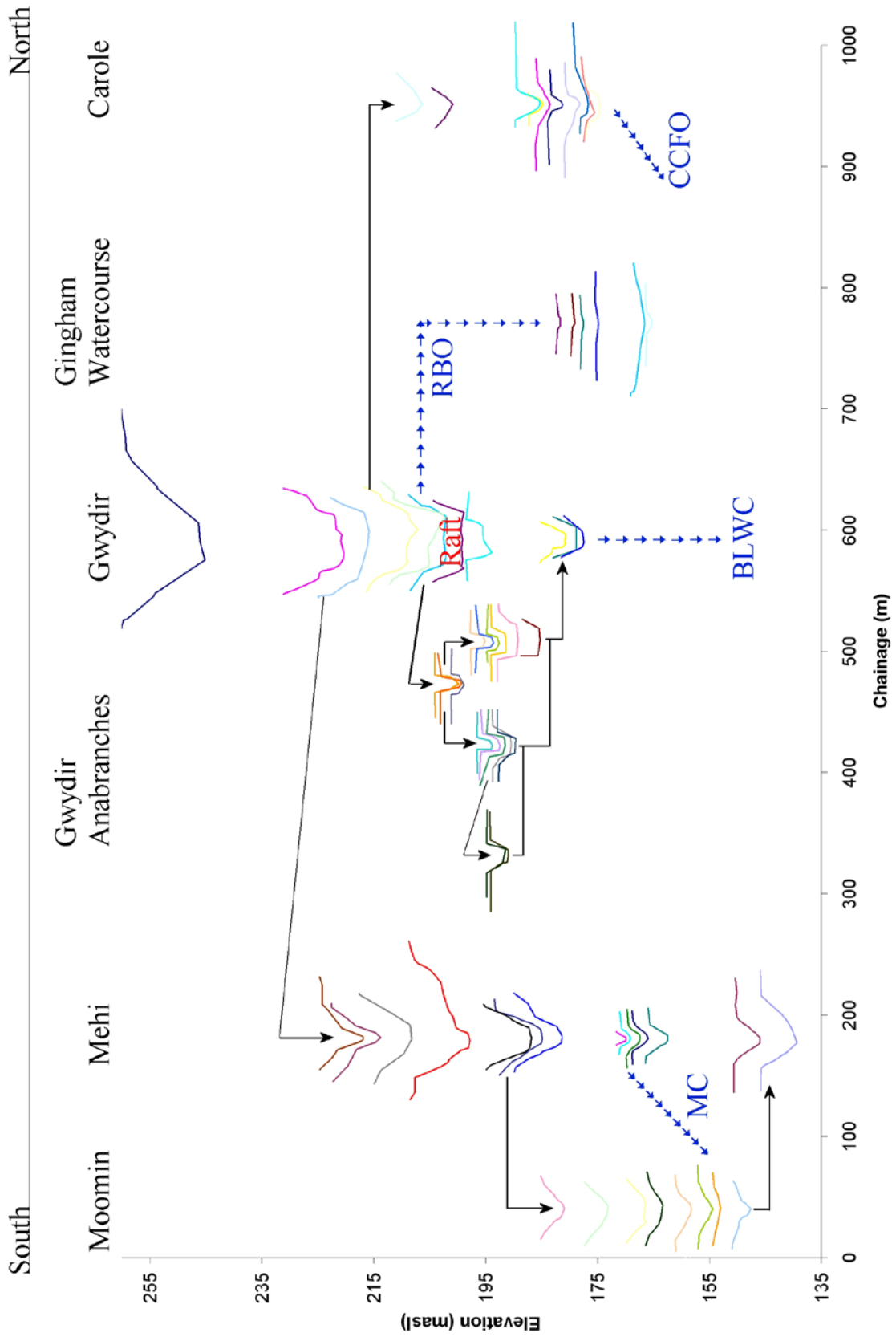


Figure 2.15 (opposite page): *Cross-section form and elevations along the contemporary fluvial system of the Gwydir fan-plain. Solid arrows represent flow distribution via effluences or confluences of channelised flow, whereas broken blue arrows represent flow distribution via predominantly overland flow. MC: Mallowa Ck; BLWC: Big Leather Watercourse; RBO: Raft break-out; CCFO: Carole Ck flood-out. Horizontal locations of channel cross-sections have been adjusted arbitrarily. Plot colours have been selected arbitrarily to enable differentiation of closely-spaced cross-sections.*

2.4.2 Mehi River

The Mehi River is a south bank distributary of the Gwydir River, its off-take from the Gwydir River being approximately 16 km down-valley of the embouchure and 20 km east of Moree. In addition to its off-take, the Mehi River receives flow from the Gwydir River from numerous interconnecting, though discontinuous, distributaries (Broadwater, Tarran-Browns and Greenbah Creeks; Goonal Anabranh), as outlined in Section 2.4.1. Approximately 355 km in length, the Mehi ranges in bankfull discharge along its length from around $575 \text{ m}^3 \text{ s}^{-1}$ at Moree to less than $5 \text{ m}^3 \text{ s}^{-1}$ upstream of the Mallowa Creek off-take. Downstream of the Mallowa Creek off-take, the Mehi River expands in size until, near its confluence with the Barwon River upstream of Collarenebri, it regains a bankfull capacity of about $100 \text{ m}^3 \text{ s}^{-1}$.

Flow in all the effluent streams of the Gwydir distributary system is determined principally by the structure of their off-takes, with the Mehi having the lowest level off-take. However, investigation of survey plans reveals that this off-take structure has been drastically altered since European settlement. Prior to engineering works being carried out the off-take for the Mehi River was approximately 3.4 m above the bed of the Gwydir (Plan 36/29), but was excavated to within about 1.1 m of the bed of the Gwydir between 1903 and 1936 (Plans 36/29; 36/30; 36/67; 36/73). This equates with a four-fold increase in flow duration, from $< 5 \%$ prior to cutting, to $> 20 \%$ afterward. Therefore, it is not productive to attempt to understand natural flow division amongst effluent streams based on flow records that are now as much artefacts of engineering works at off-takes as reflections of natural processes. Although flow division and flow

recurrence are artefacts of engineering works, the size and shape of channels downstream of off-takes, are not.

The Mehi River, following an initial increase in size, contracts over most of the first half of its length, then expands again in its lower reaches (see Chapter 3). Although there is some association between this process and the location of bifurcations (i.e. Moomin, Mallowa and Ballin-Borra Creeks) and confluences (i.e. Goonal, Browns and Moomin Creeks), standard discharge accounting is not sufficient to explain all such changes. Inputs and outputs, such as non-channelised flow, evaporation and percolation, not related to confluents or effluents, must in part be responsible. It can be seen in Figure 2.11 that, upstream of the Mallowa Creek off-take where channel size falls to a minimum, flooding is extensive. Furthermore, much of the water escaping to the north seems to be recaptured (or at least dammed) by the reach of the Mehi River immediately downstream of the Mallowa Creek off-take. In plan-form, this pattern of channel expansion-contraction-expansion is broadly repeated. It is apparent that both sinuosity and meander wavelength increase then decrease in inverse association with channel size (Figure 2.16). Moomin Creek also displays this same form of development downstream. The Mehi River is linked to its anabranch, Moomin Creek, via Mallowa Creek (Figure 2.1), a shallow, broad channel that breaks down to floodout numerous times, such that for most of its length Mallowa Creek has no defined channel (Plan 36/1205).

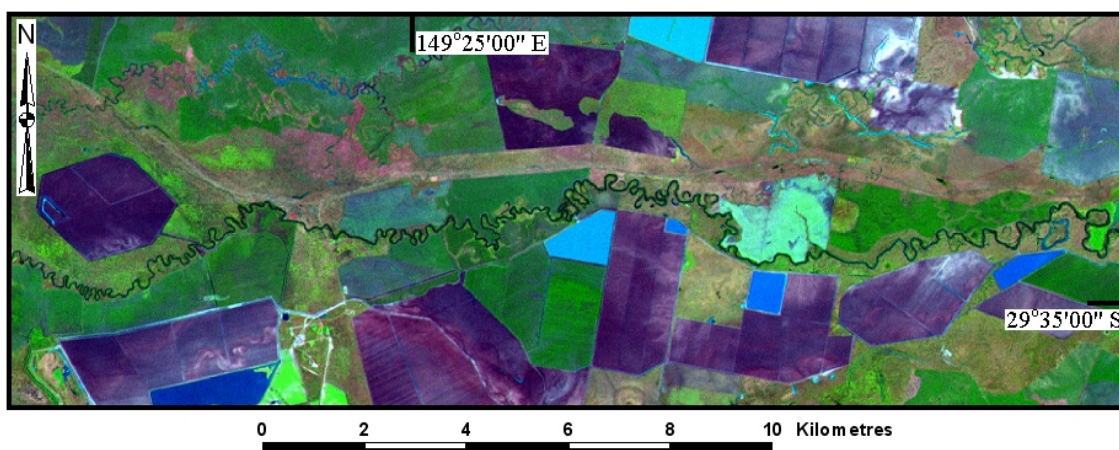


Figure 2.16: Composite LANDSAT / SPOT image of section of the Mehi River above Mallowa Ck off-take. Flow is from right to left. Note decline in scale of meandering, as well as low amplitude meandering of entire channel belt.

Cross-sections of the Mehi (Figure 2.15; see Chapter 3 for a more comprehensive analysis) show it to have lower width/depth (W/D) ratios than the main Gwydir channel, but slightly higher W/D ratios than the anabranches of the Gwydir. For the most part, W/D ratios in the main channel of the Gwydir are maintained, whereas all the other streams show a marked increase in W/D ratio downstream.

2.4.3 Carole Creek

Carole Creek takes off from the north bank of the Gwydir River, approximately 25 stream km west of the Mehi offtake, from where it flows 90 stream kilometres to the north-north-west before losing definition in a floodout, 8 km from Gil Gil Creek (Figure 2.1). Instead of following the apparent channel of Carole Creek and joining Gil Gil Creek to the north, data from the 2001 flood (Figure 2.11) showed that this floodout drained to the west, however it is not known if this happens in all floods. During the 1890s (Plan 36/7) a straight channel was cut through the flood-out, providing a direct link with Gil Gil Creek (Figure 2.1). This cut channel, over 100 years old, is only now displaying incipient meandering, indicating that even under the influence of long-duration, high flows (for irrigation purposes), channels in this environment adjust their planform very slowly.

Early survey plans (e.g. Plans 36/27; 36/30) show the head of Carole Creek situated approximately 2 km away from the bank of the Gwydir River. Thus, prior to European settlement, flow in the Gwydir had to be out-of-banks before the Carole could receive *any* water from the Gwydir. Surveys of the 1920s (Plan 36/77) show an offtake very high on the north bank of the Gwydir River, indicating that a small interconnecting channel had been artificially cut between the beginning of the Carole and the bank of the Gwydir. During the 1940s a significant connecting channel was cut to facilitate the operation of Carole Creek at lower flows in the Gwydir (Figure 2.17). Finally, the 1980s saw the construction of Boolooroo Weir, which now totally regulates flow into Carole Creek.

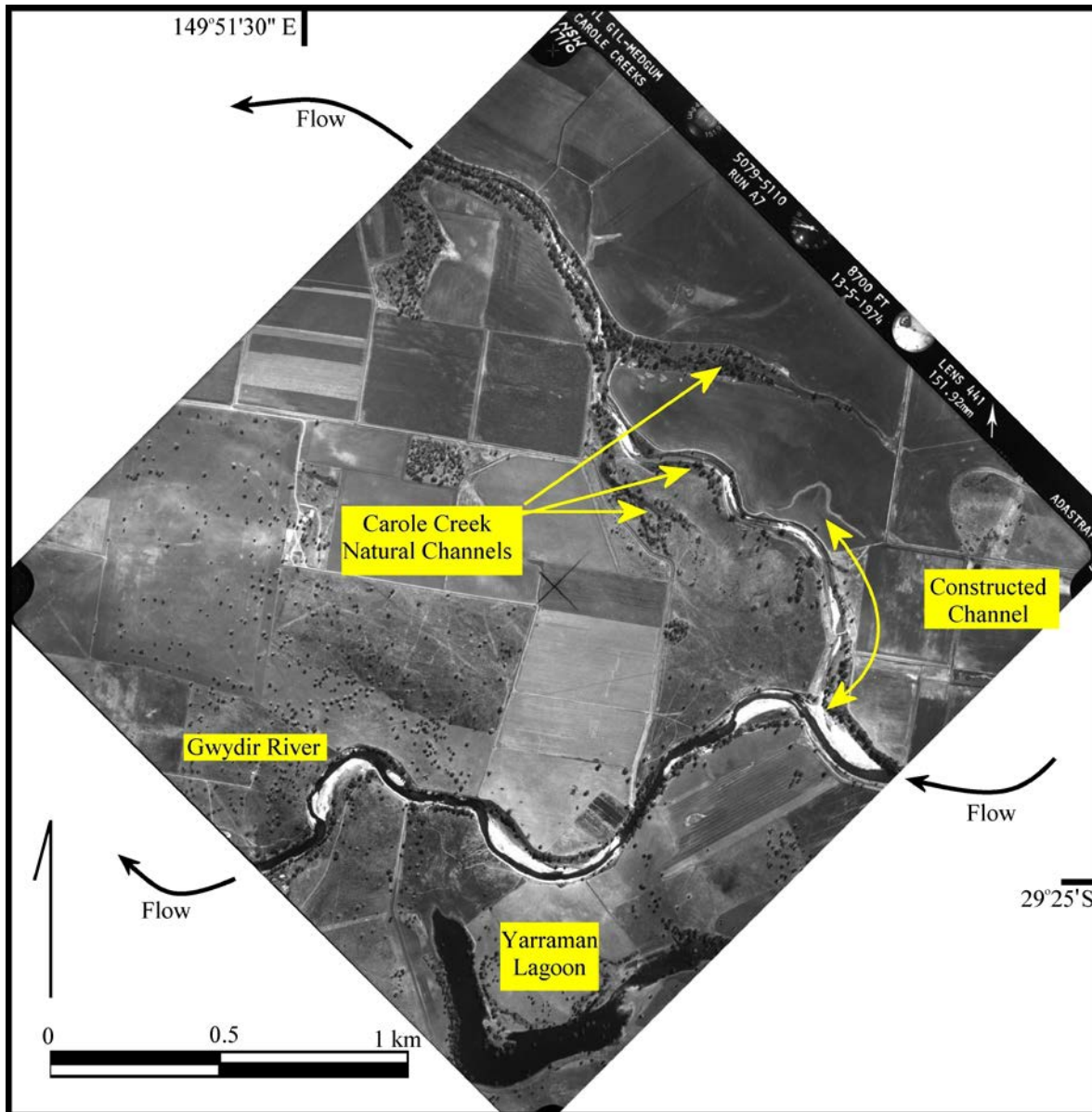


Figure 2.17: 1974 Air photo of the Gwydir River – Carole Creek bifurcation, showing the natural channels of the Carole Creek beginning approximately 750 m from the Gwydir River.

2.4.4 Moomin Creek

Moomin Creek is a 312 km anabranch of the Mehi River that follows a quasi-parallel course to the Mehi, with two major direction changes in broad sympathy with the path of the Mehi (Figure 2.1). Moomin Creek is the most sinuous of the studied streams and, though by virtue of it being a distributary of a distributary and therefore having little or

no bedload, it also has the greatest W/D ratio. This characteristic is considered in detail in the following two chapters.

The history of off-take modification progressing from minor works to weir construction, as outlined above for the Mehi River and Carole Creek, is similarly reported in survey plans (Plans 36/9; 36/37; 36/142) for the Moomin Creek off-take. In 1901, Moomin Creek would not run until the Mehi River was running at 8 m above its bed (Plan 36/37); it is now fully controlled by the Combadello Weir.

The principal hydrological effect of off-take modification for the Mehi, Carole and Moomin has been changing flow periodicity. Accompanying this is perhaps a slightly increased bedload discharged into distributaries in response to lower bed levels at the off-takes. The direct geomorphic effect of these changes is unknown but, because bedload in these rivers is very low, it could be assumed to be minor. Most sections of channel display very low stream power (e.g. $> 0.5 \text{ Wm}^{-2}$ for the lower reaches of Moomin Creek), and this presents a significant impediment to channel change, as displayed by the virtually unchanged cut channel between Carole and Gil Gil Creeks.

2.4.5 Big Leather and Gingham Watercourses

The movement of water outside channels is a quintessential characteristic of the Gwydir fan-plain. Flow along watercourses is un-gauged, and furthermore, is greatly affected by minor geomorphic or hydrological disturbances. Depending on hydrograph shape, vegetation status and (recently at least) land management, watercourses can either be flow conduits or water and sediment sinks (Figure 2.18).

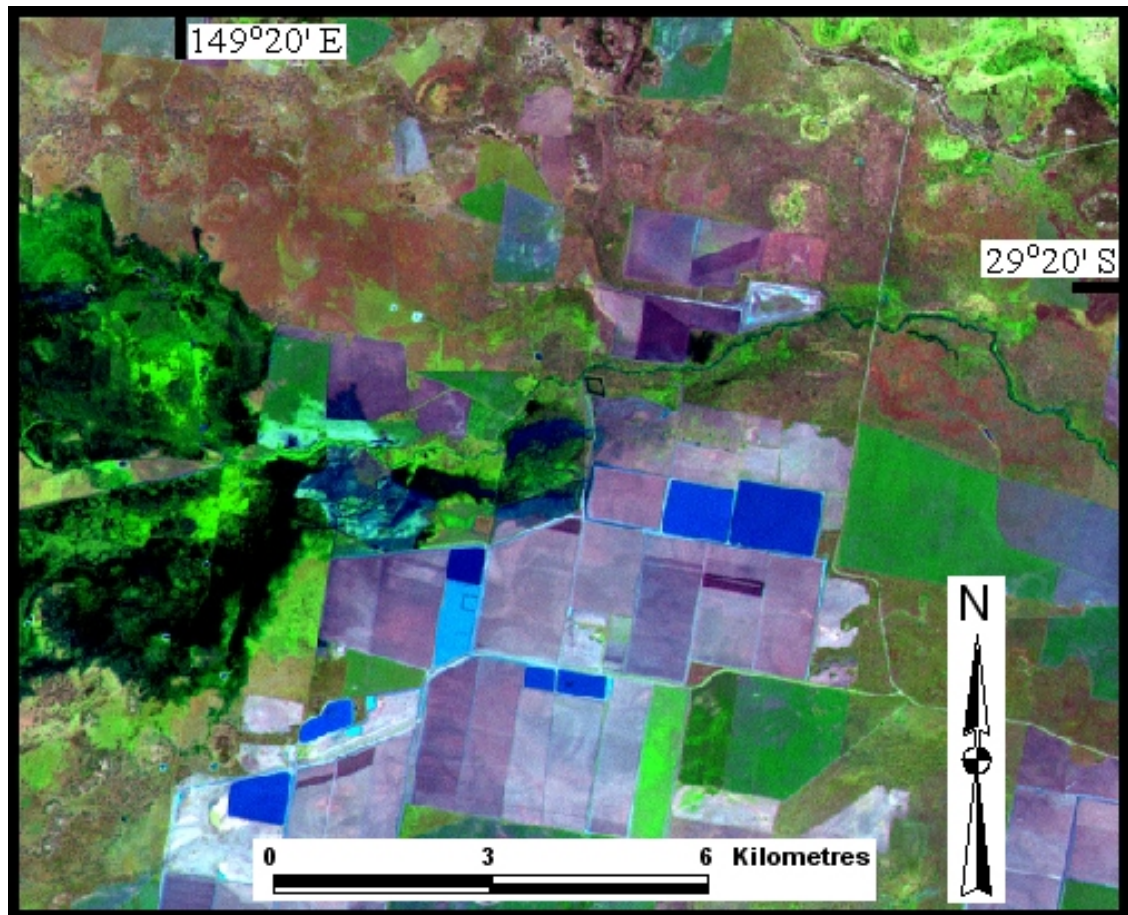
In some places, watercourses follow obvious palaeochannel remnants, with much of the Gingham Watercourse providing examples of this. However, such inheritance is not necessary, as displayed by much of the Big Leather Watercourse. Though in part channelised, Mallowa Creek too degrades into largely overland flow in its lower reaches without any evidence of its flow being constrained by palaeochannels. Recourse to inheritance does, therefore, not seem to be available in seeking explanations for the display of unchannelised flow behaviour. Consequently, unchannelised watercourses are

best understood within the context of declining stream power under the influence of a declining slope, the invasion of channels by vegetation and the siphoning of water into aquifers such that maintenance of a channel is no longer physically possible (Figure 2.19).



Figure 2.18: *Flow along the Big Leather Watercourse impeded by a ‘biological dam’.*
Note that photo was taken in 2001 after traversing ~5 km of similarly flooded country.

Figure 2.19 (opposite page): *Composite LANDSAT / SPOT image of Gwydir River in the vicinity of Wandoona Waterhole, showing channelised flow, right, grading into unchannelised flow, left. Note that linear boundary within wetland is a constructed bank. Flow is to the left.*



2.5 Palaeochannel Systems

Individual palaeochannels on the Gwydir fan-plain consist of segments that often differ in form but are apparently contiguous. This presents difficulties in mapping and describing whole palaeochannels. Breaks in channel expression, due to dissection by younger channels or overprinting by flood-borne deposits, further complicate the mapping task. Chronological correlation has been employed here to enhance the mapping program and gain an understanding of the chronology of palaeochannel changes, however, the intensity of dating necessary to fully resolve the palaeochannel chronostratigraphy is beyond the scope of the present study.

Palaeochannel segments have two basic forms: those that are topographically identifiable, and those that have little or no topographic expression. The latter are detectable only where quarries have been cut through the black clay cap to win road building material (Figure 2.20, 2.21) or, alternatively, where floodwaters highlight soil

texture differences, vegetation response or micro-topographic detail (Figure 2.22). Additionally, the radiometric signature of many palaeochannels differs from more recent deposits and thus provides further aid to their detection and mapping (Figure 2.23).



Figure 2.20: Bullarah quarry from the air (Above) and quarry face (Left). Note the lack of any obvious palaeochannel features at the surface of the plain, and the black clay overlying sandy and gravelly palaeochannel deposits evident in the quarry face. See Figure 2.1 for location of the quarry.

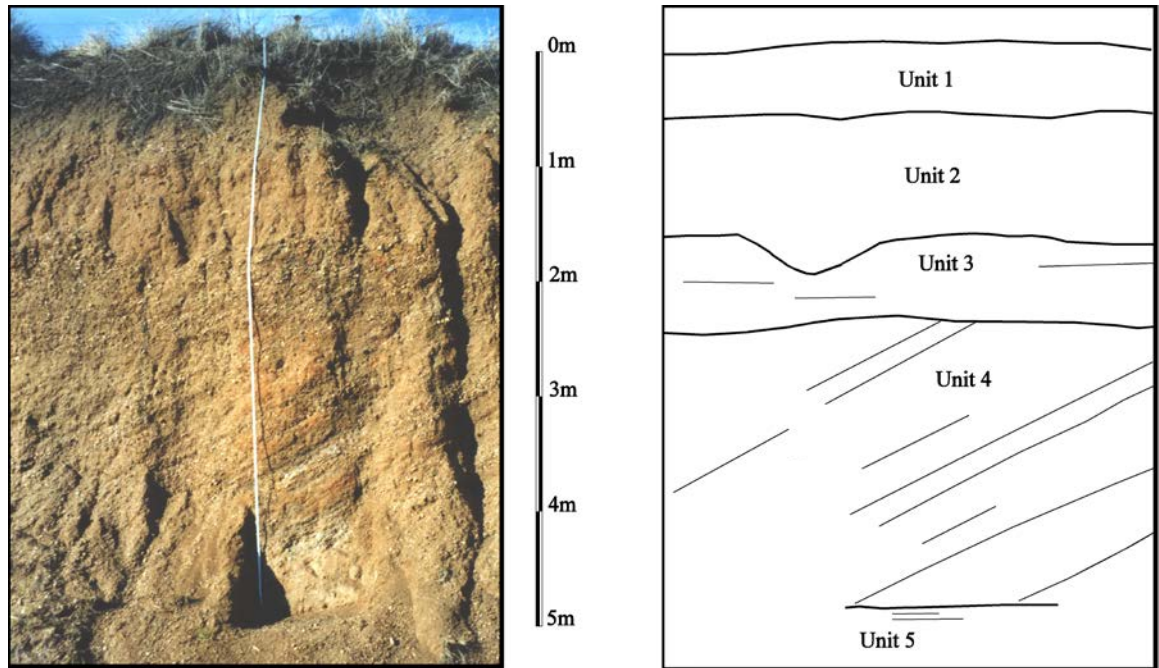


Figure 2.21: Challicum Pit, defunct council quarry beside Watercourse Rd, ~20 km west of Moree (756 000, 6739 300). Unit 1- Black clay vertisol, Unit 2 – Red brown silty loam, no bedding structures visible. Unit 3- Horizontally bedded gravelly clay, maximum grain diameters 25 mm. Unit 4 – High angle inter-bedded coarse sand and gravel. Unit 5 – Horizontally laminated sand and fine gravel.



Figure 2.22: Saturated soil on the property 'Gingham' highlighting palaeochannel location. See Figure 2.1 for general location of this site.

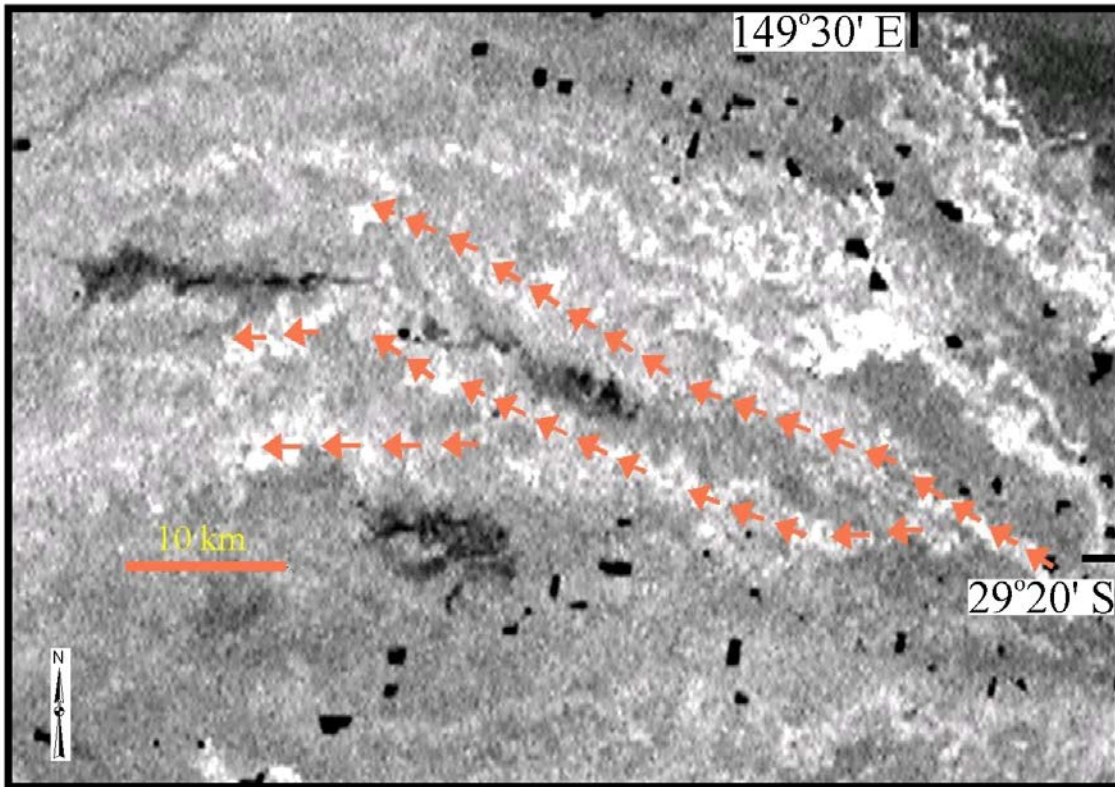


Figure 2.23: Airborne radiometry data showing palaeochannels identified by their radiometric signature. Note palaeochannels to the immediate north are topographically distinct so are not traced in this figure. Also note large wetland areas (dark coloured) associated with the Gingham Watercourse (upper) and the head of the Big Leather Watercourse (lower).

Topographically distinct palaeochannel segments have some or all of their meander belt elements raised above the surrounding floodplain, including levees, point bars, large splays and in some cases channel fills. They are therefore unaffected by small floods (Figure 2.24 and see Figure 2.4). Being largely free from floodwaters, these features project through the almost ubiquitous black clay capping. Standing out as different in colour, these are referred to locally as ‘red ridges’. The accession of aeolian material onto the general landscape has been well documented throughout eastern Australia (e.g. McTainsh, 1989), as well as locally (Cattle *et al.*, 2002). It could therefore be proposed that red ridges are so coloured because, along with being generally better drained, they provide sites of accumulation of aeolian parent material unmodified by flood-borne black clays.

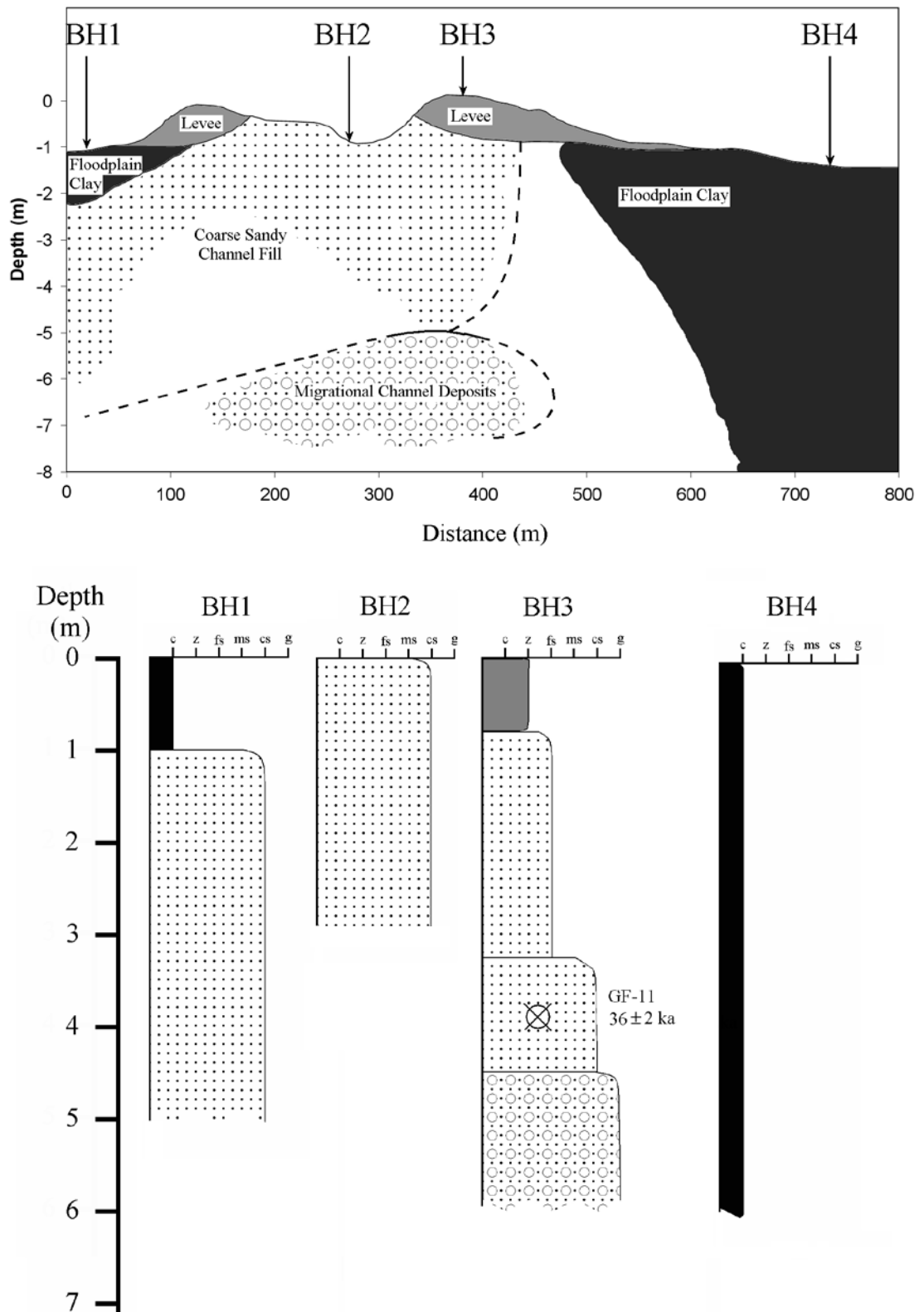


Figure 2.24: Topography and borehole data of 'Tara Loop', part of the Coocalla Palaeochannel discussed in subsequent chapters. See Chapter Six for discussion of derivation of chronology. See Figure 2.1 for location.

Of the palaeochannels that have elements standing above the general level of the floodplain, some appear to be laterally isolated, low sinuosity levee bound channels similar to the classic Murray basin ‘prior stream’ form of Butler, (1950; 1958), whereas others are closer to the ‘ancestral stream’ form described by Pels (1964a; 1966; 1969), being highly sinuous and consisting of laterally extensive true meander belts. In some places palaeochannels can be traced simply as a sequence of remnant sandy point bars with crests elevated slightly above the intervening floodplains.

Although drillers’ records show that sand and gravel deposits extend in many places to the basement rock that can be up to 60 m below the surface, most quarries have been sunk to a depth of only about 5 m, with none being greater than 12 m deep. This, along with the physical limits on hand augering, has restricted the available stratigraphic data available for this study. A sample of the data collected is presented in Figure 2.24 as roughly representative of the form many raised palaeochannels take.

With the aid of a GIS package, (ArcView 3.3) identified palaeochannel segments were collated into map form (Figure 2.25 inset). From these disparate palaeochannel segments the best preserved examples were selected to form the basis of a palaeochannel map (Figure 2.25). The meander belts presented are just one likely configuration, however, importantly the map demonstrates the difference in meander scale between the preserved palaeochannels and the contemporary channel system. The planform of the best preserved palaeochannels is easily discernible and these can be analysed in the same way as contemporary channels (see Chapter Four). Additionally the palaeochannel map provides a working model of the connectivity of disparate palaeochannel segments, a model which is tested geochronologically in Chapter Six.

2.6 Summary and Questions Arising

The Gwydir fan-plain is a low gradient alluvial surface, mantled by low-potassium black clays through which potassium-rich palaeochannel remnants project (Figure 2.2). The palaeochannels preserve in their form, sedimentology and scale a hydrological picture unlike the present, while the surficial clays appear to be genetically related to the flood-prone contemporary fluvial system. It could be supposed that contemporary styles

of flow are instrumental in the widespread distribution of clay, with numerous low gradient, vegetation-rich floodways, floodouts, and waterholes ensuring that a large proportion of the suspended load carried by the streams of the Gwydir fan-plain settles out of the water column. Where channels exist, they invariably diminish in size downstream, either grading into floodways via flood-outs, or becoming relatively wider and more sinuous. Four streams (Gwydir, Mehi, Moomin and Carole) have been chosen as representative of the range of fluvial styles, with the architectural arrangement of the distributary system, particularly the height of channel off-takes, ensuring that each has a unique hydrological and sedimentological character. Although the recent re-engineering of the distributary system of the Gwydir fan-plain obscures the natural function of the fan-plain channels, records of prior channel forms are sufficient to allow 'reconstruction' of natural channels, as well as enabling inferences regarding natural channel function.

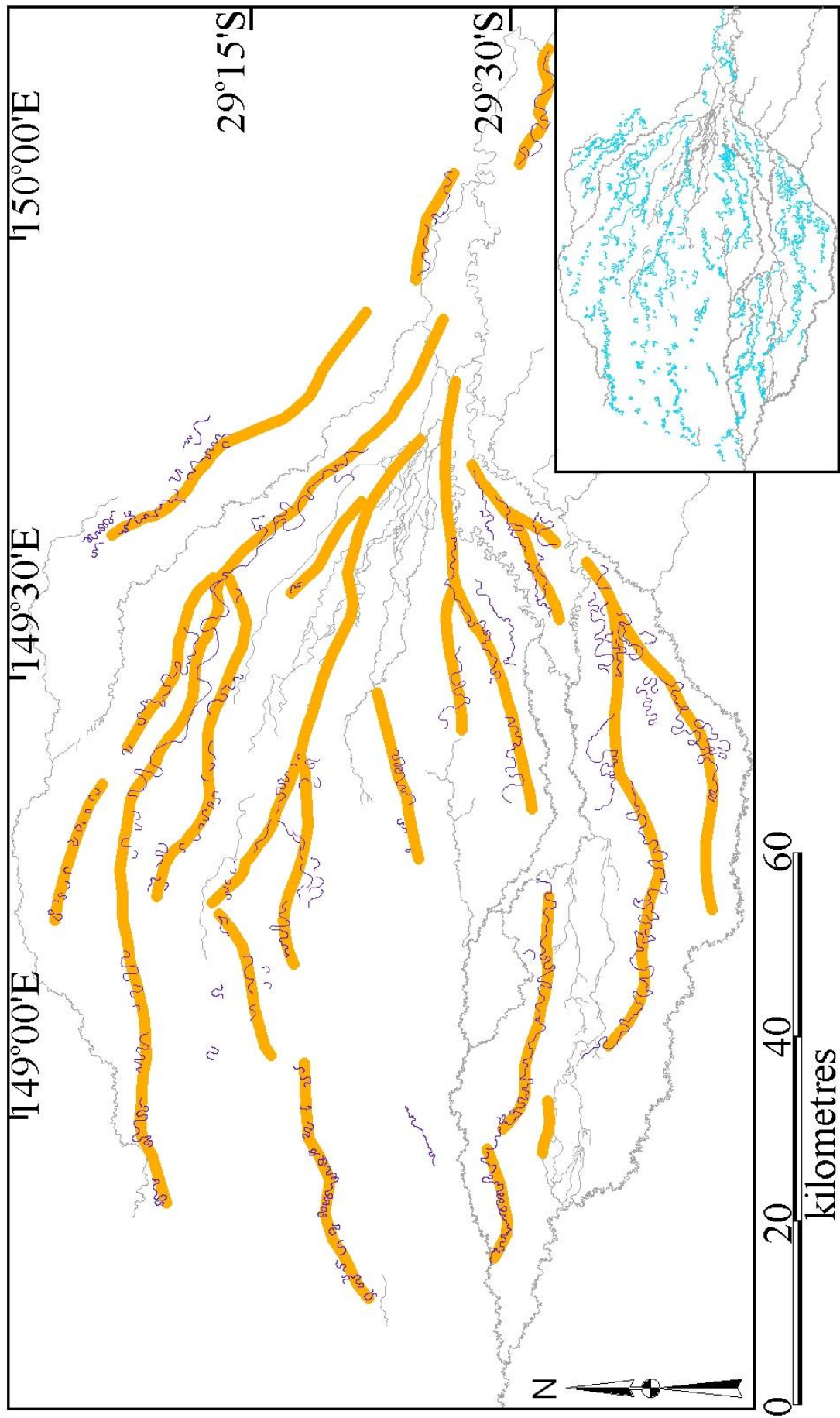
Two fundamental questions regarding the form and function of the channels of the Gwydir distributary system are considered worth pursuing. The first relates to the *contemporary system*, and can be phrased thus: What is the detailed nature of downstream channel changes in the Gwydir distributary system? Derivative questions arising include: is it possible to distinguish the causes from the effects of these changes? How do these form changes relate to discharge and slope, and why do different streams in the system change in different ways or at different rates? Following on from these questions are observations about the apparent peculiarity of the channels of the Gwydir system in comparison to channels elsewhere: why are the channels so sinuous yet so wide, so low in stream power and so prone to floodout and/or bifurcation?

The second fundamental question relates to the timing of events in the Late Quaternary and arises out of the observation that, in addition to the spatial changes within the contemporary system, the palaeochannels indicate considerable temporal change. Palaeochannels occur over a variety of scales and most of those that have been preserved are significantly larger than any of the contemporary channels. There has also been a change in the general sediment load delivered to the lower Gwydir from coarse grain, potassic sediments to fine grain, low-potassium sediments. What is the timing of these changes and is it possible to determine principal causes? A particular challenge linking the two fundamental questions is converting measurements of changes in

contemporary and palaeo form magnitude (e.g. meander wavelength) to estimates of changes in function (i.e. palaeo-discharge).

Addressing these two central questions, and the challenges issuing from them, will be the basis of the next four chapters. Chapter Three examines downstream changes in channel cross-section as discharge declines along the four main streams of the Gwydir distributary system (Gwydir, Mehi, Carole and Moomin). It relates these changes to discharge using simple bivariate hydraulic geometry. Identification and quantification of non-discharge controls on channel shape is also attempted using multivariate hydraulic geometry models. Chapter Four examines downstream changes in planform for the four main streams using four different morphometric techniques. Chapter Four also includes results of planform analysis of four of the best preserved palaeochannels segments. Chapters Five and Six provide an account of a luminescence dating program undertaken to place the developments in palaeochannel form (and derived process) within a temporal, and therefore palaeoclimatic, context. Chapter Seven illustrates the dependence of quartz luminescence sensitivity on environmental history, specifically the number of exposure-reburial cycles the quartz has experienced, and shows the potential for this to be used to trace the provenance of quartz, as well as providing insights into contemporary and palaeoenvironmental processes in river channels. Chapter Eight discusses the results of the luminescence dating in terms of the broader picture of late Quaternary climate changes in eastern Australia.

Figure 2.25 (opposite page): *Palaeochannel map of the Gwydir fan-plain. Black lines show palaeochannel remnants with surface preservation, with channel belts highlighted. Map constructed using 1967 air photo mosaics (NSW Land Information Centre), 1999 aerial obliques (Moree DIPNR), 2001 LANDSAT / SPOT composite and 2002 radiometrics (NSW BMR).*



Chapter 3 Hydraulic Geometry

3.1 Bivariate Hydraulic Geometry

3.1.1 Introduction

The cross-sectional geometry, flow velocity and to some extent roughness and slope of self-adjusting fluvial channels are scale-dependent variables, with the principle determinant of channel scale being discharge, or at least its ‘channel forming’ component(s) (Leopold and Wolman, 1957; Wolman and Miller, 1960; Woodyer, 1968; Pickup and Reiger, 1979).

*Large channels run flat, small channels steep,
Large channels are shallow, small channels deep,
Large channels run fast, small channels [creep].*
(Blench, 1957, p. 34)

Changes in scale in response to changes in discharge, at a single cross-section through time, or spatially along a channel, do not occur equitably across the three basic domains of width, depth and velocity, nor in relation to roughness and gradient. Rather, a channel adjusts its scale allometrically to accommodate a change in discharge by variable adjustment of its shape and flow parameters depending on which parameters are free and which are constrained. Hydraulic geometry interpretations are aimed first, at identifying which parameters are free to adjust and which are partially or largely constrained, and second, at deriving physical explanations for variable rates of change amongst different shape parameters through identification of the constraining agents.

As mentioned in Chapter Two, the four main channels of the Gwydir distributary system (Gwydir, Mehi, Carole and Moomin) are all very different, both in their gross characteristics, as well as how they change in form downstream. The Gwydir is relatively narrow and fast flowing, maintaining its width/depth (W/D) ratio downstream. At the other end of the spectrum, the Moomin is relatively wide and slow, displaying

dramatic adjustments in W/D ratio downstream. The Mehi and Carole, like the Moomin, are wide and slow and, like the Moomin and unlike the Gwydir, become relatively more so in their downstream reaches. These differences between channel form and function indicate that the constraints on channel shape and function must also be different for each of the four streams. From first principles alone, it would seem that this is anomalous, as all the channels sit in the same climatic, geographic and geological context. The following presents an investigation of the downstream hydraulic geometry of these four streams, undertaken to identify and quantify the differences between each of them. So called ‘at-a-station’ hydraulic geometry relationships are not considered.

With data obtained from several North American rivers, Leopold and Maddock (1953) were able to illustrate that streams adjusted their width, depth and velocity to downstream increases in discharge in what is often a remarkably consistent manner which they described using simple power relationships:

$$W = aQ^b \quad (3.1)$$

$$D = cQ^f \quad (3.2)$$

$$V = kQ^m \quad (3.3)$$

Given that:

$$Q = W \times D \times V \quad (3.4)$$

And:

$$Q = aQ^b \times cQ^f \times kQ^m \quad (3.5)$$

It follows that:

$$a \times c \times k = 1 \quad (3.6)$$

And:

$$b + f + m = 1 \quad (3.7)$$

Similar bivariate functions relating discharge to slope, roughness and sediment load were also included in the original suite of hydraulic geometry equations (Leopold and Maddock, 1953). Each of these three variables has a more complex relationship with discharge than the aforementioned width, depth and velocity, as each is dependent on

discharge, but only within a range of values determined by wholly independent factors. For example, valley slope is independent of the short term operational slope of a river. However, within the constraints imposed by valley slope a river can adjust its channel slope, thus making it within the range of normal variation in a self adjusting alluvial channel, a dependent variable. Likewise, regional sediment loads are largely independent, determined by lithology, climate and tectonics, but rivers can adjust sediment loads to match available water discharge, and therefore in the short term sediment load is highly dependent on discharge. Roughness too, is partly determined by independent factors such as riparian vegetation; however, roughness elements on the bed (ripples, dunes and bars) will develop in response to discharge changes (e.g. Simons and Richardson, 1966; Chang, 1979), therefore, roughness can be considered a dependent variable. Given these complexities, and the fact that only the Gwydir has appreciable bedload, only the width, depth and velocity relations are initially considered.

For the comparison of downstream changes in hydraulic geometry, the selection of an appropriate discharge to compare is not without theoretical and methodological difficulties (Richards, 1977; Park, 1977; Pickup and Rieger, 1979; Rhodes, 1987). In practice, however, either a discharge of known recurrence interval is used where the catchment is well-gauged, or some measure of channel-forming discharge (usually bankfull) is estimated where the gauging history is incomplete. There is an implicit assumption that the chosen discharge is the dominant flow controlling the geometry of the channel. As originally envisaged, downstream hydraulic geometry relationships required the identification of a flow that was both dominant in controlling the geometry of the channel and constant in frequency of occurrence along the channel (Leopold and Maddock, 1953). Bankfull discharge has often been selected as appropriate. However, in many situations there is no guarantee that the constancy condition is met (e.g. Kilpatrick and Barnes, 1964; Harvey, 1969). In the case of the Gwydir streams and most of the west flowing streams of the Murray-Darling basin, this is manifestly not the case (Riley, 1975a; Kemp, 2001). Though using a discharge of constant recurrence interval was emphasised in the original Leopold and Maddock (1953) paper, such a condition has not been adhered to in most subsequent hydraulic geometry exercises. This is because of both the impracticalities it presents, and for the simple reason that a flow of a single recurrence interval may have different geomorphic significance at different points

along the channel (e.g. Richards, 1977). So, in line with numerous other hydraulic geometry studies, the approach here is to use bankfull discharge, even though this does not necessarily have a constant recurrence interval downstream.

For downstream hydraulic geometry globally, average exponents b (for width), f (for depth) and m (for velocity) are typically found to be of the order ~ 0.5 , ~ 0.4 , and ~ 0.1 respectively, indicating that for streams studied, thus far at least, width is most responsive to discharge, followed by depth, with velocity being the least responsive. Given that these exponents are similar across a wide range of physiographic settings, it has been suggested that they may in fact be invariable, perhaps describing a fundamental characteristic of mobile-boundary hydraulics. Departures from the standard exponent values, at least for width, have been seen as a result of fittings across multiple coefficient - single exponent data sets (Osterkamp, 1979). Furthermore, the commonly found close proximity of b , f and m to the values predicted by minimum variance theory (0.53, 0.37, 0.10, respectively) has been used to provide corroborative evidence for the validity of application of an essentially metaphysical proposition to complex natural systems (Leopold and Langbein, 1962; Langbein, 1964). Further encouragement for accepting $b \sim 0.5$, $f \sim 0.4$ and $m \sim 0.1$ as universal or somehow fundamental, is their close agreement with empirically derived exponents that together make up so-called 'regime theory', developed in self-adjusting artificial canals. Blench (1957 p. 98) notes that the early investigations into the hydraulic geometry of natural streams (Leopold and Maddock, 1953; Wolman, 1955; Leopold and Miller, 1956) provided width and depth exponents (i.e. 0.5 and 0.33 respectively) "exactly in accordance with...regime theory equations".

Regime adjustment exponents, derived empirically through observation of correlations among measurable canal variables, have been used to predict the geomorphic behaviour of self-adjusting irrigation canals (Lacey, 1946; Blench, 1957; Simons and Albertson, 1960). As such, 'regime theory' is not actually a theory, and, as suggested by Blench (1957), is more appropriately termed 'mobile-boundary hydraulics'. Regime exponents provide descriptions of 'ideal' behaviour, where slope, discharge and bank material are largely imposed. They are therefore useful for describing channel adjustment behaviour in settings free from the complications of natural systems. However, the apparent strength of the empirical evidence supporting the suggested universality of these given

exponent values, in both hydraulic geometry and ‘regime theory’, does not necessarily translate into strong theoretical models of high explanatory power. Hickin (1983, p. 69) goes so far as to state that:

“...hydraulic geometry simply describes what is there. It has little or no theoretical significance. Even the power function form ascribed to the relations is done as much for convenience as for any other reason.”

Though the empirical evidence gathered from both hydraulic geometry investigation of natural channels and empirical observations by canal designers indicates that the aforementioned b - f - m tripartite relationship is common, it is by no means universal. Unlike physical laws, which describe necessary situations, empirical ‘laws’ describe common situations.

The first caveat that must accompany any observation of the apparent universality of these exponents is that, because of flow continuity, the geometric exponents must sum to unity (Equation 3.7). Their ranges and interrelationships are thus constrained. Secondly, the data collected thus far displays considerable scatter, both in the bivariate relationships themselves, and in the values for the derived exponents (Figure 3.1). This fact is often lost or obscured when results of hydraulic geometry exercises are presented as exponents, or, in some cases, as average exponents. A third, and most significant qualification of the apparent universality, or at least commonness, of the $b \sim 0.5$, $f \sim 0.4$ and $m \sim 0.1$, ratio is that underlying this empirical observation are physical relationships which are not in themselves universal. So, while it is possible to identify valid physical reasons for the commonness of $b \sim 0.5$, $f \sim 0.4$ and $m \sim 0.1$, it is also possible to envisage physical circumstances that would result in deviations from this norm.

Exponent b (for width) is typically three to four times exponent m (for velocity), indicating that velocity is generally more constrained than is width. Along with responding to discharge, velocity also responds to additional variables. It can be seen that an increase in discharge is, in most cases, accompanied by a decrease in slope, which will tend to moderate velocity, and, an increase in width/depth (W/D) ratio. This generally observed increase in W/D ratio will also tend to moderate velocity, and occurs because the height of banks is physically constrained by their material strength, while

the distance between the banks is generally unconstrained (Church, 1992). This constraint on bank height is reflected in an f exponent (for depth) intermediate between b and m . So, the common ordering $b > f > m$, can be explained by the common relationship between discharge and the co-variables slope and W/D ratio, without any real need to make reference to a detailed rational model.

The co-variables slope and W/D ratio are related to discharge in that they generally co-vary in a downstream direction as streams flow from upland to lowland areas (e.g. Leopold and Maddock, 1953). So, while an increase in discharge should reduce relative boundary resistance and increase velocity, in most cases this effect is countered by the downstream changes in slope and W/D ratio. Downstream increases in velocity are therefore usually slight (resulting in low m values). Where streams decline in discharge downstream, as is the case for the four streams studied here, the relationship of discharge to these co-variables will be reversed, such that an upstream increase in discharge is accompanied by an increase in slope and a decrease in W/D ratio. Examination of the hydraulic geometry relationships of streams with declining downstream discharge enables observation of the effects of these co-variables under an interesting set of alternative conditions. For while discharge declines downstream, other variables such as slope vary in much the same way as for streams with downstream increasing discharges. Interestingly, streams with downstream declining discharges are therefore not simply mirror images of streams with upstream declining discharges, as the following analyses will demonstrate.

A point of clarification regarding the term *downstream hydraulic geometry* is warranted. Downstream hydraulic geometry examines the channel response by way of changes in its geometry, velocity, roughness and water surface slope to *spatial* changes in discharge. The direction of this spatial change is, procedurally, regarded as immaterial, hence the term *downstream* hydraulic geometry could be misunderstood if it is taken as implying each incremental increase in discharge corresponds to an incremental progression *downstream*. While this may very well be the case in most streams, it is by no means necessary. Indeed as Mackin (1963) emphasized, it was not the case in the original relationships developed by Leopold and Maddock (1953). This fact needs to be seriously considered when interpreting common generalities that often arise out of hydraulic geometry exercises. For example, the commonly given explanation for the

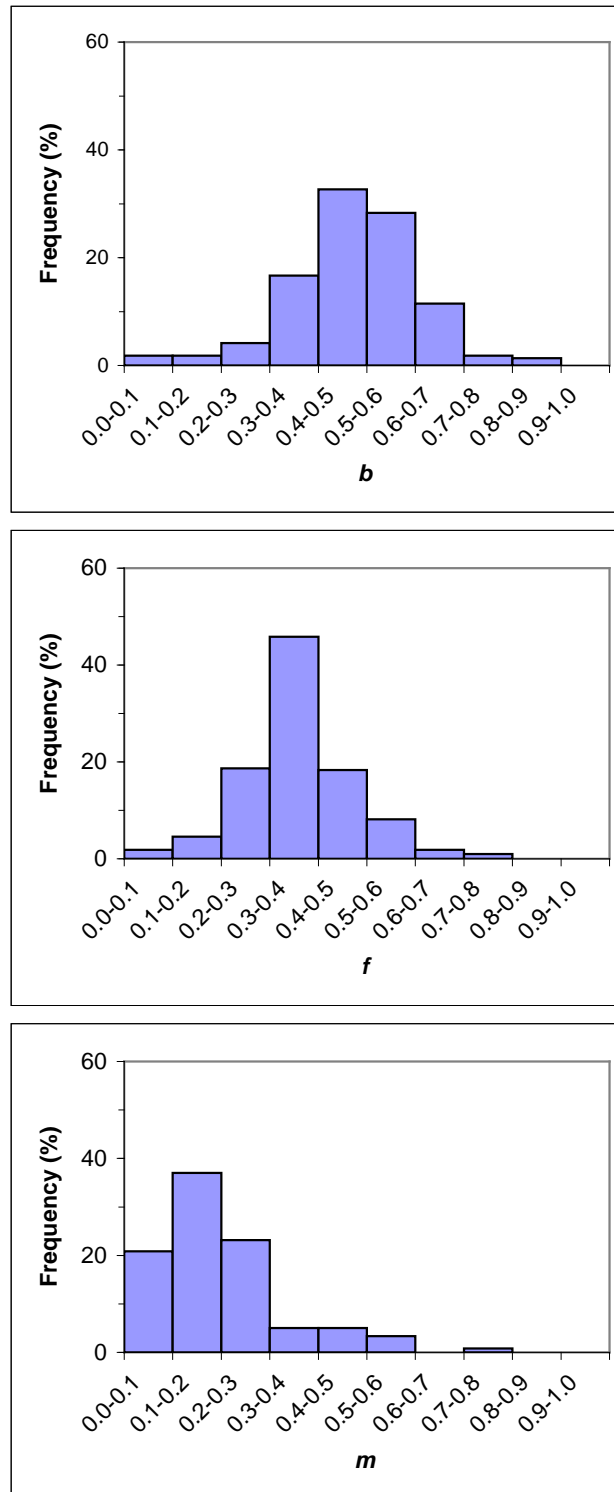


Figure 3.1: Frequency distributions of downstream hydraulic geometry exponents from 110 datasets as collected by Rhodes (1987).

low value of the velocity exponent outlined above (i.e. the generally found inverse association between discharge and slope) will be valid only if discharge increases downstream and, as is usual, slope declines. Furthermore, Richards (1977) observed that the $W \propto \sqrt{Q}$ relationship occurs only if a certain slope-discharge relation applies. To reiterate: interpretations of the significance of exponent magnitudes must take into account the direction of discharge increase because co-variables of discharge will affect exponents differently, depending on whether they are positively or negatively associated with discharge.

Perhaps then, the term downstream hydraulic geometry should be replaced by a term more reflective of the essential difference between downstream and at-a-station hydraulic geometry. Several possible candidates suggest themselves. *Along-stream* hydraulic geometry could be suitable as it more accurately captures the directionless nature of the measurement process, allowing greater appreciation of the possibilities for channels to increase and decrease in discharge multiple times throughout their downstream extent. If the original suggestion of Leopold and Maddock (1953) to use a flow of constant recurrence interval were commonly observed then *constant-recurrence-interval* hydraulic geometry could be used, which would necessarily distinguish it from at-a-station hydraulic geometry. Likewise *bankfull* hydraulic geometry could be used. Given the tendency to use this as a reference discharge in most subsequent hydraulic geometry exercises, it is perhaps more appropriate. Both of these approaches are aimed at identifying a formative discharge, which would suggest that both could be considered variants of *formative-discharge* hydraulic geometry, for this term accurately captures the essential element of downstream hydraulic geometry, that is, exploration of the way in which the channel *as a whole* accommodates discharge change. Though possibly simply an issue of semantics, the unusual circumstances of the channels of the Gwydir tributary system do require that care be taken in both their description and in the interpretation of technique application. Having flagged these issues of appropriate terminology, the remainder of this thesis will use the term *bankfull hydraulic geometry*, as the analyses below are based on estimates of bankfull discharge.

3.1.2 Data Collection

As outlined in Section 2.1, the current form of the Gwydir, Mehi, Moomin and Carole are partly the result of engineering works carried out during the establishment of broadscale irrigated agriculture in the region during the late 1970's. Present day surveys would therefore not accurately record the natural adjustment of channels to downstream changes in bankfull discharge. Fortunately, a large proportion of the length of these streams had been surveyed, in some cases multiple times during the preceding century. It is this survey data that forms the basis of this chapter, with the assumption that this survey data accurately records the 'natural' form of the channels.

Access to all government survey data held by the NSW DIPNR was granted by the Custodian of Plans, and a total of 583 survey plans were digitally scanned. Examples of these are presented in Appendix B. From these plans cross-sections and long-sections were selected in a semi-random way from meander inflection points to reduce the complications introduced by cross-section asymmetry. The coordinates of individual cross-sections were then entered into a database. Concentrations of study sites evident on Figure 3.2 are, in the case of the Mehi, Moomin and Carole, along reaches that required full canalization and were therefore particularly well surveyed. In the anabranching section of the Gwydir, high-density surveying was undertaken to find an appropriate channel to carry water diverted around the Raft.

Measurement of channel cross-sectional area and calculation of discharge become somewhat subjective exercises due principally to the arbitrary way channel limits are defined, specifically the height of the water surface at bankfull. Estimation of discharge is further subjectified by the need to account for channel roughness. For this study, coordinates for individual cross-sections were analysed using a custom written Visual Basic program to extract width, depth, cross-sectional area, mean depth and wetted perimeter. Most of the surveyed channel sections continued on to the floodplain proper and this provided a useful means of delineating bankfull stage. Given the subdued nature of the floodplain and the canal-like form of most channel sections, the abrupt change between channel bank and floodplain was readily identifiable.

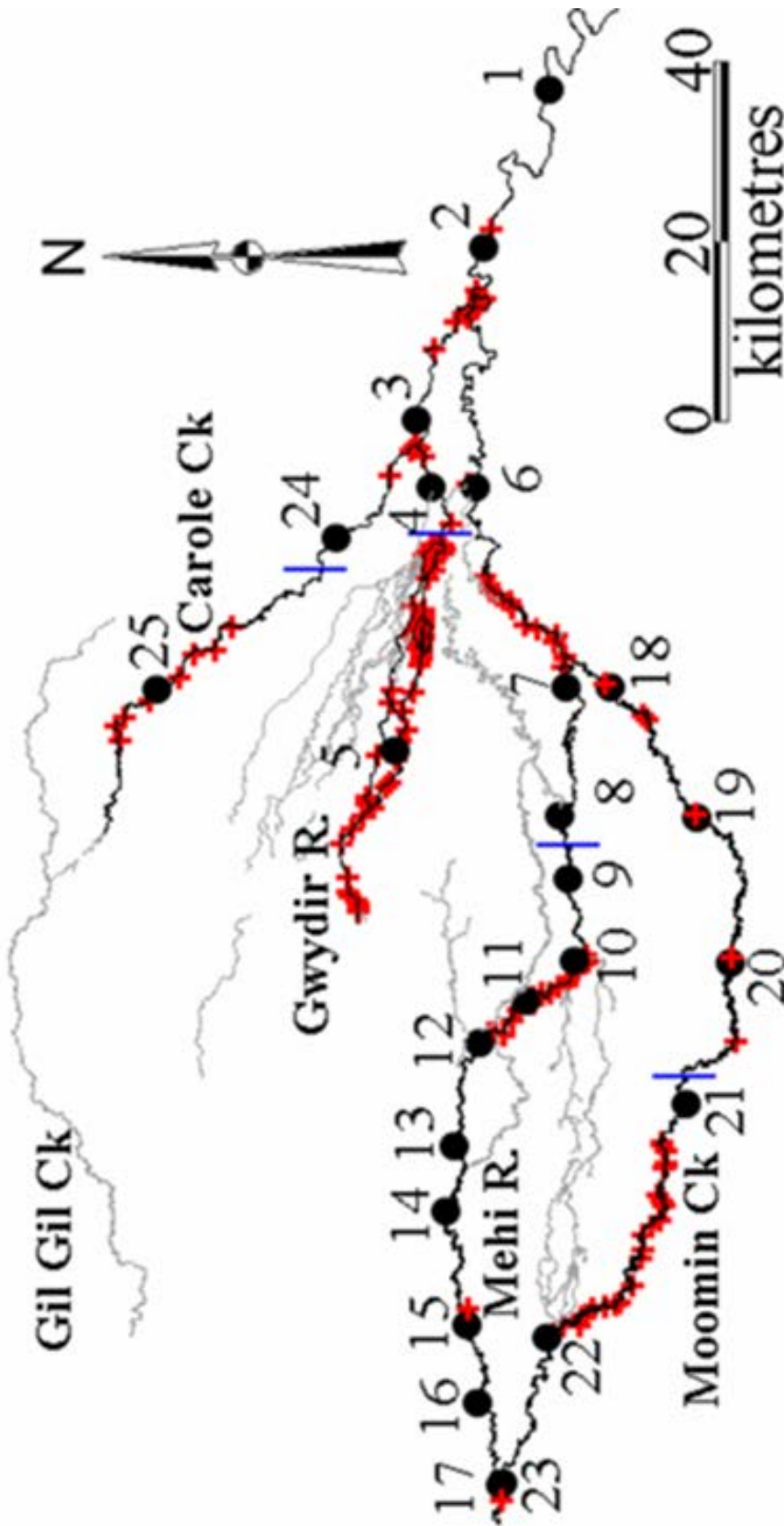


Figure 3.2: Cross-sections (red crosses) and sediment sampling sites (closed circles) for hydraulic geometry analysis. Vertical blue lines divide each channel into upper and lower reaches subsequently referred to in Section 3.2.3 and Table 3.4.

Measurement of water surface slope presents significant methodological difficulties. It is therefore common practice to resort to using bed-slope as an approximation of water level surface slope. For the channels of the Gwydir fan-plain though, long sections of channel bed reveal that for distances of less than about 20 km, channel bed slope is in fact a poor indication of water level slope (e.g. plans 36/68; 36/1620): in some cases channel bed slopes are negative over distances of up to 3 km. Although over greater distances bed slope approximates water level slope, over the localised lengths examined here it was necessary to use some other measure of water level slope. This was made possible by the fact that all the survey data used has been reduced to a common datum. This has enabled measurement of the bankfull water level slope based on the absolute elevation of the bankfull level at each cross-section.

Channel length was measured from rectified composite SPOT/Landsat imagery using Arcview software. This method was favoured over lengths provided in surveyed plan sections as the latter were based on straight line distances between successive survey points, whereas the curvature of the channel could be readily incorporated into digitised channel mid-lines when using satellite imagery.

As bankfull discharge was estimated using the Manning's equation (Equation 3.8) a value for Manning's n was estimated for each site.

$$Q = \frac{A \times R^{\frac{2}{3}} \times S^{\frac{1}{2}}}{n} \quad (3.8)$$

This was done by combining estimates obtained using three separate means; visual inspection, interpolation from sites of known n , and by adjustment of n as recorded by engineers. The first method involved simply visiting the sites and comparing them visually to tabulated examples of n for various stream types (e.g. Barnes, 1967; Hicks and Mason 1991). However, given the large number of sites it was not practical to visit them all. Interpolation of n from gauging stations with 'known' values of n , back calculated from stream flow records and survey data (NSW DLWC, 2002), was also used. The third method was to use the n values estimated by locally experienced engineers and recorded on some survey plans (e.g. Plan 36/3014_3) for the purposes of estimating the capacity of the channels to carry water for irrigation.

Estimating n visually is as likely to be too high as too low, depending on the very recent history of the site examined, whereas the other two methods for estimating n result in values that are almost certainly too low. This is because gauging stations are usually constructed at locations that are hydraulically relatively simple and therefore not representative of the channel as a whole. Furthermore, some of the engineer's n values refer to channels in their 'post-engineered' state. However, both cases, although probably underestimating n , should not do so by a large amount as most gauging reaches in the Gwydir distributary system are visually indistinguishable from adjacent channel reaches. Additionally the post-engineering channels are usually not run at bankfull and therefore the engineer's value for n refers to a sub-bankfull flow. Given that n will decrease with increasing discharge it is likely that the post-engineering sub-bank-full n estimate is close to the pre-engineering bank-full n value. The estimate of n used for each site is a composite of the multiple values arrived at using each of the three stated methods, with due cognizance given to the likely direction of error involved in each estimate.

3.1.3 Bivariate Hydraulic Geometry of the Gwydir, Mehi, Carole & Moomin

The Gwydir, Mehi, Moomin and Carole are all examples of streams with downstream declining discharges (Figures 3.3(e), 3.4(e), 3.5(e) and 3.6(e)). Derived b , f and m exponents were calculated using ordinary least squares regression fitting for log transformed data. The data and derived plots are presented in Appendices B and C, with Figure 3.7 presenting the b - f - m relationships within ternary space with two of the divisions suggested by Rhodes (1987). In a geomorphological context the derived hydraulic geometry relationships are not solutions in themselves, but rather they allow comparison of streams in order to identify the relative importance of each of the controls on channel shape (Mackin, 1963). As already noted, of suggested importance in the study streams is the fact that, on average, discharge decreases downstream. This goes some-way to explaining the difference in exponents between the study streams and streams elsewhere. However, for the four streams studied, the challenge is not only to discern why they differ from streams studied elsewhere, but also to attempt explanation of why they differ from each other.

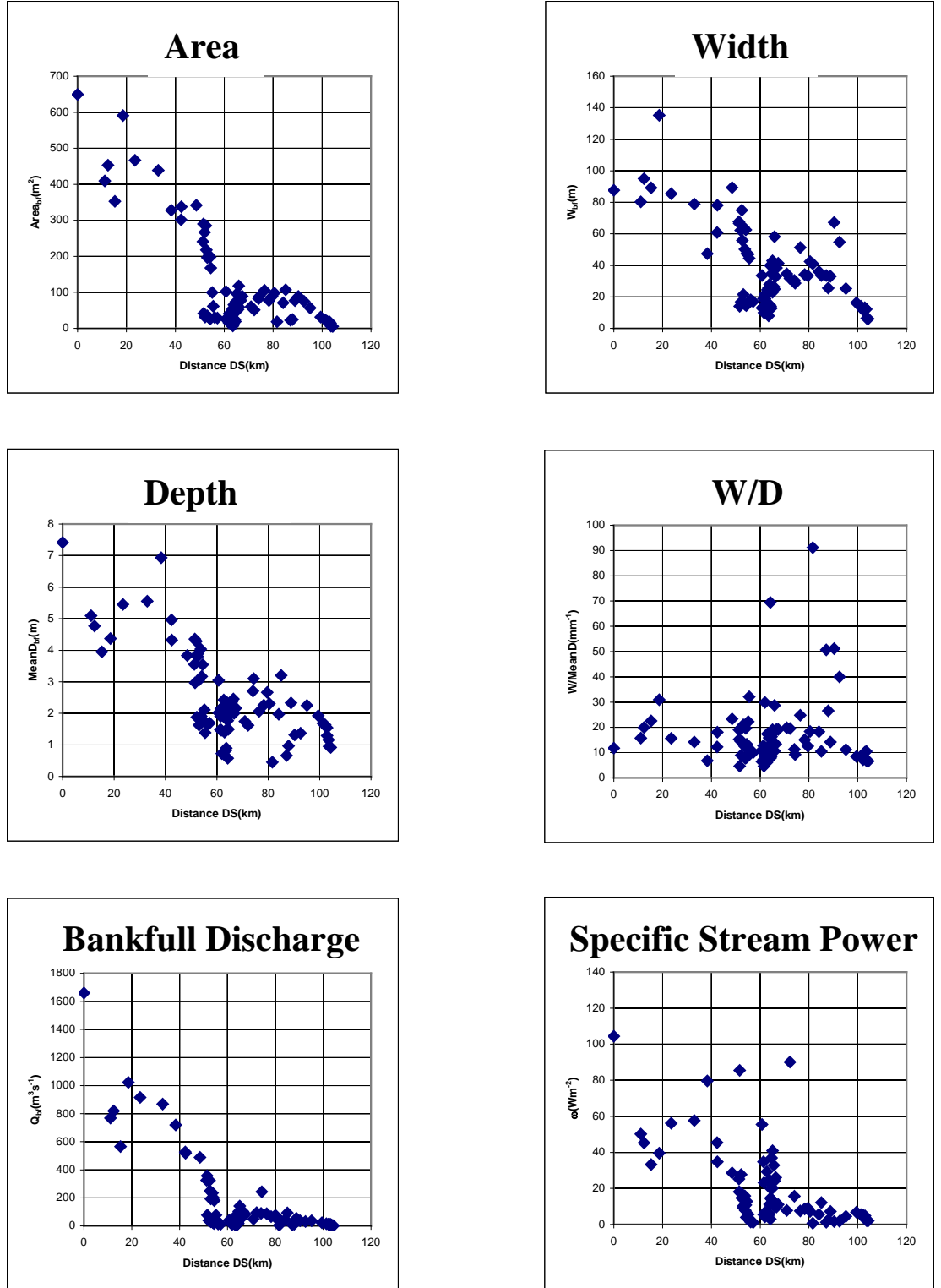


Figure 3.3: Gwydir River: downstream variation in a) bankfull mean depth, b) bankfull width, c) W/D ratio, d) bankfull mean velocity, e) bankfull discharge and f) bankfull specific stream power. Distances are downstream of Pallamallawa. See also Appendix B.

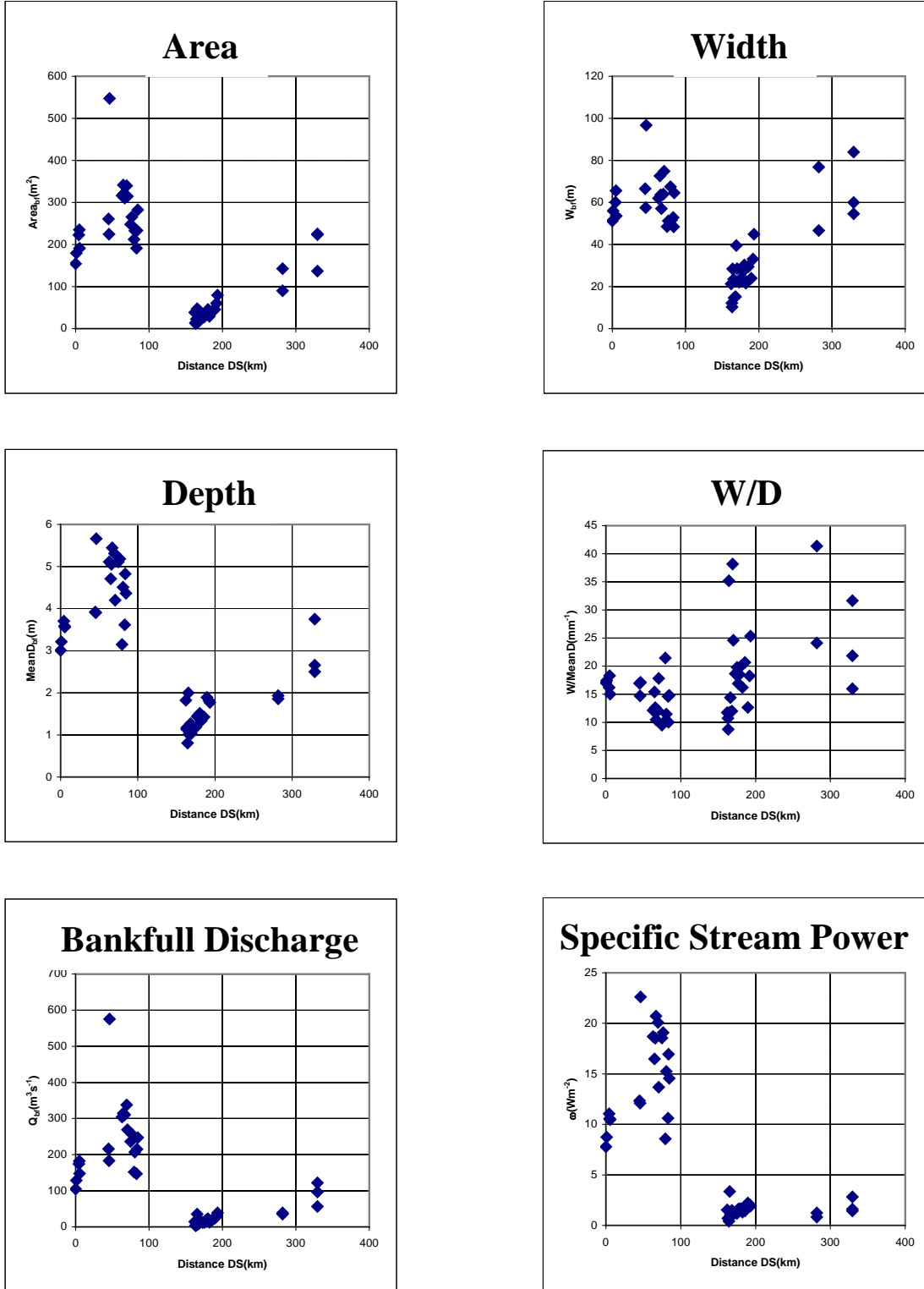


Figure 3.4: Mehi River: downstream variation in a) bankfull mean depth, b) bankfull width, c) W/D ratio, d) bankfull mean velocity, e) bankfull discharge and f) bankfull specific stream power. Distances are downstream of off-take. See also Appendix B.

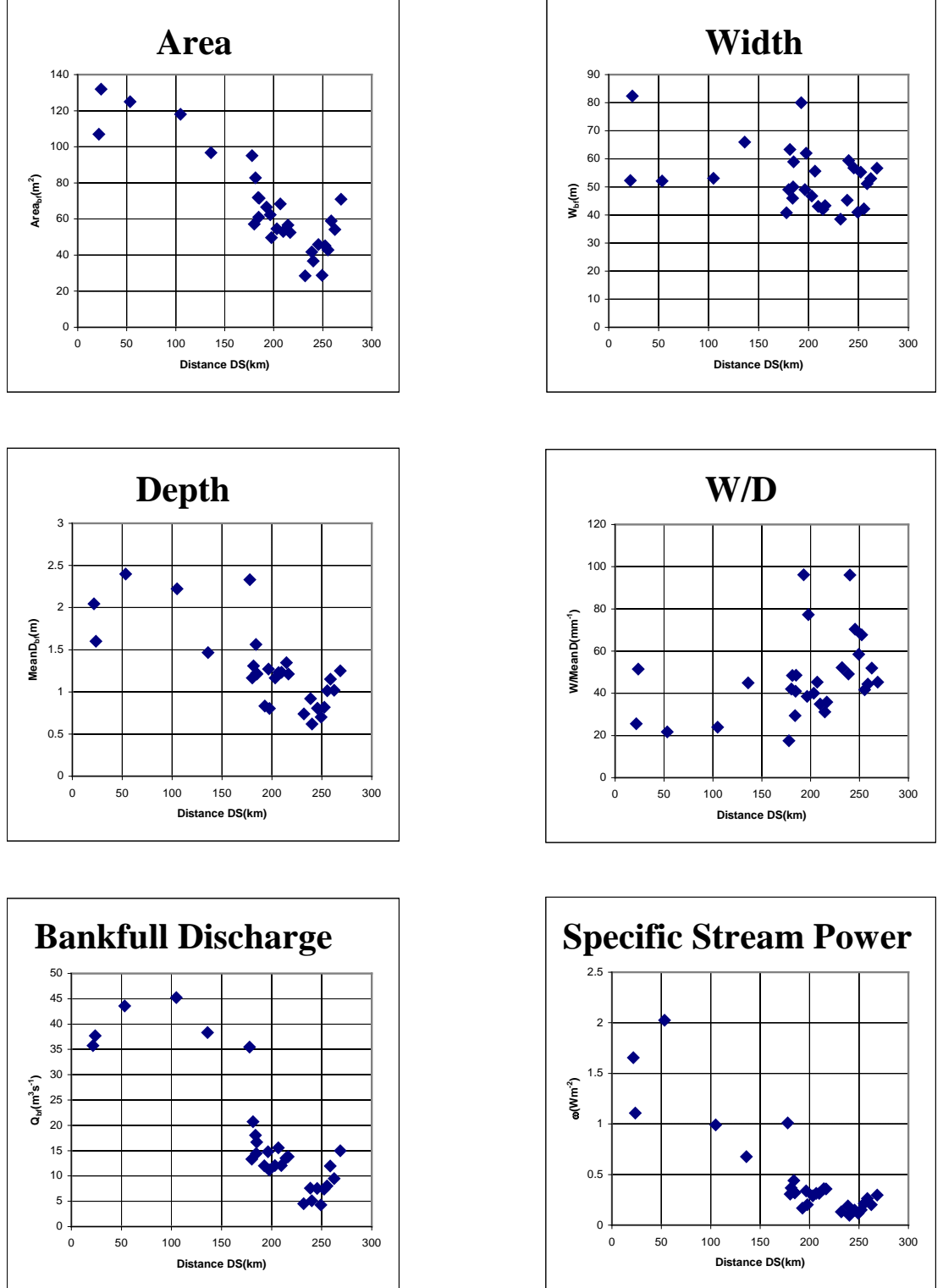


Figure 3.5: Moomin Creek: downstream variation in a) bankfull mean depth, b) bankfull width, c) W/D ratio, d) bankfull mean velocity, e) bankfull discharge and f) bankfull specific stream power. Distances are downstream of off-take. See also Appendix B.

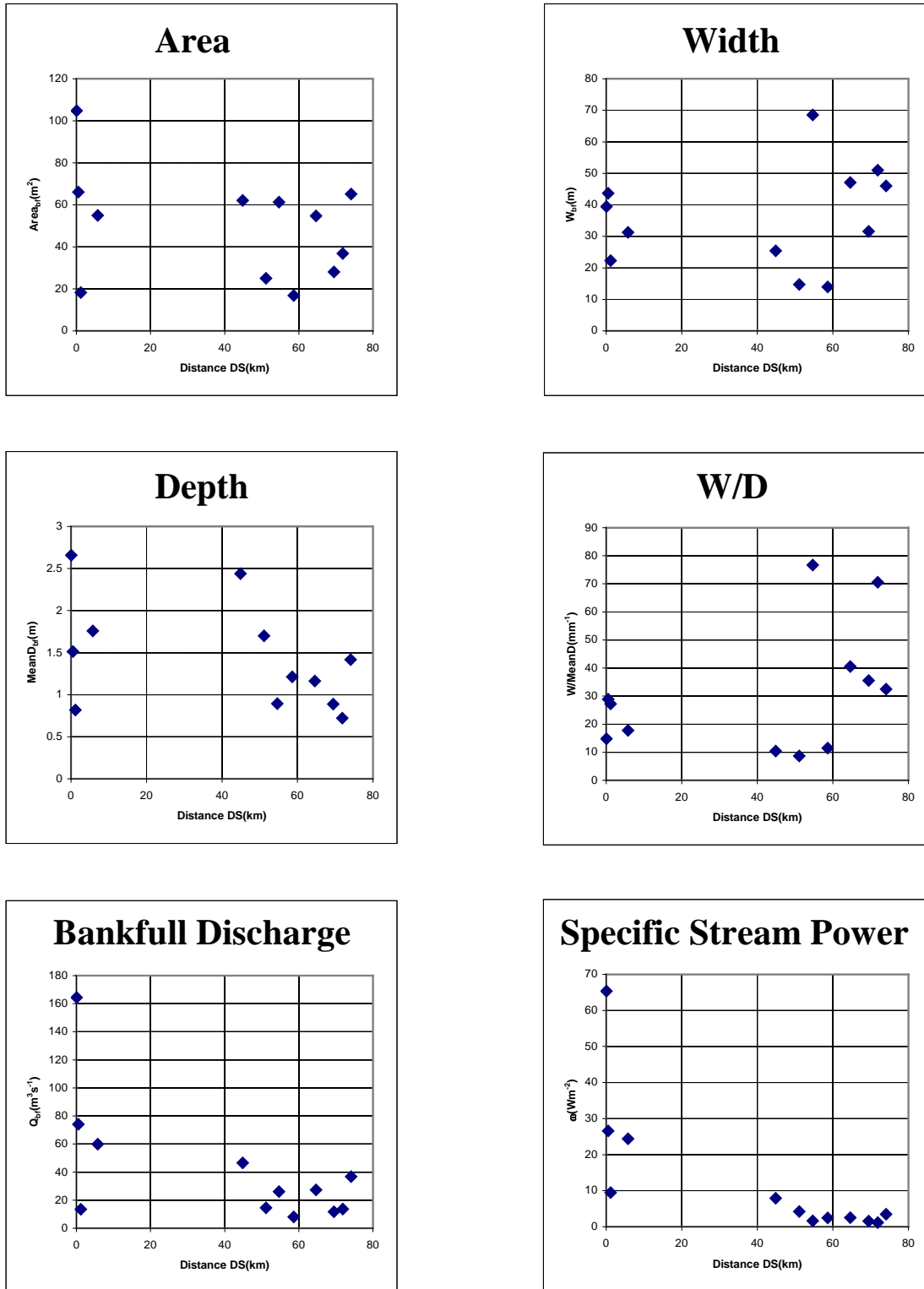


Figure 3.6: Carole Creek: downstream variation in a) bankfull mean depth, b) bankfull width, c) W/D ratio, d) bankfull mean velocity, e) bankfull discharge and f) bankfull specific stream power. Distances are downstream of off-take. See also Appendix B.

Plotting b , f and m values within ternary space allows simultaneous comparison of all three variables. The b - f - m coordinates of the majority of rivers so far studied are concentrated, with over 85% of the rivers reported by Park (1977) and Rhodes (1987) plotting within the trapezoid highlighted in Figure 3.7. All the channels described in this study fall outside this region, emphasising the distinctive nature of the Gwydir fan-plain channels. Rhodes (1987) has shown how the ternary space can be divided into regions of unique geomorphic associations, with the line $b = f$ providing the simplest example, separating those streams that increase in W/D ratio with increasing discharge (left side) from those that decrease in W/D ratio with increasing discharge (right side). However, the specific divisions identified by Rhodes (1987) have most relevance to streams which increase in discharge downstream, therefore only the two divisions that relate most clearly to channels with downstream declining discharges are retained here, i.e. the aforementioned $b = f$ line, and the $m/f = 1/2$ line. Only the Gwydir falls on the left side of the $b = f$ line, indicating that it alone has a W/D ratio which increases with discharge, and therefore declines downstream. A downstream increase in W/D ratio is usually interpreted as a downstream increase in the ability to transport bedload (Lane 1937, Mackin 1948, Leopold and Maddock, 1953), and therefore on initial consideration, it might be assumed that the relative bedload transport ability of the Gwydir declines downstream. This is argued below to be an over-simplistic interpretation though, as, under special circumstances, optimal sediment transport occurs through channel narrowing and multiplication, i.e. anabranching, rather than widening.

The ratio m/f describes the rate of change of velocity (m) relative to the rate of change of depth (f). All four study streams plot considerably above the $m/f = 1/2$ line (Gwydir $m/f = 0.76$; Mehi $m/f = 0.64$; Moomin $m/f = 0.82$; Carole $m/f = 1.23$) indicating that for all four, depth increases with increasing discharge at less than twice the rate that velocity increases. Rhodes (1987) argues that the m/f ratio can be used to describe the nature of downstream changes in suspended sediment concentration, citing earlier hydraulic geometry and regime theory workers (e.g. Leopold and Maddock, 1953; Langbein, 1965) who observed that where $m/f < 1/2$ (below the line) suspended sediment concentration decreases with increasing discharge. For the channels of the Gwydir fan-plain, which all have m/f ratios $> 1/2$, suspended sediment concentration is likely to decline with declining discharge. Thus, not only is the total volume of water discharge declining downstream, but it is also likely that the suspended sediment concentration of

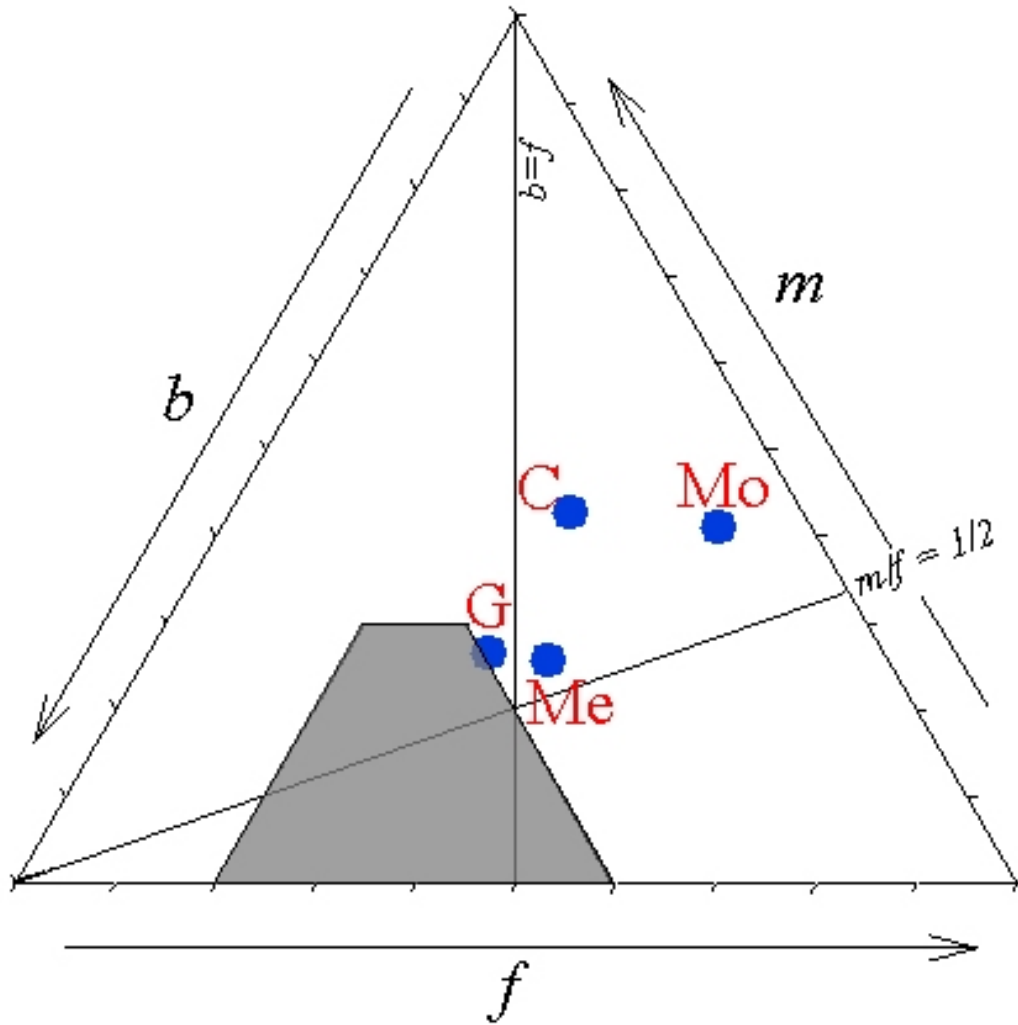


Figure 3.7: The combined exponents of the Gwydir (G), Mehi (Me), Moomin (Mo) and Carole (C) along with two of the divisions suggested by Rhodes (1987). Three other divisions suggested by Rhodes have been omitted as their interpretation requires that slope decreases with increasing discharge, which is not the case for the Gwydir fan-plain channels. The line $b = f$ separates those streams for which W/D ratio increases with increasing discharge (left side) from those streams that decrease in W/D ratio with increasing discharge (right side). The line $m/f = 1/2$ is suggested by Rhodes (1987) to indicate the nature of changes in suspended sediment concentration with increasing discharge, with Rhodes (1987) and several prior workers (e.g. Leopold and Maddock, 1953; Langbein, 1965) stating that when depth increases twice as fast as velocity (i.e. $m/f = 1/2$), neither channel scouring nor channel siltation occurs. The shaded region, bounded by $f = 0.2$, $b = 0.4$ and $m = 0.3$ represents the location of the majority of rivers studied elsewhere. For example, Park (1977) and Rhodes (1987) provide b , f and m values for a total of 107 separate rivers, with just over 85% of these plotting within the shaded region. See also Appendix C.

that water is declining, which in combination serve to illustrate the high sediment trapping efficiency of the Gwydir fan-plain channels.

Table 3.1 shows that the Gwydir alone has the standard ranking of exponents albeit that discharge is declining downstream, with width being, statistically, the most responsive to discharge (and/or its co-variables) and velocity the least. For the other three streams depth is more responsive to changes in discharge than width, with width being the least responsive variable for both the Moomin and Carole. Also apparent from Table 3.1 is that the velocity exponent, m , is far higher for all streams in the Gwydir system than most values reported for other systems (see Figure 3.1). The Gwydir and Mehi have m values ~ 2 times the values commonly found to apply in other rivers, while the Moomin and Carole have values ~ 4 times values commonly found elsewhere. In other words, the rate of downstream *decline* in flow velocity in the channels on the Gwydir fan-plain channels is greater than the rate of downstream *increase* in flow velocity in most other channels. This reflects the large impact of the downstream decrease in slope on the fan-plain (Figure 3.8). In the channels of the Gwydir fan-plain, the increase in velocity due to the decline in relative boundary resistance associated with a larger discharge is actually amplified by the accompanying change in slope, rather than moderated as is usual.

Table 3.1: Bankfull hydraulic geometry exponents for the lower Gwydir channels, with b = width exponent, f = depth exponent and m = velocity exponent. [] indicate R^2 values, with* indicating that the exponent is not significantly different from zero at the 95% confidence level.

Stream	b (width)	f (depth)	m (velocity)	Relative Exponent Value
Gwydir River	0.399 [0.724]	0.341 [0.844]	0.259 [0.688]	$b > f > m$
Mehi River	0.345 [0.798]	0.401 [0.943]	0.255 [0.786]	$f > b > m$
Moomin Creek	0.092 [0.104*]	0.498 [0.859]	0.410 [0.911]	$f > m > b$
Carole Creek	0.234 [0.179*]	0.344 [0.529]	0.423 [0.691]	$m > f > b$

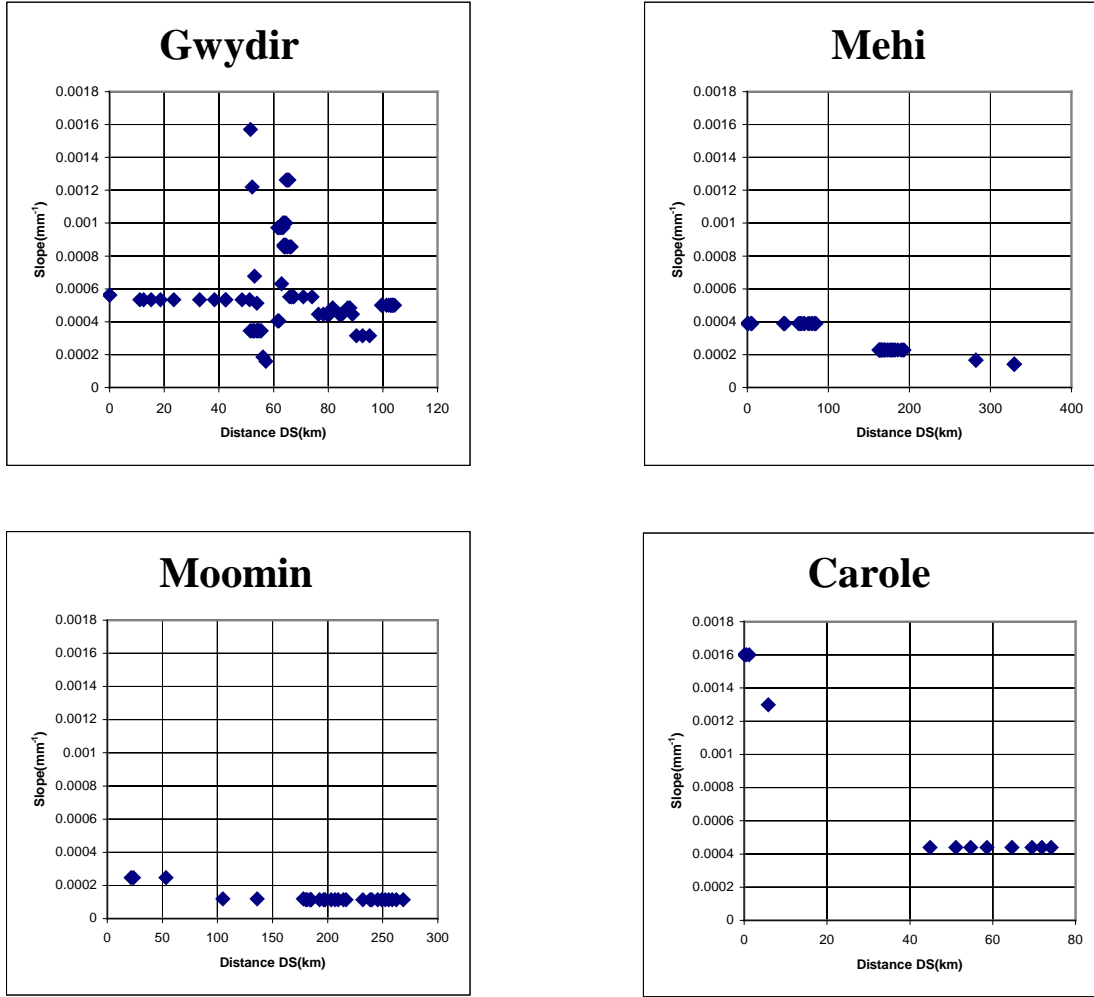


Figure 3.8: Slope vs. Distance Downstream: a) Gwydir River, b) Mehi River, c) Moomin Creek and d) Carole Creek. Distances are downstream of off-take, in the case of the Mehi, Moomin and Carole, and downstream of Pallamallawa in the case of the Gwydir River.

In most cases where downstream hydraulic geometry has been investigated, W/D ratios generally increase downstream as discharge increases. In three of the streams studied here, exponent f (for depth) is steeper than exponent b (for width), indicating that W/D ratios are also increasing downstream, but in this case with *decreasing* downstream discharge (Figures 3.4(c), 3.5(c) and 3.6(c)). In the absence of a downstream increase in discharge, this must be related to other variables that change in the downstream direction. In the context of a downstream increase in discharge, the limitation that bank strength places on achievable bank heights, and the constraints this places on flow depth, results in channels accommodating a greater proportion of their discharge

increase through increases in width rather than in depth (Church, 1992). However, the fact that W/D ratios increase downstream for streams here with declining downstream discharge indicates that the limitation on bank strength is not the sole reason for increasing W/D ratios. Downstream changing variables other than discharge that may affect W/D ratios include slope, sediment load, sediment calibre and flow resistance (channel roughness).

Slope differences have already been mentioned as significant for controlling the expression of the velocity exponent m . However it is also apparent that W/D ratio is inversely related to slope (Figure 3.9). The association between W/D ratio and slope was observed by Lane (1957) and Chang (1979) who found that steeper slopes result in wider channels. The general tendency for the Mehi, Moomin and Carole channels to increase in W/D ratio with *declining* slope is therefore apparently anomalous, as lower stream energies should allow higher stream-banks and therefore in the absence of other factors, narrower channels. The complex relationship between slope and the cross-sectional geometry of the Gwydir fan-plain channels is further emphasised by the fact that the Gwydir River does not increase in W/D ratio downstream, even though this might be expected given that it carries significant bedload. One possible avenue for explaining these unusual observations, in the Gwydir River at least, may be the changing significance of bedform roughness as the channel contracts downstream.

Chang (1979) drew attention to the indirect effect of W/D ratio on bedform roughness, whereby increases in width cause a reduction in specific stream power, allowing the form of roughness increasing bedform elements to change. This is obviously not relevant to the three streams here which do not transport significant bedload and don't show bedform development as a result of flooding. However, for the Gwydir River, which does transport significant bedload, this effect of W/D ratio on roughness may be important. Chang (1979) emphasized the discontinuity in channel roughness and flow velocity caused by the transition from upper to lower flow regime. All bankfull flows in the Gwydir River are subcritical, with Froude numbers of ~ 0.3 in the upper reaches falling to ~ 0.1 in the lower reaches. However, if the specific stream power of the Gwydir River is plotted onto the bedform existence fields of Simons and Richardson (1966), it can be seen that between the upper and lower reaches of the Gwydir River there is the potential for a major change in bedform configuration (Figure 3.10). In its

upper reaches the Gwydir River at bankfull transports sediment over a plane bed of limited roughness, whereas in its lower reaches, the transport of sediment as dunes contributes to channel roughness. Furthermore, as water is lost through distributaries and overbank flow, the in-channel coarse sediment concentration will increase. This extra roughness and sediment concentration downstream should have implications for the hydraulic geometry of the Gwydir River, as changes in bedform configuration will occur in concert with channel shape and slope (sinuosity) adjustment. As the slope of the Gwydir River can not be reduced through further straightening (it already has a sinuosity approaching 1), the principle adjustment will be in channel shape rather than sinuosity.

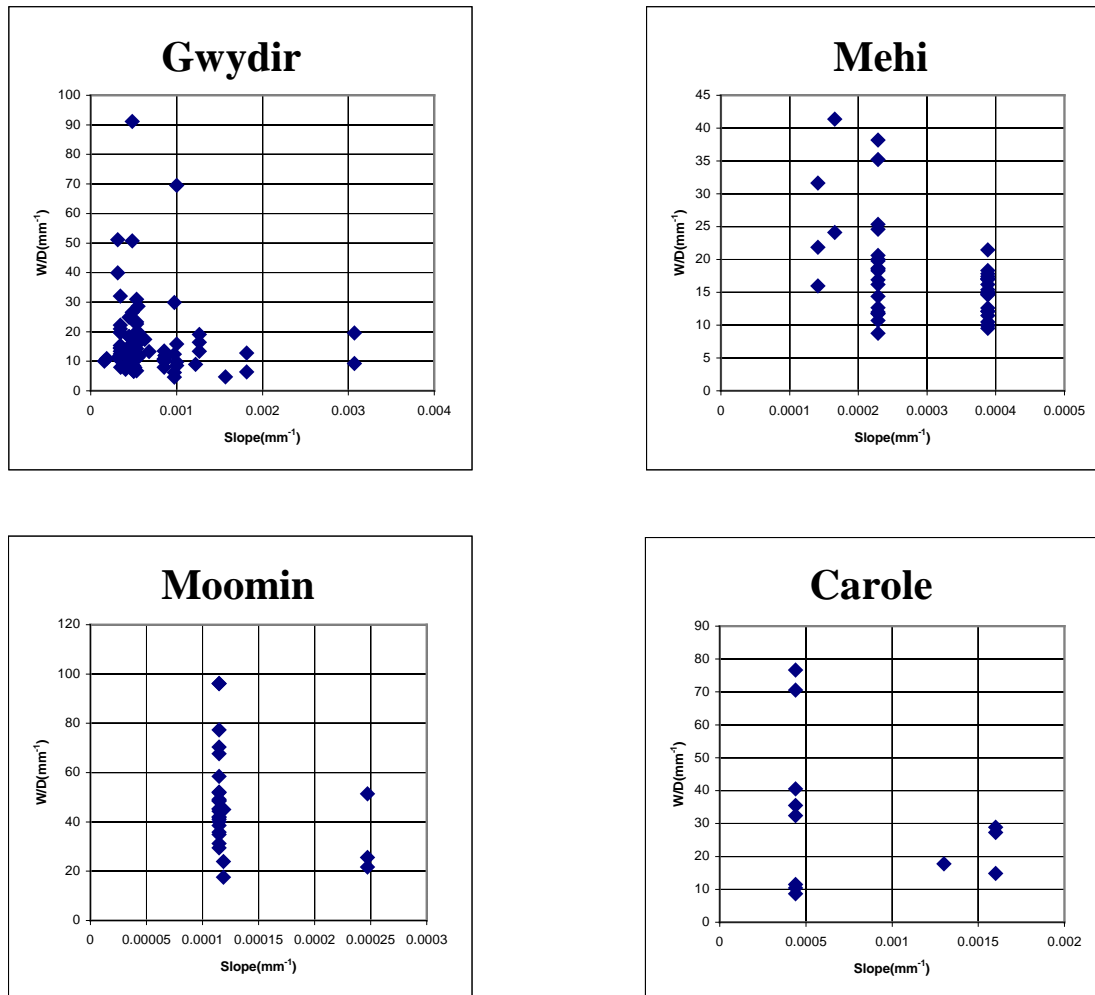


Figure 3.9: *W/D ratio vs. Slope: a) Gwydir River, b) Mehi River, c) Moomin Creek and Carole Creek. Distances are downstream of off-take, in the case of the Mehi, Moomin and Carole, and downstream of Pallamallawa in the case of the Gwydir River.*

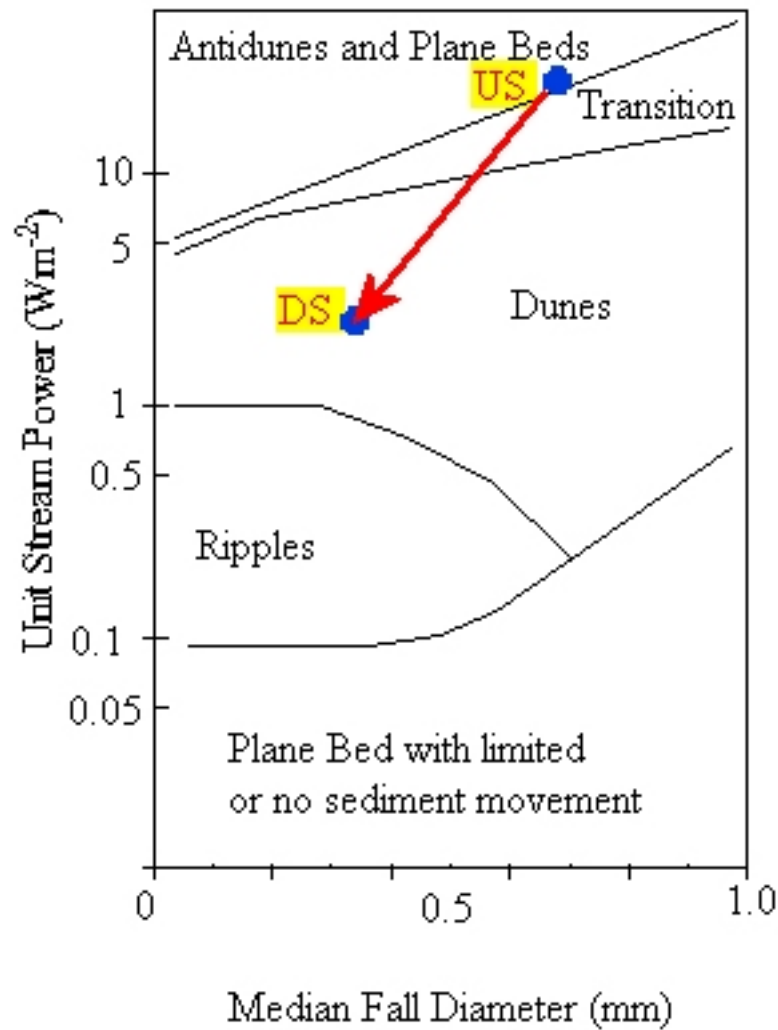


Figure 3.10: Bedform existence field of Simons and Richardson (1966) with the approximate locations of the upstream (US) and downstream (DS) reaches of the Gwydir River at bankfull flow plotted.

Huang and Nanson (2000) added to the attempts at understanding channel adjustment using extremal hypotheses, an approach pioneered in geomorphology by Langbein and Leopold (1962). Huang and Nanson (2000) argued that streams adjust to attain a condition of maximum flow efficiency, which they defined as maximum sediment transporting capacity per unit available stream power. Chang (1979) argues that there is an inverse association between bedform roughness and the amount of stream power required to transport each unit of bedload. Thus, in some instances, a deeper, narrower flow will allow larger bedforms, maximizing the bedload transport for the available

stream power (e.g. Jansen and Nanson, 2004). In such cases reductions in W/D ratio with a decline in discharge will tend to be enhanced where there is a shift in bedform configuration from plane beds (or at least washed out dunes) to dunes. This in part may explain why, of the streams studied here, the Gwydir River has the lowest depth coefficient, remembering that, in the context of a downstream decline in discharge, a low exponent implies the maintenance, and therefore relative increase, of that variable downstream. However, it is apparently unusual for a channel to attain maximum sediment transport through deepening, as most channel banks can not resist the high flow velocities which result (Ferguson, 1986).

An alternative explanation for the downstream decline in W/D ratio in the Gwydir River may be that in the downstream reach it develops an anabranching channel pattern (Figure 3.11, Figure 2.1). Anabranching is postulated to be a form of channel arrangement that may be either a transitional state, characteristic of active floodplains (e.g. Smith *et al.*, 1989; Schumm *et al.*, 1996; Makaske, 2001) or, alternatively, an equilibrium state reached through maximising some element of channel efficiency by adjusting the number of channels, rather than changing channel planform, geometry or bed configuration (Nanson and Knighton, 1996; Nanson and Huang, 1999; Jansen and Nanson, 2004). If the anabranching reach of the Gwydir River is in some form of equilibrium, and its largely unchanged form since being first surveyed suggests this, then its presence may be taken as reflective of, firstly, the need to increase efficiency beyond that which can be achieved through shifts in channel sinuosity, channel geometry or bed configuration, and, secondly, the presence of the sedimentary and vegetative conditions which make anabranching possible.

Nanson and Knighton (1996) identify erosion resistant banks as being necessary for the development of an anabranching channel pattern. It may be that the abundant bank vegetation of the Gwydir River (see Figure 2.13) is not just coincident with the anabranching form, but is in part responsible for it, as bank vegetation will in large part determine bank strength. While the effects of vegetation are thought to be significant for all channels in this study, not just the Gwydir; this point is considered in detail after an investigation into downstream bank sedimentology.

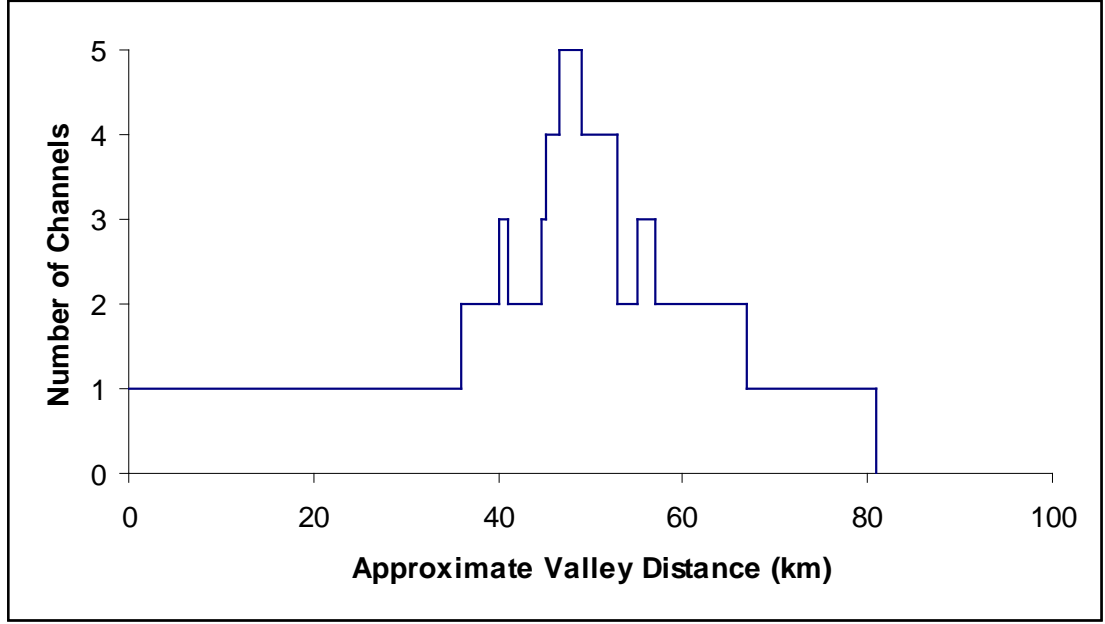


Figure 3.11: Plot of number of channels of the Gwydir River against approximate ‘valley’ distance from Pallamallawa. Note that the Gingham Channel breakout is from ~ 38 km to ~ 50 km, with this reach being the likely site of most dramatic increase in bedload sediment to water ratio.

Along with vegetation, bank sediment type also plays an important role in determining bank strength, and therefore in influencing channel shape and channel pattern. Indeed, parameter variability within Equations 3.1, 3.2 and 3.3 has almost always been attributed to variations in channel boundary composition (Schumm, 1960; Richards, 1977; Ferguson, 1986; Rhoads, 1991). For this reason the sedimentology of the lower Gwydir is investigated. Figure 3.2 shows the location of sediment sampling sites for particle size analysis (PSA), with Table 3.2 listing the results in terms of raw measurements and Schumm’s (1960) weighted silt index M :

$$M = \frac{(Bed_{Silt+Clay} \% \times W) + (Bank_{Silt+Clay} \% \times 2D)}{W + 2D} \quad (3.9)$$

Figure 3.12 illustrates the downstream development of sediment character for the Gwydir fan-plain channels. The almost uniform nature of the sedimentological characteristics of the Mehi River, Carole Creek and Moomin Creek is apparent. This contrasts dramatically with those of the Gwydir River, the only stream to carry

Table 3.2: Results of particle size analysis for 25 sites in the Gwydir distributary system. Note that at Sites 1, 2, 3 and 4, the channel bed consisted of a gravel bar, therefore an estimated maximum silt + clay % has been assigned. The value (3 %) is likely to be an over-estimate. However, the effect of this estimate on the calculated *M* value is of the order of 0.03 units.

Site No.	Distance Downstream (km)	Channel	% Silt + Clay in Bed	% Silt + Clay in Bank	Schumm's M
1	0	Gwydir	3%	82%	0.19
2	25	Gwydir	3%	68%	0.12
3	47	Gwydir	3%	93%	0.14
4	56	Gwydir	3%	53%	0.09
5	93	Gwydir	85%	87%	0.85
6	46	Mehi	81%	93%	0.82
7	90	Mehi	73%	96%	0.76
8	125	Mehi	92%	97%	0.93
9	144	Mehi	95%	96%	0.95
10	166	Mehi	90%	91%	0.90
11	180	Mehi	89%	93%	0.89
12	197	Mehi	90%	97%	0.90
13	227	Mehi	75%	91%	0.77
14	250	Mehi	80%	96%	0.81
15	282	Mehi	85%	93%	0.86
16	306	Mehi	88%	93%	0.88
17	330	Mehi	61%	89%	0.63
18	10	Moomin	85%	87%	0.86
19	54	Moomin	93%	95%	0.93
20	105	Moomin	95%	96%	0.95
21	162	Moomin	96%	95%	0.96
22	269	Moomin	90%	86%	0.90
23	310	Moomin	72%	85%	0.73
24	15	Carole	86%	94%	0.88
25	60	Carole	89%	92%	0.89

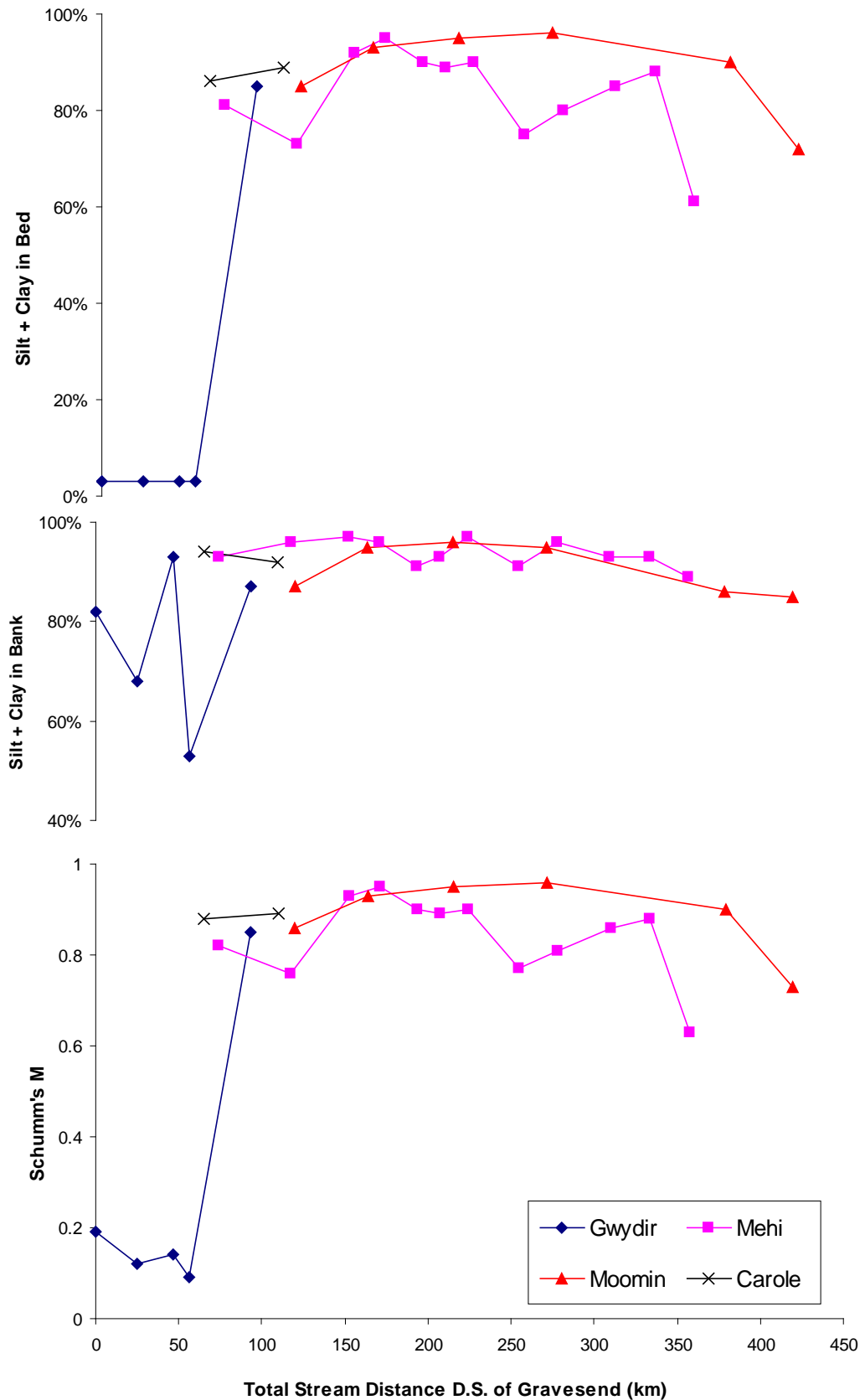


Figure 3.12: Downstream development in channel boundary sediments. For distributary channels, distance downstream includes the length of the trunk stream(s) upstream of the off-take.

significant bedload. The lack of bedload in the distributaries is almost certainly due to the nature of the off-takes (Figures 3.13 A and B). The Gwydir River, being the trunk stream, carries almost all the bedload, whereas the Mehi River and Carole Creek, being high-bank distributaries of the Gwydir, carry very little. Moomin Creek, being a high-bank distributary of the Mehi, and therefore a ‘second order’ distributary, carries almost no bedload. Even the post-European enlargement of the off-takes for irrigation water distribution does not appear to have affected the hierarchy of bedload transport.

While there is a stark difference between the bedload of the Gwydir River and the other three study streams, the variation in bank composition between all four channels is too slight to be significant (Table 3.2). Bank composition can therefore be discounted as contributing to differences in their hydraulic geometry relationships. Likewise, for three of the streams, bedload differences are minimal.

It has previously been observed (e.g. Leopold and Maddock, 1953; Schumm, 1960; Church, 1992) that for streams that carry virtually no bedload, a low W/D ratio is the most likely. Consequently, the very high W/D ratios displayed for the downstream reaches of the suspended-load Mehi River, Moomin Creek and Carole Creek appear to be anomalous. Schumm (1960) argued that channel form could be related to boundary sedimentology via:

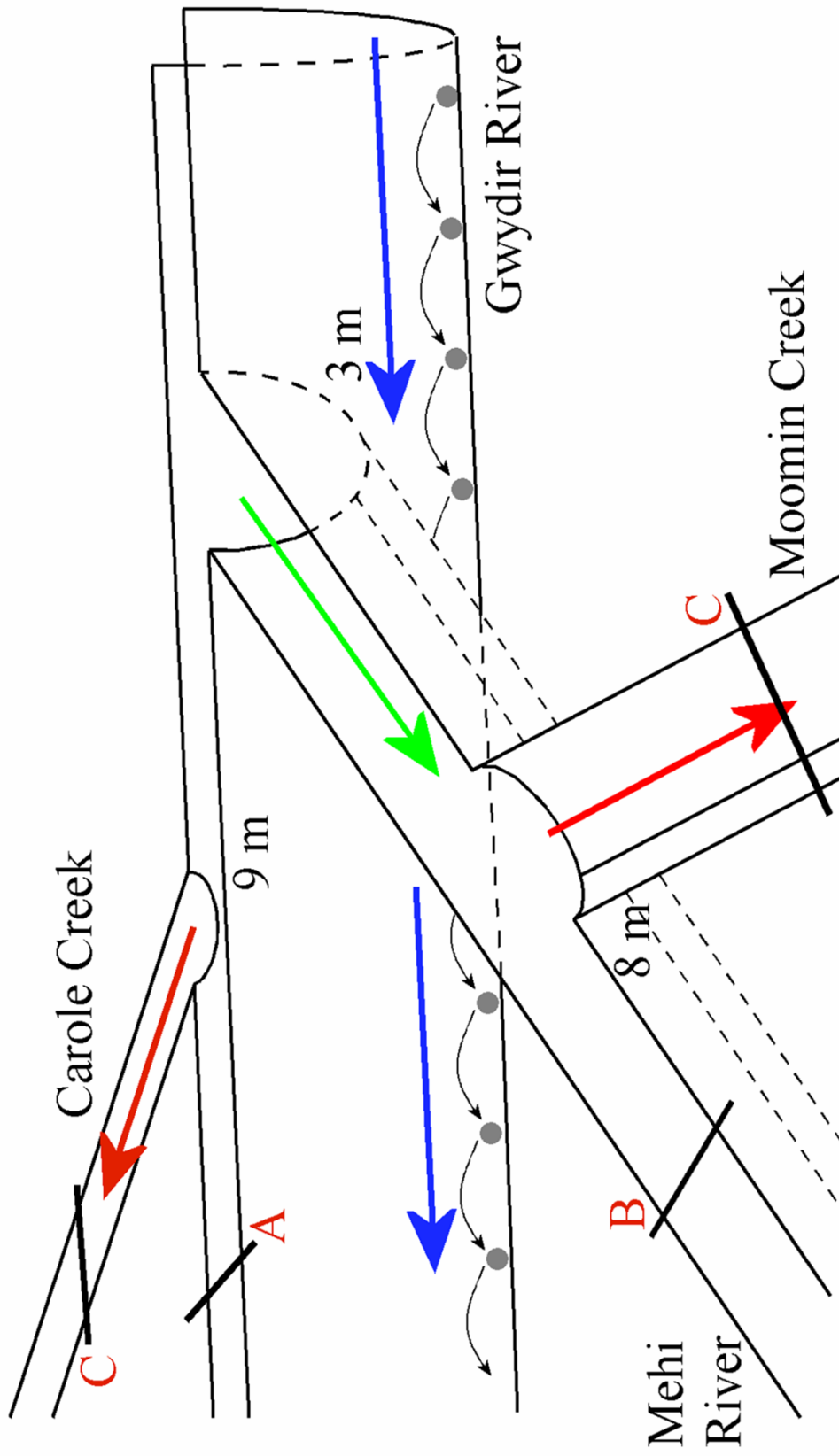
$$\frac{W}{D} = 255M^{-1.08} \quad (3.10)$$

The only place in Australia where this relationship has subsequently been tested is, by coincidence, in the study area, with Riley (1975b) finding that for streams of the Namoi and Gwydir systems, the relationship does not hold (Figure 3.14). This may not have been a suitable location to test Schumms’ relationship though, for some other process which controls channel form irrespective of boundary sedimentology must be operating here. Note that the data presented in Figure 3.14 is that collected for this project; however, this figure is almost identical to that found in Riley (1975b), suggesting that the channel alteration works of the late 1970s have not altered the sedimentology of the study streams.

An increasing W/D ratio downstream with declining discharge implies a greater relative reduction in depth than width. The problem arises, then, in identifying mechanisms that, with progressively smaller flows, can cause a downstream reduction in depth while allowing the relative (and in the case of the Moomin, absolute) maintenance of width. In the context of the streams under present study, explanations for downstream increases in W/D are to be found in the factors that are free to change downstream, and that also affect bank and bed accretion or their resistance to erosion. Two mechanisms can be envisaged which, by changing independently of bank-full discharge, operate nonetheless to reduce bank accretion downstream, thereby enabling channel width to be maintained while channel depth decreases. These mechanisms are related to the interconnected effects of stream hydrology and in-channel vegetation.

3.1.4 The Hydrology / Vegetation / Bank-Strength Hypothesis

The nature of a channel's off-take controls not only the amount of available bedload but also the frequency and duration of in-channel flows. The Mehi River is a tributary of the Gwydir River and, therefore, will usually not flow until the Gwydir River is full to at least the height of the off-take (~ 3 m above the bed). Furthermore, because of the bed-height differential, the transfer of bedload from the Gwydir to the Mehi will be minimal. The off-take for Carole Creek is further downstream from the Mehi River and considerably higher up the bank (~ 9 m above the bed) than the Mehi River off-take. Carole Creek will therefore flow with lesser frequency than the Mehi, and will not take any sediment from the bed of the Gwydir. In terms of flow frequency and bedload discharge, the three streams in declining order are the Gwydir, Mehi and Carole. Moomin Creek off-takes (at ~ 8 m above the bed) from the Mehi River, and therefore must also flow less frequently and with less bedload than the Mehi. However, its frequency and bedload discharge relative to Carole Creek is uncertain. Given the height of the Carole Creek off-take it is unlikely that Carole Creek would run without the Gwydir River being sufficiently high to fill the Mehi to a height such that water will flow into the Moomin Creek. It is probable that these differences in flow characteristics and sediment load have a profound effect on the development of in-channel vegetation and therefore on the shape of the channel.



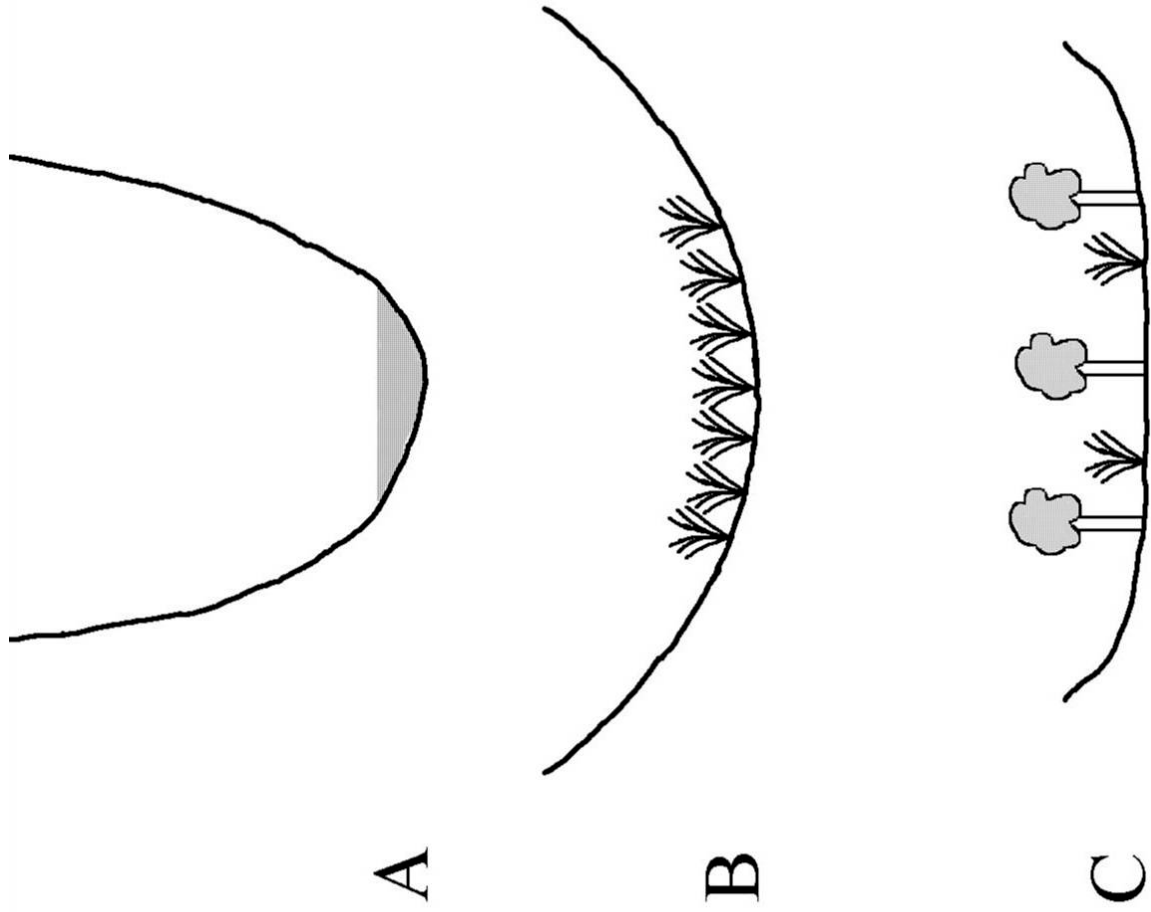


Figure 3.13: Schematic representation of the architectural arrangement of channel off-takes of the Gwydir distributary system, as well as the suggested associated channel forms and vegetation communities. Values beside each off-take are heights of off-takes above bed of trunk channel. Note the possibility of bedload transport in the Gwydir at flows below the level necessary to allow distributary flow. Where stream flow is more-or-less continuous, deep, narrow channels can occur such as that at cross section A. No vegetation can become established in the channel. For channels which, due to their intermediate level offtakes receive periodic flushes (cross-section B), early-succession vegetation communities can become established, with channels widening due to flow being displaced towards the banks. Where channels rarely carry water due to their high level offtakes, (cross-section C), permanent vegetation communities become established preventing erosion of the channel bed and encouraging channel widening.

Channels that are rarely dry (i.e. the Gwydir River) have well-vegetated banks and un-vegetated beds. Channels which are dry for short periods only, such as the Mehi River, will likewise have well-vegetated banks. They will differ from rarely dry channels though, in that their beds will be colonised by reeds, grasses and small bushes, which are periodically removed by floods. Channels such as Carole and Moomin Creeks which are dry for extended periods may also have well-vegetated banks, but are also characterised by more advanced ecological succession on their beds, such that robust under-storey plants, small trees (wattles and the like) and even permanent large trees become established. When waters return to these vegetated channels, flow is diverted around the well established bed vegetation increasing the stream energy expended on the banks. This maintains relatively wide channels with small discharges.

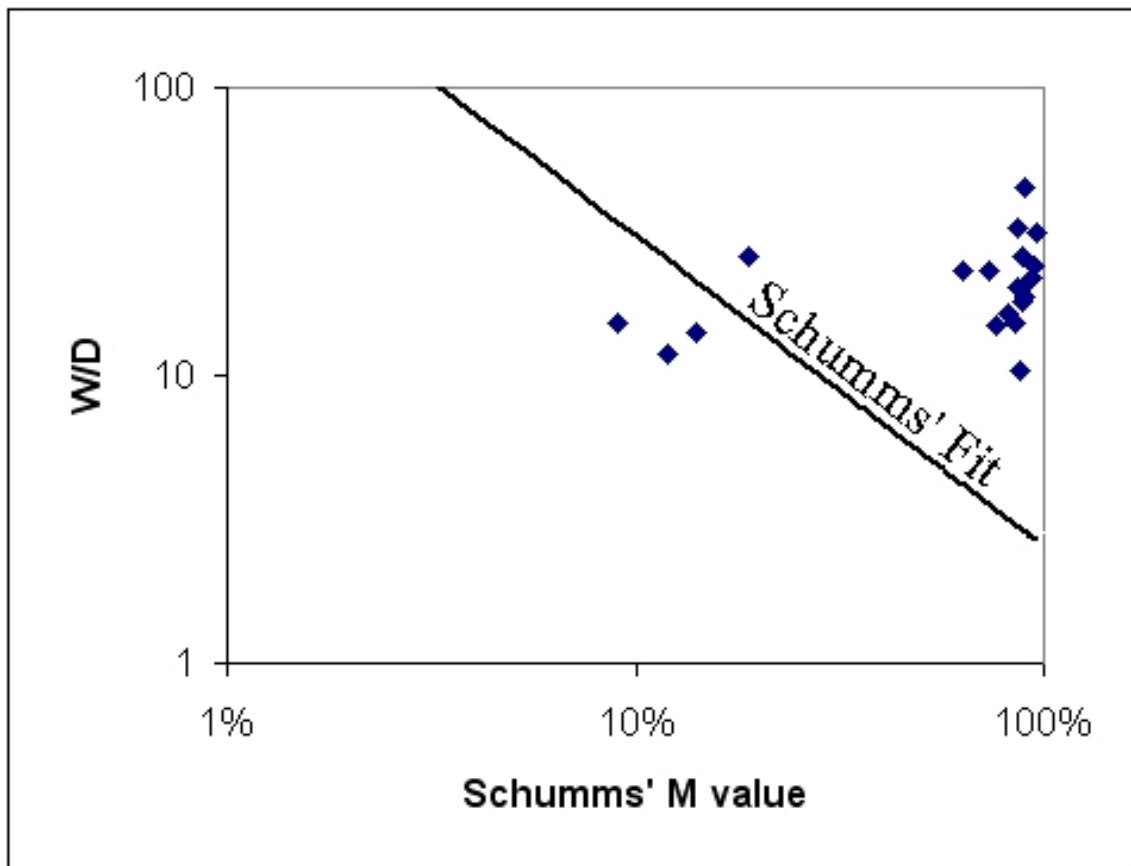


Figure 3.14: The relationship between Schumms' *M* value and *W/D* ratio for channels of the Gwydir Distributary System. The trace is the $W/D = 255M^{-1.08}$ ratio that Schumm determined.

The in-channel vegetation, at least temporarily, acts to reduce bed scour and encourage deposition, albeit that those rivers other than the Gwydir transport very little bedload. The high silt and clay contents of the channel beds (Table 3.2) reflect the deposition of mostly suspended load within the vegetation. Channel banks, on the other hand, are adjusted through downstream narrowing of the channel, probably by a process of oblique accretion of suspended load (Page *et al.*, 2003). Such narrowing however, is limited by the deflection of flow into the banks from in-channel vegetation. The banks therefore become exposed to a greater proportion of the total shear stress than the W/D ratio would suggest.

The presence of in-channel vegetation in controlling the form of ephemeral streams has rarely been recognized, with the greater width of some ephemeral channels due to a *lack* of vegetation having been remarked upon (Wolman and Gerson, 1978). Park (1977) observes that ephemeral streams generally have low width exponents and high velocity exponents, though this in part seems related to how ‘flashy’ these streams are (Leopold and Miller, 1956) rather than to their ephemeral nature *per se*. On the basis of a restricted dataset Wharton (1995) argues that ephemeral streams will become wider as flows become rarer, presumably because generally dryer conditions inhibit the growth of bank vegetation. Indeed, dryland channel *narrowing* in the presence of channel vegetation has been observed (Hadley, 1961; Graf, 1978; Blackburn *et al.*, 1982); it is interesting to note however, that these studies have all been on sand bed streams, where the effect of vegetation appears to add coherency to otherwise incoherent sand banks and bars. This may have relevance to the streams of the Gwydir fan-plain, where the sand transporting trunk stream (the Gwydir) is relatively narrow compared to the suspended-load distributaries (Mehi, Moomin and Carole).

Recent studies of Tooth and Nanson (2000a; 2004) have identified the importance of bank vegetation in increasing bank strength of dryland rivers. Furthermore, Wende and Nanson (1998), Tooth and Nanson (1999, 2000b) and Jansen and Nanson (2004) have discussed the impact of in-channel vegetation on channel shape and flow efficiency, suggesting that it is a major contributor to the development of anabranching in some dryland and seasonal monsoon rivers. Occasional channel inundation provides an irrigation effect, allowing verdant growth in an otherwise dry environment. Although the distributary channels of the Gwydir fan-plain are not in an arid environment, their

natural hydrology resembles that of arid environment rivers, due to the arrangement of off-takes discussed above. Hence it is likely that in-channel vegetation is encouraged by occasional flows interspersed with long periods of no flow during which vegetation can reach a size and strength sufficient to survive subsequent flows.

3.1.5 Supporting Evidence

Present day inspection of the four channels reveals little difference in vegetation communities on channel beds. However, this is simply a function of both the extensive channel clearing works undertaken in the late 1970's and the current management of channel flows which are entirely regulated. Investigations of other streambeds in the study area that have been unused for 1-2 years demonstrate the tendency for dry channels to be quickly colonised. Discussions with the vegetation officer at Moree DIPNR who is responsible for approving channel clearing works, and the accumulation of recently removed vegetation beside irrigation channels in the district, also attest to the rapid growth and thickness of in-channel vegetation in some locations. Indications of the effects of prolonged inundation are available in the form of large stands of dead trees along the Gingham Watercourse, the death of which local landholders attribute to unusually prolonged flow events manipulated to facilitate the construction of Copeton Dam and its associated diversion works in the early 1970's.

Direct evidence for the prior vegetation status of the channels of the Gwydir distributary system is rare. As outlined in Chapter Two, alterations to channel forms began soon after European settlement, hence photographic records are largely absent. However, plans of the Moomin Creek dated 1901 (e.g. Plan 36_40) show Coolabah trees on the bed. This suggests that Moomin Creek stayed dry sufficiently long to allow tree establishment. Furthermore, where channels have been prepared for irrigation, engineers' plans (e.g. 36/2952) state that they must be cleared of 'snags and other vegetal matter'. Even though channel alterations are known to have been occurring since the beginning of the 20th century, the available air-photo record shows that the greatest channel alterations occurred between 1974 and 1979, with air-photos dating to 1974 or earlier showing long reaches of channel with relatively intact vegetation communities, along with shorter reaches where major channel alteration is obvious.

A complete pre-1975 air-photo record was unable to be obtained for this study, excluding the possibility of a quantitative analysis of tree densities. However, from the record that is available some simple observations can be made of the type discussed above, comparing visually the vegetation communities evident in channels at different locations within the distributary stream network. Immediately obvious in Figure 3.15 is the absence of vegetation in both the upper and lower reaches of the Gwydir, compared to the relative density of vegetation in the other channels. The upper reach of the Mehi River, shown here at bankfull, has a low density of trees, while in its lower reaches, shown here at no-flow, the density of trees is high. Likewise, for the downstream reach of Carole Creek shown, again at no flow, the density of in stream vegetation is very high. The Moomin, also shown at no-flow, shows a considerable density of in-channel trees.

Perhaps the clearest examples of ecological response to periods of no flow are found where sections of channel have been isolated from the main flow (Figure 3.16). Some time prior to 1974 when the air photograph shown in Figure 3.16 was taken, the entire flow of the Moomin Creek was dammed and redirected south. The reach of channel below the dam is clearly vegetated, while the area upstream of the dam contains the stumps of trees that have died due, it is assumed, to prolonged inundation.

In addition to photographic evidence it is possible to find anecdotal evidence of the former state of instream vegetation. In 2001 the NSW Department of Fisheries commissioned '*Fish Everywhere – an oral history of fish and their habitats in the Gwydir River*' (Copeland *et al*, 2003) in which interviews with land holders and fishing club members have been distilled into an evocative account of the former state of the river, as well as the changes they have observed. The authors note:

'In the eastern end of the study area, those interviewed spoke of a great loss of instream vegetation. In the western end of the valley, residents reported a massive loss of wetland vegetation...there were many references to stock eating large amounts of vegetation, and of the current regime of high water flows preventing it growing' (Copeland *et al*. 2003, p.45).

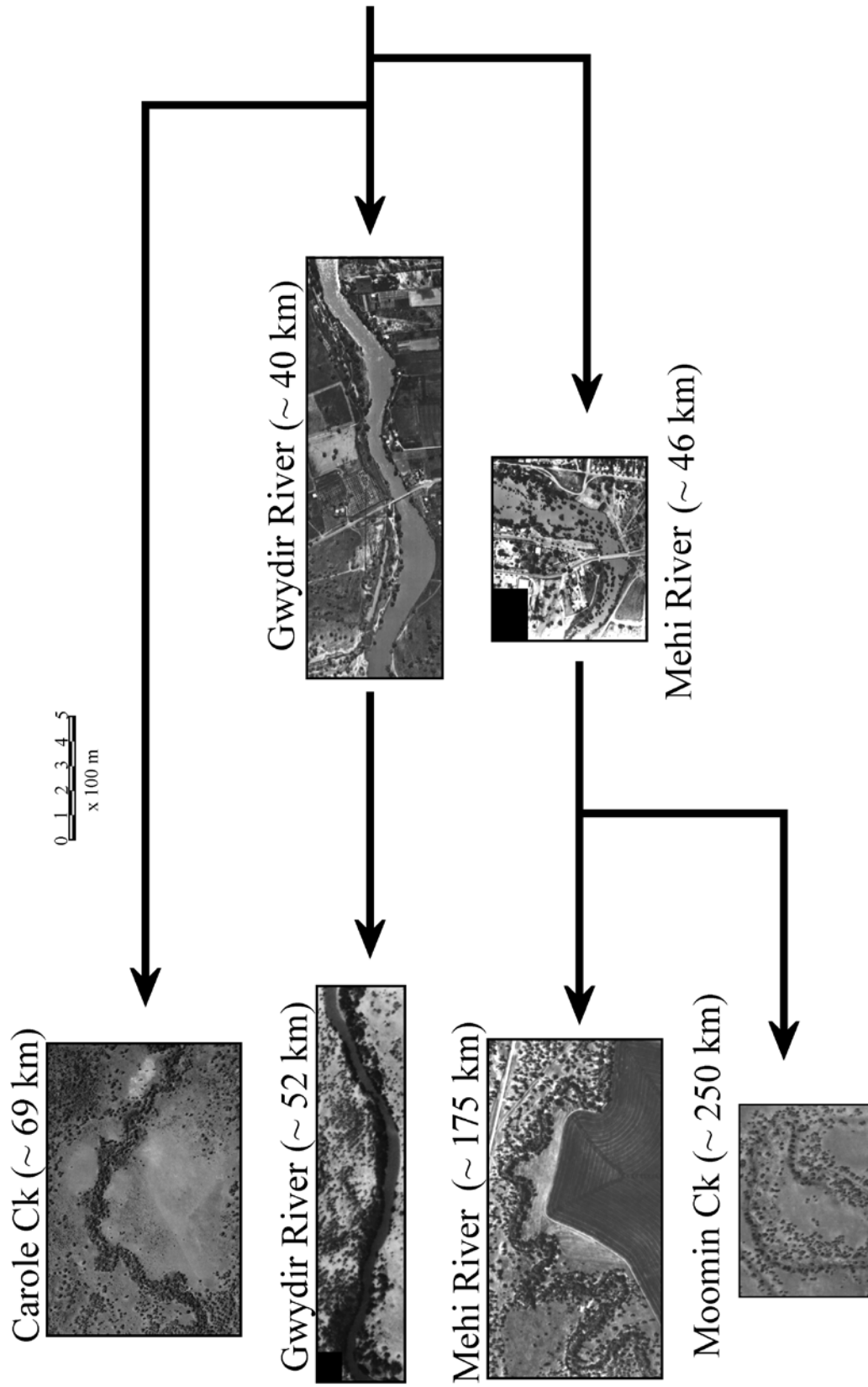


Figure 3.15: Air photo extracts of the Gwydir distributary system, showing increase in density of in-channel vegetation in the downstream reaches of the effluent channels in contrast to the maintenance of a vegetation free channel in the Gwydir River. All air photos taken prior to 1974, when major channel clearing works were undertaken.

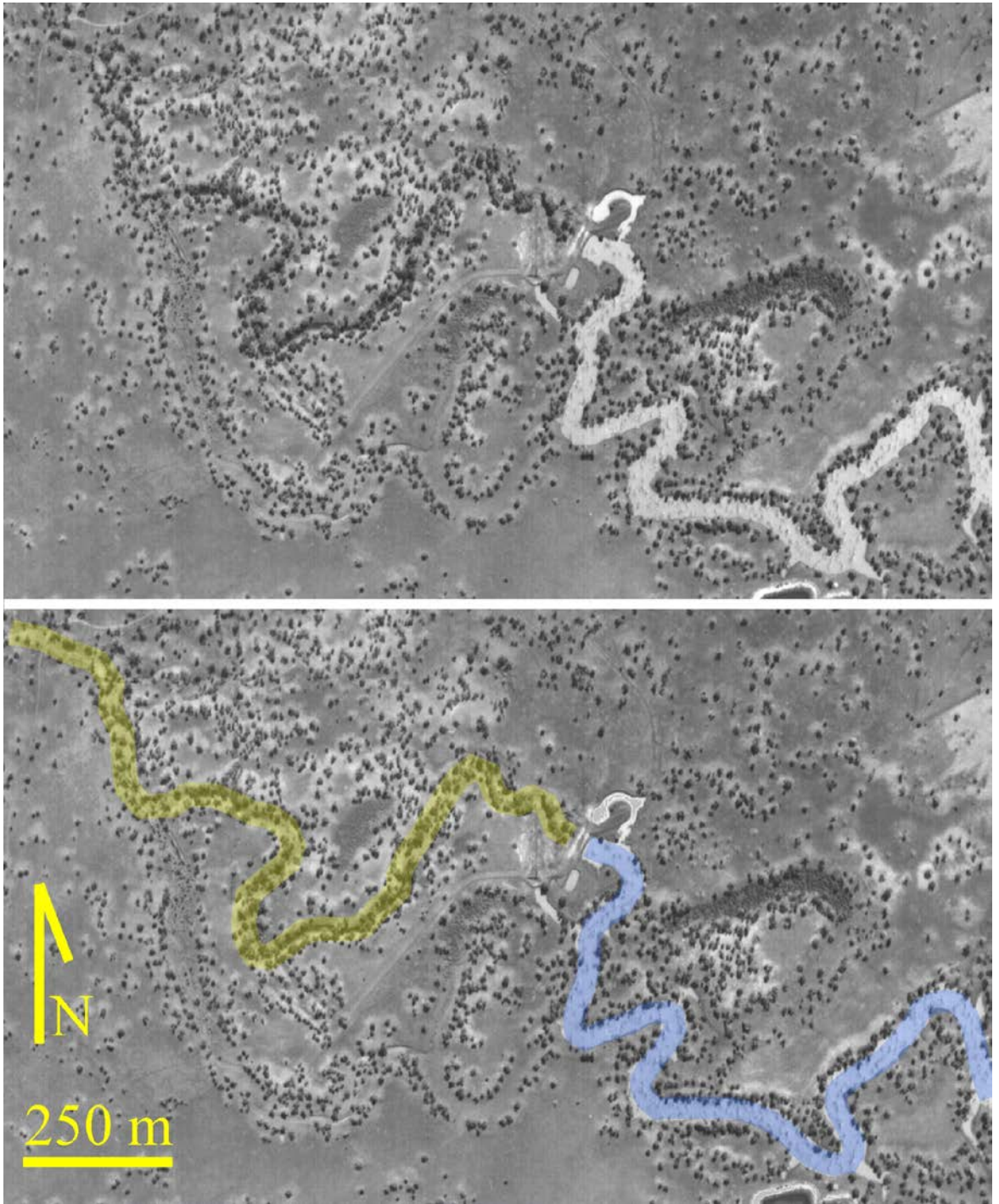


Figure 3.16: Air photograph (1974) of section of the Moomin Creek showing effects of flow disruption. At the approximate centre of the photograph a dam completely isolates the lower section of the channel, allowing revegetation of the stream-bed to occur. Upstream of the dam, the grey speckling of the water surface indicates the presence of standing dead trees, the result of prolonged inundation.

Quotes from some of the interviewees are reproduced below:

'On this section of the Mehi there's not too many trees left because of the 'stream improvements' undertaken by the Water Commission...Red river gum once gathered along the whole river. Most of them were taken out...' (p.44)

'There are fewer plants in the bottom of the river, for sure.' (p.46)

'There seems to be something about the rivers here [Moree]; there's absolutely no growth at all on them [at present]. Its only just dust, you know...' (p.44)

'This area...used to be the main watercourse back in the fifties, sixties, seventies, and round here there'd be sags [a locally used term for Bolboschoenus and Typha], oh, they'd be a couple of feet over your head when you were sitting on a horse...' (p.46)

Clearly, long time residents of the study area remember a river system very different from that found today, with the former presence of in-stream and wetland vegetation contrasted with its absence today.

3.1.6 Summary of Bivariate Hydraulic Geometry

Description of the bivariate hydraulic geometry of the Gwydir fan-plain channels has revealed some interesting differences between these channels and most channels previously studied, as well as differences between the channels themselves. In terms of their *b-f-m* coordinates, all four channels sit outside the region which contains the majority of previously studied channels (Figure 3.7). As a group the channels of the Gwydir fan-plain tend to have highly responsive velocities, while depth and especially width are relatively insensitive to changes in discharge. A downstream declining discharge and, therefore, a positive relationship between slope and discharge, is the main cause of these differences. The relative insensitivity of the width of Gwydir

fan-plain channels to discharge change is also distinctive. The Gwydir River is distinctly different from the other three channels, having a W/D ratio which does not increase downstream. Given that the Gwydir is the only stream which carries significant bedload it could be expected to be the widest. However, the adoption of an anabranching pattern could in part explain its apparently anomalously low width, as anabranching could provide an alternative means of maximising bedload transport (Jansen and Nanson, 2004). It is noted that Figure 3.11 shows a peak in number of channels in just the reach where coarse sediment would become more concentrated due to the loss of water via the Gingham Watercourse breakout. The three distributary channels (Mehi, Moomin and Carole) have obvious within-channel vegetation (Figure 3.15). This appears to increase in density downstream where, perhaps not coincidentally, W/D ratios are at their highest. Where channel water levels have been artificially managed, such that parts of the channel can be almost permanently dry or almost permanently full (Figure 3.16), distinct vegetation communities become established, allowing inferences to be made regarding the likely relationships between off-take height, hydrology, vegetation and channel cross-sectional geometry.

Hydraulic geometry is based on the prescription of a causal relationship between changes in discharge and channel width, depth and velocity. From the preceding results, it would appear that these relationships between discharge and channel variables can exist in proportions outside the ranges previously reported, if, as in the case of the Gwydir fan-plain channels, slope is positively rather than negatively correlated with discharge. Furthermore, it appears that consideration should be given, not only to the magnitude of bankfull discharge, but also to its frequency, as the timing of channel inundation will in large part determine the nature of in-channel vegetation that in turn will affect channel geometry.

3.2 Multivariate Hydraulic Geometry

3.2.1 Introduction

Discussion so far has been predicated on the hypothesis that discharge is overwhelmingly the most important independent variable controlling channel width, depth and flow velocity. However, hydraulic geometry is in reality a multivariate problem, with several researchers having attempted to quantify those variables other than discharge which influence channel width, depth and velocity (Osterkamp, 1979; Richards, 1977; Huang and Warner, 1995). When all sites in the study area, regardless of their location, are examined (Figure 3.17), the influence of factors other than discharge can be seen to be causing considerable scatter. Mean depth appears to be the factor most consistently related to discharge, suggesting that factors other than discharge have less influence on depth than they do on width and velocity.

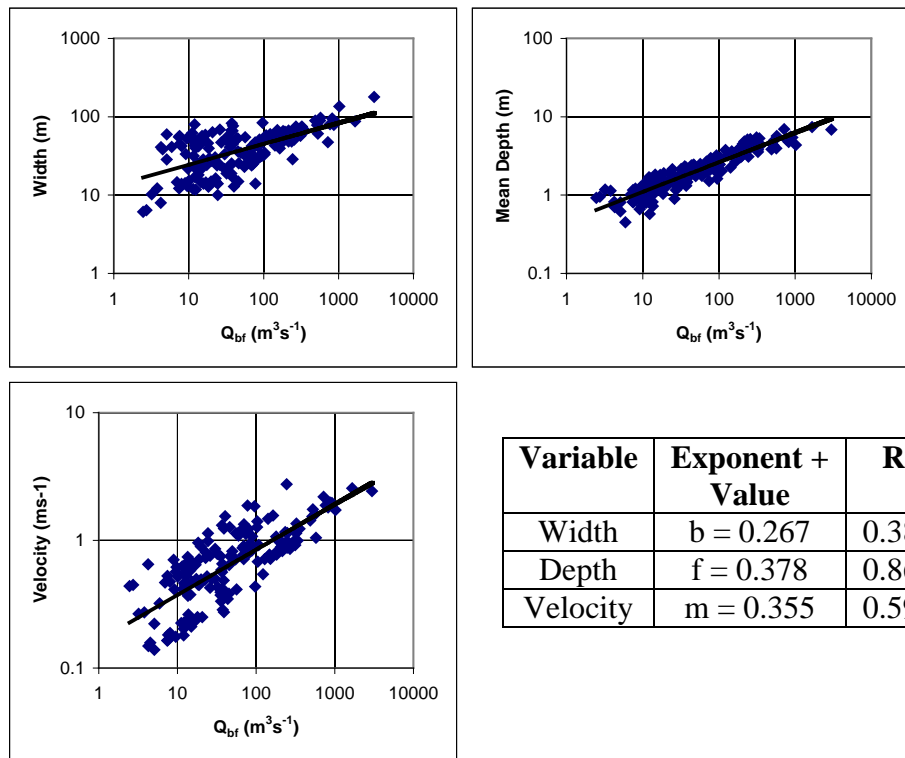


Figure 3.17 : Bankfull hydraulic geometry relationships for all sites. Table shows calculated exponent values and relevant correlation coefficients.

3.2.2 The Huang and Co-Workers Model of Multivariate Hydraulic Geometry

Huang and Warner (1995) and Huang and Nanson (1997, 1998) demonstrate that hydraulic geometry is best understood with reference to discharge, slope, channel

roughness and bank strength. While the first three variables can be readily measured or mathematically modelled, measuring bank strength has proved particularly difficult given the many complicating factors that affect bank strength. Huang and Warner (1995) and later Huang and Nanson (1998) adapted shear distribution models developed from the flume studies of Knight (1981); Knight *et al.*, (1984) and Knight and Patel (1985) (Figure 3.16), combined with a large data set of field observations, to develop a multivariate model of channel geometry incorporating the influence of bank strength. The model is of the form:

$$W = C_W \times Q^{0.5} \times n^{0.355} \times S^{-0.156} \quad (3.10)$$

$$D = C_D \times Q^{0.3} \times n^{0.383} \times S^{-0.206} \quad (3.11)$$

$$A = C_A \times Q^{0.8} \times n^{0.738} \times S^{-0.362} \quad (3.12)$$

where W , D , n and S are as above with A = channel cross-sectional area. In a study across a wide range of natural channels, Huang and Warner (1995) found the coefficients C_W , C_D and C_A to vary according to the critical shear stress for the incipient motion of bank materials. They also found the coefficients C_W , C_D and C_A to be theoretically interrelated thus:

$$C_D = C_W^{-0.6} \quad (3.13)$$

and

$$C_A = C_W^{0.4} \quad (3.14)$$

Note that given:

$$A = \frac{Q}{V} \quad (3.15)$$

it follows from Equation 3.12 that:

$$V = \frac{1}{C_A \times Q^{-0.2} \times n^{0.738} \times S^{-0.362}} \quad (3.16)$$

For the purposes of this study, the phrase ‘critical shear stress for incipient motion of bank materials’ is regarded as equivalent in practice to the term ‘bank strength’. Therefore C_W , C_D and C_A integrate the effects of both vegetation and sediment type, combining the attempts of Hey and Thorne (1986) and others to relate hydraulic

geometry to bank vegetation with the attempts of Schumm (1960) and others to relate hydraulic geometry to bank sediment size.

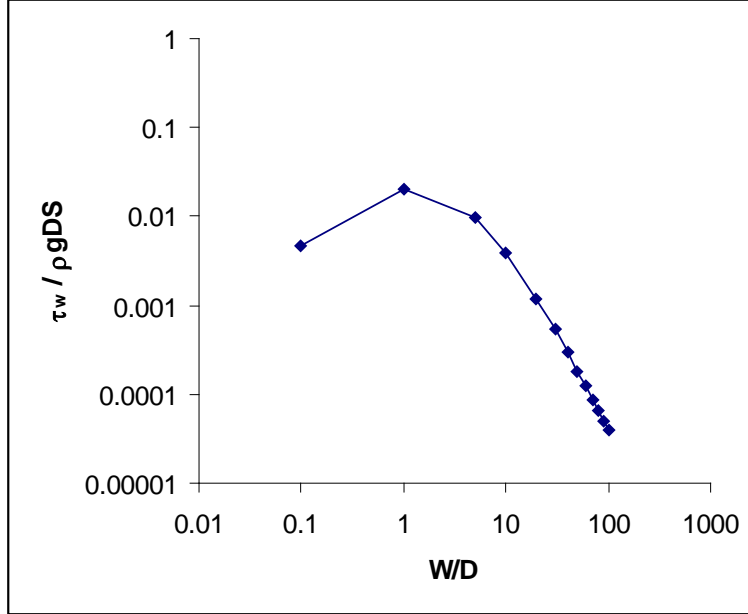


Figure 3.18: The relationship between W/D ratio and the ratio of shear stress acting on the walls (τ_w) to channel two-dimensional shear stress ($\rho g D S$) (after Huang and Warner, 1995).

It may be noted that the Huang and co-workers model involves the use of invariant exponents, and furthermore, that the absolute value of their invariant discharge exponents for width, depth and velocity (i.e. 0.5, 0.3, -0.2) are similar to the modal values for the wide range of global data presented in Figure 3.1. Using invariant power functions in place of, for example, Equation 3.1, divests significance from the exponent and instead focuses on the effects on the coefficient of additional in(ter)dependent variables (Figure 3.19). The coefficient can be considered an axis of variation, orthogonal to the gradient represented by the chosen exponent. Shifts along this axis have been found to correspond with changes in some of the covariables mentioned in Sections 3.1, 3.2 and 3.3 above. Ostercamp (1979), for example, shows shifts in the coefficient of the invariant power function:

$$Q = aW^2 \quad (3.17)$$

to be positively correlated with silt/clay content. Similarly, Hey and Thorne (1986) relate changes in vegetation to variations in the coefficient of a fixed exponent power function. The approach of Huang and Nanson (1997, 1998) is a more sophisticated example of this method. They incorporate both the effects of vegetation and silt-clay content, which they argue affect geometric influence through altering bank strength, as well as slope and roughness.

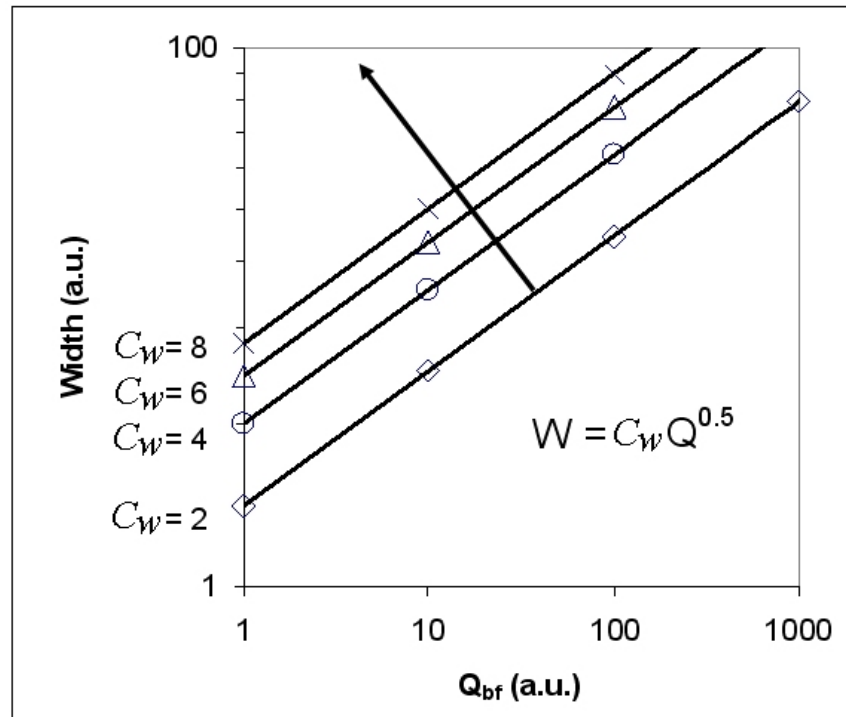


Figure 3.19: Representation of the use of an invariant power function in place of Equation 3.1. The different symbologies represent stream groupings based on some third in(ter)dependent variable affecting width (e.g. boundary cohesion or silt-clay content). The parallel lines all conform to $W = C_w Q^{0.5}$, while the solid arrow describes the directional shift caused by variations in the third variable.

3.2.3 Multivariate Hydraulic Geometry of the Gwydir, Mehi, Carole & Moomin

The hypothesis outlined in Section 3.1.4 above, relating hydrological differences to vegetation (and the minor effect of enhanced boundary fracturing), can be tested using the multivariate model of Huang and Nanson. If, as suspected, the downstream widening of the channels is due to an increasing proportion of the available energy being expended on the banks, then this should be reflected in a downstream increase in

C_W . Although the banks may not change compositionally (see Table 3.2 / Figure 3.12), they will *appear* to change in their strength because of changes in the stream energy expended on the channel boundary. If, as suggested, vegetation acts to protect the bed, the proportional distribution of energy between bed and banks will be altered, resulting in the banks appearing to be weaker. This effect will be in proportion to the opportunity for vegetation to be established on the bed. Hence, due to their different vegetation communities caused by variations in flow periodicity, not only will each of the four study streams have different apparent bank-strength characteristics, but there should also be a gradient of apparent bank-strength downstream. This will occur because the downstream decline in flow frequency inherent in the system will lead to an increased likelihood of vegetation establishing within the downstream reaches of each channel, causing the channels to widen.

Calculation of C_W values for the lower Gwydir channels is achieved through representation of Equation 3.10 as:

$$W = C_W \times W' \quad (3.18)$$

where

$$W' = \frac{Q^{0.5} \times n^{0.355}}{S^{0.156}} \quad (3.19)$$

and regressing W against W' to determine C_W (Figure 3.20; Table 3.3). Values for C_D and C_A are similarly calculated:

$$D = C_D \times D' \quad (3.20)$$

$$A = C_A \times A' \quad (3.21)$$

using:

$$D' = \frac{Q^{0.3} \times n^{0.383}}{S^{0.206}} \quad (3.22)$$

$$A' = \frac{Q^{0.8} \times n^{0.738}}{S^{0.362}} \quad (3.23)$$

respectively.

In the Moomin and Carole, the relatively small range in width leads to poor fits for Equation 3.18. Hence there is a large uncertainty associated with C_W values for these channels (Table 3.3). The uncertainty associated with the fit for Equation 3.21 is,

however, very low, and therefore it is instead used, in combination with Equation 3.14, to calculate C_W for all channels. In addition to the derivation of a C_W value for each channel, each channel has been divided approximately in two (see dividing bars along each channel in Figure 3.2) to allow comparison of the bank strength values of the upper and lower reaches of each channel.

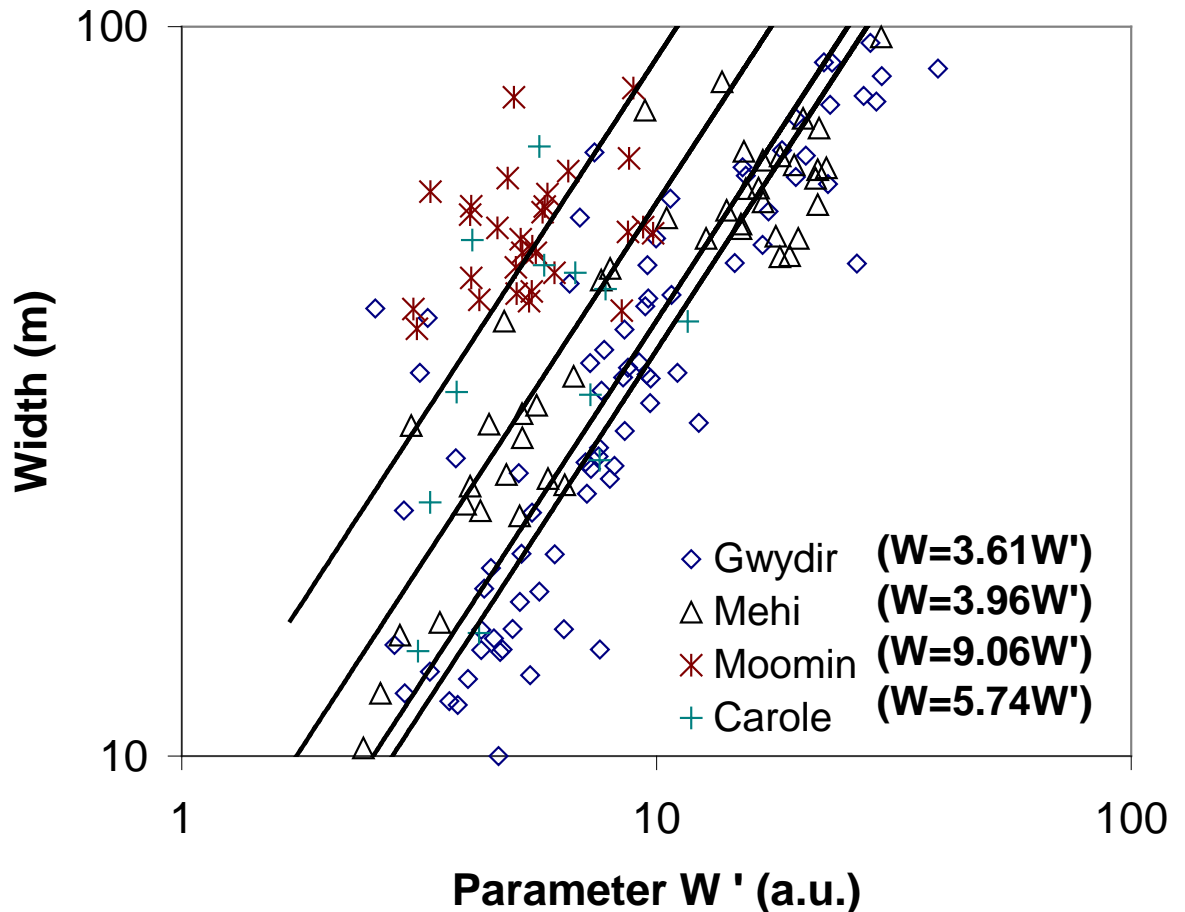


Figure 3.20: Derivation of C_W values for channels of the lower Gwydir.

Comment needs to be made on the influence of n on the derivation of C_W . The n parameter is the most difficult variable to estimate, and furthermore it will be significantly altered by the presence of in-channel vegetation. As this is the very scenario envisaged, the effect of increases in n needs to be modelled. Figure 3.21 shows the effect of increases in n on the W / W' relationship for the Mehi River. It can be seen that if n is increased in line with a vegetated bed, the calculated C_W actually increases and banks appear weaker. This occurs because increases in the $n^{0.355}$ term (in the case of Equation 3.10) are mostly cancelled out by reductions in the $Q^{0.5}$ term (see Equation 3.8).

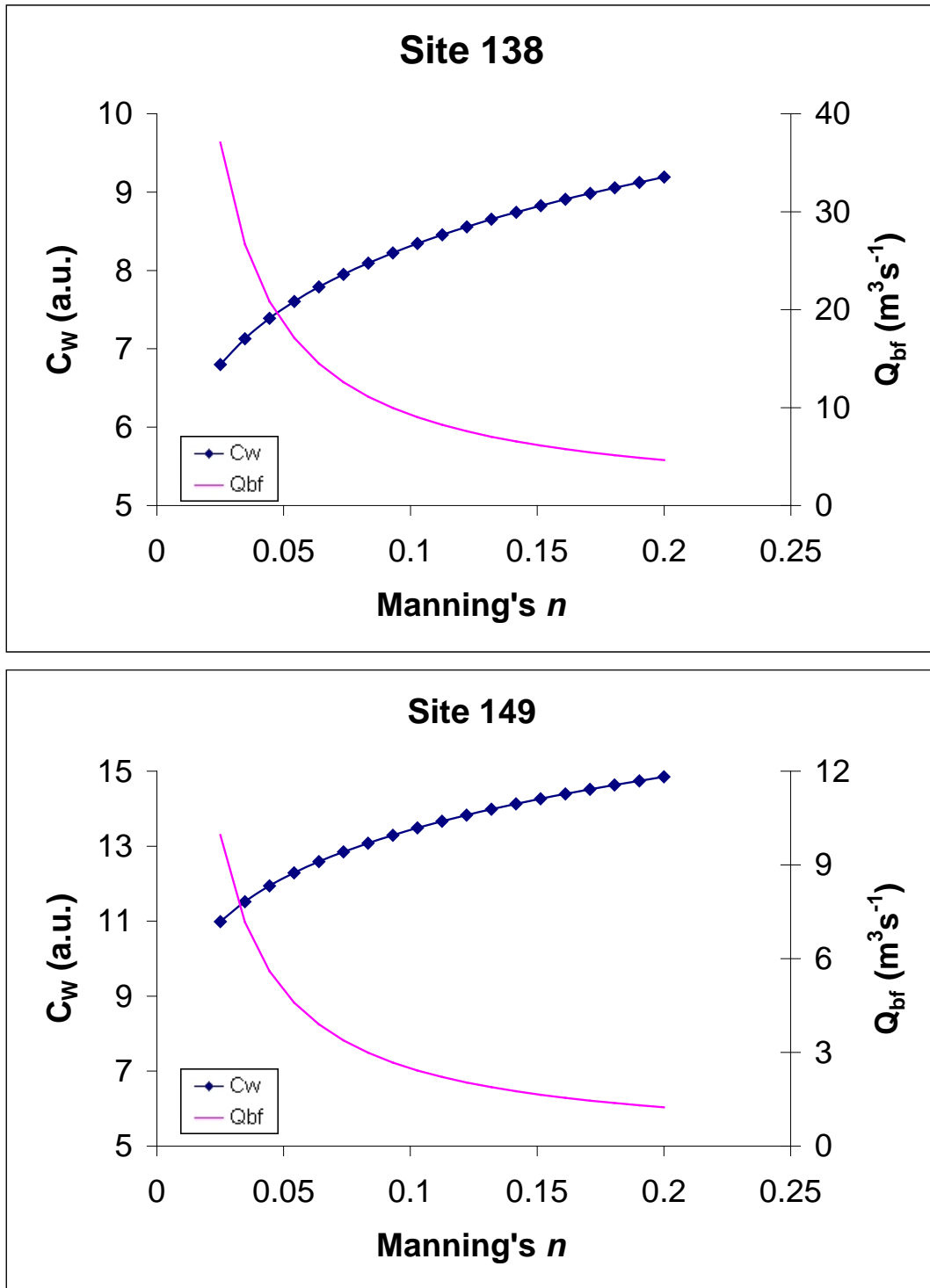


Figure 3.21: The effect on C_w of using different estimates of Manning's n for exemplar cross-section Sites 138 and 149. The plain trace indicates the effect on bankfull discharge of using different estimates of Manning's n .

Table 3.3: Direct and indirect derivation of C_W for the study streams. Upper and Lower refer to divisions of channels shown in Figure 3.2.

Channel	C_W	R^2	C_A	R^2	C_W calculated as $C_A^{\frac{5}{2}}$ (see Equation 3.14)
Gwydir	3.61	0.73	1.71	0.99	3.80
Mehi	3.96	0.64	1.75	0.99	4.08
Moomin	9.06	0.18	2.38	0.88	8.70
Carole	5.74	0.10	2.07	0.92	6.20
Upper Gwydir	3.03	0.45	1.58	0.95	3.14
Lower Gwydir	3.80	0.61	1.75	0.98	4.02
Upper Mehi	3.25	0.03	1.62	0.95	3.35
Lower Mehi	5.35	0.81	1.96	0.99	5.39
Upper Moomin	na	na	2.03	0.26	5.90
Lower Moomin	9.93	0.26	2.48	0.85	9.68
Upper Carole	4.58	0.03	1.89	0.98	4.94
Lower Carole	6.57	0.22	2.18	0.87	7.05

3.2.4. Comparison with Previously Examined Channels

The multivariate model has been applied to field observations from many parts of the world (Huang and Nanson 1998) to determine appropriate values of C_W (and therefore C_D and C_A) for a wide variety of channels. Table 3.4 shows the gross ranges of variation in C_W for various bank types, and provides a semi-quantitative method for incorporating bank strength into hydraulic geometry equations. Unfortunately, none of the bank type classes identified by Huang and Nanson (1998) accurately describes the conditions found in the study area. However, relative comparisons can be made.

Table 3.4: Gross ranges of variation in C_w for various bank types. (After Huang and Nanson, 1998). Cohesivity is taken as representing silt-clay content, where highly cohesive banks have high silt-clay contents.

Bank Type	C_w
Banks with non-cohesive sand	6.0-6.25
Gravel banks	4.5-6.0
Banks with moderately cohesive sand	3.5-5.0
Banks with highly cohesive sand	2.5-3.5
Moderately vegetated and moderately cohesive sand banks	3.0-4.0
Heavily vegetated and highly cohesive sand banks	2.1-3.0

From consideration of Table 3.4 and Figure 3.12 it may be supposed that streams of the Gwydir distributary system should have C_w values between 2 and 3. However, this is not the case. Table 3.3 shows that even though all the studied channels have clay banks, they have bank strength coefficients that are equivalent to sandy banks, and, intriguingly, they become increasingly ‘sandy’ (i.e. weaker) in the downstream direction. Furthermore, in the lower reaches of Carole and Moomin Creeks, bank strength coefficients reach values considerably higher (i.e. the banks appear much weaker) than any of the streams included in the original Huang and Nanson (1998) study. A slight downstream decline in bank vegetation density commensurate with the increasingly arid regional climatic gradient (Figure 2.3) may in part be responsible for the downstream decline in bank strength. However the aforementioned effects of variable hydrology and bed vegetation are thought to be more significant. Support for this argument is found in the relative ordering of stream channels by their bank strength (Table 3.3). The Gwydir River appears to have the greatest bank strength, followed by the Mehi River, then Carole Creek and finally Moomin Creek with apparently the weakest banks. Furthermore in all streams C_w values increase in the lower reaches. A 1-2 unit increase in C_w indicates an order of magnitude decrease in physical bank strength (Huang and Nanson, 1998); however, the silt and clay content shows little change along the study channels (Table 3.2, Figure 3.12). Accordingly, it is unlikely that the increasing C_w values downstream represent a true decline in physical bank

strength. The increase in C_w values may represent some effect of bank weakening due to wetting and drying cycles in the clay, but it is more likely that bed vegetation, by creating channel morphologies unlike any that were included in the original data set analysed by Huang and Nanson, results in the derivation of abnormally high C_w values. Interestingly, sites with in-channel trees were excluded from the Huang and Nanson (1998) study because it was noted that such reaches were abnormally wide, believed at the time to be due to the effect of flow diversion into the banks (Nanson pers. comm. 2005).

3.2.5 Implications for Future Channel Evolution

If the channels of the Gwydir distributary system were adjusted to a certain hydrological regime, then the question of what channel change has resulted from recent human-induced hydrological changes becomes an interesting one. Since the use of the Gwydir distributary system channels to supply irrigation water has required the removal of in-channel vegetation, and the change in hydrology has prevented its return, it may be expected that some channel change will be observable. For most of the length of the study streams, present day cross-sectional geometry is simply a reflection of the canalisation works carried out in the late 1970s'. However, the reach of Moomin Creek around the Moomin Plains Gauging Station (~ 240 km), does not appear to have been re-engineered, as it does not conform to the design specifications (i.e. a 20 m wide bed, and banks that have a 1 on 2 batter) stipulated for all works in the area (Plan 36/2954). It is possible that engineering works were not carried out so as to preserve the integrity of the gauging station. Assuming this to be the case, Figure 3.22 shows the change in cross-sectional geometry of the Moomin Creek at Moomin Plains between 1974 and 1993. It can be seen that over a relatively short period of time there has been a significant change in channel geometry. At this stage it is unknown whether this is just an isolated situation, or whether similar changes are occurring throughout the distributary network. It does appear however, that without the protective cover of vegetation, channels incise, causing width depth ratios to drop dramatically.

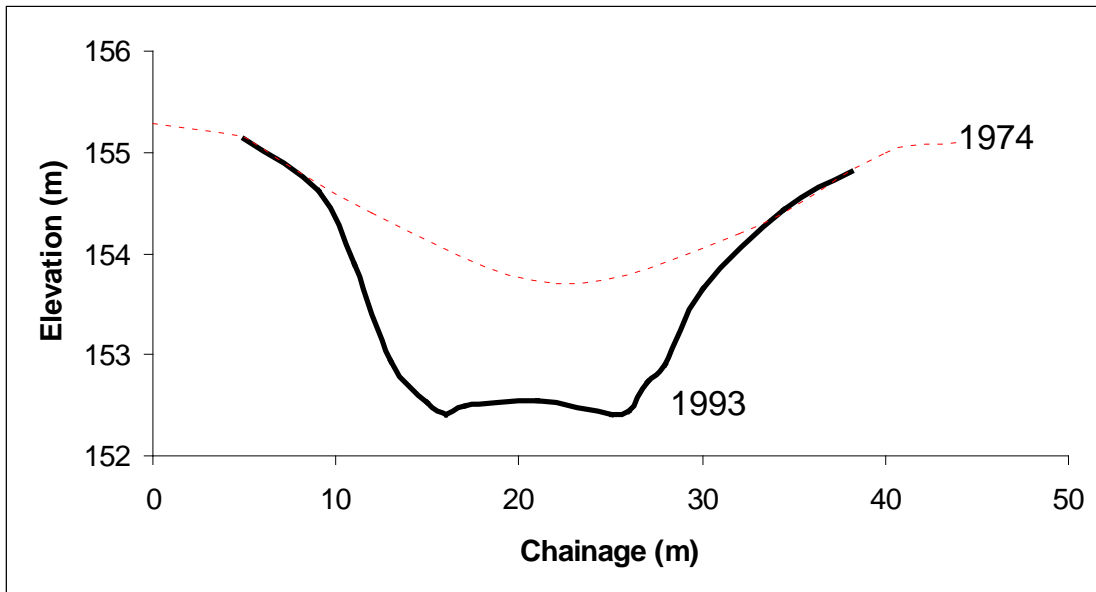


Figure 3.22: Development in channel shape at Moomin Plains (~240 km) following establishment of hydrological regime suitable for irrigation. 1974 survey from Plan 36/2847(1). 1993 survey data from Pineena 7.

3.3 Summary of Multivariate Hydraulic Geometry

The multivariate hydraulic geometry model of Huang and co-workers explicitly incorporates those variables which, in addition to discharge, control the hydraulic geometry of natural channels. It may be noted that explanations given in Section 3.1 above for differences in bivariate hydraulic geometry amongst the four study streams were founded on general discussions of slope, roughness and the effects of vegetation on the proportional distribution of stream energy. Likewise, the multivariate model of Huang and co-workers incorporates slope and roughness. However, in the model the proportional distribution of stream energy is inferred to be a function of bank strength, with weak banks unable to resist a large proportion of the boundary shear, hence the channel widens, reducing the proportion of stream energy expended on the banks. Even though the final form of the model presented by Huang and Nanson (1998) does not take into account the effects of channel-floor vegetation, it is argued that the bank-strength factor can, in the absence of compositional differences in bank material, be used as a proxy for in-stream vegetation density. This is because the model effectively

identifies those channels which are 'over-wide' for their specific complement of discharge, slope and roughness. In the context of the Gwydir distributary system, the width of channels appears not to be related to bank strength, which probably doesn't change that much, but rather to the density of in-channel vegetation.

Analysis of the hydraulic geometry of the channels of the lower Gwydir has revealed distinct differences in form and suggested function, both amongst the channels themselves and between these channels and most channels previously investigated. The principle mechanism causing this difference (apart from the effects of a downstream decline in discharge) appears to be the arrangement of the channel off-takes, which, by controlling the hydrology of each of the streams, results in different patterns of within-channel vegetation and, consequently, different patterns of channel form.

The data collected here provides a useful addition to the stream categories of Huang and Nanson (1998), as presented in Table 3.4. Ephemeral stream channels in temperate to semi-arid areas, prone to colonisation by vegetation will generally display channel forms not consistent with the material strength of their banks. The effect of in-channel vegetation obstructions on the proportional distribution of energy within channel flow should therefore be considered in the application of hydraulic geometry models, whether bivariate, exponentially invariate or multivariate.

Chapter 4 Channel Planform Characteristics

4.1 Introduction

Channel planform is but one river variable amongst many interdependent variables which mutually adjust to changes in controlling environmental parameters. Although these variables are physically interrelated, explanatory physical models have been difficult to construct and remain contentious (Rhoads and Welford, 1991). Empirical relations have therefore been widely developed; however, such relations are simply observations and not necessarily explanations. It can be observed that channel cross-sectional size in, for example, the Mehi is correlated with discharge (see previous chapter). However, it is not clear whether channel contraction causes a greater proportion of discharge to flow out of channel, or whether the decline in discharge itself causes a contraction in channel size. Identification of the cause, or independent variable, and the effect, or dependent variable remains problematic. Ferguson (1986) argues a similar point, stating that planform change both causes, and is an effect of, changes in hydraulic geometry. While these interdependencies frustrate attempts to produce definitive physical models, a related problem is that there are more unknowns than equations to solve them, hence a conclusive physically-based mathematical model can not achieve closure and identify causation. Defining empirical relations therefore remains a necessary precursor to discussion of physical mechanisms, albeit that such discussion must be in general or metaphysical terms, given the absence of physical models.

Two distinct methodologies are used in this Chapter to analyse planform characteristics. Firstly, sinuosity and meander wavelengths are measured manually in the standard manner. Secondly, following Hickin (1977), series analysis is used to measure radii of curvature, enabling the construction of a frequency distribution for each reach. In addition to using series analysis for the production of radii of curvature distributions, sinuosity and wavelength can be assessed using the spatial series (Fergusson, 1977; Hickin, 1977). These approaches comprise an objective method of verifying the manually measured sinuosity and meander wavelength values. The accuracy of the

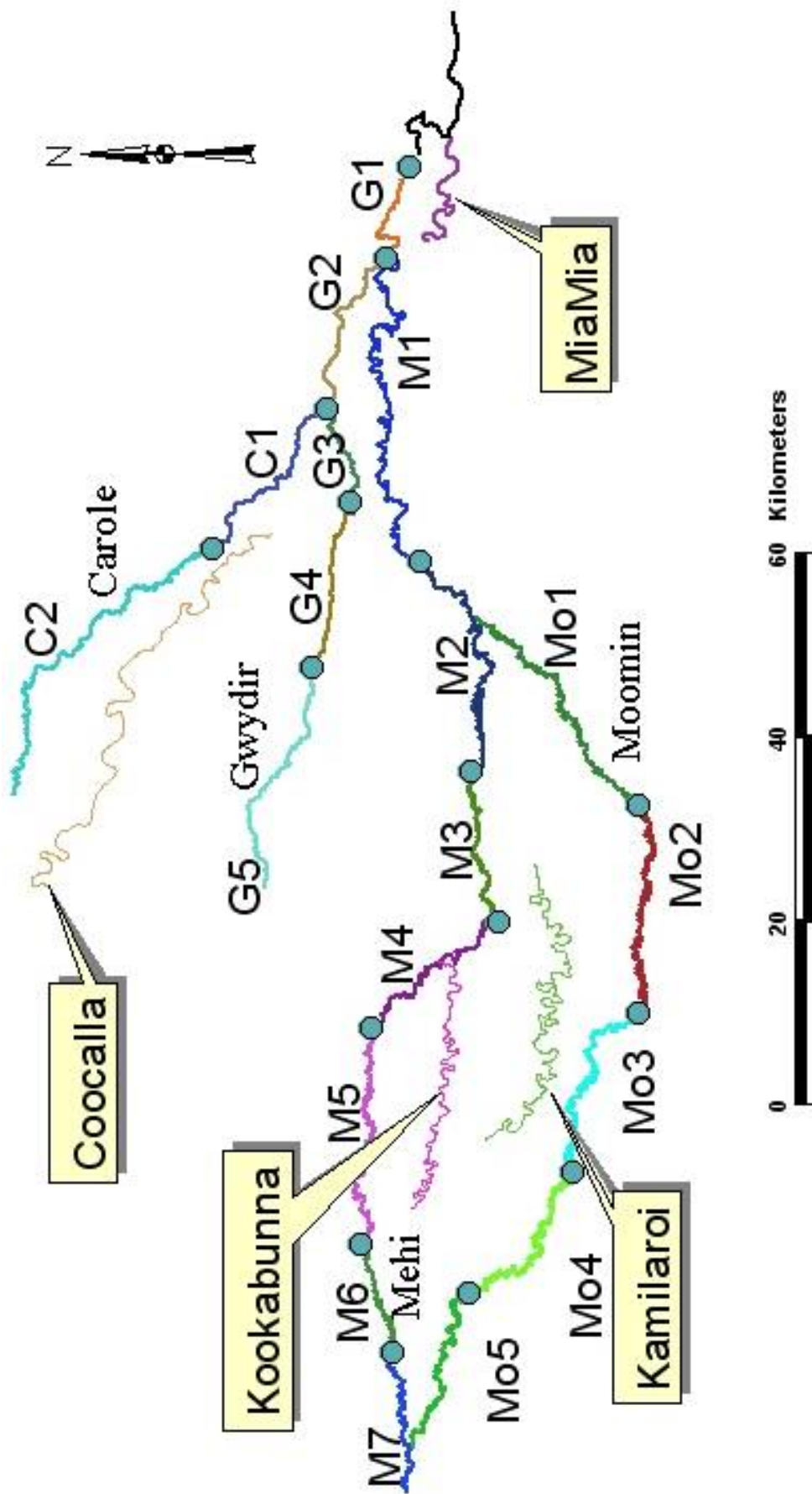


Figure 4.1: Channel Reaches for Planform Analysis. Note that colours have been arbitrarily chosen to highlight each reach. The palaeochannels studied are labeled with text boxes. See Appendix D for large scale images of individual reaches.

series approaches can in turn be tested by applying them to mathematically constructed meander traces, which have known sinuosities, wavelengths and radii of curvature.

4.2 Data

To analyse downstream changes in planform, channels were divided into approximately 20 valley km lengths. Actual lengths chosen were dictated by the location of bifurcations and major channel-train direction changes (Figure 4.1). While in some channels such lengths represent a significant decline in discharge, shorter lengths were avoided because of the computational challenges presented by a larger number of smaller channel lengths. Channel lengths were, for the most part, digitised from rectified satellite imagery (using ArcView 3.3). Channel reaches that have been significantly altered by canalization works were digitised from 1967 air photographs, flown before major channel realignment. Palaeochannels were likewise digitised from a combination of satellite imagery and air photographs. Unlike the contemporary (pre 1967) channel system, palaeochannels did not show obvious downstream planform development and were therefore analysed as whole units rather than sub-divided. Manual measurement of sinuosity and meander wavelength was undertaken ‘on-screen’. For the series analysis procedures channel data were analysed as series of X,Y coordinates in the spreadsheet program Excel, using custom written Visual Basic programs.

4.3 Techniques

4.3.1 Standard Planform Measures

Manually measured sinuosity (P), defined as:

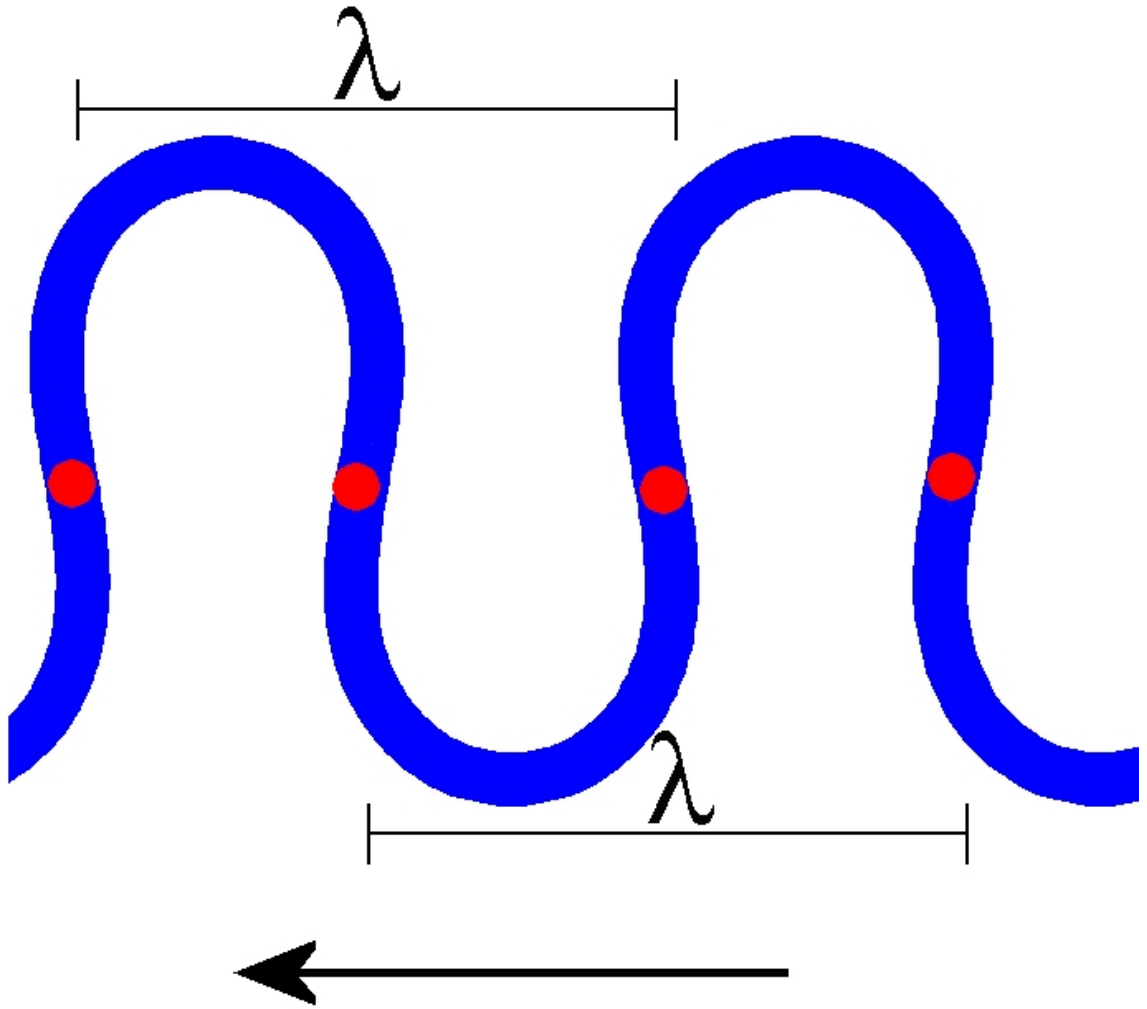
$$P = \frac{\text{Channel Pathlength}}{\text{Meander Train Length}} \quad (4.1)$$

was calculated in most cases by measuring the straight line distance between the beginning and the end of each channel reach and using this value as the denominator in Equation 4.1. However, for some reaches (C2, G5, M2, Mo3, Mo4), see Figure 4.1, the meander train did not follow a straight line, having one or two major direction changes. These direction changes were incorporated into the meander train length measurement for these channels, and hence an element of personal judgment in this measurement is incorporated. Meander wavelength (λ), defined as the straight line distance between an inflection point and the second downstream inflection point (Figure 4.2), was likewise measured in a subjective manner. This was done by measuring the length of all identifiable full meander sequences in each channel reach, then calculating the average ($\bar{\lambda}$). This method was designed to minimise the subjectivity inherent in selection of ‘representative’ meanders. It is assumed that the mean meander wavelength thus calculated is directly comparable to meander wavelength measurements of previous studies (e.g. Dury, 1977).

4.3.2 Series Analysis Planform Measures

Series analysis techniques described here are based on series of Cartesian coordinates describing channel centrelines. The as-digitised channel trace is generalised by re-sampling the original trace at equidistant intervals, and it is this generalised trace which is analysed. The chosen sampling density determines the level of channel trace generalisation, and this in part weakens the major advantage of series analysis, that is, the minimization of subjectivity. However, though the choice of sampling intensity remains a subjective decision, its influence can be tested iteratively on meander models which resemble the natural channel but for which known values exist.

Figure 4.2 (opposite page): *Measurement of meander wavelength (λ). The solid blue trace represents actual channel line, with inflection points identified. Arrow shows cardinal channel direction.*



Producing a radius of curvature frequency distribution for each reach is achieved by calculating the radius (R_C) of the circle subtended by pairs of chords between each consecutive and successive triad of equally spaced channel coordinates (Figure 4.3), where:

$$R_C = \frac{(AB)^2}{2(BC)} \quad (4.2)$$

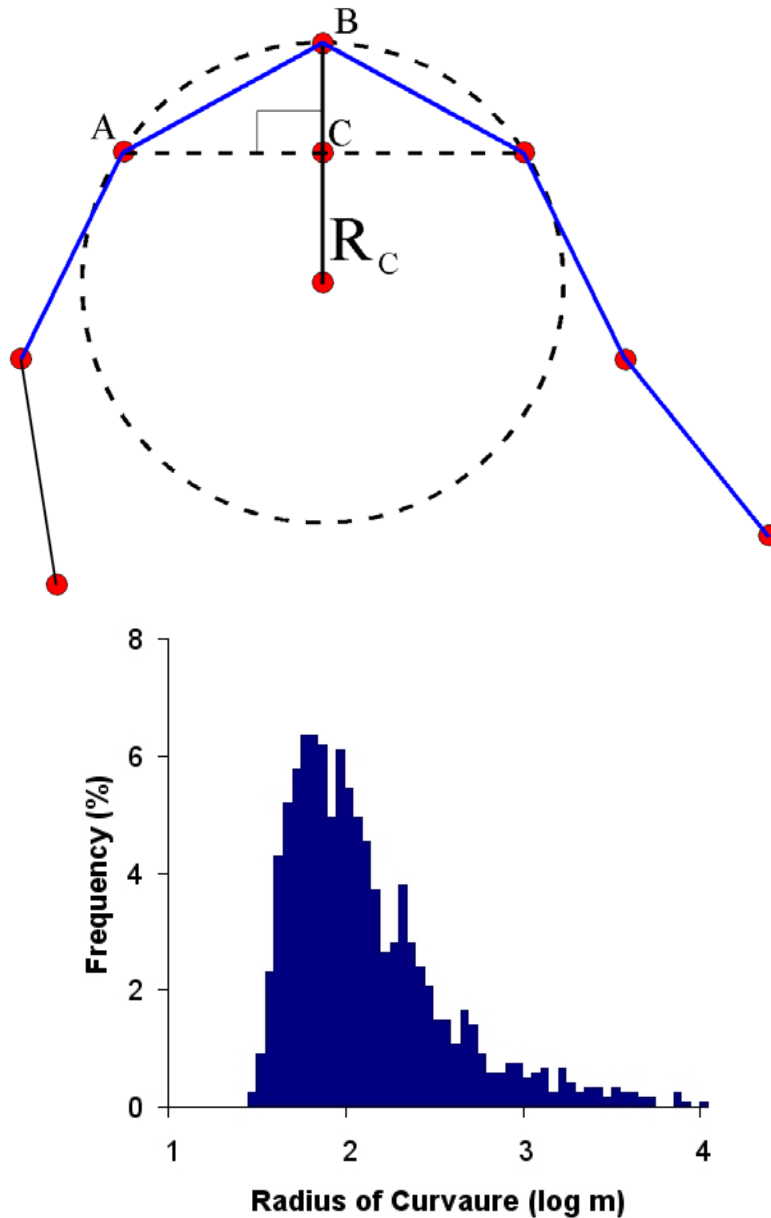


Figure 4.3: Calculation of R_C (above) with the resulting frequency distribution histogram for Reach M5 shown as an example.

Following the original approach of Hickin (1977), radii greater than $200 W$ (~ 10 km in the study streams) are considered representative of straight sections of channel and therefore are omitted from the radii frequency histogram. The number of omitted radii is taken as representative of the proportion of the channel length which is sensibly straight. Hickin (1977) found that about 20 % of the alluvial reach of the meandering Beaton River in Canada could be considered straight. It will be seen below that the proportion of straight reaches in the channels of the lower Gwydir is very much lower than this (see

Table 4.2, Section 4.5.1). Possible explanations for this difference will be offered in Section 4.5.1.

Hickin (1977) proposed that frequency analysis of channel direction series should result in statistics that are relevant to the empirically-based meander relations of Leopold and Wolman (1957, 1960):

$$\frac{\lambda}{W} \cong 10 \quad (4.3)$$

$$\frac{\lambda}{R_c} \cong 4 \quad (4.4)$$

$$\frac{R_c}{W} \cong 2 \quad (4.5)$$

$$\lambda \cong 54 Q^{0.5} \quad (4.6)$$

As these relations were derived using essentially the same approach as described in Section 4.3.1 above, they are based on a subjective extraction of the characteristic style of planform oscillation. Analysis of frequency distributions of radii of curvature should likewise result in the extraction of channel planform measures that are characteristic, though in the case of series analysis, such characterization is done in a mostly objective manner. Furthermore, extra information is available via simple statistical characterisation of the frequency distributions: mean, mode, coefficient of variation and kurtosis.

In addition to radii of curvature, meander wavelength can also be computed and frequency distributions constructed. Wavelength is calculated as the straight-line distance between each inflection point and the next, plus 1, inflection point along the meander trace, just as is done in the manual measurement of wavelength. However, in this case inflection points are identified using an automated Visual Basic procedure. From the generalized channel trace, a direction series is produced, and from this series a

direction difference ($\Delta\text{direction}$) series is produced. Using the $\Delta\text{direction}$ series, inflection points can be identified where the sign of direction difference changes (Figure 4.4). Some filtering of the resulting list of inflection points is then required to remove those inflection points which are the result of digitising error. This is achieved by placing a distance threshold between inflection points equal to the average width of each channel reach. Thus an inflection point which is spaced less than the width of the channel downstream of the preceding inflection point is assumed to be a result of digitising error and is rejected. Some of these may also be due to minor disturbances in the overall channel form, such as that caused by localised woody debris. Their removal from the data set acts to preserve the larger-scale planform description sought here.

The series approach to sinuosity measurement applied here is that of Fergusson (1977). This technique provides an objective measure of sinuosity and is calculated using the variance (V) of channel direction values, or rather their difference from the channel's cardinal direction (see Figure 4.4), which Ferguson (1977) showed to be related to manually measured channel sinuosity (P) via:

$$P = \frac{1}{\left\{1 - \left(\frac{V}{2}\right) + \left(\frac{V^2}{8}\right) - \left(\frac{V^3}{48}\right)\right\}} \quad (4.7)$$

where:

$$V = \frac{n \sum x^2 - (\sum x)^2}{n(n-1)} \quad (4.8)$$

Sinuosity as calculated using the series approach will be referred to as P_{series} to distinguish it from manually measured sinuosity (P). Likewise, the mean meander wavelength measured using the series approach will be referred to as $\bar{\lambda}_{\text{series}}$, as distinct from $\bar{\lambda}$.

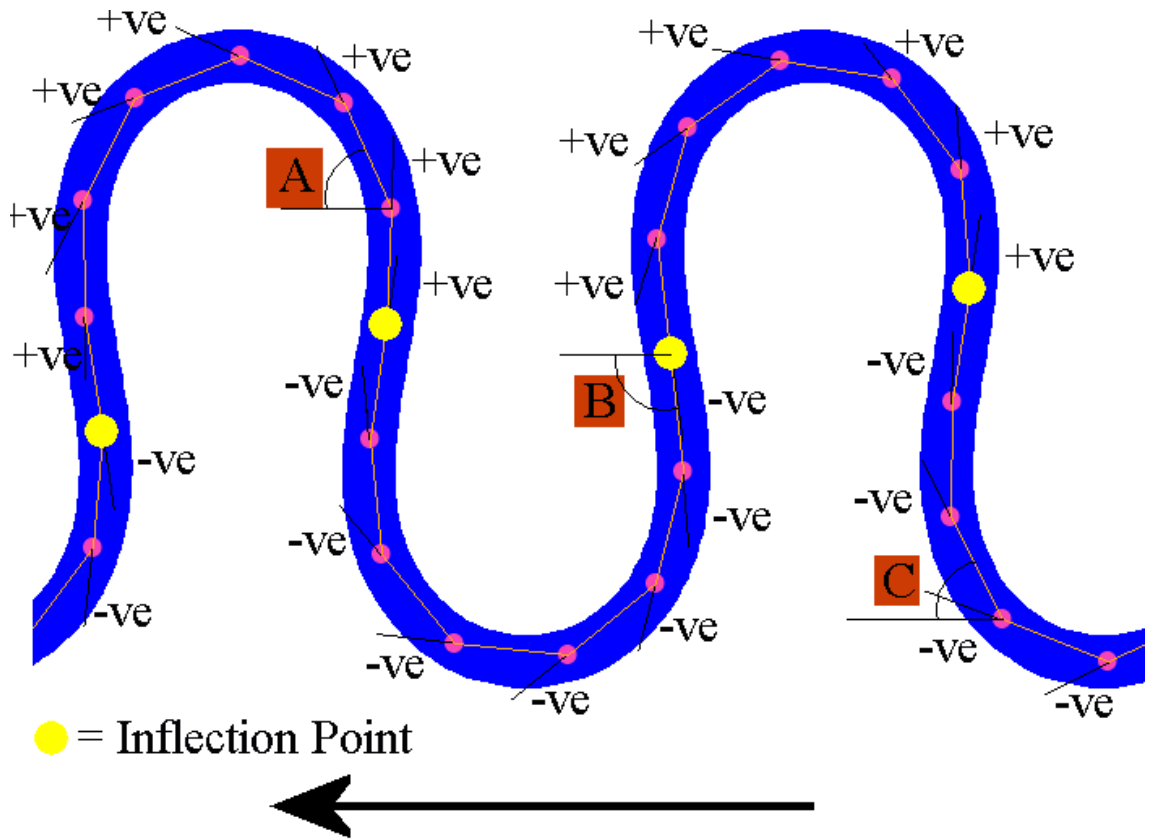


Figure 4.4: Inflection point location and sinuosity determination. The solid blue trace represents actual channel line. The segmented line represents channel generalization via equidistant re-sampling. Inflection points are located where the direction difference between successive segments ($\Delta\text{direction}$ – signified by short lines extending beyond each vertex) changes sign. The large arrow indicates cardinal direction, against which angles A, B and C are calculated to provide the angular deviation of the channel centerline. Note that for illustrative purposes only three angles are shown.

4.4 Verification of Series Analysis Techniques

The central assumption made for each of the series analysis techniques is that the equidistant re-sampling of each channel does not result in information loss. To check this assumption each of the series analysis techniques has been tested on the meander model of Langbein and Leopold (1966):

$$\theta = \alpha \sin kx \quad (4.9)$$

where θ = channel direction, being a sinusoidal function of channel distance, x ; with parameters α (maximum deviation angle) and k where:

$$k = \frac{2\pi}{(\lambda^*)} \quad (4.10)$$

with λ^* = meander pathlength (not wavelength). This model has solvable relations between the variables α and k and the expected results of each of the series analysis techniques, thus allowing the accuracy of the techniques and the appropriateness of the assumptions used in their application to be tested.

Fergusson (1973), in review of regular meander models, such as the Langbein and Leopold model, suggested that all were simply variations of a general family of differential equations, containing a scale parameter and a sinuosity, or ‘wiggleness’, parameter. Furthermore, later, more sophisticated models (e.g. Ferguson, 1976), which attempt to describe full channel traces, not just bends, contained only one more parameter, (or family of parameters), describing irregularity. The irregularity parameter is designed to account for the variable boundary conditions experienced by most natural river channels along their course. While more complicated models of meandering may produce more realistic analogues, it is the regular meander path model of Langbein and Leopold that has been chosen to demonstrate the application of the three methods outlined above. This is partly for expediency’s sake, as definable relationships exist between the results of each of the analyses and the input parameters. The main reason, however, is that non-regular meander path models apply random perturbations to an underlying functional relationship, and it is this underlying, non-random element in natural channels that is sought to be retrieved using the three series analysis techniques. The random element, i.e. that which distorts the expression of the non-random element, is intentionally filtered out. So, while application to a regular model does not allow testing of this filtering process, it does provide precise results, free from random distortions, for comparative analysis of techniques. Additionally, empirical ‘laws’ built using standard techniques are based on selectively choosing meanders which are most regular, thus they are most relevant to regular meander models.

Langbein and Leopold (1966) showed that their form of curve, where direction varies as a sinusoidal function of distance, results in a meander trace with a lower ‘sum of squares’ of direction change, than any other common curve. From this they infer that the form of river meanders can be understood in a thermodynamic sense, suggesting that the model is inherently similar to natural meanders. Regardless of the underlying reasons, sine-generated curves do bare an intuitive similarity in form to natural meanders. They are thus considered here to be a suitable pattern on which to test the series analysis procedures.

4.4.1 Modelled Meander Traces

A matrix of 25 model channel traces is created, 15 of which are shown in Figure 4.5, with λ^* values 100 m, 200 m, 500 m, 1000 m and 2000 m; and α values 20° , 40° , 70° , 100° , 120° .

4.4.2 Expected Results

Exact analytical expressions for the planform properties of the meander analogues are available in the literature and are therefore reproduced here with minimal comment.

4.4.2.1 Radius of Curvature

Langbein and Leopold (1966) noted that the tangent to the sine function is the reciprocal of the instantaneous radius of curvature. Thus:

$$\text{Radius of Curvature} = \left| \frac{1}{\tan(\alpha \sin kx)} \right| = \left| \frac{1}{\alpha k \cos(kx)} \right| \quad (4.11)$$

Note that the sign of radii alternates with direction of concavity, hence the absolute bars.

From Equation 4.11 it can be seen that, as kx approaches $(\pm) 90^\circ$, 270° , 450° etc. (i.e. $\cos(kx) = 0$), radius of curvature approaches infinity, thus describing an inflection point.

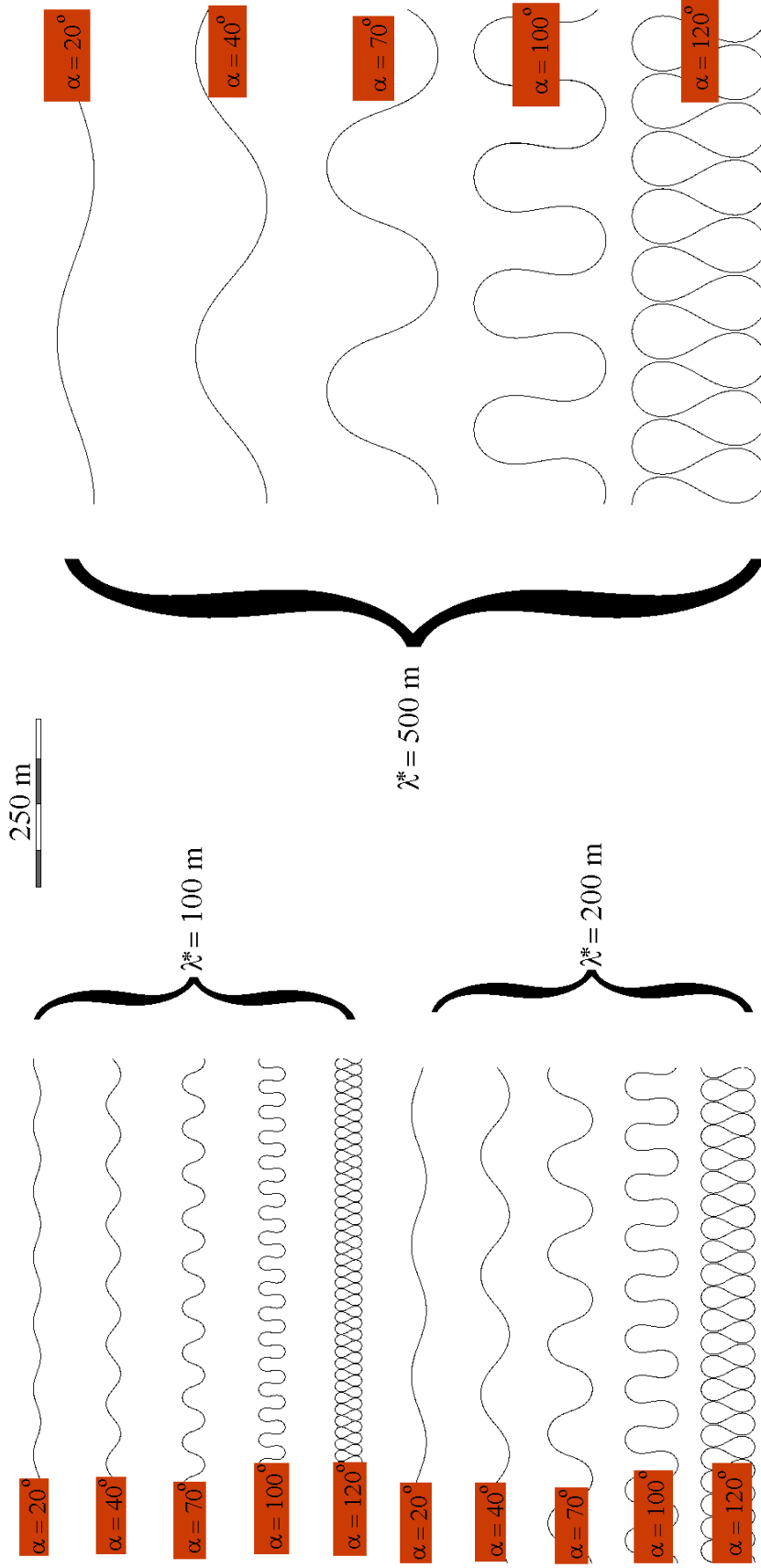


Figure 4.5: Examples of sine generated curves used to test automated series analysis techniques. For clarity, $\lambda^* > 500$ m models not shown.

Conversely, where $kx = (\pm) 180^\circ, 360^\circ, 540^\circ$ etc., (i.e. $\cos(kx) = \pm 1$), then radius of curvature will be a minimum, thus describing the instantaneous curvature at the midpoint of each loop. The radii of curvature frequency distribution for a sine generated curve resembles an inverse power function, where the modal radius is also the minimum. Thus for sine-generated curves, the modal radius of curvature, the minimum radius of curvature, and the radius of curvature concordant with the centre of each loop, are all defined as:

$$\frac{1}{k\alpha} \quad (4.12)$$

4.4.2.2 Wavelength

Fergusson (1973) showed the axial wavelength of a sine generated curve to be a zero-order Bessel function of α :

$$\lambda = \lambda_* \left[\sum_{\kappa=0}^{\infty} \frac{-1\kappa}{\kappa! \Gamma(\kappa+1)} \left(\frac{\alpha}{2} \right)^{2\kappa} \right] \quad (4.13)$$

where:

$$\Gamma(\kappa+1) = \int_0^{\infty} e^{-\alpha} \alpha^{\kappa} d\alpha \quad (4.14)$$

Note that in the Bessel function, the ' κ ' is kappa, (the Γ function variable) and not ' k ', the path-length coefficient in Equation 4.9.

4.4.2.3 Direction Variance

Ferguson (1977) demonstrated that for the sine generated curve:

$$V = \left(\frac{\alpha^2}{2} \right) \quad (4.15)$$

We now have three series analysis techniques describing plan-form properties, twenty-five analogues of meandering streams to demonstrate their use, and three analytical expressions, i.e. Equations 4.12, 4.13, and 4.15 (in combination with Equation 4.7) to define their expected results. From plots of measured values against their expected values we can identify where the geo-morphometric techniques have failed, thus providing an assessment of the appropriateness of their use in the case of natural streams.

4.4.3 Results of Series Analysis of $\theta = \alpha \sin kx$ Models

Figure 4.6 provides scatter-plots of the measured $\overline{R_C}$, $\overline{\lambda_{series}}$ and P_{series} against the theoretical values for each meander model. It can be seen that all the techniques fail for the smallest meander traces ($\lambda^* = 100$ m or $\lambda^* = 200$ m when $\alpha > 70^\circ$), however all perform well for $\lambda^* > 200$ m for all values of α . The failure of the series analysis techniques for the smaller meander models is due to the generalization technique mentioned before. Obviously the equidistant re-sampling of the smaller meander models has resulted in distortion of the original meander form, such that erroneous values result. It may therefore be concluded that if applied to natural channels, the series analysis techniques described here will only produce valid results if the natural channels resemble meander analogues which have $\lambda^* > 200$ m. None of the study streams have λ^* values of < 200 m (Table 4.1).

Figure 4.7 shows a comparison of a section of one of the smaller sets of meanders in the Gwydir distributary system, against the meander model which best approximates it. As the natural channels of the Gwydir distributary system generally resemble meander models of $\lambda^* = 500$ m, $\alpha = 100^\circ$, it is concluded that their planform characteristics will be accurately measured using the automated series approach developed here.

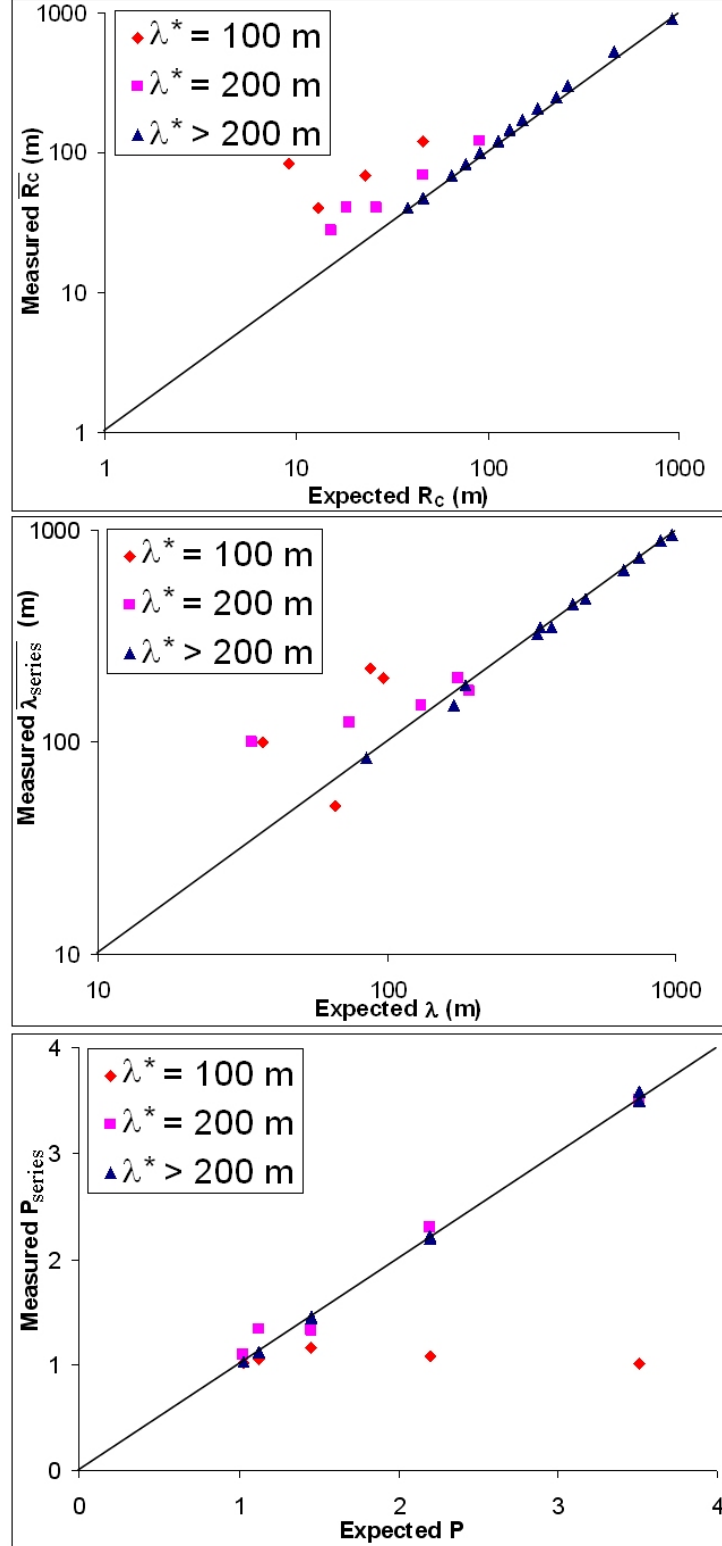


Figure 4.6: Comparisons of measured $\overline{R_c}$, $\overline{\lambda_{series}}$ and P_{series} values with expected values. Where λ^* is greater than 200 m the techniques are accurate. Where $\lambda^* = 200$ m and α is high all the techniques fail. For all the $\lambda^* = 100$ m traces the techniques fail. Lines of equal value shown.

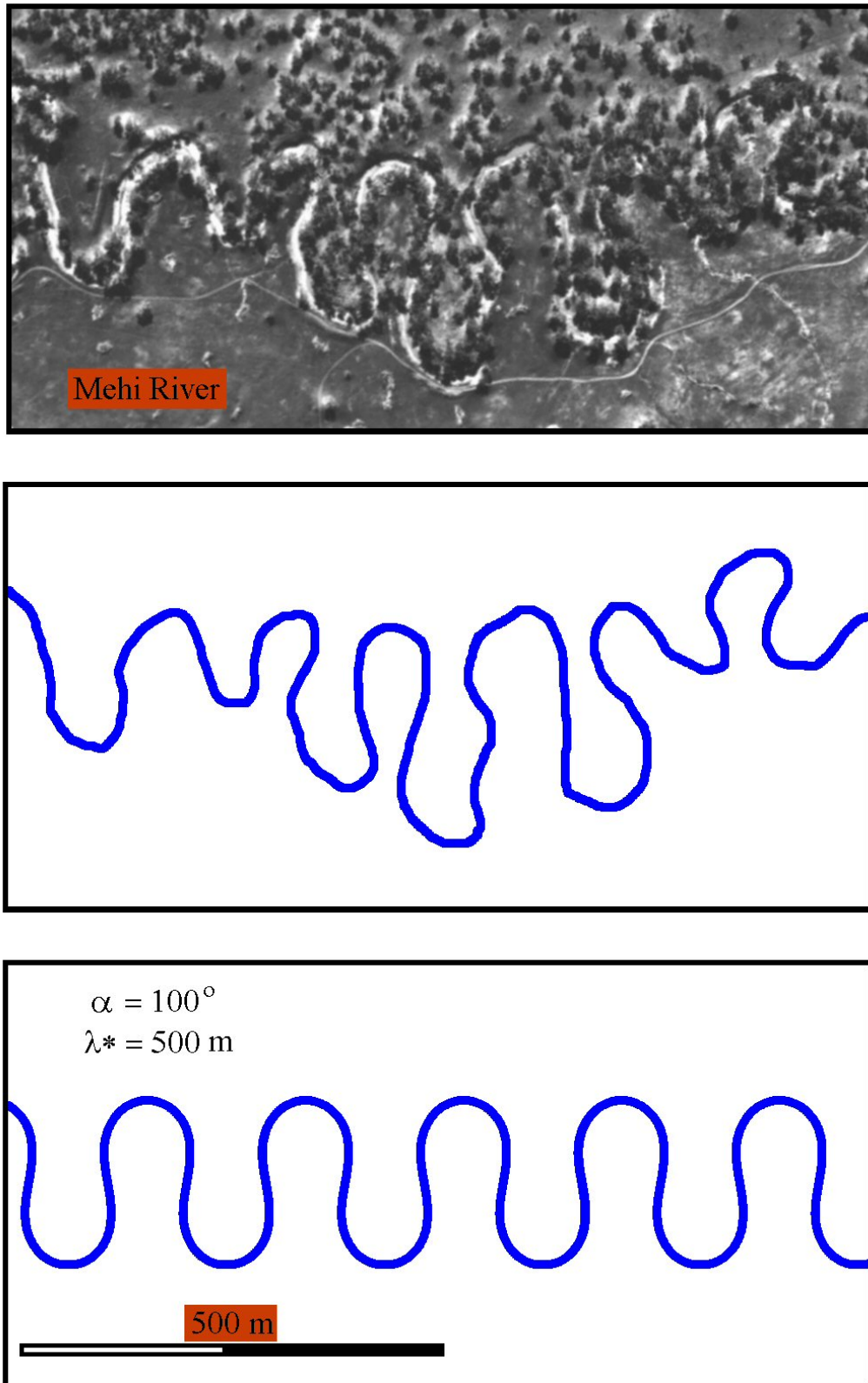


Figure 4.7: Comparison of section of Mehi River (near Cross-Section 20) with sine generated curve of approximately equal scale and angularity.

4.5 Results

Table 4.1 lists the results of all planform analysis techniques undertaken here, with the seven columns on the right providing hydraulic geometry data relevant to each reach. For convenience, the cross section (see previous chapter) closest to the centre of each reach is taken as representative of the reach as a whole. Figure 4.8 illustrates the relationships between the subjective and (mostly) objective measures of sinuosity and wavelength. Given the demonstrated accuracy of the series analysis techniques, they may be taken as providing benchmark values against which the subjectively measured P and $\bar{\lambda}$ values can be compared (Figure 4.8). The rough equivalence of the P to P_{series} and $\bar{\lambda}$ to λ_{series} indicates that the planform characteristics of the Gwydir distributary system channels have been accurately defined using the subjective methodology. Rather than continue using two roughly equivalent values of each measure in subsequent discussions, only the P and $\bar{\lambda}$ values will be used. Using the P_{series} and λ_{series} values would result in minor differences but not change the resulting conclusions.

4.5.1 Downstream Variation in Planform

The Gwydir River shows a downstream decrease in $\bar{\lambda}$, accompanied by a decrease in $\overline{R_C}$ and P , below the off-takes of the Mehi and Carole and the overflow into Gingham Watercourse (Figure 4.9). The final reach of the Gwydir is downstream of a confluence of anabranches (one of which is represented in Figure 4.9) and hence shows a modest increase in $\bar{\lambda}$ and $\overline{R_C}$, as well as a slight increase in P . The Mehi River shows a dramatic downstream decrease in $\bar{\lambda}$ and $\overline{R_C}$, apparently related to the location of the Moomin off-take. Unlike the Gwydir River, this decrease in channel scale is accompanied by an *increase* in channel sinuosity. Interestingly, the downstream confluence of the Moomin Creek causes a very slight but detectable adjustment in the scale parameters $\bar{\lambda}$ and $\overline{R_C}$.

Table 4.1: Planform analysis results of all study reaches of the Gwydir distributary system. Hydraulic geometry data relating to central most cross section also provided.

Reach	Stream km	P	P _{series}	$\bar{\lambda}$ (m)	$\bar{\lambda}_{series}$ (m)	R _C (m)	Q _{bf} (m ³ s ⁻¹)	w (m)	\bar{d} (m)	v (m s ⁻¹)	S	S _V	ω (W m ⁻²)
Gwydir 1	0-13	1.97	2.01	1150	1094	398	1660	88	7.4	2.56	0.00056	0.00111	104
Gwydir 2	13-37	1.33	1.38	1100	937	282	916	86	5.5	1.96	0.00053	0.00071	56
Gwydir 3	37-51	1.23	1.29	830	759	224	527	61	5.0	1.75	0.00053	0.00066	45
Gwydir 4	51-74	1.24	1.23	350	397	141	68	33	2.7	0.77	0.00045	0.00055	9.0
Gwydir 5	74-108	1.55	1.32	460	391	158	37	25	2.3	0.65	0.00031	0.00049	4.5
Mehi 1	0-70	2.06	2.17	670	671	178	575	97	5.7	1.05	0.00039	0.00080	23
Mehi 2	70-123	2.09	2.28	430	586	141	215	48	4.8	0.92	0.00039	0.00081	17
Mehi 3	123-163	2.45	2.18	240	391	71	15	21	1.8	0.38	0.00023	0.00055	1.5
Mehi 4	163-205	2.35	2.18	220	468	63	20	27	1.5	0.49	0.00023	0.00054	1.6
Mehi 5	205-273	3.41	3.50	195	371	63	35	47	1.9	0.39	0.00017	0.00056	1.2
Mehi 6	273-302	2.40	2.15	190	448	63	39	77	1.9	0.27	0.00017	0.00040	0.8
Mehi 7	302-343	2.65	2.36	230	400	79	97	84	2.7	0.43	0.00014	0.00037	1.6
Moomin 1	0-65	3.06	2.34	265	307	89	36	52	2.0	0.33	0.00025	0.00076	1.7
Moomin 2	65-139	3.31	2.97	220	260	71	45	53	2.2	0.38	0.00012	0.00039	1.0
Moomin 3	139-200	2.93	3.12	240	276	79	35	41	2.3	0.37	0.00012	0.00035	1.0
Moomin 4	200-265	3.64	3.33	255	276	89	14	43	1.2	0.26	0.00011	0.00042	0.4
Moomin 5	265-312	2.63	2.46	220	277	79	15	57	1.3	0.21	0.00011	0.00030	0.3
Carole 1	0-29	1.44	1.38	350	411	126	59	31	1.8	1.09	0.00150	0.00217	28
Carole 2	29-91	1.66	1.71	275	352	100	15	15	1.7	0.58	0.00044	0.00073	4.2

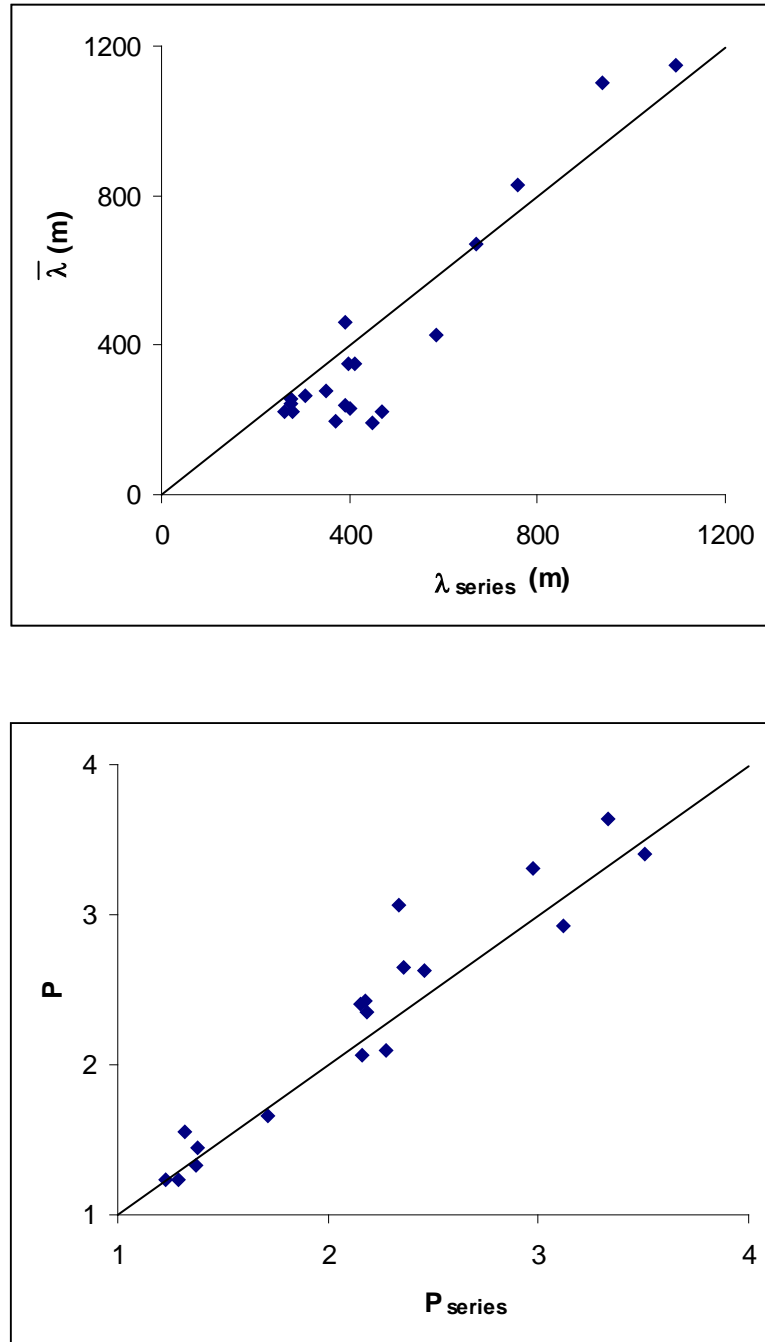


Figure 4.8: Comparisons between manually measured λ and P and the equivalent series analyses. Divergences from equality are considered to be as likely a result of inconsistencies in the manual measurement of each value as from errors in the series analysis techniques.

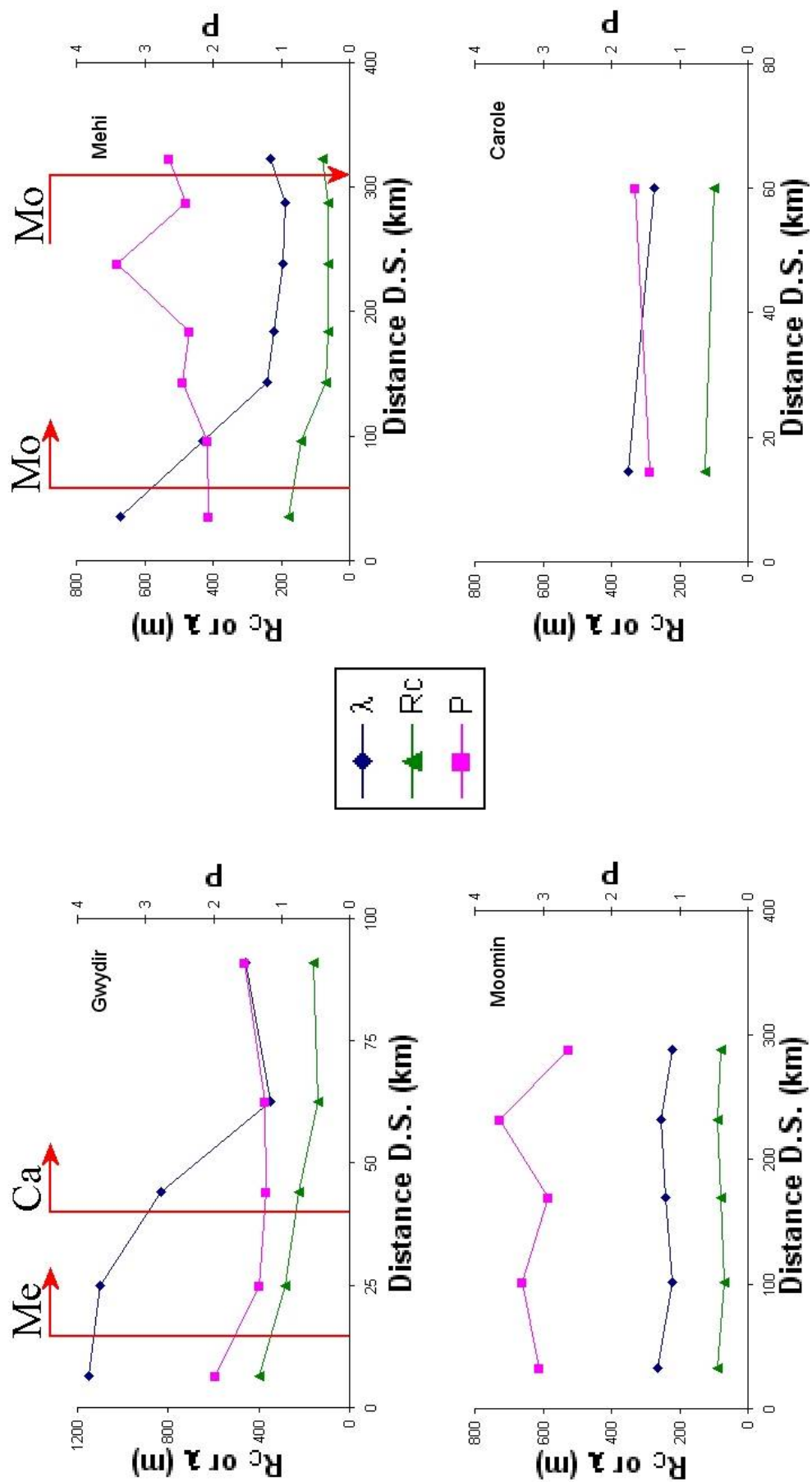


Figure 4.9: Downstream planform development in the Gwydir distributary system. The x-axes show distance of the midpoint of each channel reach downstream of the channel off-take, or Pallamallawa in the case of the Gwydir River. Arrows indicate locations of off-takes (horizontal arrow heads) and confluences (vertical arrow heads). Note variable scales on axes.

Table 4.2: Additional data describing radius of curvature and meander λ distributions.

Reach	Stream km	Radius of Curvature				Meander λ		
		Count	C.V.	Kurtosis	% > 10km	Count	C.V.	Kurtosis
G1	0-13	643	1.5	9.6	27	24	0.32	-1.1
G2	13-37	424	1.5	13	11.9	20	0.26	1.9
G3	37-51	239	1.6	21	10.2	13	0.33	-0.2
G4	51-74	404	2.0	21	10.4	23	0.33	-0.7
G5	74-108	624	1.8	27	4.9	34	0.40	-1.2
M1	0-70	1313	1.8	18	5.4	74	0.32	-0.4
M2	70-123	1017	1.9	28	2.6	73	0.36	1.4
M3	123-163	738	2.5	41	0.8	46	0.40	2.9
M4	163-205	777	2.6	43	0.9	50	0.41	1.1
M6	205-273	1215	2.6	65	0.9	78	0.45	2.0
M7	273-302	545	1.9	60	0.5	31	0.47	4.5
M8	302-343	751	2.3	67	0.8	46	0.35	1.5
Mo1	0-65	1211	2.1	32	2.2	117	0.34	-0.7
Mo2	65-139	1390	2.3	84	0.4	135	0.35	0.0
Mo3	139-200	1128	2.3	76	0.9	110	0.37	2.7
Mo4	200-265	1238	2.3	45	1.0	108	0.33	0.5
Mo5	265-312	869	2.2	48	0.7	97	0.32	1.3
Cc1	0-29	947	2.0	31	14.7	56	0.35	-0.3
Cc2	29-91	2266	2.2	34	7.2	127	0.40	1.0

All channels show a downstream decline in the proportion of each channel reach that is straight, that is, having a radius of curvature of over 10 000 m (Table 4.2). While the Gwydir and Carole have significant proportions of straight reaches, the Mehi and Moomin are virtually 100 % curved. Hickin (1977), in explanation of the ~ 20 % straight reaches present in the highly sinuous Beattoon River, highlighted the method of channel migration whereby significant limb extension occurs either side of a prominent bend, hence each curved reach is bounded by limbs of essentially straight channel. Also,

in an actively migrating river, the formation of meander cut-offs produces significant lengths of straightened channel. Additionally, though some channel reaches of the Beaton River were straight, their beds were deformed in a manner reflecting the downstream oscillatory distribution of boundary shear. Limb extension, channel straightening via meander cut-off formation, and oscillatory bed deformation are all apparently absent in the Moomin and Mehi.

The downstream changes in scale of the Mehi and Gwydir seem to be readily explainable by reference to effluents and confluents, whereas, both the Moomin and Carole have dramatic downstream declines in discharge with barely detectable changes in channel planform scale. This insensitivity of planform scale to discharge mirrors the previously observed insensitivity of width to discharge in these channels (Table 3.1). Developments in sinuosity and overall channel straightness do not appear to be directly related to discharge changes. With the possible exception of the bedload dominated Gwydir River, differences in boundary sediment likewise do not provide an explanation for the downstream changes in sinuosity (see Figure 3.12). One possibility causing the downstream changes in channel sinuosity and the insensitivity of planform scale to discharge is that downstream developments in hydraulic geometry underlie the planform developments.

4.5.2 Planform – Hydraulic Geometry Relations

Simple linear regressions have been employed to explore the relationships between planform and hydraulic geometry parameters. Table 4.3 presents the results of 12 linear regressions of either $\bar{\lambda}$ or $\overline{R_c}$ against hydraulic geometry variables. Keeping in mind that correlation does not necessarily equal causation, the results provide a picture of which channel changes occur in concert.

Channel width (W) is a very poor predictor of planform $\bar{\lambda}$ and $\overline{R_c}$ (Equations 4.16; 4.22; R^2 values of 0.30 and 0.20, respectively), contrary to the expectation arising from the Leopold and Wolman λ/W and R_c/W relationships (Equations 4.3; 4.5). Channel depth (D), is consistently related to planform scale (Equations 4.17; 4.23; R^2 values of

0.82 and 0.80), however the best predictor of channel planform scale (either $\bar{\lambda}$ or \bar{R}_c) is velocity (V) (Equations 4.18; 4.24; R^2 values of 0.90 and 0.93), which is, presumably, principally dependent on cross-sectional area ($W \times D$) and S . Given that D has a relatively constant relationship with planform scale, maintenance of an approximately constant V - planform scale relationship requires that adjustments in W and S occur in concert. Thus, while neither W nor S is well correlated with planform (Equations 4.16, 4.19, 4.22 and 4.25), the product of W and S is (Figure 4.10). Channel slope is adjustable through changes in sinuosity, hence channels that are forced to become exceptionally wide, through, for example, the presence of in-channel vegetation, can adjust by increasing their sinuosity and thereby reducing their gradient.

Table 4.3: Equation parameters for all study streams for linear functions of the form:

$$\bar{\lambda} = M(W \text{ or } D \text{ or } V \text{ etc}) + B$$

and

$$\bar{R}_c = M(W \text{ or } D \text{ or } V \text{ etc}) + B.$$

	$\bar{\lambda}$				\bar{R}_c			
	M	B ⁽¹⁾	R ²	Eq. #	M	B ⁽¹⁾	R ²	Eq. #
W	7.8	0	0.30	(4.16)	2.4	0	0.20	(4.22)
D	144	0	0.82	(4.17)	44.5	0	0.80	(4.23)
V	497	0	0.90	(4.18)	130	30	0.93	(4.24)
$S * 10^5$	14.7	0	0.67	(4.19)	4.5	0	0.67	(4.25)
$S_v * 10^5$	10.5	-190	0.50	(4.20)	3.2	-57	0.56	(4.26)
ω	10.6	260	0.88	(4.21)	3.2	83	0.94	(4.27)

⁽¹⁾All linear relationships have been forced through the origin, except where the use of a non-zero intercept results in an increase in R^2 value of greater than 0.04.

Sinuosity (P) is negatively correlated with specific stream power (ω) slope (S) and valley slope (S_v). Furthermore these three relationships are best described using logarithmic functions of the form $P = 2.67\omega^{-0.15}$, as provided in Table 4.4. Once again, correlation is no indicator of causation, however, at the very least, such modeling allows

identification of the sign of relationships (i.e. positively or negatively related) and the type (linear or logarithmic).

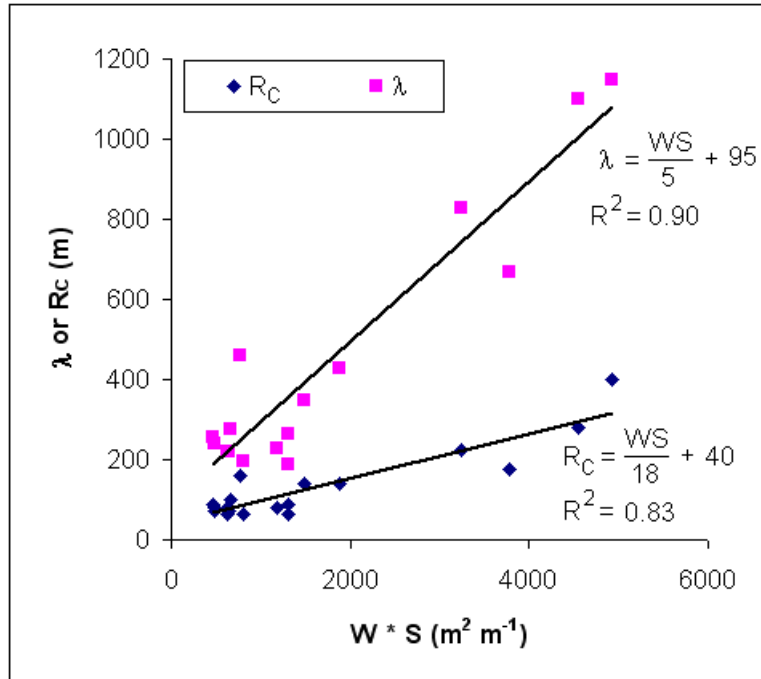


Figure 4.10: Linear relationships between planform scale ($\bar{\lambda}$ or \bar{R}_C) and the product of W and S for all study streams.

Table 4.4: Equation parameters for exponential functions of slope and stream power against sinuosity for all study streams. Square brackets indicate relationship not significant at the 95% confidence interval.

	P		R^2	Eq. #
	Coefficient	Exponent		
ω	2.67	-0.15	0.55	(4.28)
$S * 10^5$	10.7	-0.49	0.70	(4.29)
$S_v * 10^5$	12.2	-0.43	[0.19]	(4.30)

The strong inverse relationship between S and P (Equation 4.29) is unsurprising, as they are essentially reciprocals of each other over a uniform valley slope, with a straight reach necessarily steeper than a sinuous one. However, the lack of a significant positive relationship between P and S_V is surprising, in that adjustments in sinuosity are thought to be primarily a means of adjusting slope (Leopold and Wolman, 1957). Each imposed S_V change should be met with a P adjustment, resulting in a strong positive correlation between these two variables. Clearly, this is not the case, with any planform responses to imposed S_V being masked by other controls on P . It is inferred that these other controls are those variables which, independently of S_V , affect W , thus requiring concomitant adjustments in S through P . Reconsideration of the distribution of bank strength coefficient values presented in the previous chapter presents a possible mechanism by which this adjustment occurs.

Attention is drawn to the negative correlation between P and ω (Equation 4.28), plotted in Figure 4.11. It can be seen that sinuous reaches exist at very low specific stream powers, below in fact previously identified thresholds which supposedly define the lower limit of streams which actively meander (e.g. Ferguson, 1981, 1987; Nanson and Croke, 1992; van den Berg, 1995). The fact that the lower reaches of the Mehi and Moomin have both high sinuosity and very low stream power is suggestive of an unusually non-uniform distribution of boundary shear. This is because development of a highly sinuous channel implies active channel bank retreat, which would not seem possible if the estimated specific stream powers of $1\text{--}2 \text{ W m}^{-2}$ were distributed between bed and banks in the standard manner (as described by Huang and Warner, 1995, in Figure 3.18).

As discussed in the previous chapter, channel width is partly a function of bank strength, or more precisely, bank strength relative to the expenditure of stream energy on the banks. It may therefore be supposed that channel reaches that have high C_W values, indicative of a disproportionately high energy expenditure on the banks, will also have high sinuosities. This is because channels having high C_W values will be relatively wide, and hence, as discussed above, relatively gentle in slope and relatively sinuous. Indeed, there is a positive correlation between C_W and P which, though not being very strong ($R^2 = 0.52$), is still significant at the 95 % confidence interval.

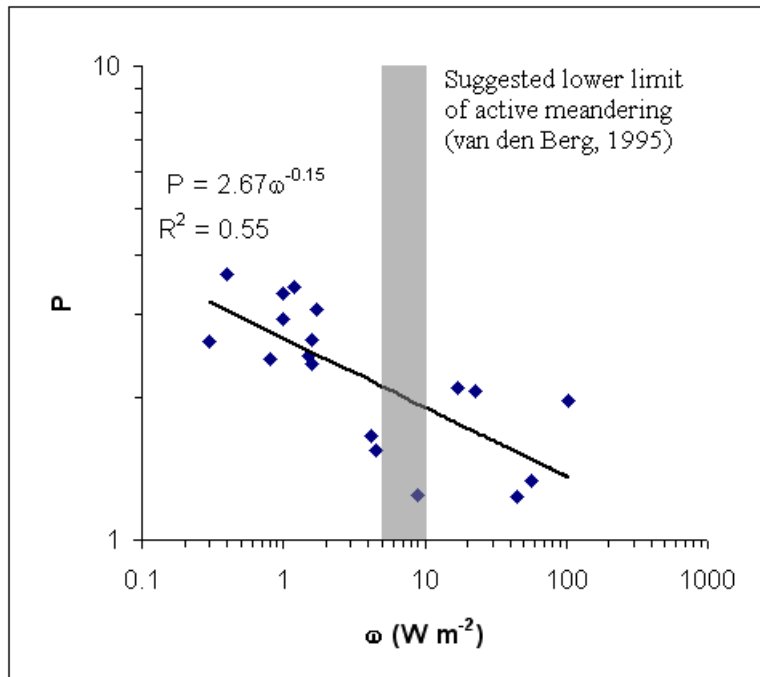


Figure 4.11: Relationship between sinuosity (P) and stream power (ω) for all study streams. Note logarithmic scale on both axes.

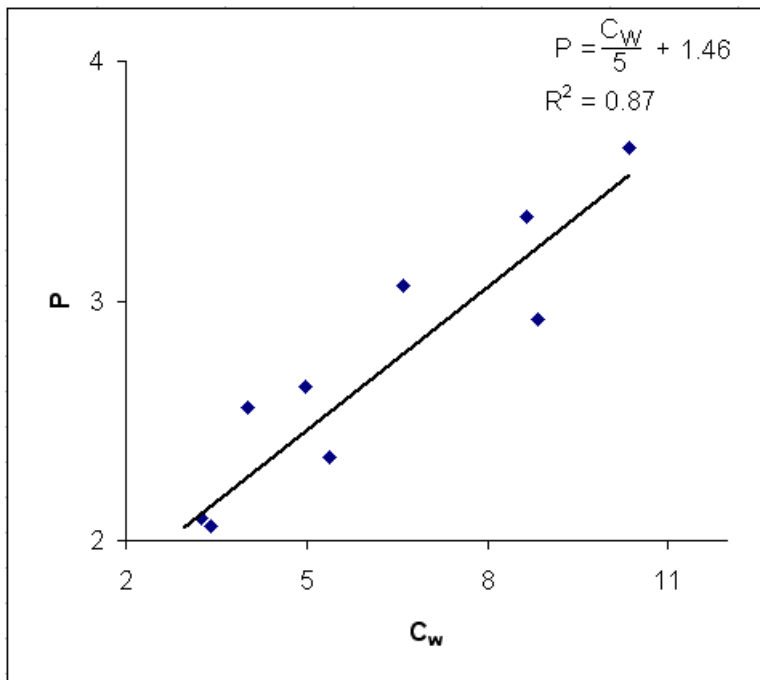


Figure 4.12: Relationship between sinuosity (P) and bank strength (C_w) for the Mehi, Carole and Moomin.

The bedload differential that exists between the streams may obscure the $P - C_W$ relationship (resulting in the low R^2 value mentioned above), as the bedload carrying Gwydir River is also the straightest. A mobile bed provides a further avenue to express oscillatory tendencies, albeit in the vertical plane (Hickin, 1977), possibly supplanting the need for channel meandering. A clearer $P - C_W$ relationship emerges if the Gwydir River is excluded from the analysis. When restricted to just the reaches of the Mehi, Moomin and Carole for which C_W can be reliably calculated, the $P - C_W$ relationship is very strong ($R^2 = 0.87$, Figure 4.12).

4.5.3 Planform – Discharge Relations and Palaeohydrology

Two planform scale - Q_{bf} relations can be constructed (Figure 4.13; Equations 4.31, 4.32) for the contemporary channels of the Gwydir distributary system. Contrary to the expectation arising from inspection of Equation 4.6, both the relationship between $\overline{R_C}$ and Q_{bf} , and the relationship between $\overline{\lambda}$ and Q_{bf} are best described using simple linear functions. In the range occupied by the study channels, the $\overline{\lambda}$ - Q_{bf} relation described here is bracketed by the Leopold and Wolman (1957) relation below and most other similar relations (e.g. Dury, 1977) above. As such, both the $\overline{\lambda}$ - Q_{bf} and the $\overline{R_C}$ - Q_{bf} relations described here fall within the range of previously described λ - Q_{bf} relations and can be taken as regionally specific palaeohydrological retrodictors. However, Williams (1983; 1984) argues that the results of regression analyses should not be manipulated algebraically for palaeohydrological retrodiction. Rather, the regression analysis should be re-run using the variable to be predicted as the dependent variable, even if the variable is not dependent in a physical sense. The equations presented below are the results of least squares regression analysis of the same data as that in Figure 4.13 conducted after reversing the dependencies of the variables.

$$Q_{bf} = 4.59\overline{R_C} - 370 \quad (R^2 = 0.90) \quad (4.31)$$

$$Q_{bf} = 1.31\overline{\lambda} - 311 \quad (R^2 = 0.86) \quad (4.32)$$

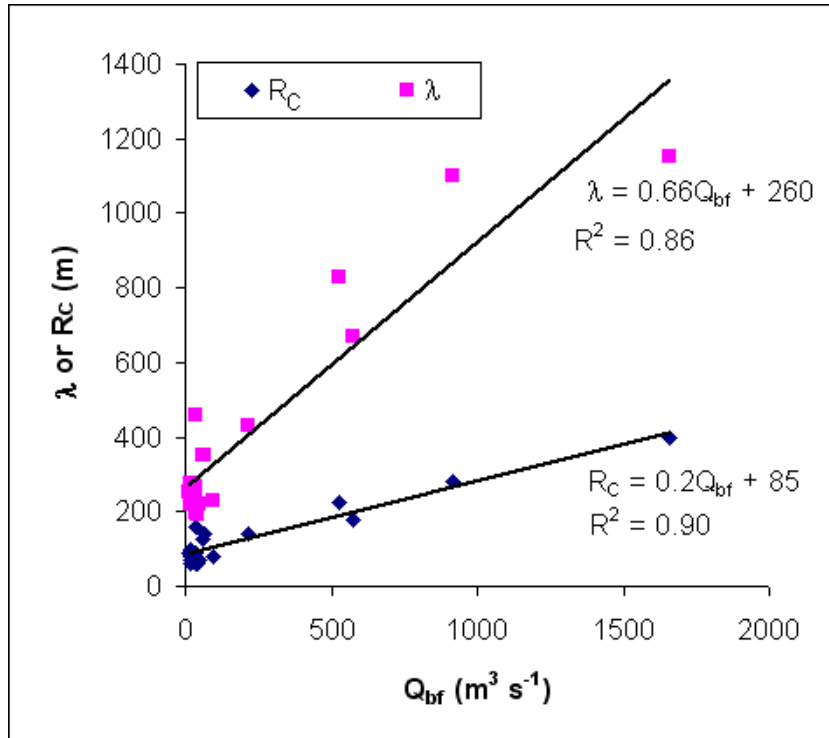


Figure 4.13: Relationship between channel planform scale ($\bar{\lambda}$ or \bar{R}_C) and bankfull discharge.

P , $\bar{\lambda}$ and \bar{R}_C values have been determined for the four best preserved palaeochannel reaches on the Gwydir fan-plain, plotted in Figure 4.1. Equations 4.31 and 4.32 have been used to estimate discharges carried by these palaeochannels with the results provided in Table 4.5.

Table 4.5: Palaeochannel discharge estimates from planform analyses.

Palaeochannel	P	\bar{R}_C (m)	$\bar{\lambda}$ (m)	Est. Q_{bf} from \bar{R}_C (Eq. 4.31) ($m^3 s^{-1}$)	Est. Q_{bf} from $\bar{\lambda}$ (Eq. 4.32) ($m^3 s^{-1}$)	Average Estimated Q_{bf} ($m^3 s^{-1}$)
Coocalla	1.63	631	2454	2523	2903	2710
Kamilaroi	2.52	355	1282	1257	1368	1310
Kookabunna	1.84	316	1298	1080	1389	1240
Mia Mia	1.72	562	2210	2209	2580	2390

The two palaeohydrological techniques provide results that are in reasonable agreement. In the case of the Coocalla palaeochannel, the $\sim 400 \text{ m}^3\text{s}^{-1}$ disparity between the techniques probably reflects the difficulty in defining meander couplets within the Coocalla palaeochannel. As meander couplets are not as clear in the Coocalla palaeochannel as in the other three palaeochannels, its mapped planform is probably not as accurate. This would have a greater impact on the measurement of $\bar{\lambda}$ than $\overline{R_c}$, for while individual bends are readily discernable, the contiguity of couplets of bends is less certain. Even so, the average values presented here provide clear indication of the decline in channel capacity over time, with the values presented here in stark contrast to the estimated total channel capacity of the contemporary system ($\sim 200 \text{ m}^3\text{s}^{-1}$ ‘mid-fan’ – see Figure 2.10). The significance of these palaeochannel discharges is discussed in Chapter 8, which focuses in the Late Quaternary evolution of the Gwydir fan-plain.

The average palaeodischarges presented in Table 4.5 are considerably different from those that would be calculated using palaeohydrological relations from the literature. Using the Dury (1977) equation, for example, would result in palaeodischarges that are between 0.58 and 0.91 times the values presented here. Although relations from the literature have had wider testing, it is unlikely that their use for the Gwydir palaeochannels would result in greater accuracy in palaeohydrological estimates. Firstly, definition of planform variables, specifically the exact method of measurement, is rarely reported in conjunction with derived relations (Williams, 1984) and therefore the application of these derived relations to a data set collected in a possibly different manner is questionable. Where the data set has been collected using a wholly different manner, such as is the case here where series analysis and frequency distributions have been used, it is even less likely that relations from the literature are likely to be applicable. The second reason for using a locally derived equation is that applying previously derived relations usually requires a degree of geographical extrapolation, whereby the environments in which the relations have been built are quite different from the environments where they are subsequently applied (Williams, 1984). However, even when using locally derived relations some level of environmental extrapolation is necessary if the palaeo-environment was different from the present environment.

4.6 Summary of Channel Planform

Planform characteristics can be analysed objectively to produce accurate descriptions of the relationships between planform, hydraulic geometry and discharge. Establishing cause and effect within these relationships remains a challenge because no truly independent variables could be identified, however, exploration of simple correlations amongst variables allows traditional explanations for planform differences between channels to be tested. The channels of the Gwydir distributary system display planform characteristics that are interestingly different compared to previous empirical models of stream planform development. Meander size ($\bar{\lambda}$ and \bar{R}_c) is scaled to depth, velocity, stream power and discharge, but not to width as has traditionally been proposed (e.g. Inglis, 1949; Leopold and Wolman, 1960; Hey, 1976), and sinuosity increases where imposed slope and stream power decline, rather than increasing with increasing slope and power, as proposed by Leopold and Wolman (1957), Schumm *et al.* (1972) and Schumm and Khan (1972).

Objective methods of channel planform analysis have been used here to both directly describe channels (\bar{R}_c) and to test the rigour of more subjective methodologies ($\bar{\lambda}$ and P). The subjective method of λ determination used here did not make use of the representative reach approach, but rather was based on averaging the values measured from all subjectively identified meander couplets. Not surprisingly this approach appears to provide results consistent with the more objective series approach, as it too is an average of all measurable meander couplets. Interestingly, both these approaches produce values that are *linearly* related to discharge, at least within the range of values present in the Gwydir distributary system. This is likely to be a result of the relatively small weighting placed on large meander couplets, which, due to their size, are necessarily fewer in number than smaller meander couplets. Previously determined non-linear relations based on the representative reach approach (e.g. Dury, 1977) are possibly the result of a tendency to overlook small scale meandering in favour of a small number of large well-defined meander couplets. This would occur less so at higher discharges as even ‘small’ meander couplets become easily distinguishable from random perturbations. Relations built using the representative reach approach will

therefore have an inherent tendency to flatten as discharge increases, regardless of any physical limit on meander size.

Application of the techniques described here has revealed that each of the channels of the Gwydir distributary system displays a distinct form of downstream planform development. Adjustments in planform scale in the Gwydir and Mehi are apparently directly related to changes in discharge, with the techniques used being sensitive enough to measure planform scale changes downstream of confluences. The Moomin and Carole however, show no real development in planform scale in response to discharge change. Insights into possible compensatory mechanisms that could enable this are available via investigations of downstream developments in sinuosity, along with reconsideration of the hydraulic geometry interpretations outlined in Chapter Three.

The non-responsiveness of width to discharge decline for the Carole and Moomin provides a limit on the decline in scale of channel meandering in these streams. Although discharge is declining downstream, the scale of meandering is prevented from declining by the 'over-wide' nature of the channels. To achieve this decline in discharge in the presence of a constant width, slope appears to be declining rapidly through the adoption of a meandering habit, which, in turn, is made possible by the concentration of stream energy at the bank. The channels would not be able to migrate and form meanders if this was not so. There is an admitted circularity in this description, which is somewhat inevitable in the absence of a physically-based model. However, it does suggest the integral role probably played by vegetation in this relatively low energy and well-vegetated channel environment in shaping both planform and cross-sectional form of fluvial channels.

The final observation provided in this chapter is both the most straightforward and perhaps the most significant. That is, the observed decline in estimated channelised flow on the Gwydir fan-plain through recent geological time. The four palaeochannels analysed record in their dimensions a hydrological picture very unlike the present, and although the values provided in Table 4.5 are just estimates, it is clear that the bankfull discharges of the palaeochannels of the Gwydir fan-plain are very much larger than any carried by the present system.

Chapter Four has focused on the decline in channelised flow as expressed in planform, with the techniques developed enabling observation of the dramatic difference in scale and discharge between the contemporary and relict systems. The following chapters will shift the focus of the thesis to the relict systems themselves, particularly their age and the climatic significance of the changes in flow regime. In Chapters 5 and 6 luminescence methods used to analyse both the relict and contemporary systems are outlined, with resulting further insights into the functioning of the contemporary system are included in Chapter 6. The chronology of the palaeosystem is developed in Chapter 7, with a discussion of the Late Quaternary history of the fan-plain in the context of other evidence for southeastern Australia provided in Chapter 8.

Chapter 5 Geochronological Methods

5.1 Introduction

Previous chapters have examined the spatial distribution of channel forms. It is clear from results of investigations into palaeochannel planforms that changes through time have been as significant, if not more so, than the downstream changes of the contemporary system. The first step in describing and attributing causes to these changes is the development of an accurate chronology for palaeochannels and their associated deposits. The Gwydir system provides an excellent opportunity to examine both contemporary and Quaternary changes in channel form and behavioural response to changes in flow characteristics.

This chapter presents a thermoluminescence (TL) – derived chronology for the palaeochannels of the Gwydir distributary system. A comparative dating exercise using both TL and optically stimulated luminescence (OSL) for a subset of the collected samples has been undertaken. This revealed a considerable age disparity between the techniques. The reasons for this disparity are explored and resolved below. Arising directly out of this investigation was the realization that an improved method of OSL analysis was required. In collaboration with Dr Jon Olley and Professor Richard Roberts, an improved method was developed, tested and has subsequently been published (Olley *et al.*, 2004a).

5.2 Existing Geochronological Data for the Lower Gwydir

Prior to this study very little geochronological information on the surficial sediments of the lower Gwydir existed. Some palynological data has been collected (Martin, 1980), which suggests a mid-Miocene age for the base of unconsolidated sediments near Moree; and burial of artefacts, including entire fence-lines (Riley and Taylor, 1978; Mahaffey, 1985), indicates that accretion is continuing to the present day. An assessment of the expected approximate age of lower Gwydir palaeochannels is available in the form of aggradation rate estimates for the plain: about 1 m in 50 ka

(Riley and Taylor, 1978), which gives an approximation of the length of time palaeochannels, typically standing 1-2 m above the surrounding plain (see Chapter 2), should remain visible at the surface. Alternative indicators of the likely ages of lower Gwydir palaeochannels are available from dated fluvial deposits in the adjacent valleys (Figure 5.1). Palaeochannels of the Namoi River (which bear a general resemblance to the lower Gwydir palaeochannels) have been TL dated at two sites by Young *et al.*, (2002) to between ~ 18 ka and ~ 6 ka, with the shift to the contemporary hydrologic regime sometime thereafter. In the Bellinger and Nambucca Valleys to the immediate east considerably more dating (TL, OSL and conventional and accelerator mass-spectrometry (AMS) radiocarbon (^{14}C)) has been undertaken (Warner, 1970; 1972; Nanson and Doyle, 1999; Doyle, 2003; Cohen, 2003), a synthesis of which was recently presented by Nanson *et al.*, (2003). They identify clustering of high terrace ages at ~50 ka, ~30 ka and, most clearly, between 20 and 13 ka. These deposits are attributed to enhanced fluvial activity producing thick floodplains, the remnants of which exist as high terraces. Nanson *et al.* (2003) attribute an absence of dates from the early Holocene on the coastal rivers of NSW as also indicating enhanced fluvial activity, arguing that during this time sediment flushing predominated over sediment deposition. The late Holocene, after about 4 ka, saw the onset of a period or relative fluvial quiescence in the Bellinger and Nambucca Valleys, characterised by vertically accreted floodplains, with narrow channels liable to debris-induced avulsion.

Full consideration will be given in Chapter 8 to the chronology of the Gwydir system in the context of other work done in south-east Australia. However, as a working hypothesis based on the extrapolated deposition rates from Martin (1980) and Riley and Taylor (1978), it may be suggested that the surface palaeochannels of the lower Gwydir are no older than Late Pleistocene. Furthermore, it might be expected that, just as the large palaeochannels of the Namoi (dated to ~ 18 ka) seem to correspond with high terraces of adjacent coastal valleys, indicating a commonality of cause most probably climate change, palaeochannels of the lower Gwydir may likewise have formed during regionally significant 'fluvial phases'. Additionally, if the shift to hydrologically quiescent conditions in the Namoi, Nambucca and Bellinger Valleys was driven by extrinsic factors (i.e. climate change) then it might be expected that no large sandy palaeochannels of the Gwydir fan should date to younger than about 4 ka, which

appears (in adjacent valleys) to be the maximum age of sediments related to the present climatic regime.

The indications available from adjacent valleys and previous investigations in the study area suggest that palaeochannels of the lower Gwydir may be unsuited to radiocarbon (^{14}C) dating. In addition to the dearth of suitable material available in the study area (only one site, GF-24, yielded suitable carbon), and the possibly questionable relationships between the age of interned carbon and the timing of its deposition (Blong and Gillespie, 1978), there is a high likelihood that at least some of the surface palaeochannels in the study area will be beyond the limit of ^{14}C . Luminescence dating, particularly OSL dating, therefore appears to be the most appropriate technique. It has a range far in excess of the 40 ka limit associated with conventional ^{14}C dating (Aitken, 1990), and it is based on quartz which is ubiquitous in the study area.

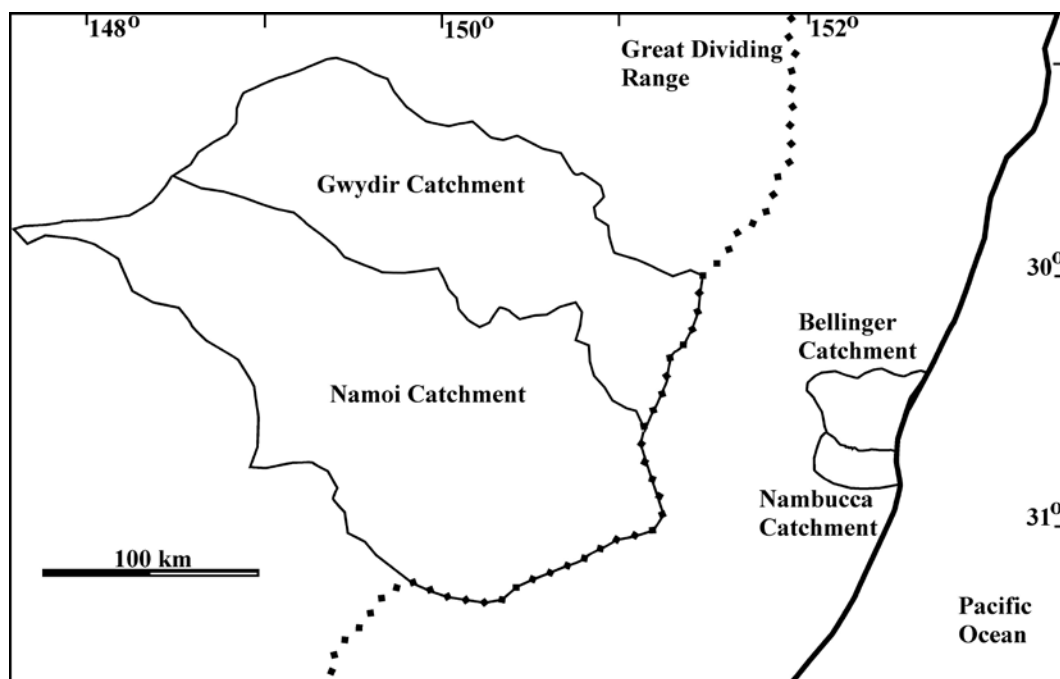


Figure 5.1: Location of nearby catchments with dated palaeochannels and terraces.

5.3 Sample Collection

As luminescence techniques are designed to provide a measure of time since last exposure to sunlight, protecting the sample from light is the over-riding consideration

during sampling. Even small amounts of light (natural or artificial) can significantly erode the luminescence signal and result in age under-estimation. Accordingly, most samples were collected by driving a light-safe tube either horizontally into a cleaned face or vertically into the base of an auger hole. This latter approach was facilitated by attaching the collection tube to lengths of steel rod, with the uppermost rod attached to a slide hammer. In the case of samples taken from vertical faces, collection tubes of 30 cm length were used, however, for down-hole sampling, tubes of 40 cm length were used. This was to ensure that the tubes were long enough to be driven through any material that had sloughed off from the side of the auger hole and collected at the hole's base. After sampling, the tubes were capped at each end and double-wrapped in thick black plastic. When returned to the laboratory, material from the first 5 cm (10 cm in the case of down-hole samples) of each end of each tube was discarded and only material from the centre of each tube was processed further.

The second consideration in sampling was to ensure that material to be dated was collected from within a 30 cm radius sphere of uniform material. This was necessary because no field measurements of radioactivity were able to be made, and therefore the concentration of radioactive elements in the samples was assumed to be representative of the radioactive concentration of the surrounding sediment (30 cm is considered to be the size of the sphere of influence from which a sample receives its dose - Aitken, 1985). While the extent of uniform material in all three dimensions was more readily assessable in the case of cleaned faces, such assessment was for down-hole samples is severely limited. Because most of the lithological variation in sedimentary strata is vertical, the auger holes were extended below the sampling depth to check that the uniformity of the sediment below the sample was similar to that above.

5.4 Luminescence Dating of Sediments

When quartz grains are buried, they begin to accumulate a population of electrons and electron holes trapped between the valence and conduction bands in crystal defects (Figure 5.2). The trapped electrons and electron holes originate from atoms ionized by incoming radiation (α , β , γ , cosmics), with measurement of the trapped charge population undertaken via laboratory evicition using either heat (TL) and/or light (OSL).

Photons produced upon recombination of the released electrons with electron holes associated with luminescence centres are related in number to the received ionizing radiation dose. Given chemical stability, the lithogenic dose rate is taken as constant over the burial period (Aitken, 1985), as the half-lives of the main parent nuclides concerned (^{238}U , ^{234}Th , ^{40}K) are many orders of magnitude longer than the practical range of luminescence dating.

Exposure to sunlight releases the light-sensitive trapped electrons, thereby resetting the luminescence signal; a process commonly referred to as ‘bleaching’. The time elapsed since sediment grains were last exposed to sunlight can be determined by measuring the luminescence signal from a sample of sediment, determining the equivalent natural dose (D_e) in grays (Gy) that this represents, and estimating the rate of exposure (D_r) in Gy ka^{-1} of the grains to ionising radiation during burial (Huntley *et al.*, 1985; Aitken, 1998). The burial age, in ka, of a sample may be obtained from the following equation:

$$\text{Burial Age} = \frac{D_e}{D_r} \quad (\text{Equation 5.1})$$

5.5 TL Dating

5.5.1 Introduction

In TL analyses, raising the temperature of the sample through defined temperature bands liberates all the available trapped electrons in a specific trap type. A TL glow curve (photon count vs. temperature) will display various peaks, each corresponding to a population of de-trapped electrons from a specific trap (Figure 5.3). This is because trapped electrons escape in a stochastic manner at a rate dependent on temperature, with peaks in a TL glow curve the result of the 100 % likelihood that all the trapped electrons will escape. At environmental temperatures, the likelihood of escape is very much lower than 100 %. For high energy traps, such as the ‘375°C’ trap generally used in TL dating, the probability of escape at environmental temperatures is virtually zero. It can therefore be assumed that electrons trapped in the 375°C trap will not escape during burial.

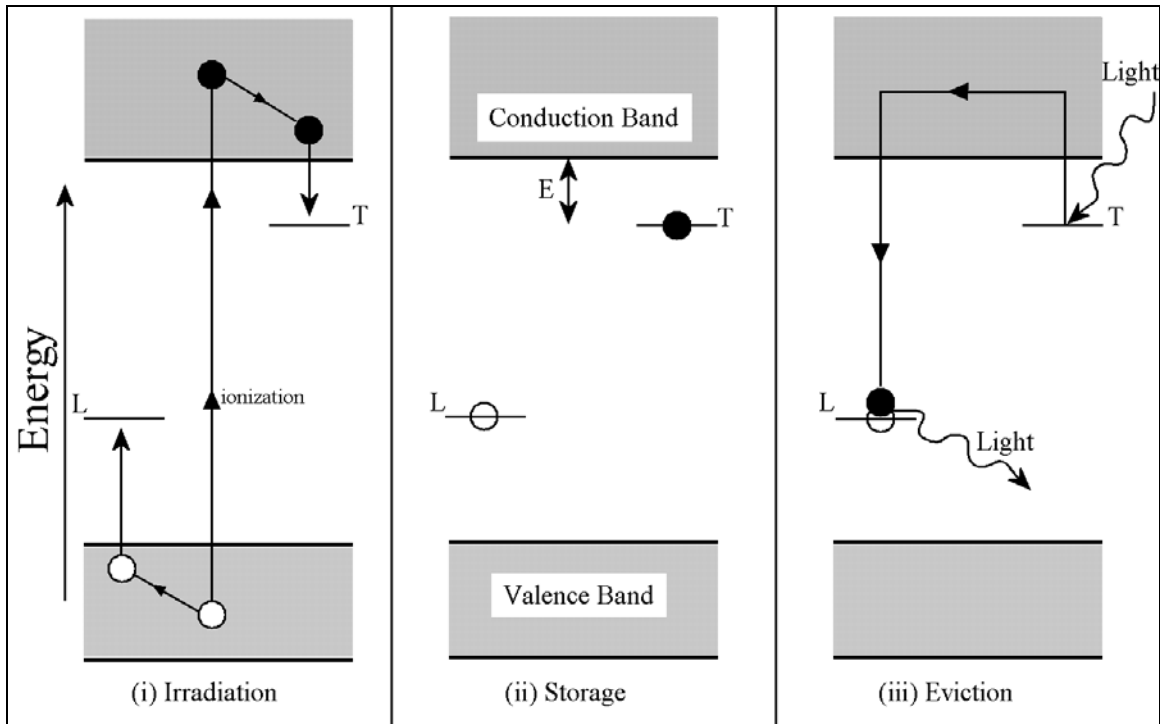


Figure 5.2: Energy-level representation of luminescence (after Aitken, 1998). (i) Collisions with high energy neutral particles (e.g. γ photons) or attraction/repulsion by charged particles (e.g. α and β) provide sufficient energy for electrons (carriers of negative charge) (here symbolised as filled circles) in the valence band to be moved into the conduction band, where they are free to diffuse through the crystal until falling into the 'forbidden' gap and becoming trapped at a defect. Likewise, the electron vacancy or 'hole' (carrier of positive charge, here symbolised as open circle) can diffuse through the valence band, becoming trapped at (or 'activating') a luminescence centre. (ii) Electrons remain trapped for lifetimes accordant with the depth of the trap (i.e. the energy necessary to move it back into the conduction band) and the storage temperature. OSL analyses aim to sample electrons from light-sensitive traps that have depths sufficient to exceed the stochastic reach of the burial time. One such trap, the '325°C' trap has an energy depth of about 1.6eV (iii) Photons with energy equal to that necessary to lift the electron to the conduction band are administered to de-trap the population of electrons. These are then free to diffuse through the crystal lattice and recombine with a lower energy hole. If the hole is at a luminescence centre then the recombination results in the production of a photon (with energy equal to the difference between the excited and recombination states). Alternatively, and more likely, the recombination can be at a 'killer' centre, where a phonon is released rather than a photon.

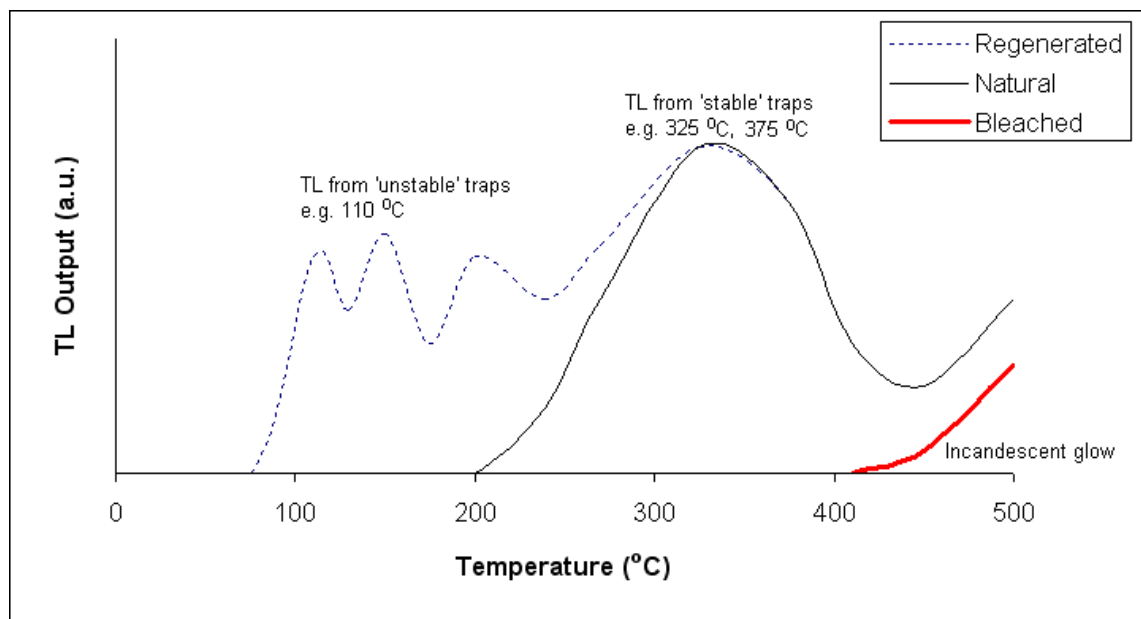


Figure 5.3: Elements of a TL glow curve. For quartz irradiated naturally (thin solid line), only the long lived, high temperature traps contribute to the emitted TL. For quartz recently irradiated (dashed line), short-lived, low temperature traps also contribute to the emitted TL. For quartz that has been completely bleached of trapped charge (thick solid line) only an incandescent glow is emitted.

The energy depth of a trap not only determines its rate of emptying, but also its behaviour when exposed to sunlight. The 375°C trap requires prolonged exposure to the ultraviolet (UV) component of the solar spectrum to empty. For this reason the 375°C trap has been labelled a slowly bleaching trap (Franklin *et al.*, 1992) as distinct from the 325°C ‘rapidly bleaching trap’. Various studies (Smith *et al.*, 1986; Spooner *et al.*, 1988; Spooner 1994) have demonstrated that the 325°C trap is the same as that sampled in the initial stages of OSL analysis. Because of the differences in bleaching characteristics of the TL trap and the OSL trap, reservations persist regarding the suitability of TL dating in sedimentary contexts as transport events may not result in sufficient exposure time, and/or may occur beneath a UV-attenuating water column. Notwithstanding these theoretical constraints on the use of TL dating, experience in Australia has generally shown that the method can be applied with a high degree of success to fluvial samples. This is probably a result of the ideal bleaching conditions produced by Australian

environments, where river bed sands may be exposed and re-exposed at the surface of bars through multiple summers.

Samples collected for TL analysis were prepared and analysed by David Price in the University of Wollongong (UW) TL laboratory under subdued yellow light. The methods outlined below are identical to techniques successfully applied in numerous other similar dating programs (e.g. Nanson *et al.*, 1992; Page *et al.*, 1996; Nanson *et al.*, 2005). A total of 15 TL samples were collected, with nine gravel pits, sunk in obvious palaeochannel deposits, and one sand dune sampled (Figure 5.4).

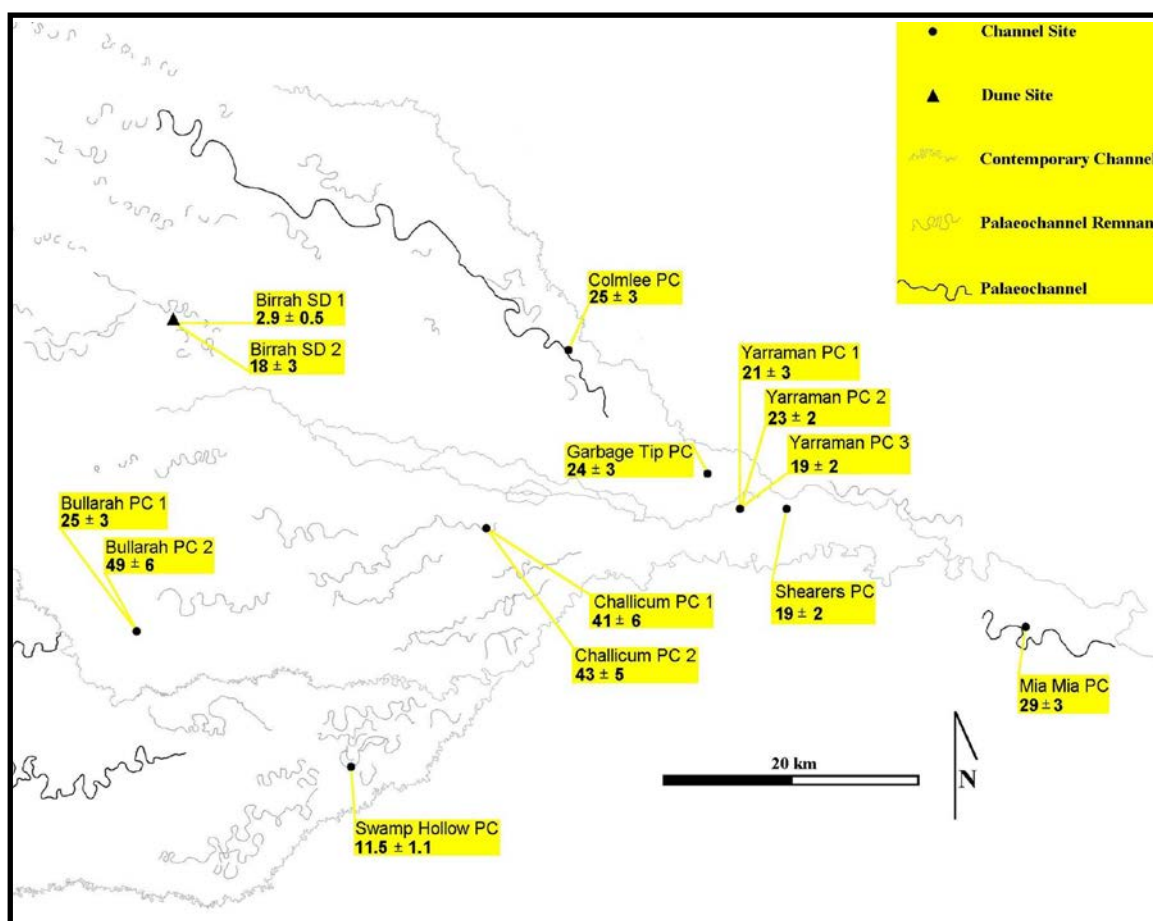


Figure 5.4: Location and calculated ages (in ka) of TL samples.

5.5.2 Sample Preparation Procedures

1. Removal of fines by multiple washings in ultrasonics as appropriate.
2. Wet sieving to obtain the 90-125 μm fraction.
3. 10 minute etch in 15 % HCL to remove carbonates as appropriate.
4. Wash with 32 % hydrogen peroxide to remove organics as appropriate.
5. Heavy liquid separation (via centrifuge) in $\text{Na}_6(\text{H}_2\text{W}_{12}\text{O}_{40})$ solution (specific gravity 2.74) to remove heavy minerals.
6. 10 minute etch in 40 % HF to remove feldspars and the outer alpha irradiated rinds of quartz.

5.5.3 Sample Analysis

The UW TL laboratory determines a single palaeodose for each sample using the modified combined regenerative additive technique of Readhead (1984; 1988). The technique begins with the determination of an appropriate analysis temperature through observation of the relationship between a natural glow curve and one following laboratory irradiation. The plot of the ratio of natural TL to artificial TL against temperature plateaus when all the low temperature short lived traps have been evacuated (Figure 5.5). The plateau region identifies electron traps of lifetimes sufficient to greatly exceed the burial period. Once an appropriate analysis temperature (375°C for all samples in this project) has been identified, the averaged TL output of 8 aliquots (second-glow normalised) is plotted onto a dose response curve built using 24 laboratory bleached (24 hr under Philips MLU300 UV lamp) then dosed (plaque β source) aliquots. Further checks on the appropriateness of the interpolated D_e are provided through fitting so-called $N + \beta$ s, aliquots that have the Natural dose plus 1, 2, 3.... units of laboratory dose.

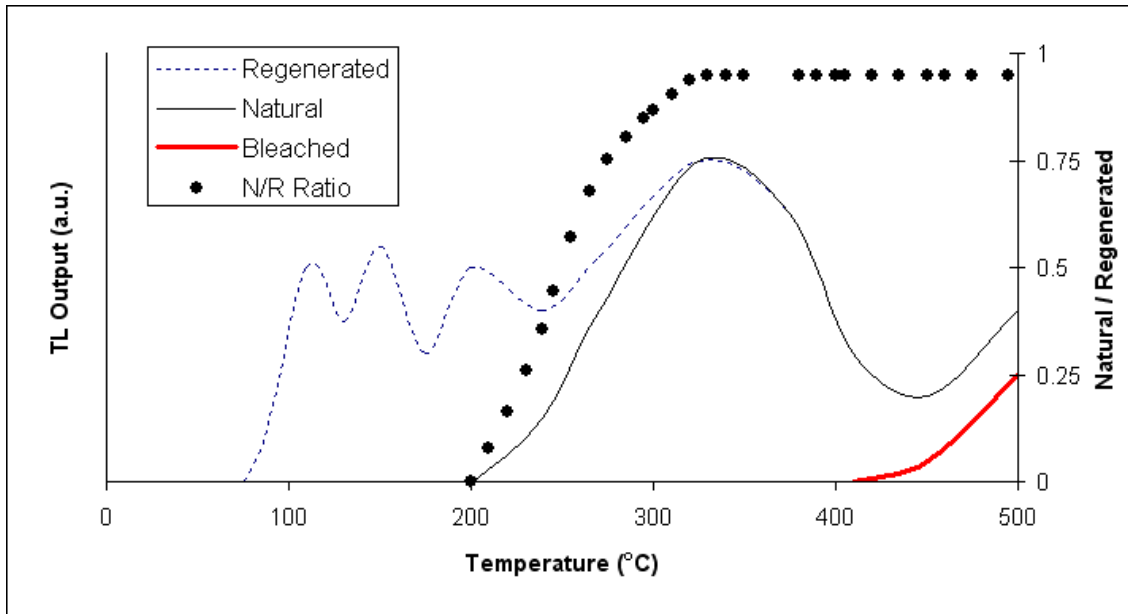


Figure 5.5: Plot of ratio of Natural to Regenerated TL output. The plateau represents the temperature range over which the TL resulting from the Natural dose can be compared to TL resulting from subsequent laboratory doses.

Previous studies at the University of Wollongong have demonstrated the equivalence of TL and OSL ages in some settings. One such study was conducted on samples from palaeochannels and floodplains of Coopers Ck by the author on behalf of a previous PhD student (Fagan 2001), with the results presented below (Table 5.1). Obviously, in the environs of Coopers Creek, the TL signal is bleached to much the same extent as the easier to bleach OSL signal.

Table 5.1: Results of Cooper Creek TL / OSL analysis (Fagan 2001).

Sample	TL Age (ka)	OSL Age (ka)
W2839	20.4 ± 1.6	21.1 ± 1.4
W2844	5.3 ± 0.5	4.2 ± 0.3
W2845	7.3 ± 0.6	6.1 ± 0.6
W2846	8.8 ± 0.7	7.5 ± 0.6
W2849	6.1 ± 0.5	7.3 ± 0.5
W2850	5.7 ± 0.6	7.2 ± 0.5

5.5.4 TL Results

Table 5.2: Details of samples taken for TL. Eastings and Northings are UTM zone 56J coordinates, rounded to the nearest 10 m. Uncertainties are as reported in TL laboratory report and incorporate all random and systematic errors. Sample names in parentheses indicate sub-samples also submitted for OSL analysis. PC = Palaeochannel, SD = Sand Dune

Sample	Eastings	Northings	Depth (m)	E _D (Gy)	Dose Rate (Gy ka ⁻¹)	Age (ka)
Yarraman PC 1	777500	6740770	7.5	39.6±5.2	1.895±0.049	20.9±2.8
Yarraman PC 2	777500	6740770	4.0	74.7±5.9	3.212±0.052	23.2±1.9
Yarraman PC 3	777500	6740770	2.8	58.5±6.3	3.044±0.051	19.2±2.1
Birrah SD 1 (GF_OSL/TL_1)	729250	6757300	3.5	11.0±2.0	3.753±0.062	2.9±0.5
Birrah SD 2	729250	6757300	6.0	56.2±9.9	3.178±0.058	17.7±3.1
Shearers PC (GF_OSL/TL_5)	781500	6740900	6.5	64.9±5.4	3.438±0.059	18.9±1.6
Colmlee PC (GF_OSL/TL_3)	763280	6754690	4.0	82.5±9.3	3.338±0.060	24.7±2.8
Weetah PC	801760	6730950	2.5	87.0±9.1	3.040±0.062	28.6±3.0
Garbage Tip PC (GF_OSL/TL_5)	774700	6744000	8.0	82.8±9.3	3.471±0.056	23.9±2.7
Challicum PC 1	756000	6739300	3.0	114±17	2.779±0.059	41.0±6.2
Challicum PC 2 (GF_OSL/TL_2)	756000	6739300	11.0	116±12	2.718±0.057	42.8±4.6
Bullarah PC 1	726160	6730530	5.8	70.3±7.4	2.770±0.060	25.4±2.7
Bullarah PC 2	726160	6730530	11.2	125±16	2.543±0.059	49.1±6.4
SwampHollow PC	744500	6719090	3.0	33.3±3.2	2.894±0.061	11.5±1.1

The TL results when viewed alone appear to mirror the findings of Young *et al.* (2002), in their study on the adjacent Namoi valley, with large palaeochannels operative up until 11 ka. However, in anticipation of the results of the TL / OSL comparative dating exercise, further discussion of the palaeoclimatic significance of the dates is deferred.

5.6 OSL Dating

5.6.1 Introduction

Optical dating has been used to date aeolian, fluvial, lacustrine and marine sediments (e.g. Olley *et al.*, 1999; Bailey *et al.*, 2001; Murray and Clemmenson, 2001; Radtke *et al.*, 2001; Hilgers *et al.*, 2001;) and in recent comparative exercises good agreement has been found between OSL dates and independent ages (Murray and Olley, 2002; Olley *et al.*, 2004a) (Figure 5.6). The principle theoretical advantage of OSL dating over TL dating is that it is based on the relatively low energy, light sensitive, 325°C trap, which is, as discussed above, easy to bleach. Transport events involving only short exposure times can therefore be dated with OSL.

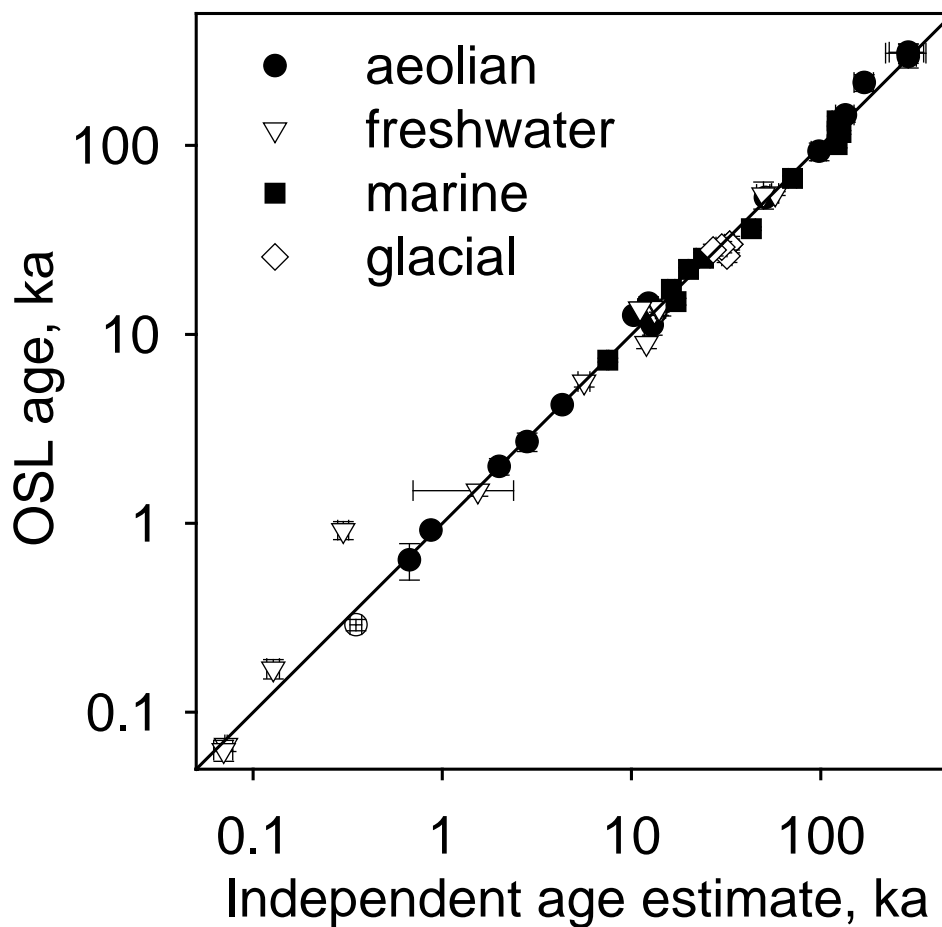


Figure 5.6: Age comparisons for 53 sites from numerous published sources. Some OSL ages are averages of multiple OSL dates of a single stratigraphic feature (after Murray and Olley, 2002).

OSL analytical strategies have evolved over the last ~ 20 yrs, with perhaps the most significant advances (save for the initial demonstration of OSL by Huntley *et al.* 1985) being in the form of development (Murray *et al.*, 1997; Murray and Roberts, 1998; Murray and Mejdahl, 1999) and formalisation (Murray and Wintle, 2000) of the Single Aliquot Regenerative-Dose (SAR) protocol. The SAR protocol involves comparing the intensity of the OSL produced on initial measurement (i.e. that resulting from radiation received while buried) to the intensity of OSL produced from a series of subsequent laboratory irradiations of the same aliquot (see Section 5.8 below). Several authors have questioned the universal applicability of the SAR protocol, with discussions focusing on sensitivity changes during measurement (e.g. Bailey, 2000; see Chapter 6). Despite these reservations, the SAR protocol has been widely adopted and is acknowledged by Wallinga (2002) and Murray and Olley (2002) to be the most appropriate technique for analysis of fluvial samples.

5.6.2 Sample Preparation

Sample preparation for OSL analyses were designed to isolate pure extracts of appropriately sized quartz grains. Treatments were applied to remove carbonates, feldspars, organics, heavy minerals and acid soluble fluorides, all of which are contaminants that can interfere with the analysis procedure. Application of hydrofluoric acid has the dual purposes of removing feldspars and etching the quartz grains. Quartz grains are etched to remove the outer α -irradiated rind of each grain. Unlike g and b radiation, α particles are heavily ionizing and thus unable to penetrate through a 180 μm quartz grain. By removing this outer rind, the analysis is restricted to just the inner core of each grain which has more or less been evenly irradiated.

Samples collected for OSL analyses were prepared by the author in the UOW OSL laboratory or the CSIRO OSL laboratory under subdued red light in the following manner:

1. Removal of fines by multiple washings in ultrasonics as appropriate.
2. Wet sieving to obtain the 180-212 μm fraction.
3. 10 min etch in 15 % HCl to remove carbonates as appropriate.

4. Wash with 15 % H_2O_2 to remove organics as appropriate.
5. Heavy liquid separation in $\text{Na}_6(\text{H}_2\text{W}_{12}\text{O}_{40})$ solution (specific gravity 2.74) to remove heavy minerals.
6. 24hr H_2SiF_6 wash to remove feldspars.
7. 5 minute etch followed by 40 minute etch in 40 % HF to remove feldspars and the outer alpha irradiated rinds of quartz.
8. 10 min etch in 15 % HCl to remove acid soluble fluorides.

5.7 TL/OSL Comparison

Table 5.3 shows the results of the OSL / TL comparative dating exercise with TL D_e s for five samples all being significantly lower than the sample of respective large aliquot OSL D_e s. Differences in the bleaching characteristics of TL-sensitive traps and OSL-sensitive traps are well understood (Huntley *et al.*, 1985; Smith *et al.*, 1986; Godfrey-Smith *et al.*, 1988; Spooner *et al.*, 1988; Spooner, 1994; Wintle and Murray, 1997; Stokes, 1999) and are often cited as being responsible for TL / OSL discrepancies. However, for the five samples analysed, the discrepancy is opposite in sense to that which can be explained by differential bleaching, *i.e.* the OSL D_e s, based on the rapidly bleaching 325°C peak are significantly *larger* than the TL D_e s. Exhaustive checks and re-analyses (using multiple instruments) of samples ruled out operator or instrumental errors in the analysis phase. As part of such checks extra samples were prepared in the OSL laboratory and D_e s determined using both OSL and TL on a single instrument by one operator, and on separate instruments by different operators. In both cases the tests showed the equivalence of D_e as determined using OSL and TL *as long as the sample was prepared identically*. It therefore appeared that the reason for the discrepancy between the OSL and TL D_e s outlined in Table 5.3 lay in the different preparation regimes.

Table 5.3: Comparison of D_e produced on large (3 mm) aliquots of quartz using OSL vs. TL. Note that the OSL D_e s presented here differ from the final given D_e s because they are based on large aliquots, analysed using the standard SAR protocol.

Sample	TL D_e	OSL D_e	TL/OSL
GF_OSL/TL_1	11.0 ± 2.0	19.5 ± 2.0	$56 \pm 12 \%$
GF_OSL/TL_2	116 ± 12	180 ± 25	$64 \pm 11 \%$
GF_OSL/TL_3	83 ± 9	125 ± 8	$66 \pm 8 \%$
GF_OSL/TL_4	65 ± 5	105 ± 10	$62 \pm 8 \%$
GF_OSL/TL_5	83 ± 9	108 ± 8	$77 \pm 10 \%$

An extensive review of each stage of the OSL preparation procedure was undertaken to investigate the possibility that the OSL D_e was being artificially elevated. Extra care (multiple heavy liquid separations, agitation during etching, use of fresh acid batches) was taken to ensure the purity of fresh sub-samples of each of the samples, however, analysis of these duplicate samples revealed no difference in D_e s from the original five samples. Attention then turned to the preparation techniques used in the TL laboratory. The two main differences between the OSL and TL preparation procedures are the HF etching times and the lighting conditions of the laboratories, and it is one or both of these factors that are thought to be responsible for the age discrepancy.

Step 6 in the OSL preparation procedure is designed to remove feldspars. Experience showed that without this step, most samples still produced an infra-red stimulated luminescence (IRSL) signal (which is known to be emitted by feldspar but not quartz) following 5 + 40 mins of etching. Furthermore, some samples still had a detectable IRSL signal (albeit small) after *one week* of fluoro-silic acid treatment. A literature search revealed that this is not unprecedented with the presence of feldspars after prolonged HF etches having been reported for Californian aeolian sands (Rendell and Wood, 1994; Rendell *et al.*, 1994). For the Gwydir samples feldspar grains were ‘surviving’ the HF treatments. Furthermore, the samples prepared for TL analysis, with only a 10 min HF etch (Step 6 section 5.5.2) and no H_2SiF_6 wash had considerably more contaminant feldspars than the respective OSL prepared sample (Figure 5.7). It is possible that these contaminant feldspars were free grains that were particularly resistant to etching. An alternative explanation is that the feldspars existed as (partial)

inclusions within some quartz grains and were therefore (partially) shielded from the etching effects of the HF. The still present IRSL signal from some OSL prepared samples after one week of flourosilic acid treatment points to this later explanation, at least for some samples.

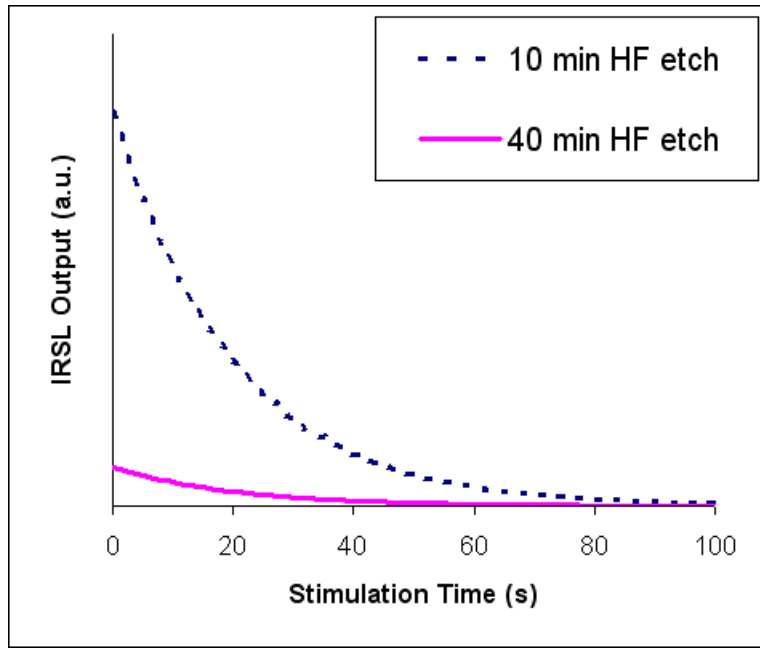


Figure 5.7: Comparison of the IRSL (emitted from feldspar but not quartz) output from 2 subsamples of GF-OSL/TL_4.

Age underestimation for TL analyses of feldspars or samples containing feldspars has been widely reported (Debenham, 1985; Balescu *et al.*, 1989; Grun *et al.*, 1989; Rendell, 1992; Packman and Grun, 1992; Wintle, 1993; Berger, 1994) and relates to both trap retention lifetimes of feldspars (both thermal and athermal or ‘anomalous’) and to the overlapping emission spectra of quartz and some feldspars (Huntley *et al.*, 1988; Andersson *et al.*, 1990; Andersson *et al.*, 1991). The phenomenon of ‘anomalous fading’, i.e. depletion of trap populations, especially in feldspars, at a rate faster than predicted by kinetics calculations (Aitken, 1985) may also be relevant here. However, Berger (1994) has argued that age underestimation could result from operator behaviour alone (i.e. choice of detection filters and laboratory light sources, or use of peak integration across curve ranges encompassing multiple trap lifetimes).

Anomalous fading was first recognised (Wintle, 1973) in feldspars derived from volcanic areas, and therefore any feldspars occurring as contaminants in the samples,

(being derived from an area rich in volcanics – see Figure 2.7) would quite probably have had partially depleted natural signals. The level of anomalous fading could be quite small, as the brightness of feldspar relative to quartz (Krbetschek *et al.*, 1997) would emphasise even a small amount of fading.

An alternative suggestion is that the lighting conditions in the TL laboratory were such that the natural TL signal from the feldspar (or even the quartz) was inadvertently bleached during sample preparation. Feldspars are usually prepared for luminescence investigation under far more austere lighting conditions than used for quartz preparation. Tests on other samples have shown that the lighting conditions in the TL laboratory are ‘safe’, (Price, *pers. comm.*), though this may not be the case for all mineral varieties. In general the TL signal from feldspar is bleached at a slower rate than the TL signal from quartz (Godfrey-Smith *et al.*, 1988); however, peculiarities in feldspar mineralogy can result in complex emission behaviour, with Krbetschek *et al.* (1997) commenting in relation to feldspar that:

“it is becoming clear that nature has been extravagant in creating mineral species with a wide range of individual luminescence behaviour”.

Some feldspar TL peaks can be very light sensitive (Robertson *et al.*, 1991) such that poly-mineral samples could have their feldspar component bleached by laboratory light sources resulting in age underestimation (e.g. Berger, 1994).

Interestingly, the TL/OSL ratios for each sample always fall within error of 67 %, indicating that there is some constancy in the error mechanism (perhaps a common feldspar concentration across all samples, or a constant level of fading, or etching) which suggests that the results of the TL analysis should not be excluded altogether. For samples not subsequently dated with OSL (Shearers Palaeochannel, Swamp Hollow Palaeochannel), it may be expected that the TL ages presented above should be about two thirds of the true burial age.

5.8 Development of an Improved OSL Method

Although the OSL D_e s presented above are thought to be better estimates than the TL D_e s, they are possibly still affected by the presence of contaminant feldspars. Even though the extended etch used in the OSL preparation procedures removed a greater proportion of the feldspars, there was still a detectable IRSL signal from all samples. It is highly likely that the feldspars existed as inclusions within the quartz, and would therefore remain regardless of the length of etching. A method which can be used to measure the OSL from quartz in the presence of feldspar inclusions is therefore required.

Olley *et al.*, (2004a) proposed a modified SAR protocol introducing IR stimulation at 125°C before each OSL stimulation (Table 5.4). They showed (Figure 5.8) that inclusion of this step before every OSL measurement enables the OSL signal from quartz to be isolated from the OSL signal from feldspar. Olley *et al.* tested the modified protocol on 12 samples of known (independent) age (Figure 5.9) and concluded that application of the modified protocol to single grains or small aliquots of quartz, using the lowest D_e population to estimate the burial dose, is the best means of obtaining reliable ages for Holocene sediments.

Whether due to anomalous fading or accidental bleaching, contaminant feldspars in both the samples prepared for TL analysis and the samples prepared for OSL analysis have resulted in age underestimation. Given that the concentration of feldspars in the TL samples was greater than in the OSL samples, the age underestimation was accordingly greater. This has resulted in the unusual situation where the apparent OSL age is older than the apparent TL age. To overcome this problem Olley *et al.* (2004a) devised an OSL analysis strategy that effectively removes the influence of contaminant feldspars. This modified SAR strategy has been applied more broadly to Gwydir samples.

Table 5.4: Comparison of the Standard and Modified SAR protocols, after Olley *et al.* (2004a).

Standard SAR (Murray and Wintle, 2000)		Modified SAR (Olley <i>et al.</i> , 2004a)	
Step	Treatment	Step	Treatment
1	Give dose* (D_1)	1	Give dose* (D_1)
2	Preheat ($240\text{ }^{\circ}\text{C}$ / 10 s)	2	Preheat ($240\text{ }^{\circ}\text{C}$ / 10 s)
3	Stimulate with green laser for 1 s at $125\text{ }^{\circ}\text{C}$ ++	3	Stimulate with infrared diodes for 40 s at $125\text{ }^{\circ}\text{C}$
4	Give test dose, D_T	4	Stimulate with green laser for 1 s at $125\text{ }^{\circ}\text{C}$ ++
5	Cut-heat to $160\text{ }^{\circ}\text{C}$	5	Give test dose, D_T
6	Stimulate with green laser for 1 s at $125\text{ }^{\circ}\text{C}$ ++	6	Preheat ($160\text{ }^{\circ}\text{C}$ / 10 s)
7	Return to Step 1	7	Stimulate with infrared diodes for 40 s at $125\text{ }^{\circ}\text{C}$
		8	Stimulate with green laser for 1 s at $125\text{ }^{\circ}\text{C}$ ++
		9	Return to Step 1

* For the first cycle, no laboratory dose is given, with only the Natural dose being measured. In subsequent cycles, doses ranging from $0 - 2 \times$ the expected natural dose are applied. One dose cycle is repeated as a check on reproducibility. ++ For samples analysed using the TL/OSL DA-12 instrument, sample is stimulated for 100 s at $125\text{ }^{\circ}\text{C}$.

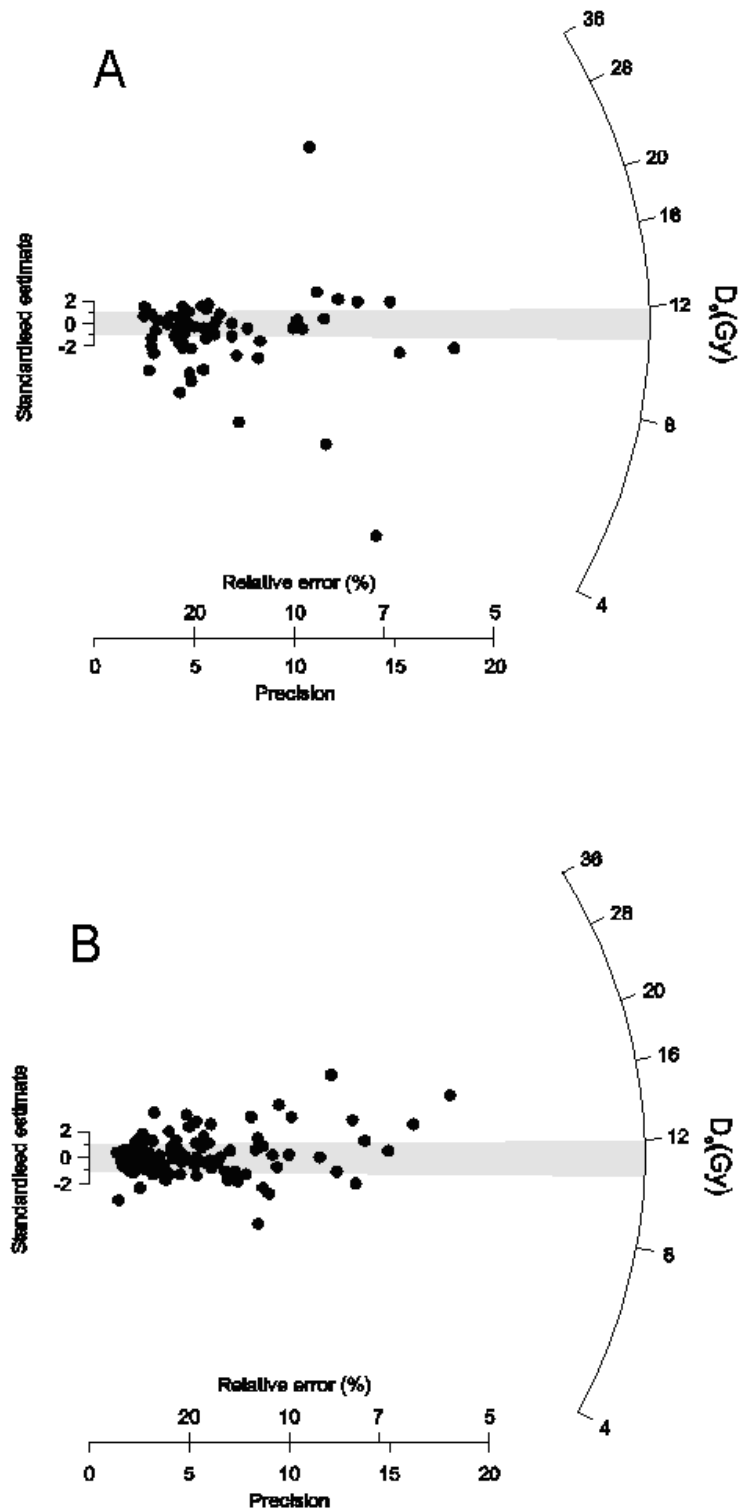


Figure 5.8: Comparison of D_e populations when using standard SAR protocol (a) and modified SAR protocol (b). See subsequent discussions in text for description of the modified SAR protocol. It may be noted that (a) above is almost identical to a distribution presented in Jacobs et al., (2003) which they attribute to contaminant feldspar grains.

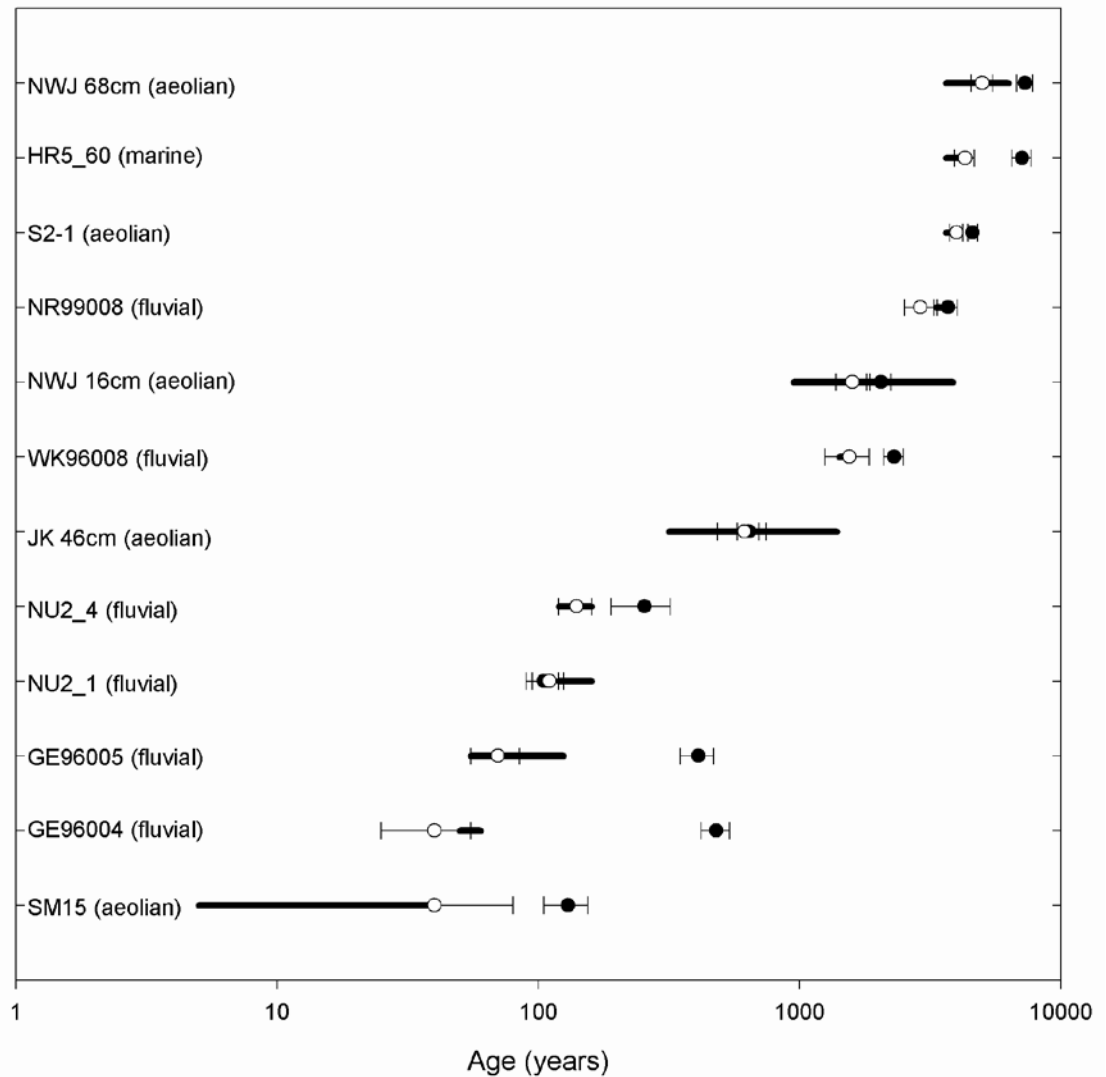


Figure 5.9: Comparisons of (modified SAR) single-grain optical ages determined using the minimum age model (open circles) with independent age estimates (thick horizontal lines) for 12 Holocene samples. Infilled circles are ages as calculated with the central age model (see subsequent discussions in text for explanation of age models). Error bars on optical ages are at one standard error. After Olley et al., (2004a).

5.9 Application of Olley *et al.* (2004a) Method to Gwydir Samples

The modified SAR protocol of Olley *et al.* (2004a) has been applied to 29 samples collected from depositional features of the Gwydir fan-plain. This section details methods and initial results with presentation of the final calculated ages presented in Chapter 7.

Single grain OSL measurements were made on grains loaded on to aluminium discs drilled with a 10×10 array of chambers, each of 300 μm depth and 300 μm diameter (Botter-Jensen *et al.*, 2000). A Riso TL/OSL DA-15 instrument was used, with OSL stimulated using a green (532 nm) laser, with filtered (7.5 mm Hoya U-340) ultra-violet emissions detected by an Electron Tubes 9235QA photomultiplier. Laboratory irradiations were conducted using a reader-mounted $^{90}\text{Sr}/^{90}\text{Y}$ β source. For small aliquot analyses, an earlier generation Riso TL/OSL DA-12 instrument was used. This instrument stimulated OSL from grains adhering as a monolayer to a stainless steel disc, using filtered light (420-575 nm) from a halogen globe.

Although it is technically possible to produce an OSL date from a single aliquot, it is normal practice to measure multiple single aliquots (or multiple single grains) in order to enable examination of any inter-aliquot variation. Typically, a sample of single-grain D_e s is over-dispersed, such that the range in D_e s is greater than that which can be attributed to measurement uncertainties alone. Three (non-experimental) sources of inter-grain variation have been suggested: partial bleaching (e.g. Murray *et al.*, 1995; Olley *et al.*, 1998; Olley *et al.*, 1999), grain migration (e.g. Galbraith *et al.*, 1999, Roberts *et al.*, 1999) and dose-rate heterogeneity (e.g. Murray and Roberts 1997; Duller *et al.*, 2000; Vandenberghe, 2003). Of these, partial bleaching is particularly relevant to fluvial sediments.

When clean quartz grains are exposed directly to sunlight, the OSL signal is reduced to a negligible level within a few seconds (Godfrey-Smith *et al.*, 1988; Wintle, 1997; Aitken, 1998). However, incomplete or non-uniform bleaching is commonplace in many depositional environments (Murray and Olley, 2002; Olley *et al.*, 2004a), due to surface coatings on grains and/or poor exposure to sunlight during sediment transport.

This results in grains being deposited with a heterogeneous distribution of residual trapped charge; the sample is said to be partially bleached. For young, partially bleached samples, where only a small proportion of the grains have a starting dose of zero, Olley *et al.* (1999) showed that the most accurate burial dose estimate was provided by the lowest measured D_e s. They suggested that the burial dose could be calculated as the weighted mean of the lowest 5% of D_e s. Since then, several techniques of varying sophistication have been applied to enable identification of the lowest dose ‘population’ (Lepper *et al.*, 2000; Fuchs and Lang, 2001; Lepper and McKeever, 2002; Fuchs and Wagner, 2003; Zhang *et al.*, 2003), with the ‘minimum age model’ (originally developed for analysis of fission track data) of Galbraith and Laslett (1993) (see also van der Touw *et al.* 1997; Galbraith *et al.* 1999) considered by Olley *et al.* (2004a) to be the most mathematically rigorous.

5.9.1 OSL Data Analysis

The ‘central age model’ of Galbraith *et al.* (1999), has been used to identify samples with D_e distributions consistent with a single population, and, where warranted, to calculate a burial dose (the dose which all grains have received since burial - D_b) based on the central tendency of the data. A distribution representative of a single population is one where the spread in the data can be wholly accounted for by measurement uncertainties on the individual data points. These uncertainties have been calculated using *Analyst 3.1b*, and include counting statistics, curve fitting errors and a 3.5 % uncertainty to accommodate the reproducibility with which the laser can be positioned.

Using the central age model, the spread in a D_e distribution is assessed using the over-dispersion parameter, ‘ σ_d ’. σ_d is calculated as the relative standard deviation of the single-grain D_e distribution after taking into account the measurement uncertainty for each grain (Galbraith *et al.*, 1999). If measurement uncertainty were the only source of spread in a distribution then σ_d would be 0 %. Olley *et al.*, (2004b) suggest a σ_d value $< \sim 22$ % to be indicative of uniform bleaching prior to deposition, and for such samples they recommend use of the central age model. For samples with σ_d values $> \sim 22$ %, and where partial bleaching is the most likely cause of the over-dispersion, Olley *et al.*, (2004a; 2004b) show that use of the ‘minimum age model’ is most appropriate. For convenience, 22 % is here adopted as a threshold value. Samples for which a σ_d value $>$

22 % is calculated, are processed using the minimum age model. Samples for which a σ_d value < 22 % is calculated, are processed using the central age model.

The minimum age model algorithm calculates iteratively the central tendency of the lowest D_e sub-population within the overall D_e population. This low D_e sub-population is identified as all D_e s lying between the lowest D_e value and the D_e at the upper edge of a theoretical normal distribution, of spread consistent with the uncertainties on each individual measurement. Use of the minimum age model is predicated on the assumption that the most significant cause of over-dispersion is a heterogeneous distribution of initial doses, such as has been described for samples from numerous sedimentary contexts (e.g. Li, 1994; Clarke *et al.*, 1999; Olley *et al.*, 2004a). For over-dispersed Holocene samples, Olley *et al.* (2004a) show that application of the minimum age model consistently produces a D_b accordant with the independently determined age. Doubt still remains as to the applicability of this approach for older samples, as it has long been envisaged that for older samples other factors (e.g. a heterogeneous dose rate) would predominate over partial bleaching (e.g. Roberts *et al.* 1999). However, Olley *et al.* (2004b) have used the minimum age model to select a D_b from a highly dispersed Pleistocene sample, resulting in good agreement with the independent age.

5.9.2 Dose Rate Determination

Lithogenic radionuclide activity concentrations were determined from measurements of U, Th and K concentrations using neutron activation analysis of dried and ground bulk samples. Dose rates have been calculated based on the assumption of secular equilibrium in the ^{238}U and ^{232}Th chains, using the conversion factors of Stokes *et al.*, (2003). High Resolution γ Spectrometry (HR γ S) analysis (Murray *et al.*, 1987) of four samples from the range of sedimentary environments was undertaken to test the assumption of secular equilibrium. Cosmic dose rates were calculated from Prescott and Hutton (1994). β -attenuation factors were taken from Mejdahl (1979) and the effective internal α dose rate (applied to all samples) has been estimated using an α -efficiency ' a ' value of 0.04 ± 0.02 (as measured previously for quartz grains from southeastern Australia e.g. Bowler *et al.*, [2003]). An assumed long term water content of 5 ± 5 % has been used to adjust dry dose rates. This value was chosen based on examination of

the distribution of measured water contents, which ranged from less than 1 % to over 12 %, with most values below 5 %. Similar sampling exercises elsewhere report water contents ranging up to 25 % (e.g. Page, 1994; Tooth, 1997). Evidently water content is highly variable through time; thus the probability of sampling at a time when the sampled water content is coincident with the long-term water content is low. Climatic and topographic changes over the burial time further complicate the task of assigning a water content to each sample. These factors negate the apparent benefits in precision of using a measured water content, hence the use of an assumed value. The 100 % relative error has been assigned to the water content estimate in recognition of the difficulties inherent in making such an approximation.

5.10 Initial Results

5.10.1 Dose Rates and Disequilibrium Investigation

The lithogenic radionuclide concentrations for the samples are summarised in Tables 5.5 and 5.6. Prescott and Hutton (1995) and Olley *et al.*, (1996) have shown that disequilibrium in the ^{232}Th chain is rare in Australian terrestrial samples. However, especially in fluvial environments, disequilibrium in the ^{238}U chain is common. It can be seen in Table 6.1, that across four different sedimentary environments minimal disequilibrium in the decay chains is detectable. Two of the samples display equilibrium in the ^{238}U series at the 1 σ confidence interval, while the remaining two samples are in equilibrium at the 2 σ confidence interval. It can be seen that for samples GF-17 and GF-30, that ^{226}Ra is apparently unsupported by the ^{238}U . However, one (GF-30) is based on a very unreliable estimate of ^{238}U activity (~ 70 % proportional error) while the other falls outside the 1 σ confidence interval but well within the 2 σ confidence interval. Based on this small sample of four, it will be assumed that decay chain disequilibrium is not significant for samples of the lower Gwydir. This assumption is supported by the observation that ^{40}K accounts for the majority ($\sim 60 - 80$ %) of the dose rate in each sample. By way of comparison, Olley *et al.*, (1996) suggest that ~ 40 % of the dose rate of typical samples comes from ^{40}K . The combined effects of these factors is shown in Figure 6.1, where dose rates, as determined using HR γ S, are compared to dose rates as

determined using NAA (or thick source α counting (TS α C) and flame photometry in the case of GF-29). At the 2 σ confidence level the dose rates are equivalent.

5.10.2 D_e Distributions

D_e distributions for samples GF-12 and GF-16 are presented as radial plots (Galbraith, 1990) in Figure 5.11 as examples, with the remainder presented in Appendix D. For samples GF-2, 3, 4, 6, 7, 8, 9, 10, 11, 16, 18, 23, 25, 28 and 29, only minor over-dispersion of the D_e distributions is evident (see also Table 7.1). Burial ages were therefore determined using the central age model. The remaining samples all had over-dispersed D_e distributions, i.e. σ_d values $> 22\%$, therefore a burial dose has been calculated using the minimum age model. It may be noted that, in general, the higher D_e samples have the greatest relative error (see x-axes on radial plots). This is due to the higher level of uncertainty produced when a D_e is determined using the higher end of the saturating exponential model (Figure 5.12), as is typical of the form of most growth curves.

Table 5.5: Radionuclide data for 4 samples from the lower Gwydir, as determined using HR γ S. See text for discussion of D_r calculation. ^{226}Ra and ^{230}Th are assumed to be in equilibrium.

Sample Name	^{238}U	^{226}Ra	^{210}Pb	^{232}Th	^{40}K	βD_r %	% βD_r from ^{40}K	Total D_r (Gy ka^{-1})
GF-6	13.7 ± 2.3	13.6 ± 0.2	13.1 ± 1.4	19.7 ± 0.5	670 ± 9	64%	87%	2.76 ± 0.15
GF-17	6.7 ± 4.4	12.5 ± 0.4	14.7 ± 2.2	16.8 ± 0.6	535 ± 12	63%	86%	2.26 ± 0.17
GF-29*	12.4 ± 3.7	14.6 ± 0.4	13.1 ± 1.8	21.3 ± 0.4	788 ± 14	65%	88%	3.15 ± 0.18
GF-30**	25.7 ± 3.9	33.8 ± 0.4	25.7 ± 2.1	41.2 ± 0.5	313 ± 6	51%	61%	2.32 ± 0.16

* Sample not submitted for NAA analysis.

**Sample GF-30 was submitted for HR γ S, however a corresponding D_e was not able to be determined, hence no date is subsequently reported for this sample.

Table 5.6: Radionuclide data for all samples (except GF-29) from the lower Gwydir, as determined using NAA.

Sample Name	^{40}K (Bq/kg)	Th (Bq/kg)	U (Bq/kg)	β D _r %	% β D _r from ^{40}K	Total D _r (Gy ka ⁻¹)
GF-1	600±6	22.7±1.1	16.9±1.8	62%	83%	2.68±0.15
GF-2	654±7	35.8±1.8	28.7±0.3	60%	77%	3.21±0.26
GF-3	673±7	23.2±1.2	13.1±2.7	63%	87%	2.84±0.16
GF-4	736±7	19.1±1.0	12.7±2.7	65%	89%	2.95±0.17
GF-5	755±8	21.7±1.1	13.5±2.6	64%	88%	3.01±0.22
GF-6	758±8	20.8±1.0	16.3±2.0	65%	87%	3.10±0.18
GF-7	715±9	28.9±2.1	15.5±2.1	62%	85%	3.13±0.17
GF-8	705±7	24.1±1.2	9.5±3.4	64%	88%	2.88±0.16
GF-9	695±7	20.2±1.0	13.5±2.6	65%	88%	2.76±0.21
GF-10	758±8	22.6±1.1	15.9±2.0	65%	87%	3.04±0.23
GF-11	575±6	45.2±2.3	27.8±0.3	58%	73%	3.14±0.20
GF-12	480±5	38.0±1.9	26.9±0.3	57%	71%	2.75±0.18
GF-13	458±5	38.8±1.9	23.1±0.5	55%	72%	2.70±0.17
GF-14	458±5	38.8±1.9	23.1±0.5	55%	72%	2.69±0.17
GF-15	547±5	36.3±1.8	22.4±0.6	57%	76%	2.89±0.18
GF-16	790±7	26.2±1.4	11.8±2.1	64%	87%	3.25±0.20
GF-17	566±6	18.5±0.9	10.8±3.2	64%	87%	2.31±0.17
GF-18	743±8	39.6±2.1	20.4±3.0	62%	80%	3.35±0.23
GF-19	600±10	25.7±1.6	14.5±2.1	61%	84%	2.71±0.14
GF-20	774±8	22.0±1.1	10.4±3.2	66%	90%	2.97±0.22
GF-21	721±7	17.8±0.9	9.3±3.5	66%	90%	2.72±0.20
GF-22	515±5	21.6±1.1	12.4±2.8	63%	84%	2.21±0.17
GF-23	597±6	34.9±1.7	21.3±0.9	60%	78%	2.88±0.23
GF-24	534±5	27.9±0.7	15.6±2.1	61%	81%	2.46±0.19
GF-25	550±5	36.4±0.2	16.1±2.1	58%	79%	2.76±0.17
GF-26	743±7	23.0±1.1	11.7±3.0	63%	88%	3.06±0.18
GF-27	651±7	19.5±1.0	10.0±3.3	64%	89%	2.67±0.15
GF-28	765±8	21.3±0.5	11.6±3.2	65%	89%	3.05±0.18

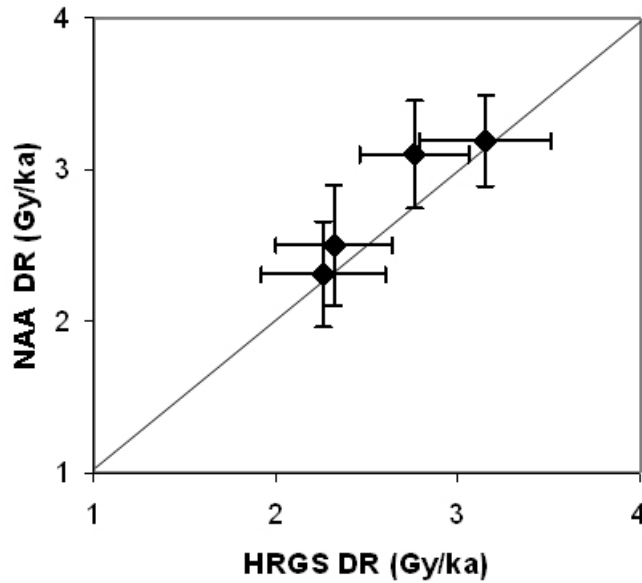


Figure 5.10: Comparison between D_r as determined using HRGS against D_r as determined using NAA or TSaC. Note that when using NAA secular equilibrium is assumed.

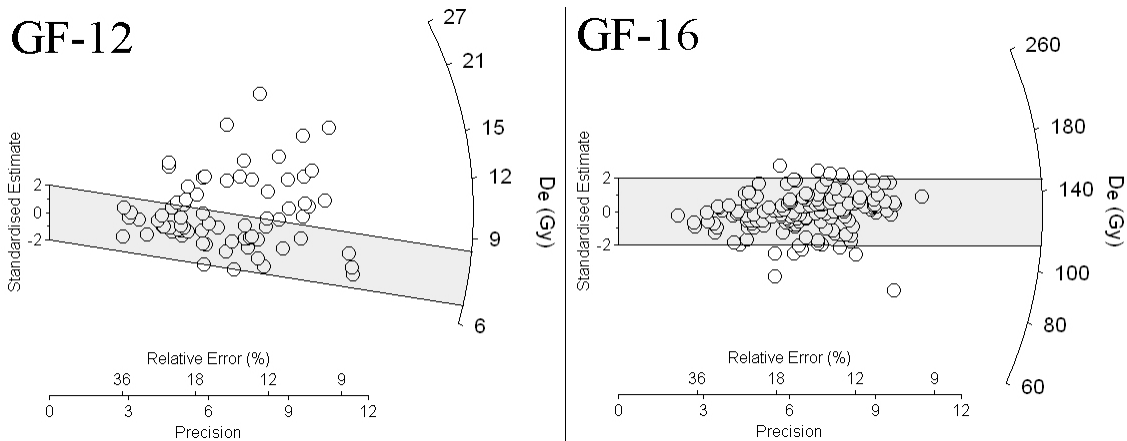


Figure 5.11: Examples of Radial Plots. The measured D_e for a grain can be read by tracing a line from the y-axis origin through the point until the line intersects the radial axis. The corresponding standard error for each D_e estimate can be read by extending a line vertically to the x-axis. The two scales on the x-axis are the relative standard error of the D_e estimate (in %) and the reciprocal standard error. Values with the highest precisions plot closest to the radial axis.

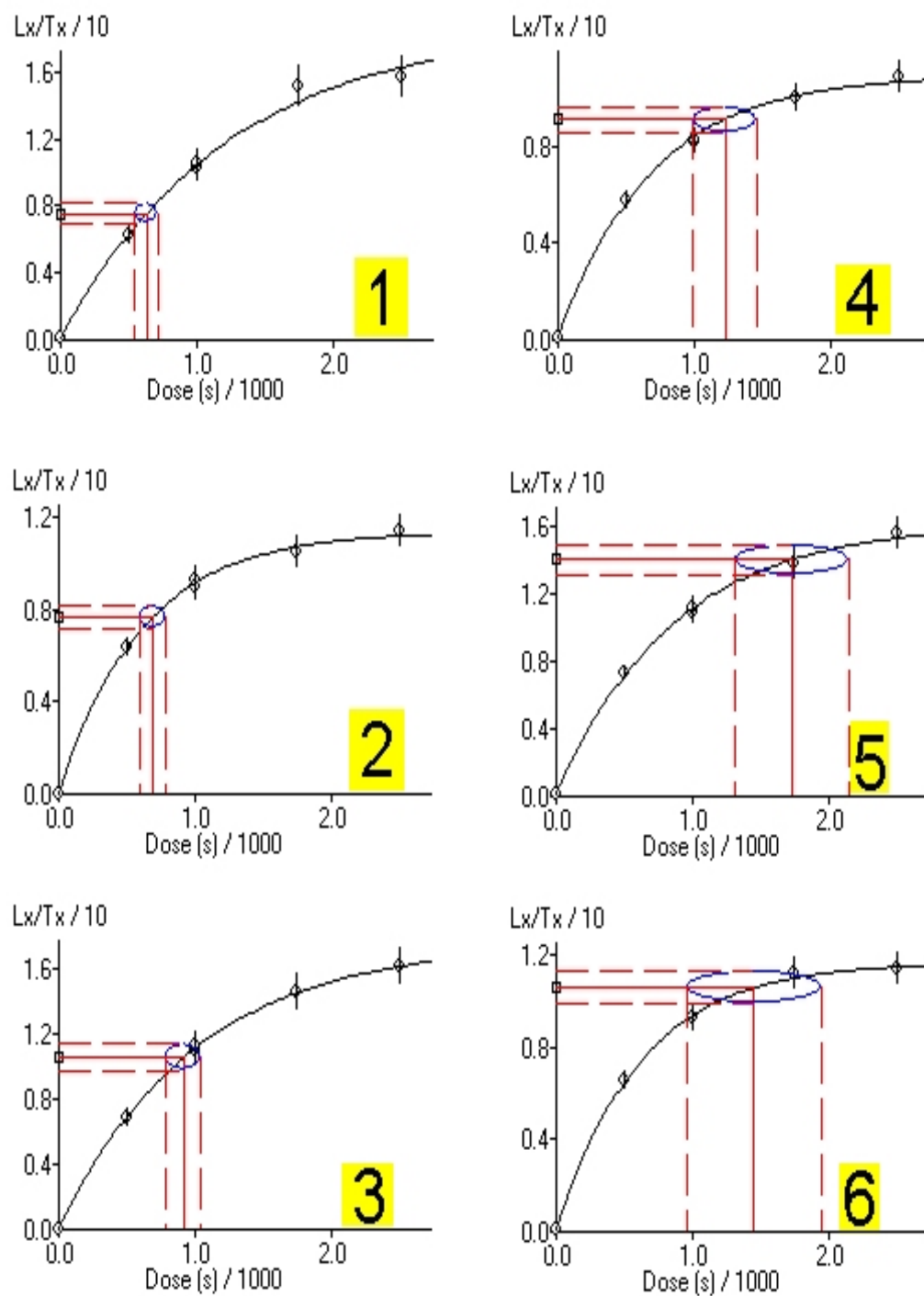


Figure 5.12: Comparison of errors associated with D_e s derived from the linear vs. the non-linear regions of the growth curve for different grains. Note that the counting uncertainties associated with the OSL measurement (i.e. the error on the Y-axis position) are comparable for each grain.

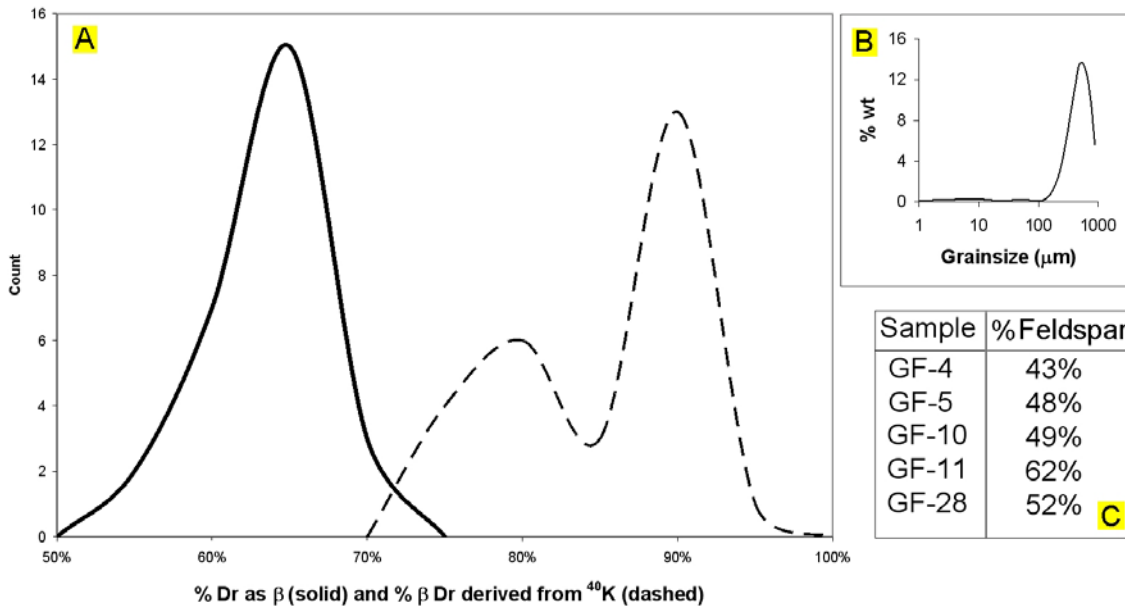


Figure 5.13: Indications of unlikelihood of dose rate heterogeneity. A) Solid line shows that, for all samples, approximately 65 % of the total dose is in the form of β dose. It may be assumed that the γ dose rate is constant across all grains (Aitken, 1985). Of the β dose, about 90 % is from ^{40}K (dashed line). This ^{40}K is unlikely to be present as a clay matrix as B) shows particle size distribution for sample GF-4, which is considered typical of the fluvial sands dated here. It is therefore likely that ^{40}K will be present as large feldspar grains. β dose rate homogeneity will result if these large feldspar grains are in high concentration. This can be shown to be so. If $\sim 2\%$ ($\sim 632\text{ Bq/kg}$) is taken as an average K content in these samples (see Table 5.6), and alkali feldspars are known to be generally 5 -10 % K (Deer et al., 1966), it follows that alkali feldspar grains must make up over 40 % of each deposit, assuming all ^{40}K is present as alkali feldspar. This assumption was tested by measuring % feldspar (by HF digestion) in five samples considered representative, the results of which are shown in C). It follows that if approximately every second grain is potassic feldspar, no β Dose Rate heterogeneity will be possible.

As stated previously, use of the minimum age model requires the assumption that the principle cause of D_e dispersion is partial bleaching rather than dose rate heterogeneity or layer mixing. In the case of the fluvial samples, this assumption can be supported by consideration of the unlikelihood of significant dose rate heterogeneity (Figure 5.13), as well as the coherency of sedimentary layers in the sampled deposits (see Figure 2.21).

In the case of samples GF-13, 14 and 15 from a soil layer, the assumption requires clarification. The soil profile in question is a typical vertisol, with cracks extending below the surface during high summer. It is therefore likely that the burial dose for these samples does not refer to the timing of initial deposition, but rather the time at which accretionary over-burden reached sufficient thickness to place the sampled grains below the depth of summer-time cracking.

5.11 Summary

This chapter has provided background information on the theory and methods of luminescence dating and has highlighted problems encountered when the sampled material contains contaminant minerals, presumably feldspars. TL and traditional OSL methods are not suitable for dating the feldspathic sands (see Figure 5.13c) of the Gwydir fan-plain as the presence of feldspar (which may have been bleached by standard laboratory lighting or lost part of its signal due to anomalous fading) results in significant age underestimation. It is likely that at least some of the feldspar in palaeochannel sands of the Gwydir fan-plain exists as inclusions within quartz, as no chemical treatment was successful in removing 100 % of the feldspar. The development of a modified SAR protocol for the OSL analysis of quartz in the presence of feldspar inclusions has been documented and methods of data analysis used here have been described. Initial results have been provided in demonstration of some of the concepts discussed, in particular dose rate data has been provided which illustrates the unlikelihood of secular disequilibrium or β dose rate heterogeneity in the samples collected from the Gwydir fan-plain. The following chapter details another use for OSL data, while the sedimentary context of the dating program is described in Chapter 7.

Chapter 6 A Non-Geochronometric Application for OSL

6.1 Introduction

This chapter presents a new method of river characterization using the OSL signal obtained from quartz. A model relating OSL properties of quartz to transport processes is developed, and some applications arising there-from are demonstrated. The model adds to the overall thesis objectives of describing channel forms and their controls in the Gwydir distributary system.

The previous chapter focused on obtaining geochronological information through analysis of the OSL signal of quartz. Further characterization of quartz is possible using the luminescence signal. Hashimoto *et al.*, (1989) and Price (1994) for example, demonstrated that TL signals could be used to trace the provenance of quartz, with glow curves having origin-specific forms. The various forms of OSL growth curves (Yoshida *et al.*, 2000; Banerjee, 2001) and shine-down curves (e.g. Bailey *et al.*, 1997; Murray and Wintle, 1998; Kuhns *et al.*, 2000; Bulur *et al.*, 2000; 2002) have also been explored; however limited investigation of the cause(s) of this variety have been reported. In this chapter the focus is on characterizing quartz in terms of OSL sensitivity, where sensitivity is defined as OSL response to a given dose.

6.2 Quartz Sensitivity

Australian researchers and Australian sites feature disproportionately highly in the luminescence literature. For some as yet unknown reason, Australian sedimentary quartz is particularly sensitive (in terms of OSL or TL response) to irradiation, such that a typical sample of Australian quartz may be orders of magnitude brighter than a sedimentologically equivalent sample from Europe. This sensitivity simplifies analytical and statistical procedures.

Although early investigations into the controls on quartz sensitivity were related to TL rather than OSL (e.g. Zimmerman, 1971; Wintle, 1985), Stoneham and Stokes (1991),

Murray and Roberts (1998) and Wintle and Murray (1998) have shown that changes in TL sensitivity (from the 110°C trap) are mirrored by sensitivity changes in the OSL response. Although initially this was attributed to a common mechanism, subsequent work by Stokes (1994) monitoring the timing of sensitivity changes indicated that the mechanism can not be wholly common. Specifically, Stokes (1994) observed that the sensitivity of the OSL response increased only when a bleach preceded dosing and heating, the latter two processes being all that was necessary to increase the sensitivity of the 110°C TL response. Itoh *et al.* (2002) have lately argued that the OSL mechanism and the (110°C) TL mechanism share only part of their luminescence pathways, in part explaining why some behavioural characteristics are common, for example heat sensitization, while others, for example luminescence spectral response, are not. Models of TL sensitivity are nevertheless relevant to OSL studies, and therefore, in the following discussion, little distinction is drawn between TL sensitivity and OSL sensitivity.

It may be assumed that quartz sensitivity is due to high charge traffic between electron traps and luminescence centres (L-centres). The most obvious determinant of the rate and/or quantity of this charge traffic is the absolute number of traps and L-centres (McKeever, 1985; Hashimoto *et al.*, 1994; 1997; Vartanian *et al.*, 2000) with this number being determined largely by crystal formation conditions. Moreover, most luminescence models (e.g. Zimmerman, 1971, McKeever, 1991; Bailey, 2001; Itoh *et al.*, 2002) include competitor traps (i.e. those that are not subsequently sampled in the measurement process) and non-luminescent centres that have been variously referred to as ‘non-radiative’, ‘phonon-producing’, ‘killer’ or ‘reservoir’. They will be here referred to as R-centres.

R-centres compete with L-centres for free charge (Figure 6.1), and are generally considered to be closer to the valence band than L-centres. The degree to which this competition from R-centres disrupts the flow of charge traffic between electron traps and L-centres will be as important as the absolute number of traps and L-centres, in determining luminescence efficiency. It may be posited then that Australian quartz must be peculiarly endowed with high numbers of traps and/or L-centres, or alternatively, the level of disruption of charge traffic by R-centres must be comparatively low.

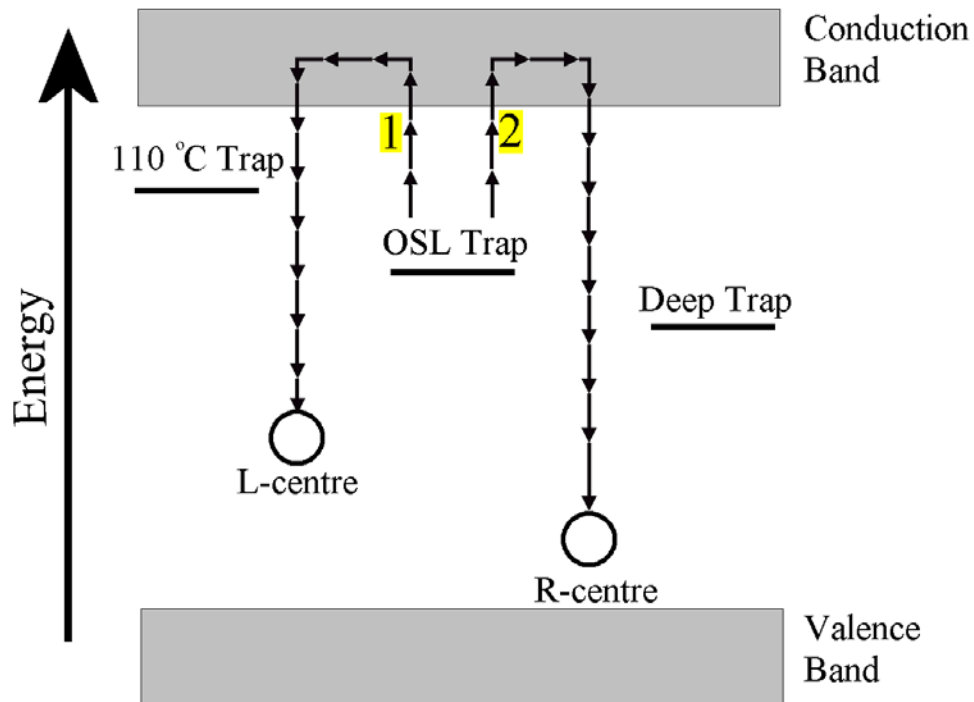


Figure 6.1: Energy band model of the competition between R-centres and L-centres for free charge. Upon eviction from the OSL trap by laboratory bleaching, charge may travel via either of the two pathways to an L-centre or R-centre (or be re-trapped at a shallower or deeper trap, e.g. the 110 °C or 375 °C traps). If the proportion of L to R centres changes through either the removal of R-centres or the creation of L-centres, then the sensitivity of the quartz will change. Note that charge re-captured at an L-centre results in photon emission, whereas charge re-captured at an R-centre results in either phonon emission, or photon emission at a wavelength outside the detection window.

While relatively little research has been directed towards quantifying the number of luminescence traps and centres in natural quartz, an extensive body of work exists recounting investigations into the effects of various laboratory treatments on the competitiveness of L-centres compared to R-centres. Heating (e.g. Aitken and Smith, 1988; Botter-Jensen *et al.*, 1995; Rhodes and Bailey, 1997; Rhodes, 2000; Wintle and Murray 2000; Bailey, 2001); bleaching (Wintle, 1985; Bowall *et al.*, 1987; McKeever, 1991; Li and Wintle, 1991; 1992; Morris and McKeever, 1993; Stokes, 1994; Zhou and Wintle, 1994) and irradiation (e.g. Zimmerman, 1971; Durrani *et al.*, 1977; Stoneham and Stokes, 1991; Bailiff, 1994; Chawla *et al.*, 1998; Benny *et al.*, 2000) have all been

shown to change the sensitivity of quartz, presumably by altering the proportional capture of charge between L-centres and R-centres. Suggested mechanisms which may determine this proportion include the thermal transfer of holes from shallow R-centres to thermally stable L-centres (Zimmerman, 1971); recombination at L-centres during irradiation (Aitken, 1985); an increase in competitiveness of the R-centres during irradiation and heating (Bailey, 2001); or the irreversible thermal conversion of R-centres to L-centres (Vartanian *et al.*, 2000). It would appear that the aforementioned proximity of R-centres to the valence band makes them liable to activation / deactivation at a rate different from that of L-centres. While the precise mechanisms by which any or all of these processes occur are currently being hypothesized, they remain largely a mystery and beyond the scope of the present work.

Though there may be some mineralogical, structural and/or chemical peculiarity to the quartz so far sampled in Australia, such that high concentrations of defects relevant to the luminescence pathway are common, the unusual sensitivity of Australian quartz must, at least in part, be a result of environmental conditions experienced by quartz within the Australian landscape. Just as the laboratory treatments outlined above alter the sensitivity of quartz, so too must their natural analogues. Very little research has been done in this area. Li and Wintle (1991; 1992) suggested that colluvial samples should be distinguishable from aeolian samples based on differential sensitization occurring during their final, pre-burial bleach (i.e. colluvial = short bleach resulting in low sensitivity; aeolian = long bleach resulting in high sensitivity). Wintle and Murray (1999; 2000) make a passing reference to the ambient temperatures experienced by Australian quartz, commenting that old Australian samples could be thermally sensitized by long storage at relatively high environmental temperatures. Although these studies suggest a link between components of the environmental history of a sample and its final sensitivity, they are perhaps somewhat simplistic in their conclusions. If ambient temperature or bleaching severity alone were the sole determinants of sensitivity it could be expected that sensitivity would be inversely related to latitude. Such a relationship has nowhere been documented, and equatorial samples with which the author is familiar are generally very insensitive. It is here proposed that rather than any of the individual ‘natural’ treatments causing Australian quartz to be highly sensitive, it is instead the effect of all of such treatments in combination. Cognizant of this possibility, Olley (pers. comm. 2001) proposed to the author a hypothesis which

promised, if proven, to open up a whole new application for OSL. The hypothesis can be stated thus:

Australian quartz is particularly sensitive because of the number of dose / heat / bleach (DHB) cycles it experiences during weathering from bedrock and transportation to its site of ultimate deposition. Repetitive natural processes operate in much the same manner as repetitive laboratory treatments, sensitizing the quartz to optical stimulation and/or increasing charge capacity.

Non-Australian quartz would be exposed to these same processes, but not to the same extent. Consider for example the path of a quartz grain in transit from a steep mountainside in the Black Forest, along nearly 3000 km of the deep, perennial Danube River to a point of deposition near the Black Sea. Or alternatively, the path of a grain hastily washed into the Fly River (Papua New Guinea) under the influence of a tropical storm, and moved quickly along below a deep, turbid water column. Compare these to the path of an equivalent Australian grain, weathered from exposed bedrock, moved slowly across a flat landscape into and along, a slow moving, often dry, Cooper Creek or Diamantina River. Even upon becoming part of the bedload of a large river, highly seasonal flows will repeatedly bury and exhume individual grains through many channel bars before final burial in a floodplain, terrace or palaeochannel. The opportunities for multiple episodes of exposure to bright sunlight, burial and exhumation are far higher in an Australian context.

Support for this hypothesis can be found in the design of the SAR protocol (see Table 5.4). Sensitivity changes during sequential OSL measurements (Figure 6.2) were first observed by Botter-Jensen *et al.* (1993) and Jungner and Botter-Jensen (1994). Compensating for these sensitivity changes was the major challenge faced by the developers of the SAR protocol (Murray *et al.*, 1997; Murray and Roberts, 1998; Murray and Wintle, 2000; Bailey, 2000). As already stated, for each of the laboratory treatments applied during the SAR protocol, natural analogues can be identified. Additionally, it is envisaged that certain environments may be distinguished by the number of DHB cycles that quartz is exposed to. In an Australian fluvial setting, quartz will experience burial (i.e. irradiation) and illumination during many episodes of remobilization, and heating in association with illumination, especially if located at the

surface of an exposed sandbar during high summer. It could therefore be expected that, just as sensitivity changes result from laboratory measurement, increased sensitivity should develop during multiple episodes of downstream transit.

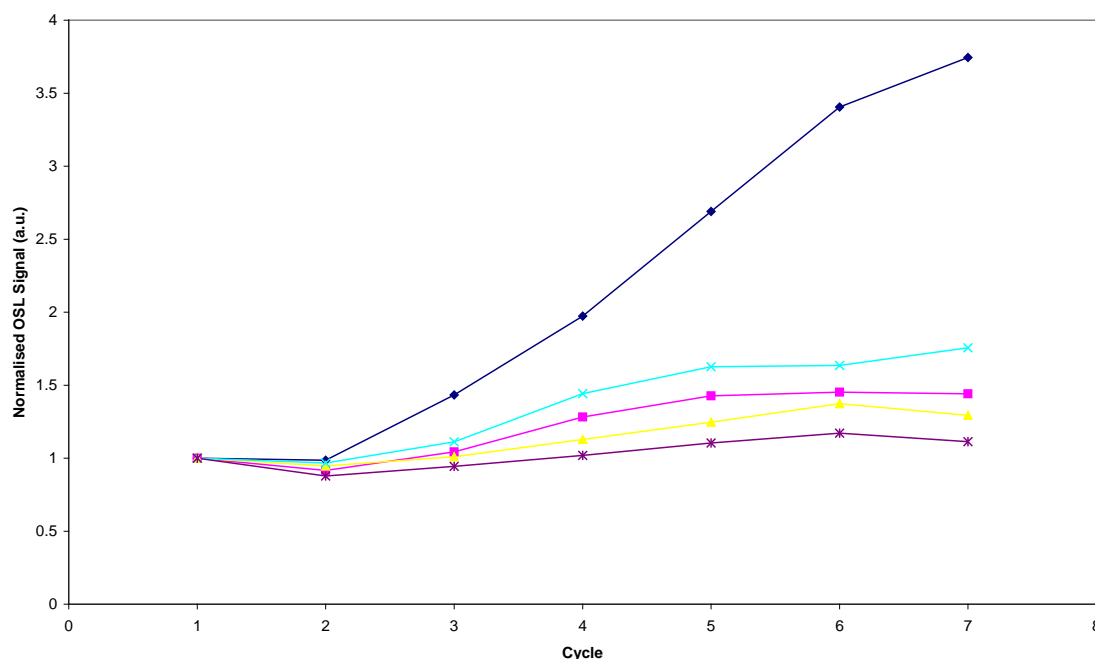


Figure 6.2: OSL response to the test dose throughout a standard SAR protocol for five large aliquots of sample GF-27. Note that OSL response is normalized using the initial value measured in cycle one.

Modelling of the likely effects of the different stages in the SAR protocol provides further indication of the importance of the combined effects of various treatments. For example, heating alone has been shown to cause sensitization (Aitken and Smith, 1988; Botter-Jensen *et al.*, 1995), although this has not been observed directly at environmental temperatures. Murray and Wintle (2000) and Bailey (2000) however suggest that temperature sensitization can be modelled via an Arrhenius type equation: that is, short period high temperature treatments are equivalent to long period low temperature treatments. Although heating will increase sensitivity, the amount of increase will be determined by accompanying treatments. For example, Wintle and Murray (1998) show that the level of sensitivity change due to heating varies depending on whether or not the sample receives a prior bleach, that is, dose plus heating = 30 % sensitivity increase; bleach, dose then heat = 300 % sensitivity increase. McKeever *et al.* (1997) have constructed computer models which suggest that the greatest sensitivity

increases will result from multiple cycles involving *incomplete bleaching*. Such a finding has obvious relevance to natural samples.

By way of conclusion to this section it may be observed that there is sufficient theoretical and empirical evidence to suggest that at least part of the reason for the sensitivity of Australian quartz is its environmental history. While it should be noted that a strong sample dependence in the direction, magnitude and timing of sensitivity changes has also been observed (e.g. Armitage *et al.*, 2000; Bailey, 2001 and see Figure 6.2), it may be hypothesized that the natural treatments received by quartz during transmission by Australian fluvial systems operate in such a way as to, on average, positively sensitize quartz. This may be due to either the overall severity, or number, or ordering of these treatments. In addition to providing an answer to the question of the origin of increased sensitivity of Australian quartz, the multiple DHB cycles hypothesis offers a way to model river behaviour through investigation of the downstream changes in quartz sensitivity. Furthermore, different rivers, with different flow regimes, will expose and rebury quartz at different rates. Perhaps most interesting of all, is the possibility for behavioural investigation of palaeochannels based on down-valley changes in quartz sensitivity. The following section details an experiment designed to test this application.

6.3 Methodology

6.3.1 Experiment 1

This section reports the results of an experiment devised to test whether river behaviour has an influence on quartz sensitivity. By sampling from a river bed at consecutive distances downstream it should be possible to detect increases in average quartz grain sensitivity with increasing stream length. It is presumed that distance downstream is a proxy for number of DHB cycles, or at least, for the number of opportunities for DHB cycling.

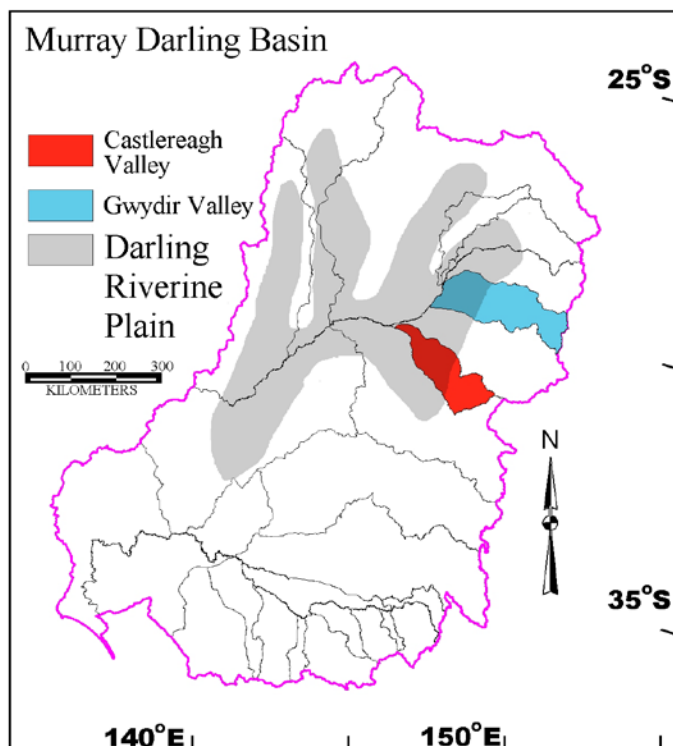
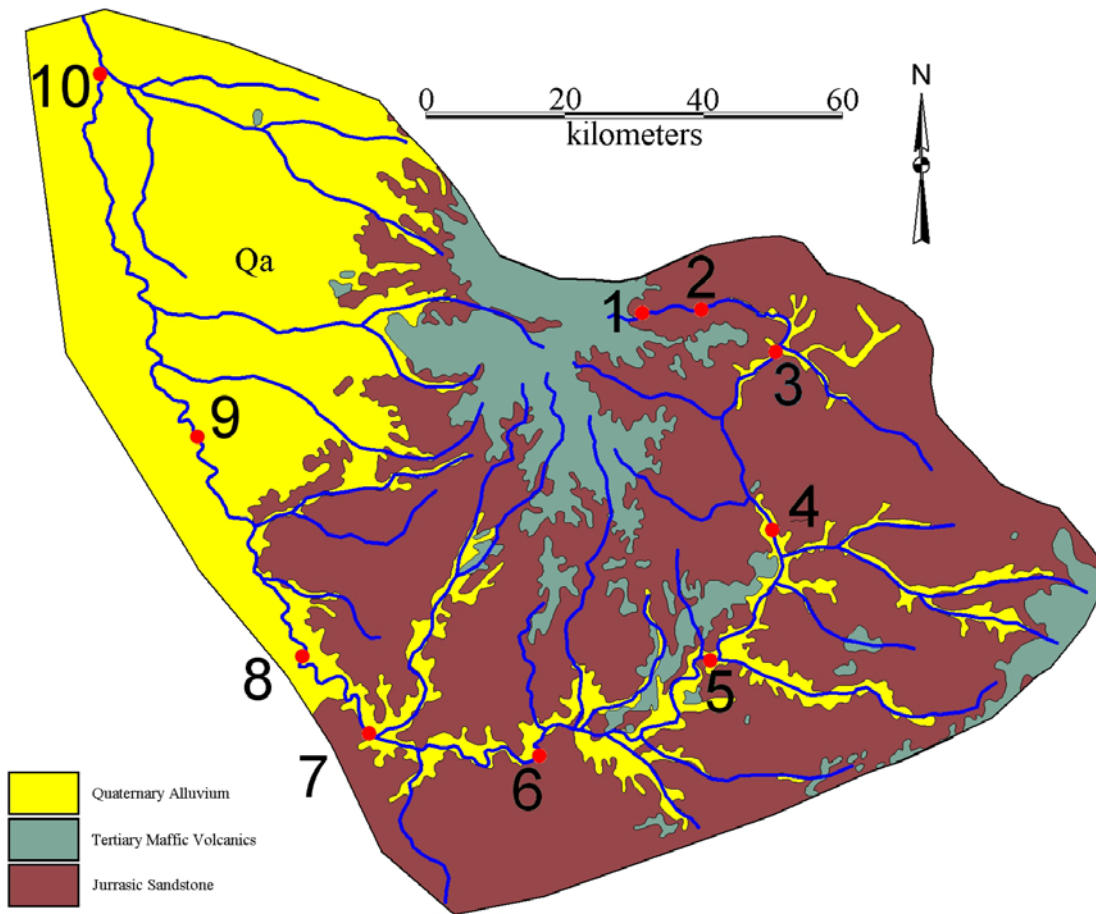


Figure 6.3: *Geology and sampling points of the Castlereagh River. Inset shows location of Castlereagh Valley within Murray Darling Basin.*

Geological Data retrieved 20/01/05 from www.ga.gov.au.

The role of the geological origin of quartz in controlling to some extent its luminescence characteristics can not be discounted. Therefore, rather than test the hypothesis within the study area (where the geology of the catchment is very complex), a more suitable geologically simpler stream was sought. The Castlereagh River (Figure 6.3) proved to be an ideal study stream, as it is in the same broad region of NSW as the main study area (the western slopes and plains); has a coarse-grain quartz bedload derived almost entirely from the Jurassic Pilliga Sandstone; and has a highly episodic flow regime. For almost its entire length, and for much of the time, the Castlereagh River has a dry sandy bed. During transport the great majority of quartz grains will be cycled from bar innards to surface many times.

Nine samples were collected from the bed of the dry Castlereagh River at approximately 20 stream km intervals (Figure 6.3). Additionally, a sample was collected from a decaying rock face close to the source of the river. An appropriate size fraction (180-212 μm) from each of the ten samples was obtained and prepared in the standard way (see Section 5.6.2), except that acid treatments were more rigorous (though standardized) to ensure complete removal of any external coatings, and most processes were undertaken under white light conditions. Sensitivity was assessed using the following sequence on five 5 mm aliquots of silicon oil mounted, weight-normalised quartz samples:

1. 240°C preheat for 10 seconds
2. IR-bleach at room temperature for 40 seconds
3. Bleach at 125°C for 100 seconds using green light
4. Application of 2 Gy β Irradiation
5. Cut heat to 160°C
6. IR-bleach at room temperature for 40 seconds
7. Measurement of OSL at 125°C for 100 seconds

For the assessment of the inherent sensitivity of quartz, the first 10 seconds of the OSL signal (measured in Step 7) were integrated and corrected for background using the final 25 seconds of the OSL signal. The errors reported here are the standard deviations on the means for each sample.

6.3.2 Experiment 2

Experiment 2 was undertaken using material from Site 1 (the decaying rock face), with the aim being to determine whether its sensitivity could be increased through application of multiple bleach / dose cycles. The inherent sensitivity of twenty-four 5 mm aliquots was measured using the sequence from Experiment 1. These aliquots were then divided into 6 sub-samples of 4, with each group of 4 being treated with either 0, 10, 20, 100, 200 or 500 runs of the following sequence:

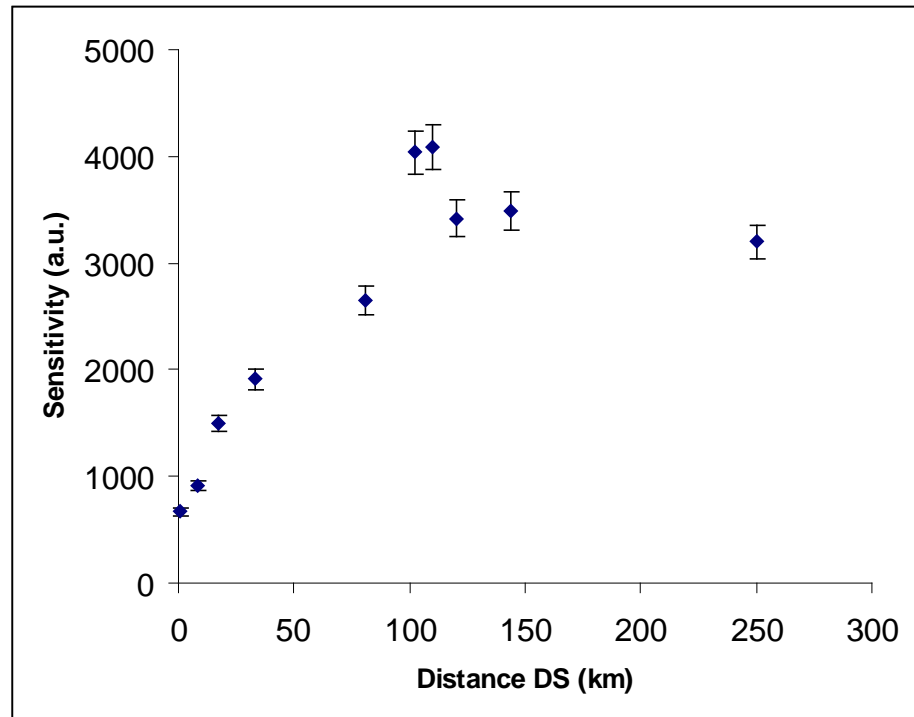
1. Application of 2 Gy β Irradiation
 2. Bleach (with instrument green light source) at 50°C for 2 min
- (Note that during these treatments the samples were not heated above what was considered a reasonable estimate of possible environmental temperatures. Note also that the effects of bleaching with the instrument light may not necessarily be the same as the effects of exposure to sunlight).

The sensitivity of each aliquot was measured again and the reported results show the average increase in sensitivity relative to the number of cycles received.

6.4 Initial Results

It can be seen in Figure 6.4 that quartz sensitivity increases with both distance downstream (Experiment 1) and with number of laboratory cycles (Experiment 2). Furthermore, it would be expected that downstream increases in average sensitivity should be suppressed by the input of 'dim' quartz from short tributaries. This is indeed the case, with a reduction in average quartz sensitivity detectable at sites 8 (120 km), 9 (144 km) and 10 (250 km), downstream of the confluences of short tributaries. The results of Experiment 2 show that low temperature cycling (using green light) is sufficient alone to increase the sensitivity of material that has only recently been released from bedrock. Further experiments could be run to isolate which part of the procedure (i.e. bleach, dose or heat) is contributing most to the sensitivity increase; however, such an exercise would be in large part a repeat of the extensive body of work referred to above.

(a)



(b)

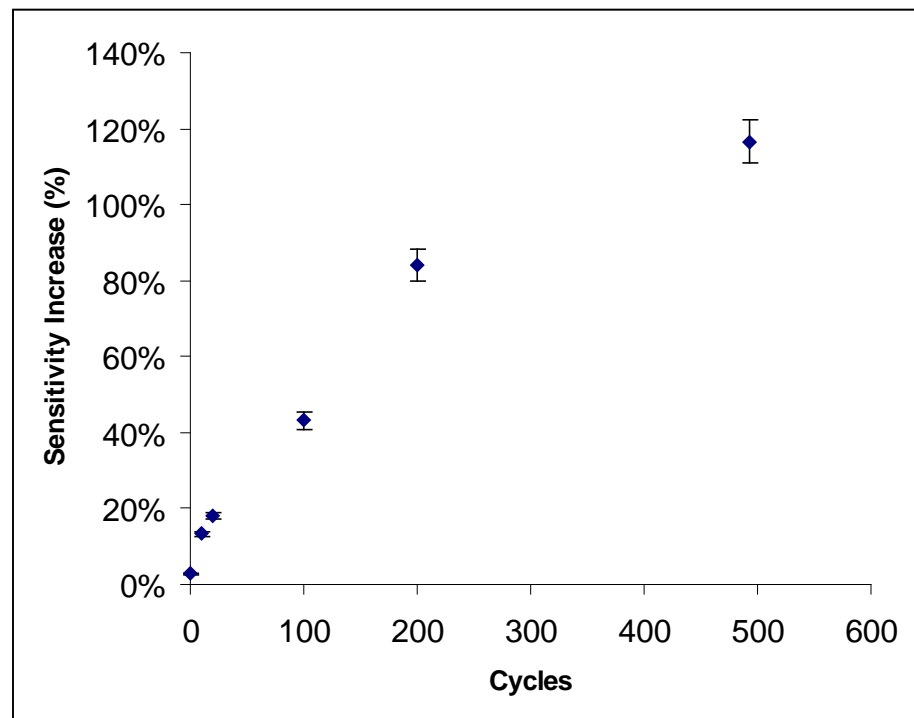


Figure 6.4: Increases in sensitivity with (a) distance downstream (Experiment 1) and (b) number of cycles (Experiment 2).

It is noted that McKeever and Morris (1994) suggest that sensitivity increases should stabilise after about 10 (of their) DHB cycles, beyond which no further increases in sensitivity are expected. While this value would depend on the intensity of each treatment within a DHB cycle, the general observation that there should be a limit to the possible increases in sensitivity is only partly supported by the data presented here. Experiment 2 shows a non-linearity in the sensitivity increase, although exclusion of the last point, would allow the growth to be interpreted as linear. Likewise the results of Experiment 1 appear to show a linear increase over the first 100 km downstream transit with increases thereafter suppressed, as argued above, by the input from short tributaries. On the evidence presented here, non-linearity in sensitivity increases are not considered likely, but such a possibility should be considered in interpretation of subsequent experimental results.

The results of Experiment 2 show that, as with quartz studied elsewhere, Castlereagh River quartz is positively sensitized by DHB cycling and that, unlike studies conducted elsewhere, this effect is observable even when the quartz is not heated above normal environmental temperatures. This therefore leads to the conclusion that the observable downstream increase in sensitivity for Castlereagh quartz is not related to any macro changes in the quartz (e.g. abrasion of surface coatings) but is related to genuine changes in the luminescence properties of the quartz.

The experiments reported here give results which align with predictions arising from previously discussed models of quartz response to laboratory treatments (e.g. McKeever, 1991; Bailey, 2001). However, by identifying natural analogues of these treatments in the way rivers, particularly Australian rivers, transport sediment, new applications for OSL present themselves. If sensitivity is related to river behaviour (specifically the rate of cyclical burial, exhumation and exposure), then different rivers should yield quartz with different levels of sensitivity.

6.4.1 A Note on Units and Uncertainties

Time constraints necessitated the use of multiple TL/DA 12 Riso machines for the experiments reported in this chapter. Corrections for sensitivity differences between

machines, and instrumental sensitivity changes of single machines over time have been duly applied. However, the use of these correction factors has made it difficult to precisely describe the units used and their uncertainty. The basis of the unit of sensitivity is a sample averaged background corrected photon count in response to optical stimulation, normalized to a standard applied dose. The precision with which the sizes of the background, photon count and applied dose could be determined varied between experiments and machines and over time, necessitating a conservative approach to uncertainty propagation, with the summing in quadrature of uncertainties generated at each measurement or correction step as well as adoption of ‘arbitrary units’ rather than the cumbersome mean sensitivity corrected, background corrected, dose normalised photon count. Given the cumbersome nature of the derived units, the results are reported in arbitrary units (a.u.) or in % change, with the size of uncertainties being largely a function of the number of correction factors (each adding to the uncertainty) which needed to be applied. Experiment 2, having been run on a single machine, has the lowest uncertainties. Experiment 1 was run on 2 machines (higher uncertainties), while Applications 1 and 2 (below) were run on 3 machines and accordingly have large uncertainties. Application 3 (below) involved the greatest number of correction factors as it uses data not collected specifically for this part of the thesis (see Section 6.6).

6.5 Applications

Three applications of luminescence sensitivity monitoring have been trialed in the Gwydir catchment. The first attempted to trace sensitivity changes as they occur throughout a drainage network, in order to develop a picture of from where in the catchment sediment is derived. The second looks to compare the distributaries of the Gwydir fan-plain in terms of their effects on quartz sensitivity. The distributary nature of the system provides the special circumstances of a common initial bedload transported through a variety of stream types, thereby highlighting the effects of river behaviour over tributary inputs. The third application is an extension of the second with the aim of determining if palaeochannels have varying rates of downstream sensitivity increase. One complication of this latter application is that most individual palaeochannels can not be clearly traced over great distances and therefore some uncertainty remains about whether the same palaeochannel is being sampled. Though

this is a problem, it also presents an opportunity for examining the connectivity of uncertainly related palaeochannels, with samples of a single palaeochannel all expected to show the same sensitivity trend.

6.5.1 Sediment Sources for the Gwydir River

The location and surrounding geology of sediment sampling sites in the upper catchment of the study area are shown in Figure 6.5, and the results of the sensitivity investigations are shown in Table 6.1. It can be seen that there is a considerable variation in the ‘initial’ sensitivity of quartz, apparently depending on its geological provenance. In the Gwydir River itself, quartz sensitivity varies significantly downstream under the influence of tributaries, with the greatest shift being a result of inputs from north-bank tributaries (Warialda Creek and Mosquito Creek), which drain a large area of Jurassic sandstone, which in fact is an extension of the Pilliga Sandstone through which the Castlereagh River runs. Though this area represents only a minor proportion of the Gwydir River catchment (i.e. ~ 7 %), it appears from the effects on the sensitivity of Gwydir River quartz that this region is contributing a disproportionately high amount of the sampled quartz fraction. The Pilliga Sandstone readily weathers to unconsolidated sand, which presumably is easily mobilized, becoming a significant component of the bedload of the Gwydir River. The granite-dominated regions of the upper catchment produce quartz with the greatest initial sensitivity; however, the initially dimmer Pilliga Sandstone dominated quartz achieves a level of sensitivity approaching that displayed by the granitic quartz after ~ 150 km transit down the Gwydir River (Figure 6.6).

If the proposition that the majority of bedload material being transported today is derived from the Pilliga sandstone is correct, then it would appear that there has been a shift in source area dominance through time. Sediments of the palaeo-fluvial systems are generally highly potassic (see Section 2.3; Table 6.2) whereas the sands weathered from the Pilliga Sandstone are low in K. Brief discussion of the possible causes of this shift in source area, from the south of the catchment to the northern region where the Pilliga Sandstone is found, continues in the Chapter Eight.

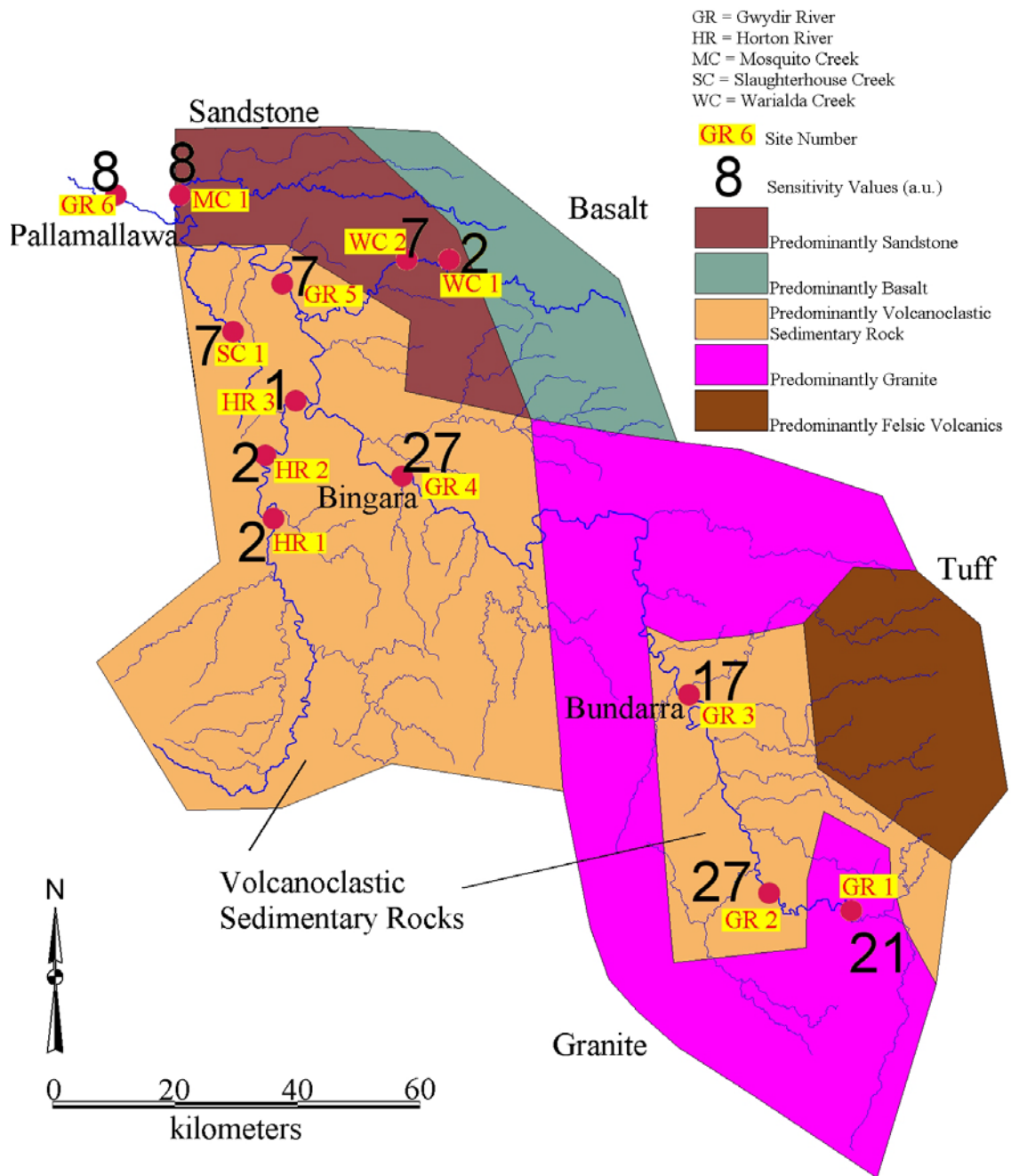


Figure 6.5 : Sensitivity values in arbitrary units ($\times 1000$, rounded to nearest integer) of quartz samples collected within the upper Gwydir Catchment. Schematic representation of major geological features shown.

Table 6.1: Sensitivity values for all Gwydir Catchment samples. Distance D.S. for sites upstream of Site GR 6 (highlighted) refers to approximate distance from stream origin. For sites on tributary channels downstream of Site GR 6, Distance D.S. is total stream distance from Site GR 6. WC 1 is a hill-slope sample taken from the Pilliga Sandstone. (Continues over two pages).

Site #	Stream	Distance D.S. (km)	Sensitivity (a.u.)
GR 1	Gwydir River	5	20900 \pm 630
GR 2	Gwydir River	25	26600 \pm 1325
GR 3	Gwydir River	65	16550 \pm 765
GR 4	Gwydir River	185	26900 \pm 1400
GR 5	Gwydir River	255	6530 \pm 390
GR 6	Gwydir River	295	8370 \pm 490
GR 7	Gwydir River	332	11750 \pm 800
GR 8	Gwydir River	369	16300 \pm 785
GR 9	Gwydir River	390	15450 \pm 1270
HR 1	Horton River	85	1515 \pm 195
HR 2	Horton River	100	2050 \pm 100
HR 3	Horton River	117	1100 \pm 100
SC 1	Slaughterhouse Ck	20	6835 \pm 490
WC 1	Warialda Ck	0*	1865 \pm 120
WC 2	Warialda Ck	45	6650 \pm 535
MC 1	Mosquito Ck	70	8350 \pm 540
MR 1	Mehi River	46	12000 \pm 630
MR 2	Mehi River	90	11350 \pm 630
MR 3	Mehi River	143	14165 \pm 1180
MR 4	Mehi River	165	10650 \pm 700
MR 5	Mehi River	180	12450 \pm 1190
MR 6	Mehi River	195	12340 \pm 1140
MR 7	Mehi River	225	16075 \pm 1070
MR 8	Mehi River	250	11670 \pm 1010
MR 9	Mehi River	280	14530 \pm 945

Site #	Stream	Distance D.S. (km)	Sensitivity (a.u.)
MR 10	Mehi River	305	17645 ± 1435
MR 11	Mehi River	330	16725 ± 1280
MC 1	Moomin Ck	10	10400 ± 630
MC 2	Moomin Ck	54	9230 ± 970
MC 3	Moomin Ck	105	11350 ± 685
MC 4	Moomin Ck	162	8025 ± 910
MC 5	Moomin Ck	270	14650 ± 1090
MC 6	Moomin Ck	310	16700 ± 1100
CC 1	Carole Ck	70	13500 ± 970

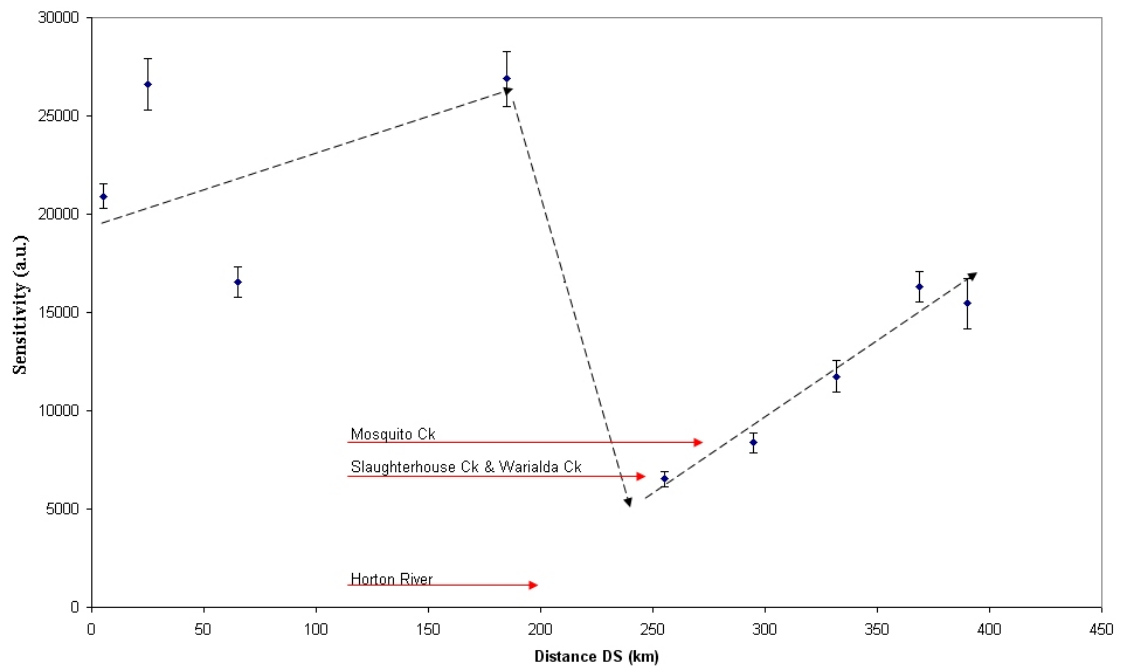


Figure 6.6: Downstream trend in sensitivity for quartz sampled from the Gwydir River. Dashed lines indicate suggested trends. Labeled lines indicate input of material from tributaries, with vertical location indicating sensitivity of tributary inputs.

6.5.2 River Description for the lower Gwydir

It may be noted in Figure 6.5 above, that each stream appears to contain quartz bedload that increases in sensitivity downstream, as would be expected based on the results of Experiment 1. However, partly due to the uncertain effects of the downstream changes in geology and partly because of the low precision of the investigation, it is not possible to make meaningful distinctions in terms of sensitizing behaviour between streams in the upper catchment. In the lower catchment, however, circumstances are more favorable.

If Site GR 6 (Figure 6.7) is considered as representative of the final mixture of bedload delivered to the head of the fan, then this can be taken as the starting point for assessment of behavioural differences in the distributaries based on the changes in quartz sensitivity downstream.

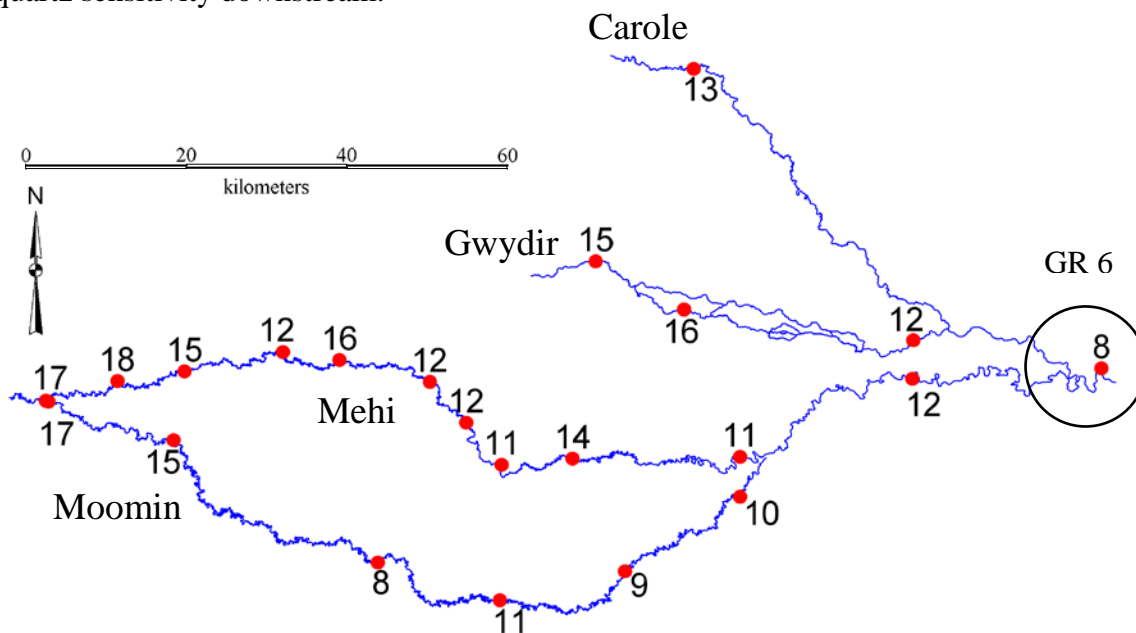


Figure 6.7: Sensitivity values in arbitrary units ($\times 1000$, rounded to nearest integer) of quartz samples collected within the Gwydir distributary system. Site labels are not shown for clarity. They are, however numbered sequentially with increasing distance downstream. The uppermost site is Site GR 6.

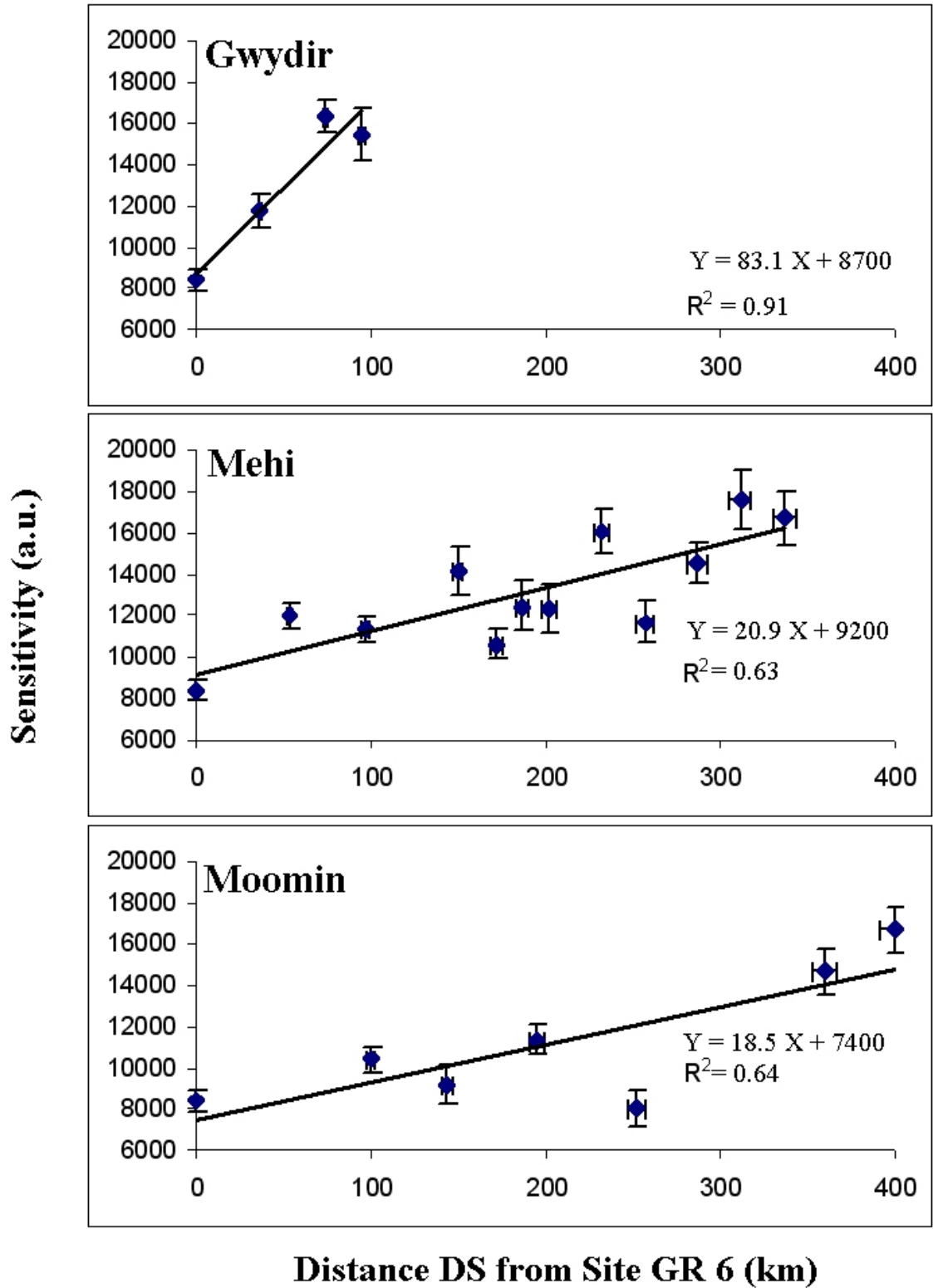


Figure 6.8: Differential sensitivity increase in arbitrary units (a.u.) for streams of the Gwydir distributary system. Note ordering of lines of best fit gradients: Gwydir (83.1) – Mehi (20.9) – Moomin (18.5). Though not plotted due to paucity of data, Carole Ck appears to have a rate of sensitivity increase similar to Moomin Ck. 2 % uncertainty added to Distance DS values.

Again considering the limited precision of the dataset, it can be seen that the Gwydir River has the greatest sensitizing effect on quartz followed by the Mehi River, with the Moomin Creek having the least sensitizing effect (only one sample was retrievable from Carole Creek, it is therefore excluded from further discussion). This is just as may have been predicted based on the arguments of flow regimes detailed in Chapter 3. As the Gwydir experiences the largest number of small flows, it will bury and exhume quartz repeatedly, thus sensitizing it the most. At the other extreme, the Moomin Creek (under a natural flow regime) flows only during high flow events. Thus, not only are the number of transport events fewer, they are likely to be more extended (moving bedload further) when they do occur. Moomin Creek will therefore sensitize quartz the least. The high likelihood of any sandy bedload in the Moomin being overlain by fines after deposition should also be considered, as this will also reduce the sensitizing effects of the Moomin.

6.5.3 Palaeochannel Connectivity Analysis

The determination of sensitivity values for quartz from ancient deposits (Table 6.2) has been undertaken using data collected during single grain dating procedures (see Chapter Five), rather than on material specifically prepared for sensitivity assessment. This was due principally to a lack of available material. Sensitivity was assessed for each single grain disc by summing the total light from all grains emitted in response to the first test dose (normalised to account for variations in the size of the test dose used). Unfortunately, the dating procedures were carried out without realization of subsequent uses for the collected data. Specifically, in loading discs not all grain wells were filled and no record was kept of the variation in grain numbers per disc, and, the size of the test dose was not kept constant across all analyses. Most samples displayed such high inter-disc sensitivity variation that the results could not be meaningfully interpreted. However, all the samples shown in Figure 7.6 (see Chapter 7) gave reasonable sensitivity results. Part of this figure is reproduced here with the sensitivity of each sample reported (Figure 6.9). As can be seen the values provide additional data on which to base stratigraphic correlations. Initially, sample GF-22 was expected on the basis of channel alignments to be part of the Kookaburra Palaeochannel, however, it can be seen from both the geochronology and the sensitivity analysis that this is unlikely

to be the case. Furthermore, it can also be observed that it is highly likely that the Kookabunna Palaeochannel is the source of the sand for the dune at Site GF-27. A similar investigation comparing the sand dune at Site GF-26 with its apparent source palaeochannel at Site GF-23 revealed a similar correspondence in sensitivity values (see Table 6.2).

Although it would obviously be highly desirable to rate palaeochannels in terms of their relative downstream sensitizing efficiency, only samples collected from the Kamilaroi Palaeochannel (GF-20, GF-21, GF-1) were sufficiently precise to reveal a downstream increase in sensitivity (48 ± 20 , 81 ± 33 , 246 ± 29). Sensitivity values of samples from the Coocalla and Kookabunna Palaeochannels had such high uncertainties that no downstream trends could be detected.

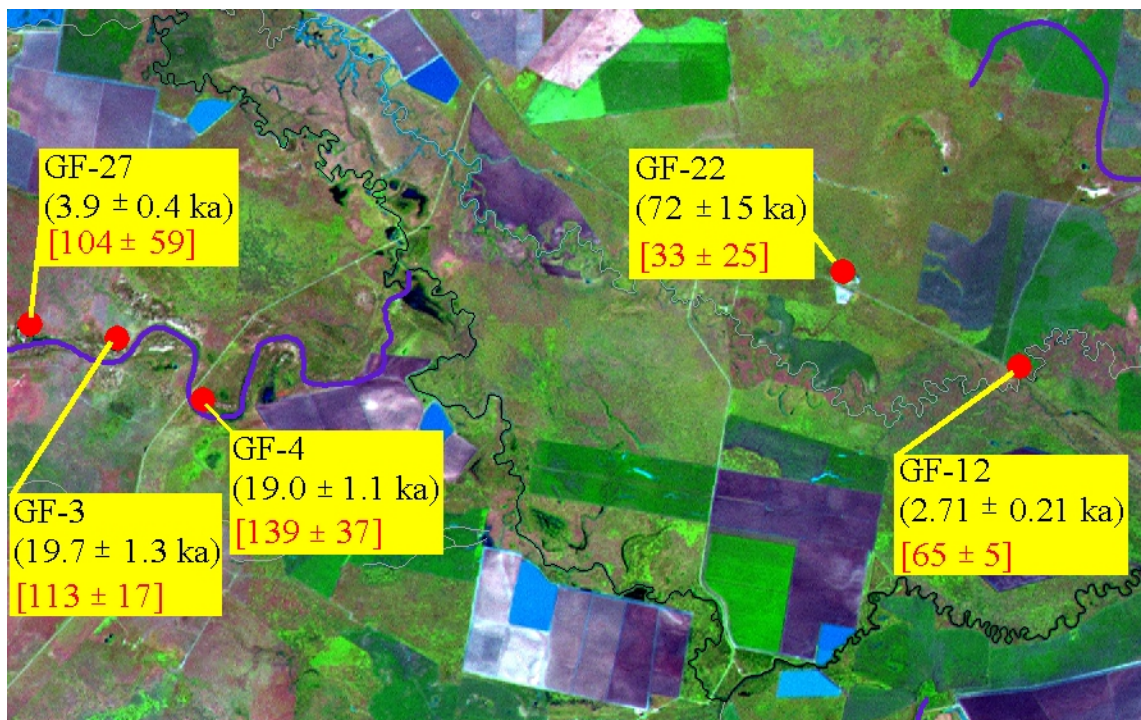


Figure 6.9: Sensitivity values (square brackets) and ages for samples from the Kookabunna Palaeochannel in comparison with Bullarah Pit (GF-22) and Browns Ck (GF-12). The dark meandering channel across the centre of the image is the Mehi River.

Table 6.2: *Sensitivity Values for ancient deposits of the lower Gwydir Valley.*

Sample	Mean \pm uncertainty
GF-1	246 \pm 29
GF-2	120 \pm 14
GF-3	113 \pm 17
GF-4	139 \pm 37
GF-5	151 \pm 25
GF-6	143 \pm 44
GF-7	145 \pm 37
GF-8	89 \pm 20
GF-9	141 \pm 31
GF-10	178 \pm 22
GF-11	165 \pm 28
GF-12	65 \pm 5
GF-16	192 \pm 18
GF-17	131 \pm 50
GF-18	135 \pm 11
GF-19	130 \pm 21
GF-20	48 \pm 20
GF-21	81 \pm 33
GF-22	33 \pm 25
GF-23	151 \pm 10
GF-24	274 \pm 19
GF-26	129 \pm 24
GF-27	104 \pm 59

6.6 Summary and Discussion

Though this study of quartz sensitivity is preliminary, it does offer the potential to add to the suite of tools available for catchment-scale investigations. Its use here is demonstrated in a limited setting and, in the case of the palaeochannels, with samples

not specifically collected and prepared for the experiment. However, even with these limitations, it is possible to see the potential value of the technique.

The most significant finding of this investigation into quartz sensitivity has been the identification of a mechanism to account for the generally observed ideal luminescence characteristics of Australian quartz, namely, the episodic downstream transport of material in large ephemeral rivers such as the Castlereagh. Repeated cycles of exposure, burial and re-exposure have been shown to increase the sensitivity of quartz (Figure 6.4), suggesting that at least part of the explanation for the high luminescence sensitivity of Australian quartz may be the predominance in Australia of the river style exemplified by the Castlereagh.

Characterising the luminescence sensitivity of bedload sediments throughout the Gwydir drainage network has enabled the identification of the principal source areas of bedload material of the contemporary fluvial system (Figures 6.5; 6.6), as well as the testing of the variable flow recurrence amongst distributary channels hypothesis outlined in Chapter 3 (Section 3.1.4; Figure 6.8). In terms of bedload contributions, the low potassium Pilliga Sandstone predominates today, though this could not have been the case in the past given the high potassium signature of the palaeochannels (Figure 2.2). Sensitivity monitoring has enabled some clarification of the distinctive imagery presented in Chapter 2, by way of highlighting the likely shift in sediment source area through time.

Sensitivity monitoring has successfully identified the ordering of distributary channels as sensitizers, as would be predicted based on their differing hydrology (see Chapter 3). Supporting evidence for the inferred hydrological differences between trunk and distributary streams has been provided by analysis of downstream changes in quartz sensitivity throughout the distributary network. On the fan-plain, the Gwydir River is the most efficient sensitizer of quartz, suggesting that its hydrological regime provides the most opportunities for transport and burial. The distributary Mehi and Moomin channels have had less impact on the luminescence sensitivity of their quartz bedload (Figure 6.8), consistent with hydrological regimes dominated by low frequency high magnitude events mediated by their high off-takes.

This chapter has provided an additional if still problematic tool to be used in the description of palaeochannel behaviour and connectivity. Unfortunately the precision of the sensitivity data relevant to palaeochannels was compromised by the analysis procedures used, however the data can be used to provide corroborative evidence for the suggested palaeochannel connectivity presented in Figure 2.7. There appears to be no theoretical impediment to high precision analyses being used to infer palaeochannel behaviour in the future, with the tantalizing possibility of being able to distinguish between palaeochannels based on their hydrological regime. Although possibly a statistical fluke, the similarity in sensitivity between aeolian dunes and nearby palaeochannels is highly suggestive of the palaeochannels having been the immediate source for dune sediments.

Chapter 7 Gwydir Fan-Plain Chronology

This chapter presents a detailed OSL chronology for palaeochannels and related features of the Gwydir distributary system on the basis of 29 dates produced using the improved analytical method (Olley *et al.* 2004a) outlined in Chapter 5. OSL analyses were undertaken on quartz grains of 180-212 μm diameter extracted from each sample and purified in the standard manner (e.g. Aitken, 1998), as outlined in Section 5.6.2. Twenty-six of the analyses were made using single grains, with the remainder undertaken on small aliquots (~100 grains).

The sampling program was designed to include geochronological characterisation of both the readily identifiable palaeochannel features, as well as those sand and gravel deposits exposed in roadside quarries where a lack of palaeochannel form at the surface makes their origin less certain. For the present purposes, depositional features of the Gwydir fan-plain have been divided into four categories: well-defined channels and palaeochannels (including the contemporary system and its flood-deposits), surficially undefined palaeochannels only visible in quarry exposures, disjunct palaeochannel remnants and aeolian dunes.

7.1 Well-Defined Channels and Palaeochannels

The four extensive, well-defined, palaeochannels described in Chapter 4 form the basis of the dating program reported here (Figure 7.1 – 7.6). The Kamilaroi and Mia Mia palaeochannels have each been sampled once (GF-1, GF-2), from quarries in obvious point bar sequences. The Kookaburra palaeochannel was sampled three times, once from a quarry (GF-3), with two additional samples (GF-4,5) taken from bore holes into the inside of meander bends. The Coocalla palaeochannel has been sampled five times, from three quarries (GF-6,7,8,9) and two bore holes (GF-10,11). In addition to the four main palaeochannels, the ‘contemporary’ system has been sampled in two places. GF-12 was taken from a bore hole into the meander belt of Browns Creek, while samples (GF-13,14,15) were obtained from the top metre of the contemporary floodplain at Yarraman.

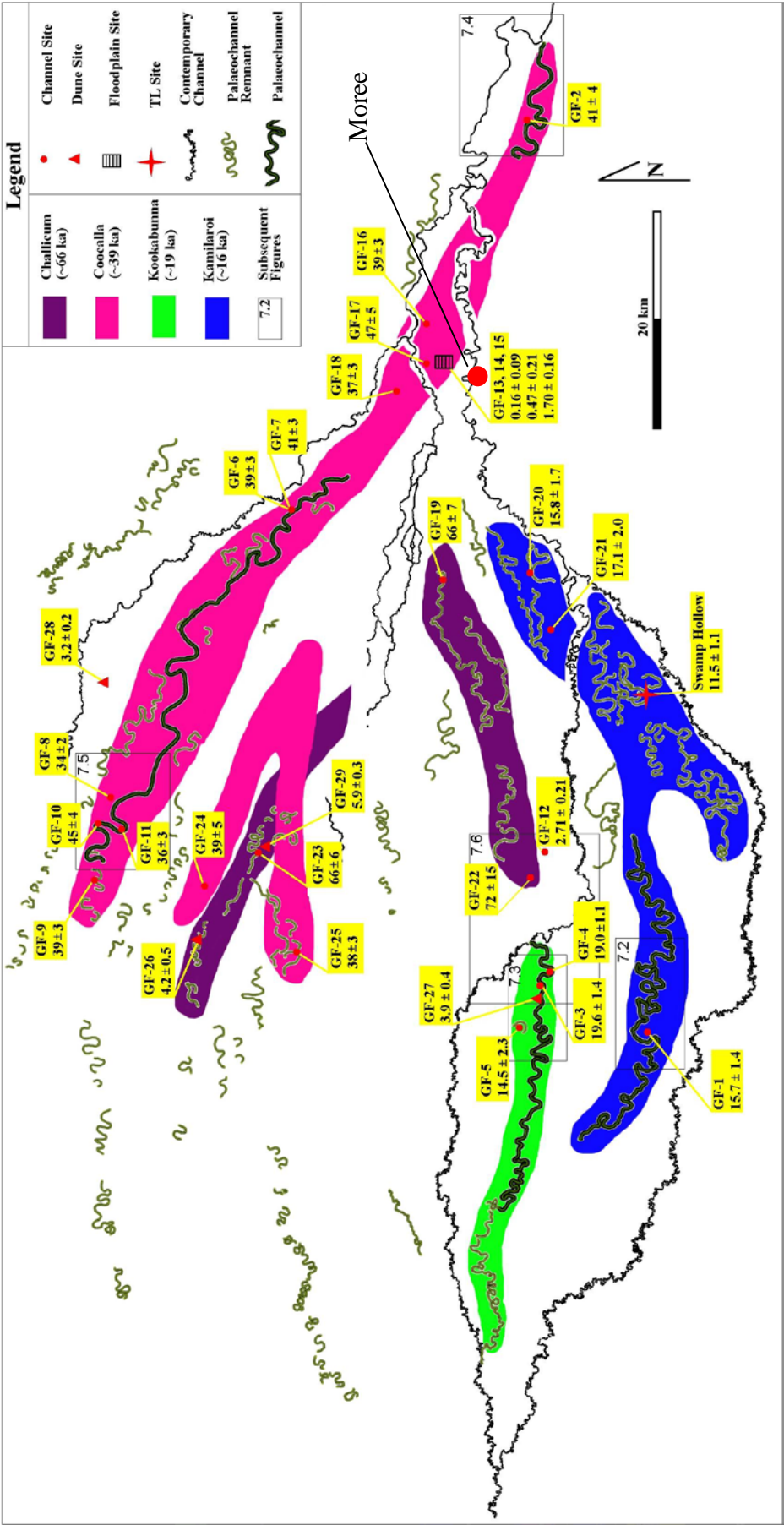


Figure 7.1: Palaeochannel age map of the Gwydir fan-plain.

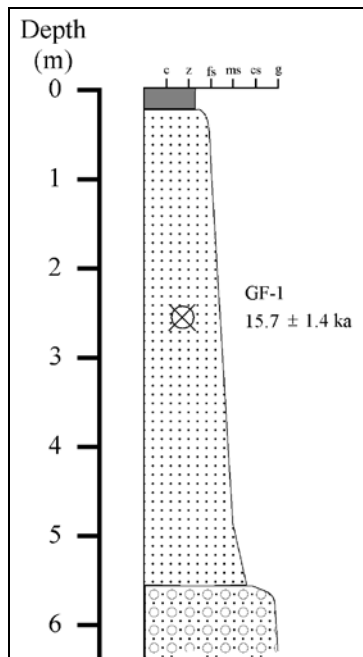
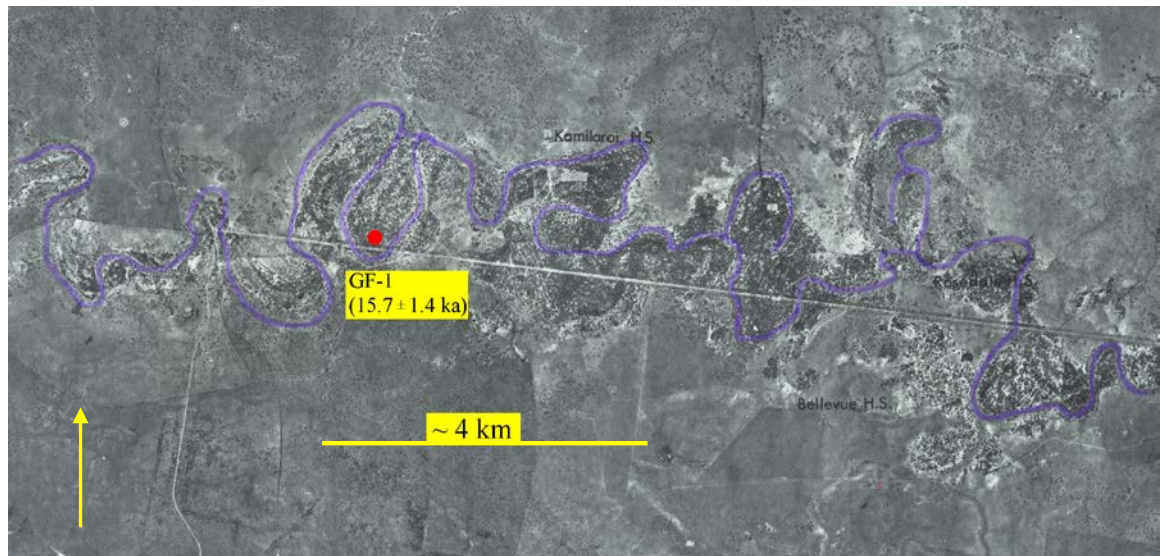


Figure 7.2: Kamilaroi palaeochannel, showing sampling location and borelog data. Estimated Q_{bf} from Chapter 4 is $1310 \text{ m}^3 \text{ s}^{-1}$.

7.2 Surficially Undefined Palaeochannels

While many palaeochannels have poor or non-existent surface expression (see Figure 2.10), several gravel pits across the fan provide excellent access to subsurface

stratigraphy (Figure 7.7). Extrapolating the general line of possible palaeochannels on the basis of these gravel pits provides an indication of their likely location, however; the exact path of such channels remains undetermined. By sampling from these sites (GF-16, 17, 18, 19, 20, 21, 22) it was hoped that the deposits could be related geochronologically to the sections of palaeochannels that could be traced by their surface expression. Of particular interest are the extensive gravel deposits at the head of the fan-plain which, due to subsequent surficial deposition, are located where there is virtually no surface expression of the original channel(s).

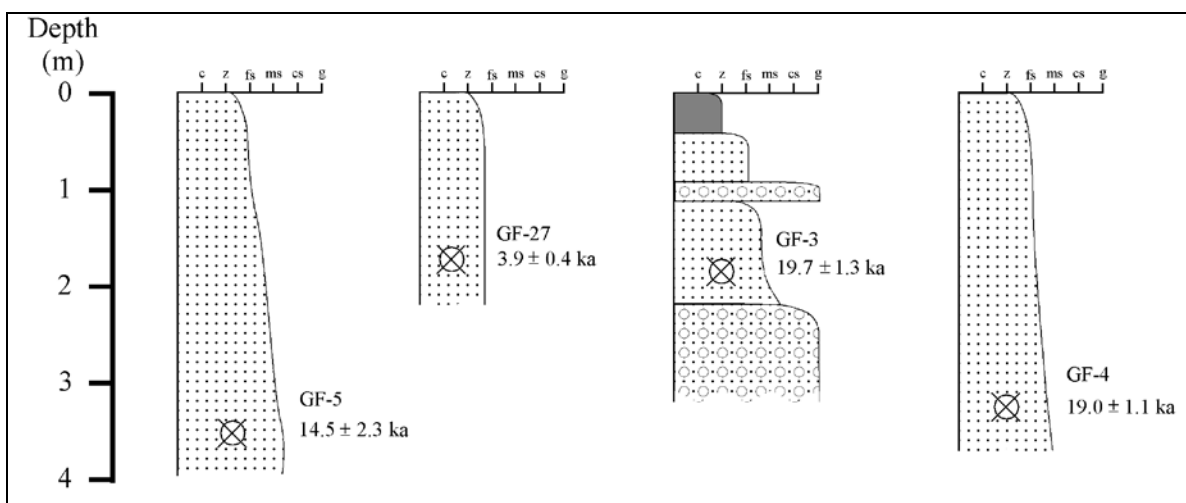
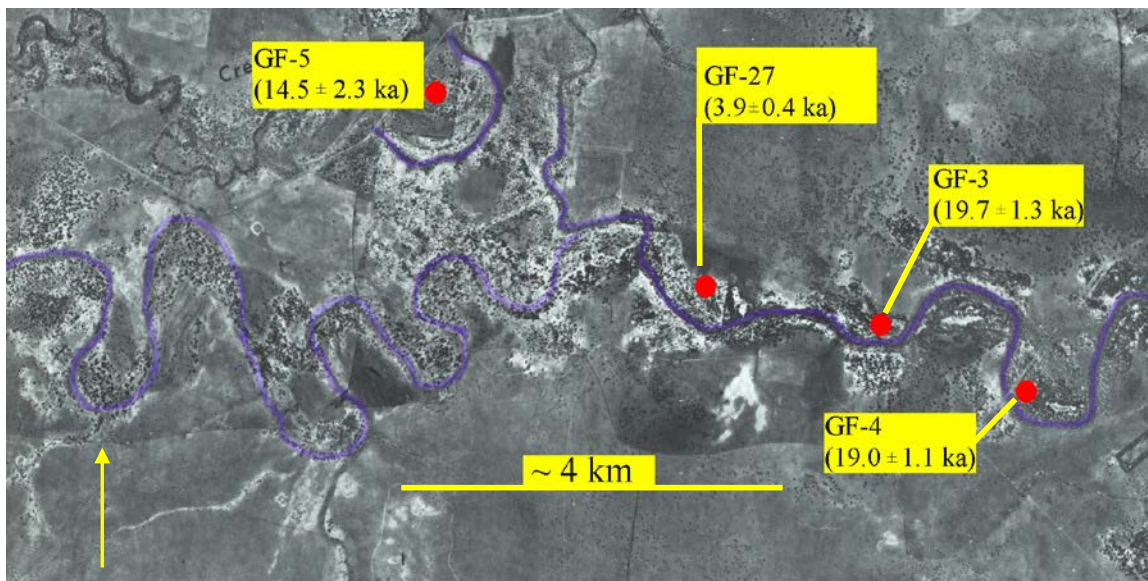


Figure 7.3: Kookaburra palaeochannel, showing sampling locations and borelog data. Estimated Q_{bf} from Chapter 4 is $1240 \text{ m}^3 \text{ s}^{-1}$.

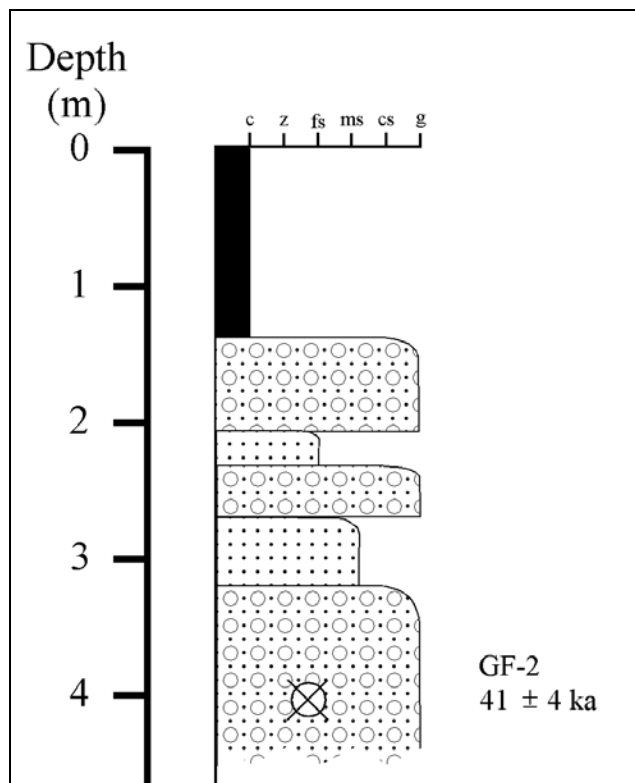
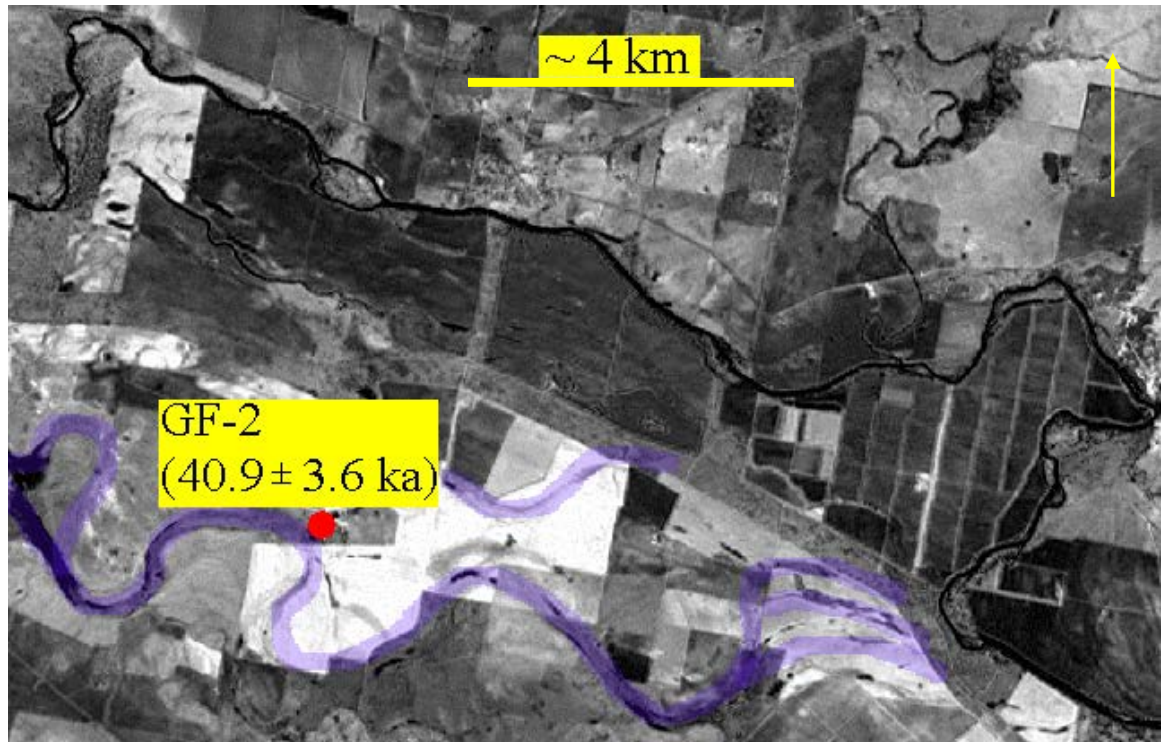


Figure 7.4: Mia Mia palaeochannel, showing sampling location and borelog data. Estimated Q_{bf} from Chapter 4 is $2390 \text{ m}^3 \text{ s}^{-1}$.

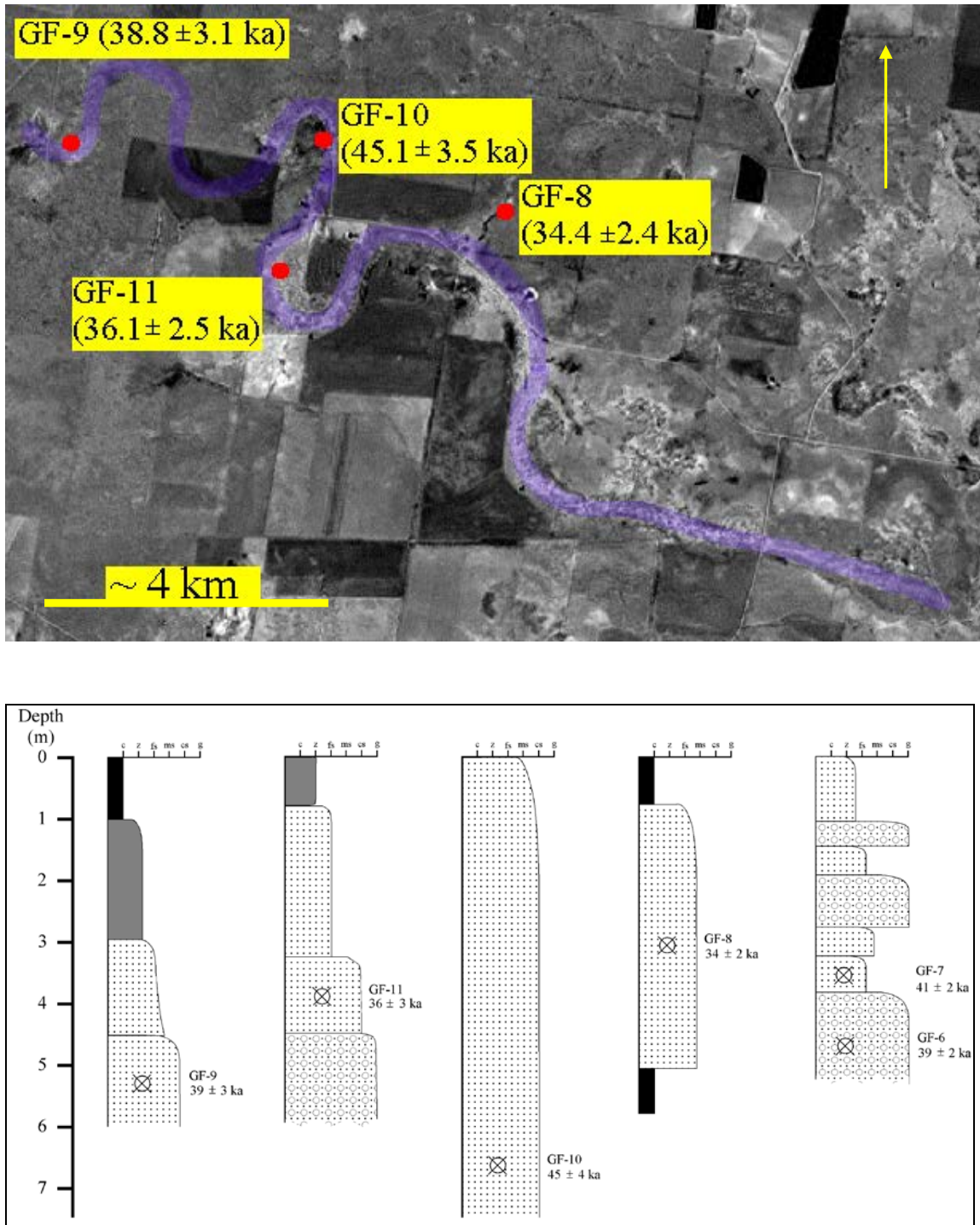


Figure 7.5: Coocalla palaeochannel, showing sampling locations and borelog data. The Coocalla palaeochannel was also sampled ~ 20 km south east of the reach shown in this photo on the property 'Colmlee' (GF-6, GF-7). Estimated Q_{bf} from Chapter 4 is $2710 \text{ m}^3 \text{ s}^{-1}$.

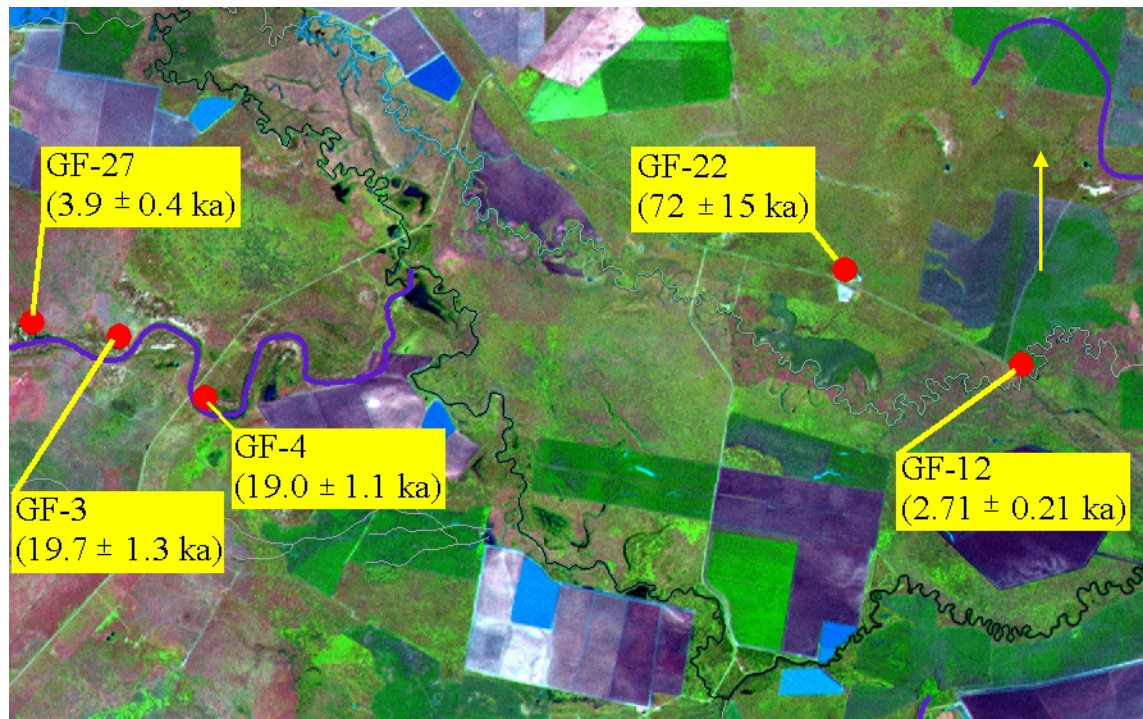
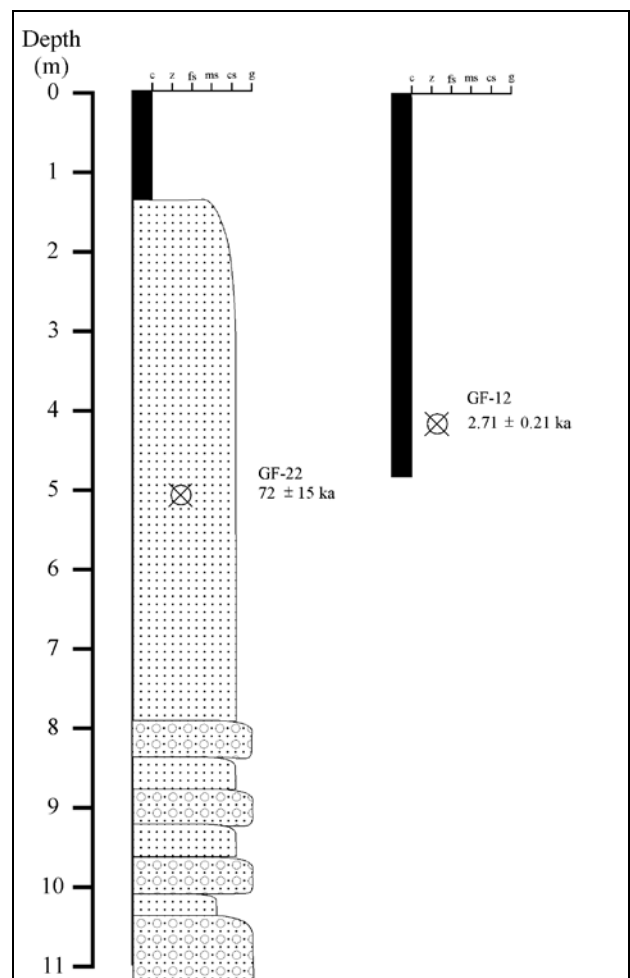


Figure 7.6: Borelog data and sampling locations on and near Browns Creek (pale blue meandering channel) (GF-12) including Bullarah quarry (GF-22) and Kookabunna palaeochannel (GF-3, 4 and 27). Borelog data for Kookabunna deposits provided in Figure 7.3. Q_{bf} of Mehi River (dark meandering channel) in this reach is approximately $20 \text{ m}^3 \text{ s}^{-1}$. Flows in Browns Creek and Mehi River are from right to upper left.



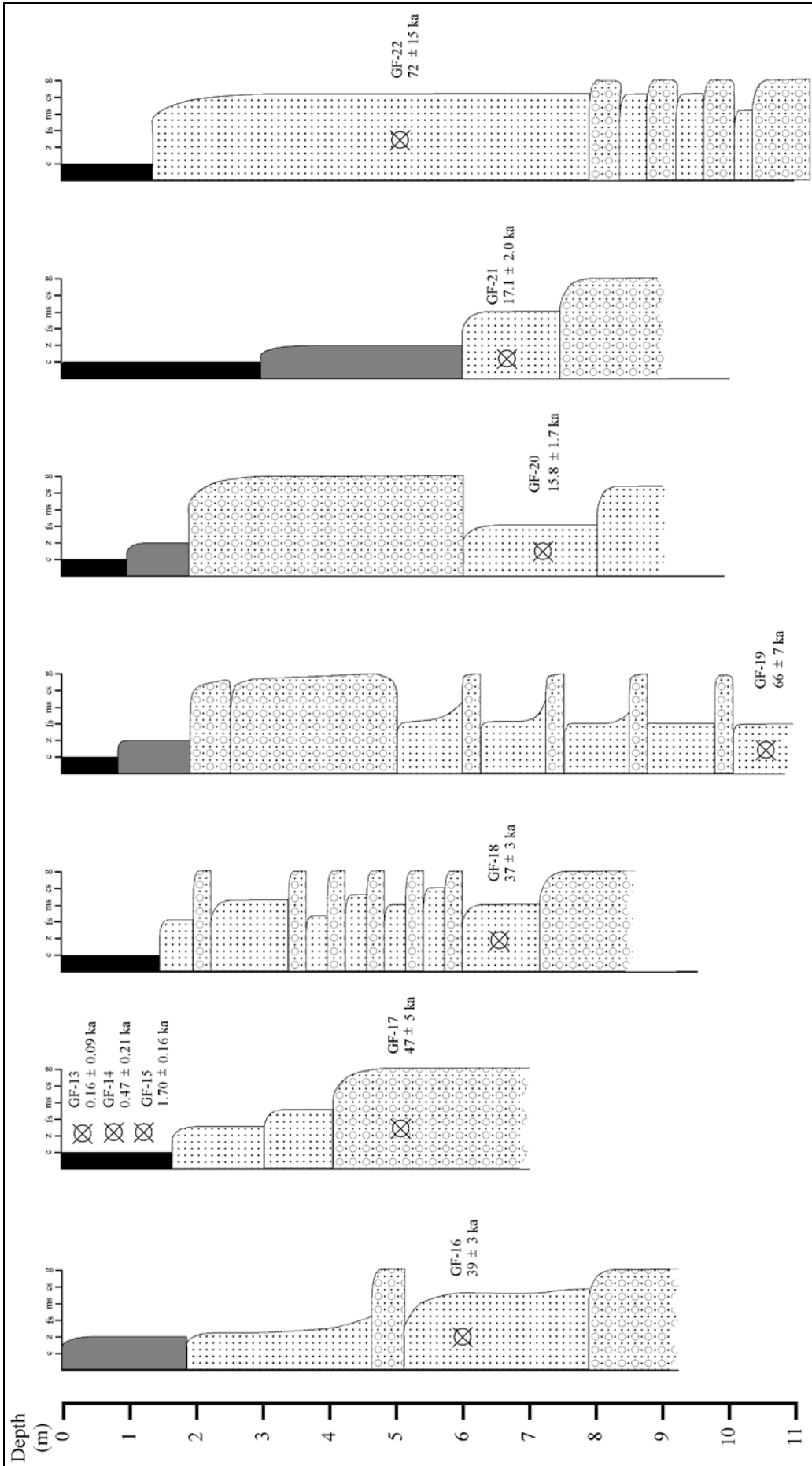


Figure 7.7: Borelog data from isolated gravel pits. See text and Figure 7.1 for locations.

Samples GF-16, 17 and 18 (Figure 7.7) lie near the apex of the fan-plain, and therefore could be related to any of the palaeochannels. However, as these gravel deposits are extensive, they have initially been assumed to be related to Coocalla, the largest of the palaeochannels. Samples GF-20 and GF-21 could relate to either the Kamilaroi or the Kookabunna palaeochannel while GF-19 and GF-22 appear to relate to the Kookabunna palaeochannel (Figure 7.7). The results of the dating exercise are reported in the Section 7.4, and, as shown by the dates in Figures 7.1 – 7.7, adaptation of these initial assumptions is required.

7.3 Palaeochannel Remnants and Aeolian Dunes

In several places short disjunct remnants of palaeochannels exist, three of which have been sampled (Figure 7.8). Given the large number of such remnants (see Figure 2.24) geochronological investigation of all of them was not possible within the resources of this study. Rather, demonstration of the complexity of palaeochannels and some representation of their ages were sought via sampling from a particularly congested part of the fan in the vicinity of Gingham Waterhole. Here multiple palaeochannels merge and/or cross with alignments at high angles to each other. GF-23 was obtained from the palaeochannel appearing in Figure 2.5 on the property 'Bunnor'. This channel can be traced to the east for a short distance, while to the west it appears to merge with the palaeochannel currently occupied by the Gingham Watercourse. Sample GF-24 was obtained from a bore hole sited 'mid-stream' in the Gingham Watercourse, where it is at its narrowest because of being constrained by the palaeochannel levees. Sample GF-25 was obtained in a sand deposit (splay?) apparently associated with the palaeochannel extending to the south west.

What are interpreted to be source-bordering aeolian dunes are an ill-defined but common feature on the fan-plain. These are found in association with palaeochannel complexes, and have a low splay-like form, generally extending ~ 2 m above the surrounding floodplain. They typically consist of well-sorted, fine to medium sand extending from the surface to a depth of at least 4 metres. Their fine well-sorted texture suggests that they are aeolian rather than directly fluvial in origin, therefore they are more likely to be source bordering dunes than fluvial splays. These features were

sampled in four places (GF-26, 27, 28, 29) (Figure 7.9). For samples GF-26 and GF-27 there is an obvious association between the dune and the adjoining palaeochannel; however, for the others, the connection is not as clear. At the GF-28 site, the sample was taken from within a small pit into well-sorted fine sand, but the aeolian source for this material could not be identified. Site GF-29 is a more extensive sand body, which is likely to be a source-bordering dune supplied from one of the near-by palaeochannels. However, the possibility that it is the remnant of a fine-grained point-bar, such as appears in Figure 2.4(d), can not be excluded.

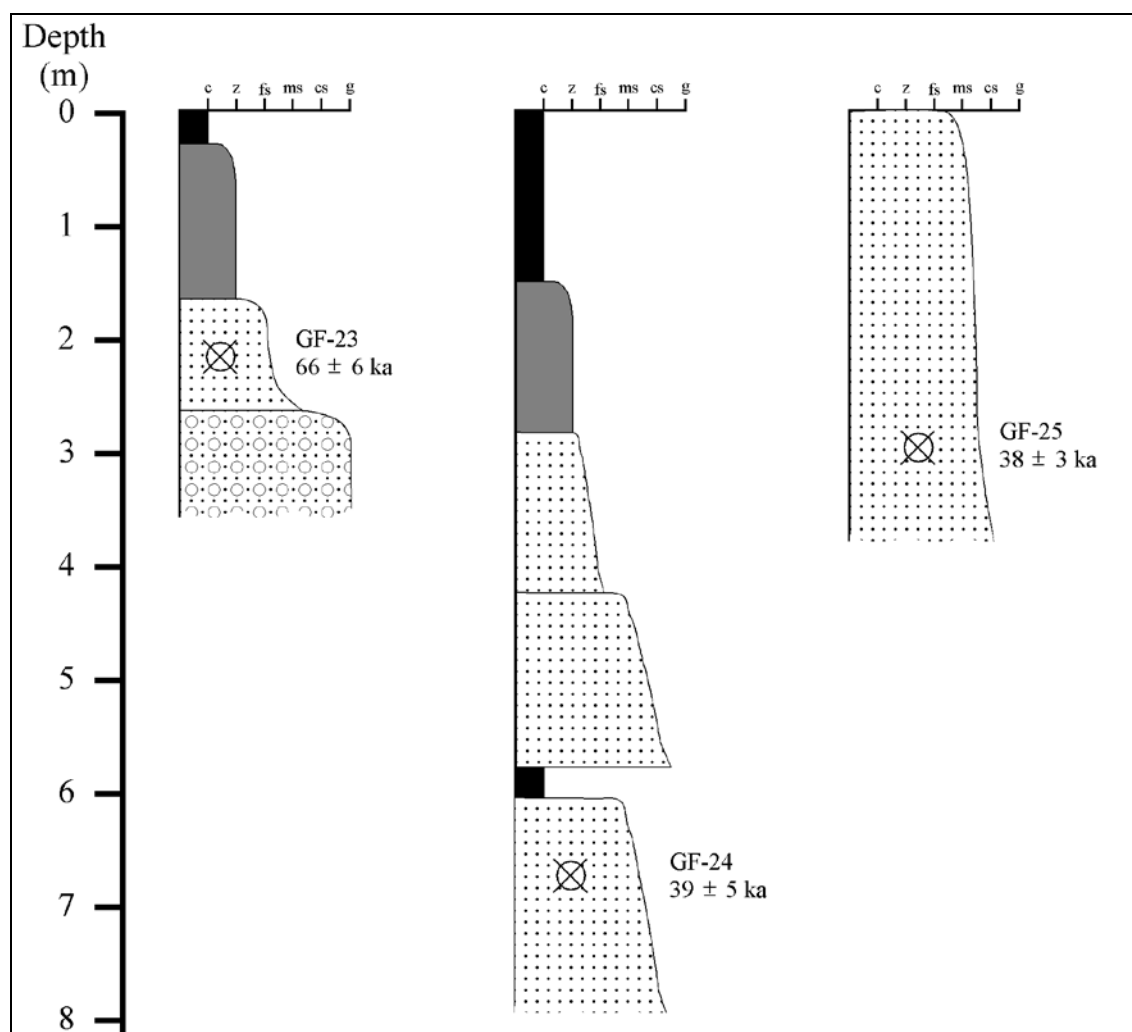


Figure 7.8: Borelog data from palaeochannel remnants. See text and Figure 7.1 for locations.

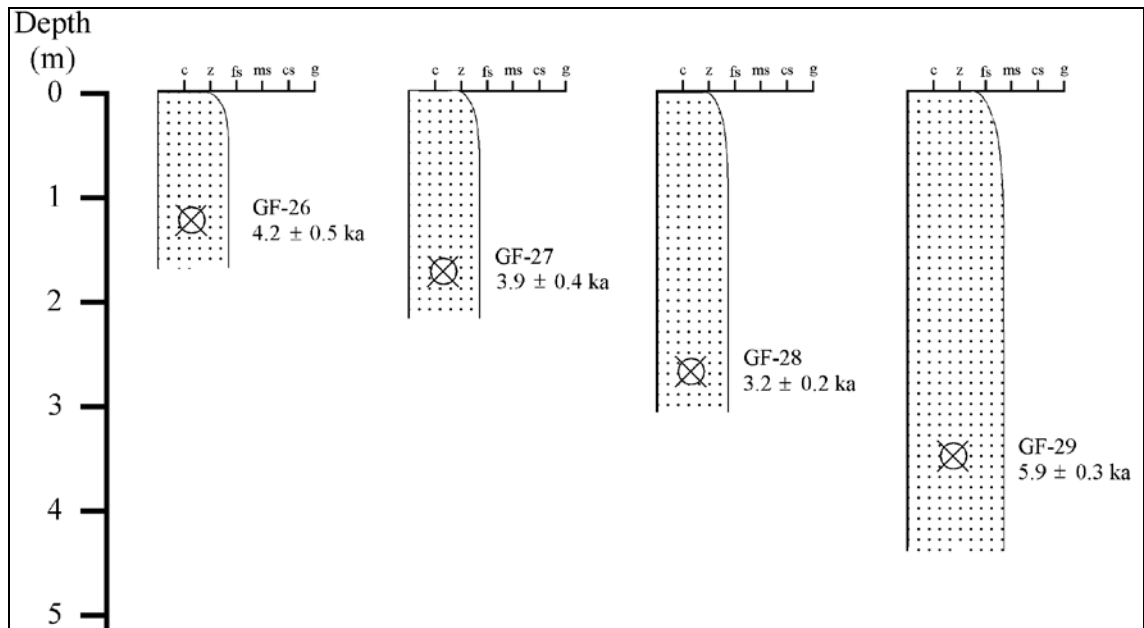


Figure 7.9: Borelog data from suspected aeolian dunes. See text and Figure 7.1 for locations.

7.4 Age Estimates

Table 7.1 lists the ages for each sample. It can be seen that where single features (e.g. the Coocalla or Kookabunna Palaeochannels) are dated using multiple samples, good agreement is found between the dates. Such internal consistency allows some confidence in the dating technique, including the data analysis procedures. Furthermore, it can be seen that samples from sites with no surface expression have ages corresponding to nearby palaeochannels, allowing them to be tentatively correlated. Exceptions to this are GF-19 (66 ± 7 ka) and GF-22 (72 ± 15 ka) which, though lying along the same general path as the Kookabunna Palaeochannel (~ 19 ka), are unrelated to it in age (Figure 7.1). GF-19 and GF-22 do, however, appear to be chronologically part of the same system despite their spatial separation by some 30 km. Hence, they are used to define the unit subsequently referred to as the Challicum Unit.

The Coocalla Palaeochannel has been dated using six samples (GF-6, 7, 8, 9, 10, 11) which have ages of 39 ± 2 ka, 41 ± 2 ka, 34 ± 2 ka, 39 ± 3 ka, 45 ± 4 ka and 36 ± 3 ka. The Mia Mia Palaeochannel has been dated at one site (GF-2) at 40.9 ± 3.6 ka. The three samples situated between the Coocalla and Mia Mia Palaeochannels (GF-16, 17,

18) have ages of 39 ± 3 ka, 47 ± 5 ka and 37 ± 3 ka. It may therefore be proposed that the Coocalla and Mia Mia Palaeochannels, and the intervening gravel deposits, are in fact one unit with an age range centred on ~ 39 ka. The Kookabunna Palaeochannel is dated at three sites (GF-3, 4, 5; 19.6 ± 1.3 ka, 18.9 ± 1.1 ka and 14.5 ± 2.3 ka, respectively). The Kamilaroi Palaeochannel has been dated to 15.7 ± 1.4 ka at GF-1 with two apparently contiguous sites (GF-20, 21) dating at 15.8 ± 1.7 ka and 17.1 ± 2.0 ka. The Swamp Hollow site has a TL age of 11.5 ± 1.1 ka, and is therefore included within the Kamilaroi Unit, based on the assumption that the TL age is approximately 70 % of the true age due to feldspar contamination (see Table 5.3). The aeolian dunes (GF-26, 27, 28, 29) appear to cluster near 4 ka, with ages of 4.2 ± 0.5 ka, 3.9 ± 0.4 ka, 3.22 ± 0.21 ka and 5.9 ± 0.3 ka, respectively, while the contemporary fluvial system is dated at Browns Ck (GF-12) to 2.71 ± 0.21 ka and at Yarraman Floodplain (GF-13, 14, 15) to < 1.5 ka. The accretion rate at Yarraman appears to be of the order of 0.5 mma^{-1} (Figure 7.10). This estimate contrasts with observations of accretion rates mentioned previously. Riley and Taylor's (1978) estimate of 1 m in 50 ka equates to an average annual rate of 0.02 mma^{-1} , while the burial of a fenceline recorded by Mahaffey (1985) requires an approximate annual accretion rate of 20 mma^{-1} (assuming burial of a 1 m fence in 50 a). Evidently, floodplain accretion is highly variable across the surface.

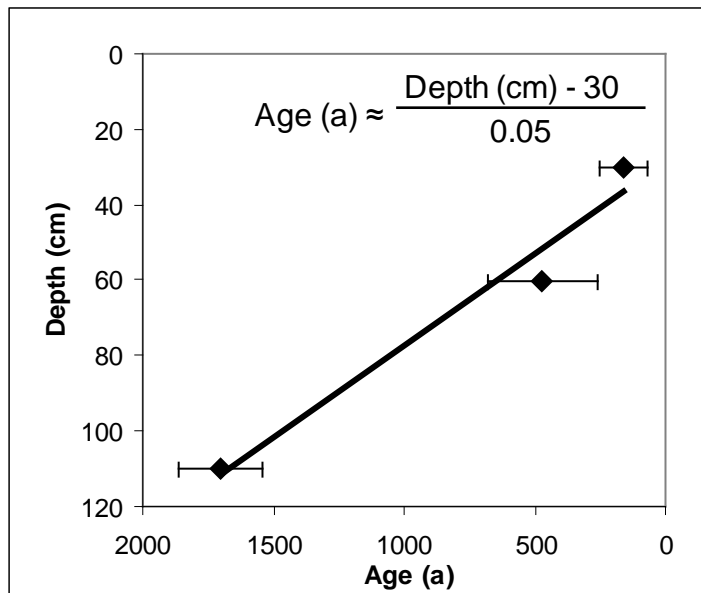


Figure 7.10: Plot of Depth vs. Age for floodplain samples at Yarraman. Note the non-zero intercept, possibly indicating the depth of soil cracking or post-European disturbance.

The sampled palaeochannel remnants (GF-23, 24, 25) indicate that disparate channel segments can be of equivalent age, with GF-23 (66 ± 6 ka) being age equivalent with the Challicum Unit (GF-19, 22); and GF24 (39 ± 5 ka) and GF-25 (38 ± 3 ka) both having the same age as the Coocalla Palaeochannel. This raises the possibility that palaeochannels, when functional, were part of a distributary network. The precision in the dates is not as yet sufficient to prove adjacent channels actually coexisted, but overlapping dates indicate that such a situation is possible and given the present situation on the fan-plain, even likely. This has palaeoclimatic significance, as hydrological shifts (as documented in Chapter 4) may be a function of changes in the number of channels, rather than (or as well as) the overall volume of water transmitted.

7.5 Summary

Figure 7.11 summarises the geochronological data collected on the Gwydir fan-plain. At ~ 65 ka, the Challicum Unit, consisting of thick (> 12 m) gravelly point-bars was emplaced in the mid-south of the fan. Virtually no surface expression of this unit remains here. However, to the north at 'Bunnor', a very well preserved remnant of a similar aged (possibly contemporaneous) palaeochannel remains. At ~ 39 ka the largest ($Q_{bf} \approx 2550 \text{ m}^3 \text{ s}^{-1}$) of the well-preserved palaeochannels, Coocalla, was operative, extending from south of the current head of the fan-plain in a north-westerly direction. This channel laid down extensive gravel deposits in the vicinity of Moree. At ~ 19 ka the Kookabunna palaeochannel ($Q_{bf} \approx 1240 \text{ m}^3 \text{ s}^{-1}$) was operative, possibly re-working the deposits of the Challicum Unit. A marginally larger channel, the Kamilaroi ($Q_{bf} \approx 1310 \text{ m}^3 \text{ s}^{-1}$), was operative slightly later at ~ 16 ka. Perhaps signaling a period of enhanced aridity or flow seasonality, aeolian dunes appear to cluster near 4 ka. Finally, the contemporary channel system (total combined channel capacity mid-fan $\approx 200 \text{ m}^3 \text{ s}^{-1}$) was operating by at least ~ 2.7 ka, laying down flood deposits that are accreting, near Yarraman, at $\sim 0.5 \text{ mma}^{-1}$. The relationships between the chronology obtained here and that for other Late Quaternary palaeoenvironments in south-eastern Australia are discussed in the next chapter.

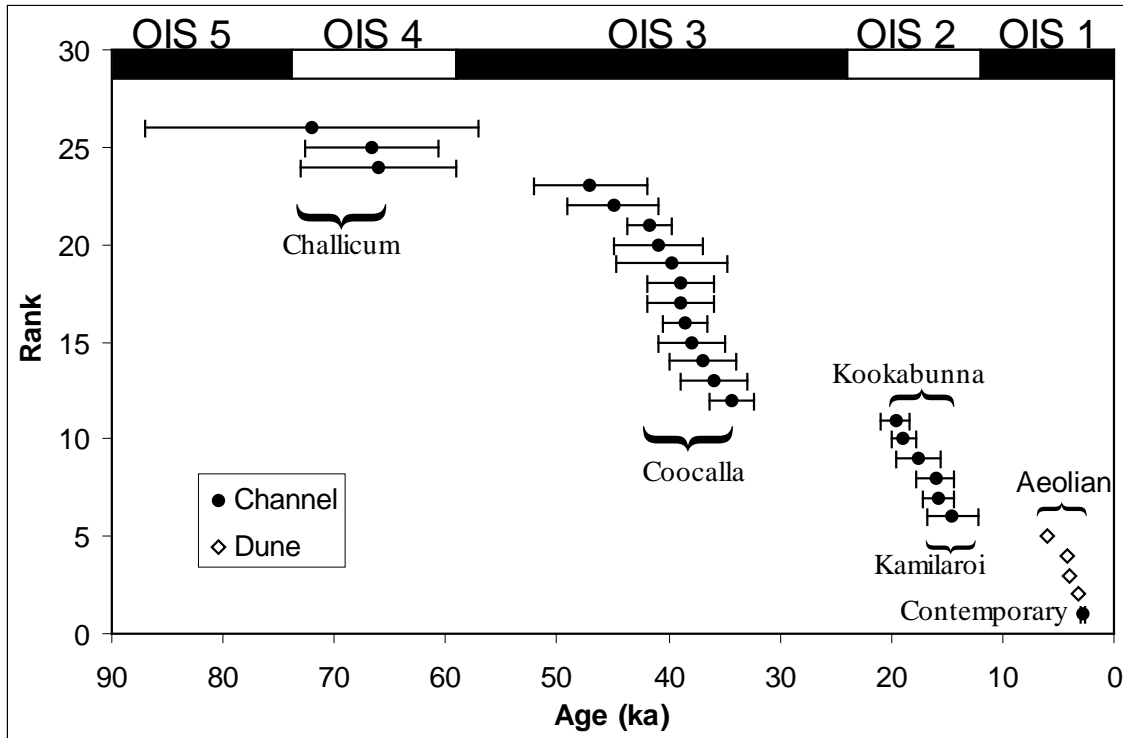


Figure 7.11: Age / Rank plot for OSL ages collected from the Gwydir fan-plain. The divisions shown on the top axis are oxygen isotope stages of Martinson et al., (1987).

Table 7.1: D_e estimate, over dispersion parameter, D_r and calculated OSL age for all samples.

Sample	Feature	D_e (Gy)	σ_d^1 (%)	D_r (Gy ka ⁻¹)	Age (ka)
GF-1	Kamilaroi PC	42 ± 3	28	2.68 ± 0.15	15.7 ± 1.4
GF-2	Mia Mia PC	130 ± 5	14	3.21 ± 0.26	41 ± 4
GF-3	Kookabunna PC	56 ± 2	19	2.84 ± 0.16	19.6 ± 1.3
GF-4	Kookabunna PC	56 ± 1	17	2.95 ± 0.17	18.9 ± 1.1
GF-5	Kookabunna PC	44 ± 6	35	3.01 ± 0.22	14.5 ± 2.3
GF-6	Coocalla PC	120 ± 3	13	3.1 ± 0.18	39 ± 2
GF-7	Coocalla PC	130 ± 3	1	3.13 ± 0.17	41 ± 2
GF-8	Coocalla PC	99 ± 4	21	2.88 ± 0.16	34 ± 2
GF-9	Coocalla PC	107 ± 3	19	2.76 ± 0.21	39 ± 3
GF-10	Coocalla PC	137 ± 3	17	3.04 ± 0.23	45 ± 4
GF-11	Coocalla PC	113 ± 3	11	3.14 ± 0.20	36 ± 3
GF-12	Browns Ck PB	7.5 ± 0.3	37	2.75 ± 0.18	2.71 ± 0.21
GF-13	Yarraman FP	0.45 ± 0.25	151	2.7 ± 0.17	0.16 ± 0.09
GF-14	Yarraman FP	1.3 ± 0.6	118	2.69 ± 0.17	0.47 ± 0.21
GF-15	Yarraman FP	4.9 ± 0.4	85	2.89 ± 0.18	1.70 ± 0.16
GF-16	Coocalla PC (?)	128 ± 2	10	3.25 ± 0.20	39 ± 3
GF-17	Coocalla PC (?)	110 ± 9	30	2.31 ± 0.17	47 ± 5
GF-18	Coocalla PC (?)	125 ± 3	10	3.35 ± 0.23	37 ± 3
GF-19	Challicum PC	180 ± 17	24	2.71 ± 0.14	66 ± 7
GF-20	Kamilaroi PC (?)	47 ± 4	0	2.97 ± 0.22	15.8 ± 1.7
GF-21	Kamilaroi PC (?)	47 ± 4	35	2.72 ± 0.20	17.1 ± 2.0
GF-22	Challicum PC	160 ± 30	33	2.21 ± 0.17	72 ± 15
GF-23	Challicum PC (?)	189 ± 6	16	2.88 ± 0.23	66 ± 6
GF-24	Coocalla PC (?)	96 ± 9	33	2.46 ± 0.19	39 ± 5
GF-25	Coocalla PC (?)	106 ± 5	14	2.76 ± 0.17	38 ± 3
GF-26	Dune	12.9 ± 1.2	35	3.06 ± 0.18	4.2 ± 0.5
GF-27	Dune	10.4 ± 0.9	56	2.67 ± 0.15	3.9 ± 0.4
GF-28	Dune	9.8 ± 0.3	8	3.05 ± 0.18	3.22 ± 0.21
GF-29	Dune	18.5 ± 0.3	3	3.15 ± 0.18	5.9 ± 0.3

Chapter 8 The Late Quaternary Evolution of the Gwydir Fan-Plain

8.1 Introduction

The chronology established for geomorphic developments in the Gwydir fan-plain presented in the previous chapters is reasonably straight forward. Three episodes of enhanced fluvial activity have been identified (Figure 7.11). The earliest of these is represented by the deposits of the Challicum Palaeochannels which date to ~66 ka, i.e. Oxygen Isotope Stage (OIS) 4 (Figure 7.1). No discharge estimates based on planform measurements were able to be made for this unit, however the depth and caliber of gravel deposits at Sites GF-19 and GF-22 suggest that the Challicum Palaeochannels had discharges comparable to that carried by subsequent palaeochannels. The next oldest fluvial phase identified is that corresponding to the Coocalla Palaeochannel (Figures 7.1, 7.11), of which the Mia Mia Palaeochannel is apparently part, which has an age near 39 ka (OIS 3) and an estimated discharge of $\sim 2550 \text{ m}^3\text{s}^{-1}$ (average of Coocalla and Mia Mia estimates in Table 4.5). The final episode of palaeochannel activity is recorded by the Kookabunna and Kamilaroi Palaeochannels at between 19 ka and 16 ka (OIS 2) (Figures 7.1, 7.11), with the estimated discharges for these two palaeochannels being $1240 \text{ m}^3\text{s}^{-1}$ and $1310 \text{ m}^3\text{s}^{-1}$, respectively (Table 4.5). Luminescence ages younger than 16 ka are found only for geomorphic units suggestive of a dramatic decline in general environmental wetness from this time. These are the sand dune deposits which indicate an apparently widespread aeolian reactivation of palaeochannel sands at around 4 ka and the extensive floodplain clays of the contemporary system dating to less than 2.7 ka (Figure 7.11).

Whether or not there were large palaeochannel systems in the intervening periods remains unknown; the absence of evidence can not by itself be taken as evidence for absence. However, it seems a reasonable assumption that the larger the system, the greater chance of it being preserved and being discovered and dated in this study. As most if not all the well-preserved palaeochannels at the surface of the Gwydir fan-plain

have been sampled for this thesis, it is tentatively suggested that it is unlikely that large palaeochannel systems existed in the intervening periods.

Along with the decline in channel size through time, there appears to have been a change in the nature of sediment load carried by the streams. Palaeochannel deposits are universally high in potassium (Figures 2.2, 2.8), whereas the coarse sediments of the contemporary channel system are dominated by sand from the Pilliga Sandstone (Figure 6.6) that are low in potassium (Figure 2.9). The changes in OSL sensitivity recorded in the sediments of the contemporary Gwydir network upstream of the Goondooindi Thrust Fault are highly suggestive of the Pilliga Sandstone being the dominant contemporary source for coarse bedload material. Although the source of the high potassium materials of the palaeochannels can not as yet be identified, it can be inferred that the Pilliga Sandstone was a less important contributor of coarse sediment during the three Late Quaternary fluvial phases identified above.

Revisiting the scenario presented in Section 5.2, it can be seen that there are slight but significant differences between the observed and expected timing of environmental change in the Gwydir. Firstly, the presence of an active fluvial phase corresponding to the largely-buried Chalicum Unit (~ 66 ka) is not reflected in the data so far collected for the Namoi, Nambucca or the Bellinger Valleys (see Figure 8.1 for locations of all sites mentioned in this chapter). Furthermore, the almost complete overprinting of this unit with black clay suggests that, in this sector of the plain, at least, the 1 m in 50 ka (0.02 mm a^{-1}) estimate of Riley and Taylor (1978) for floodplain aggradation is a significant underestimate. Secondly, the period of sediment flushing during the early Holocene (the 'Nambucca Phase') inferred by Nanson *et al.* (2003) on the basis of an absence of sediment dating to this time, also shows up as a 'gap' in alluviation in deposits of the lowland Gwydir fan-plain. Its absence on the Gwydir fan-plain is contrary to expectations, as material being flushed from the highlands should be found deposited in adjacent low-land areas. The absence of Gwydir fan-plain dates corresponding to the Nambucca Phase is similarly repeated in the Namoi alluvial plain, with the youngest palaeochannels TL dated to 12.1 ± 1.6 ka (Young *et al.*, 2002) and an equivalent sandy lunette (indicating lake full conditions) TL dated to 13.2 ± 1.7 (weighted average of two TL dates presented by Ward, 1999). In the Gwydir and Namoi valleys at least, there is no evidence for enhanced alluvial deposition between 12 and 3

ka. A more likely scenario to explain the absence of alleviation during a period of independently determined hypsithermal of enhanced temperatures and precipitation is that the upland catchments were very well vegetated and highly stable. The larger flows may well have consisted of relatively low sediment concentration leaving little by way of alluvial signature (Cohen and Nanson, in review).

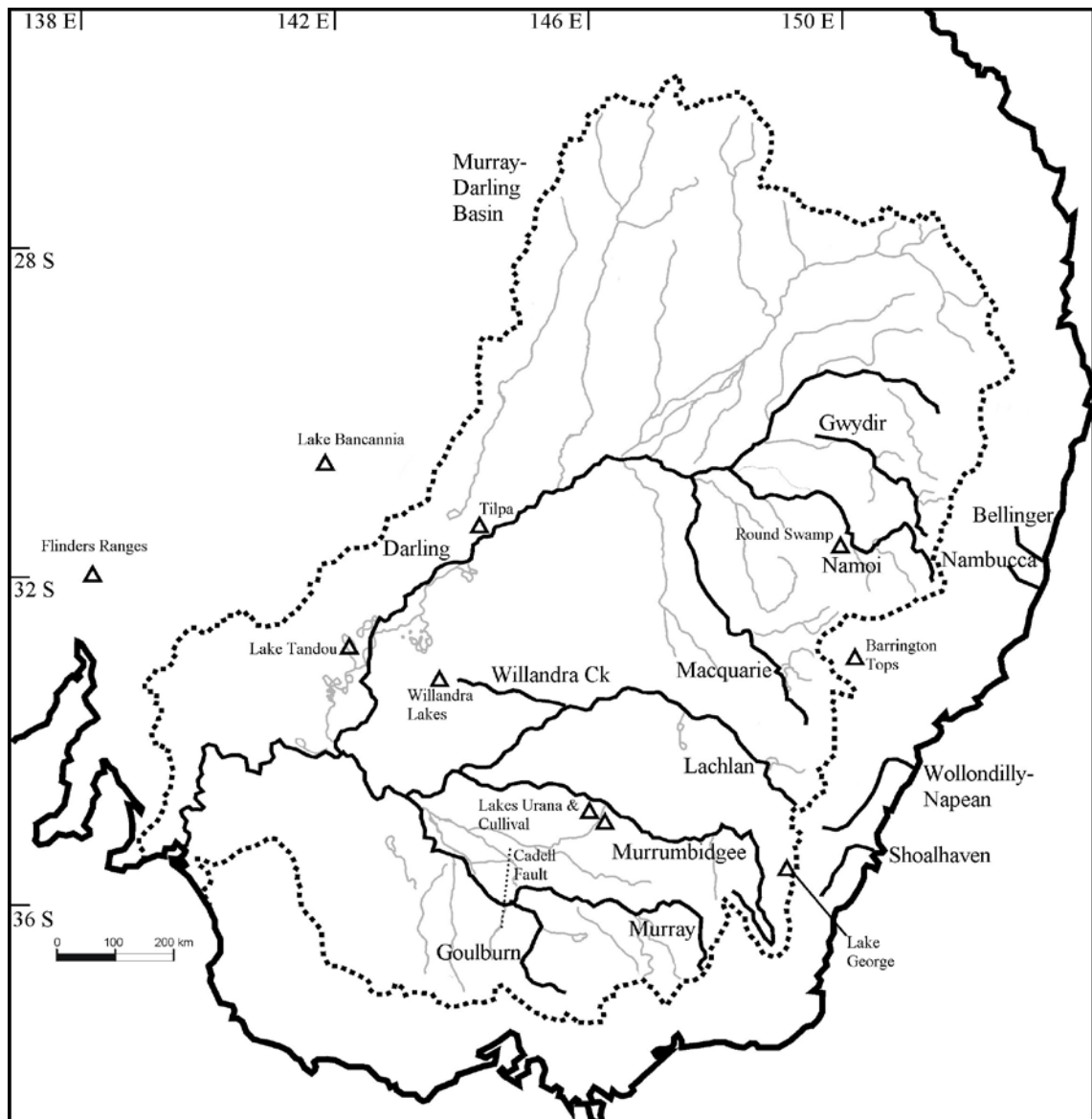


Figure 8.1: Map of southeastern Australia showing locations of sites discussed in Chapter 8.

The suggestion of Nanson *et al.* (2003) that climatic conditions approximating that of the present were established around 3 ka is supported by the evidence presented here, as

the contemporary channels appear to post-date the aeolian phase of ~ 4 ka. Although the evidence from immediately adjacent valleys is most relevant to the results presented in this thesis, the broader context allows greater sense to be made of the unexpected aspects of the environmental record.

8.2 Quaternary Australia

The contemporary Gwydir distributary system has played a relatively minor role in the construction of the Gwydir fan-plain. Rather, construction of the bulk of the fan-plain has been effected over many millennia by innumerable palaeochannels, some of which are still visible at the surface. To understand this history, it is necessary to appreciate Australia's Quaternary past. Prior to the onset of the Quaternary, subtropical humid conditions extended to the southernmost continental margin of Australia (Lowry and Jennings, 1974). The Australian continent experienced the same Tertiary cooling evident elsewhere. However, the prime geomorphic accompaniment was not glaciation but rather aridification of the continent as northward migration of the continent into latitudes characterised by persistent high pressure cells promoted dry conditions. By the Miocene – Pliocene boundary, drying of previously high lakes was underway (Bowler, 1976). Reduced evaporation from the by then cooler Southern and Indian Oceans reduced the penetration of warm, moist air masses into the Australian interior. Onset of full-scale aridity inland is first recorded by the appearance of the gypseous Winmatti Beds at Lake Amadeus in central Australia, prior to 0.91 Ma (Chen *et al.*, 1993), and the demise of Lake Bungunnia on the western Riverine Plain after about 780 ka (An *et al.*, 1986). With time aridity spread coastward (Chappell, 1991).

Cycles of glacials and interglacials across the globe had their expression in an Australian context in the form of oscillating landform development. Lakes filled and emptied; rivers increased in size and then diminished; dune fields advanced and retreated; dust concentrations waxed and waned; glacial areas expanded and contracted. However, this wealth of evidence for change is arranged in such a way that it is difficult if not impossible to draw simple, broadscale climatic inferences. Numerous complications exist which colour the interpretation of previously gathered evidence. The fog of uncertainty that surrounds the accuracy of previously gathered

geochronologies (see Chappell, 1991) is a severe impediment to basic understanding of climate change. However, a more fundamental problem is the at times uncertain connection between climate and the landform expressions interpreted as proxies for palaeoclimate.

The connection between climate change and landform development is rarely if ever unequivocal. Williams (1994) cautions that climate is a second-order concept inferred from first-order interpretations of environmental records. This is especially the case for fluvial environments (Nanson and Tooth, 2004), where, along with the prime climate variables of temperature and precipitation, rivers are a function of seasonality, vegetation, soil permeability and snow/ice retention and sudden melting. The accuracy of the palaeoclimate record will, therefore, always be subject to the accurate interpretation of the palaeoenvironmental record. In addition, the tempo of environmental change established through the collection of geochronological data may be subject to question if the interpretations of the gathered data are themselves open to question (see Appendix G).

8.3 Lacustrine History of the Murray-Darling Basin and Surrounds

While it would be too large a task to review here all forms of Late Quaternary palaeoenvironmental evidence for eastern Australia, the regions lacustrine evidence does invite plausible comparison with flow regime changes. However it needs to be borne in mind that while lakes and rivers both respond to increased precipitation, lake levels are also very responsive to changes in evaporation.

Figure 8.2 summaries the results of research into three of the better known lake systems in the Murray-Darling basin. Examination of water level histories for Willandra Lakes, Lakes George, Urana and Cullival demonstrates that there has been widespread high lake levels in OIS 3 and a decline in water levels in lakes of the Murray-Darling basin since OIS 3. Complications of geomorphology, geochronology or past interpretation exist at all sites (see for example Appendix G), however, the broad similarities in history allow some general inferences to be drawn. During the last glacial maximum (LGM) there is evidence for an inflow/outflow ratio less than unity at Willandra Lakes,

however, such evidence has not been found at Lake George (see Appendix G) or Lake Urana. Furthermore, these are not isolated examples of high water levels during OIS 2. Outside the Murray-Darling basin, the Flinders Ranges have ‘wetland’ deposits initially interpreted as lacustrine (Cock *et al.*, 1999) but subsequently interpreted as swampy meadows, and which date to the LGM (Williams *et al.*, 2001). The quartz sand Bootingee Unit at Lake Tandou (Hope *et al.* 1983) in western NSW also dates to OIS 2 indicating that high lake levels persisted through this time. Closer to the main study area Sweller and Martin (2001) have deduced from palynological and sedimentological evidence in lake-floor cores the sequence of climatic developments at Barrington Tops at an elevation of 1000-1500 m ASL. Here the lake level was high between 40 and 30 ka while apparently drying out from 30 – 21 ka, with a dryland periglacial phase of accelerated sedimentation recorded thereafter (21-17 ka). However, as with the situation in the coastal valleys of northern NSW (Nanson *et al.* 2003), it is not clear whether the absence of a lake between 30 and 21 ka is due to increased fluvial activity eroding the lake basin, or a reduction in the inflow/outflow ratio. In the Namoi to the immediate south of the Gwydir Valley, the sandy lunette adjoining Round Swamp has been TL dated to ~13 ka, (Ward, 1999) (a value which may be erroneously low given the similar geology of the Namoi and Gwydir catchments and the problems experienced with TL determinations in this study – see Chapter Five) while high water levels at Lake Bancannia in north-western NSW have been ¹⁴C dated at one site to 17 ka (Dury, 1973). Clearly conditions in the Murray-Darling basin during much of OIS 2 were favourable for lake expansion, with the most likely explanation being that the combined effects of increasing runoff efficiency and decreasing evaporation due to lower temperatures were more than compensatory for the decline in precipitation. Following the LGM, rising temperatures have caused the balance to shift in favour of outputs (evaporation) over inputs (direct precipitation and runoff). The reasons for high lake levels persisting through OIS 3 are less clear.

It is possible that relative to the LGM, evaporation was lower during OIS 3 even though temperatures were higher, due to wind activity that was low compared to the high wind conditions of the LGM (e.g. Galloway, 1965; Bowler, 1986). Alternatively, lake levels could have been high because evaporation declined faster than precipitation following the last interglacial with the greatest divergence occurring sometime during OIS 3. From the dominant role played by precipitation onto the lake surface at Lake George, to

the almost totally runoff dominated Willandra Lakes, all the lakes have different proportional inflow characteristics. A modest decline in evaporation would have a major effect at ‘evaporimeter-like’ Lake George (Galloway, 1965) but very little effect at Willandra Lakes. The fact that all three lake systems have recorded high water levels is strongly indicative of widespread increased precipitation.

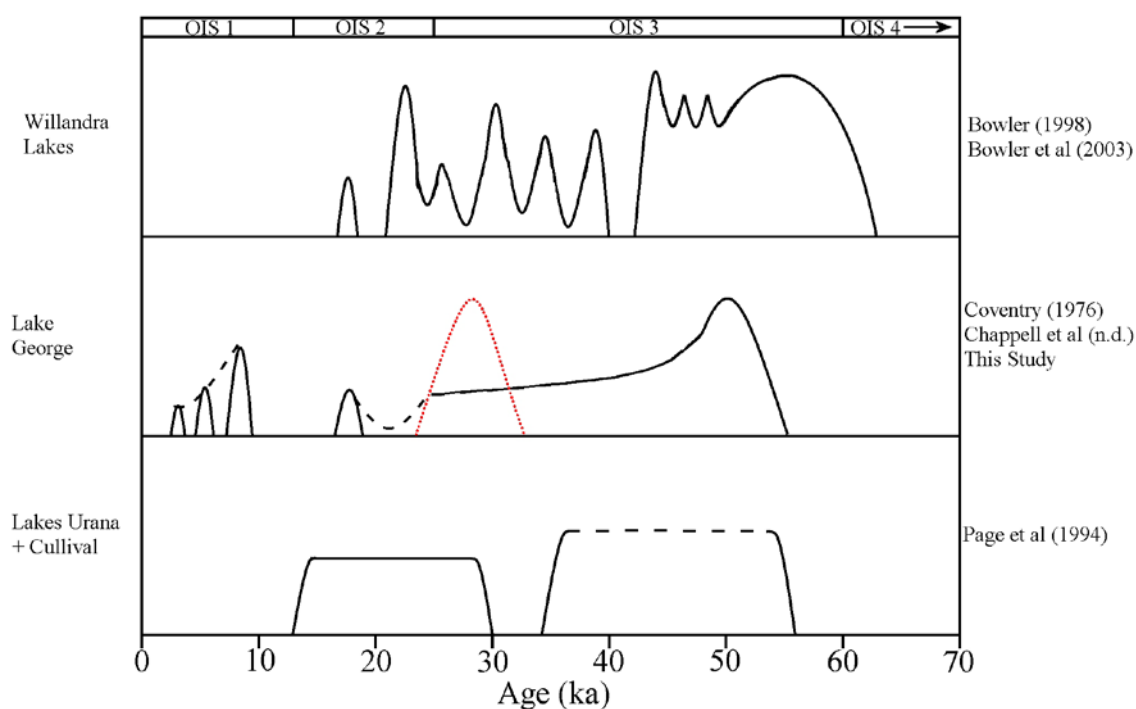


Figure 8.2: Water level curves for Willandra Lakes, Lake George and Lakes Urana and Cullival. Red peak in Lake George record corresponds to Winderadeen Embankment as dated by Coventry (1976), argued in Appendix G to be more accurately positioned at ~50 ka.

8.4 Late Quaternary Fluvial Records

Most, if not all, investigations into the Quaternary history of the river systems of the Murray-Darling basin (e.g. Bowler, 1978; Page *et al.* 1996; Kemp, 2001; Young *et al.*, 2002) begin with the observation that the palaeochannels of a particular river system are larger than the contemporary channels. While this in part may be simply because larger palaeochannels have a greater preservation potential than smaller palaeochannels, it also indicates that formative discharges have been considerably larger during previous

fluvial episodes. However, ascribing climate conditions commensurate with larger formative discharges is not straightforward, not least of all because of the number of different climate ensembles which can result in the same formative discharge. This is especially true in catchments strongly effected by snow accumulation and seasonal meltwater as well as the direct effects of varying amounts of precipitation.

Critical to correctly inferring past climates from fluvial environments is the observation that fluvial environments, in contrast to lacustrine ones, are adjusted to actual precipitation events as translated into runoff. While a lacustrine beach may form at a level coincident with the long-term balance between inflow and outflow, a stream channel will expand to accommodate a discharge which flows for only a small proportion of the time, on which changes in evaporation will have very little effect. This discharge, known as the formative discharge, may correspond with bankfull discharge (Wolman and Leopold, 1957; Williams, 1978) a flow that has been identified as probably that which does the most geomorphic work (Wolman and Miller, 1960). In some cases it appears that it is the sequence of events that is important in controlling channel dimensions, rather than any single discharge. Whether channel dimensions relate to a single discharge or to a specific sequence of discharges, it is events (or series of events) that have significance in shaping channels, as opposed to general climatic conditions. As such, mechanisms which increase the size of events need to be invoked in explanation of large palaeochannels, not simply increases in general environmental wetness.

Somewhat paradoxically, though gross palaeochannel *scale* is related to the size of the formative discharge, preserved palaeochannel *form* appears to be related to the way the river behaved just before it ceased to function. Palaeochannel segments isolated by avulsion will largely preserve their form, while palaeochannels which atrophy under the influence of an increased coarse sediment load will tend to shallow, widen and straighten before finally becoming defunct. This basic difference in the nature of channel extinction is set out in the migrational / aggradational stratigraphic model of Page and Nanson (1996) discussed below.

8.5 Episodes of Enhanced Fluvial Activity

Surficial palaeochannels of the Murray-Darling basin so far dated extend in age to about 400 ka (e.g. Watkins and Meakin, 1996) with the period since the last interglacial having the most complete record. The Riverine Plain remains the most intensively studied Quaternary fluvial sequence in Australia and it is from the Murrumbidgee sector of the Plain that the most comprehensive geomorphic and chronological models have been built (Page and Nanson, 1996; Page *et al.*, 1996). The work on the Riverine Plain has been instrumental in interpreting the physical geography of the other main area of fluvial archives in the Murray-Darling basin, the Darling Riverine Plain (Watkins and Meakin, 1996; Young *et al.*, 2002) containing the main study area. In most similar studies in the Murray-Darling basin the number of reported dates has been too few to build an independent history. For example, Watkins and Meakin (1996) report four dates for the Macquarie, Kemp (2001) reports three dates for the Lachlan and Young *et al.* (2002) report 8 dates for the Namoi. Hence, to contextualize individual interpretations based on few dates into a broader chronological story, all three studies rely heavily on the history already interpreted by Page *et al.*, (1996) for the Murrumbidgee.

8.5.1 The Murrumbidgee Throughout the Last Glacial Cycle

On the basis of detailed stratigraphic information and nearly 40 reported TL dates on palaeochannels and source-bordering dunes on the Murrumbidgee sector of the Riverine Plain, Page *et al.* (1996) were able to identify four main phases of palaeochannel activity: Coleambally, 105 to 80 ka; Kerarbury, 55 to 35 ka; Gum Creek, 35 ka to 25 ka and Yanco, 20 to 13 ka. This chronological framework is also based on supporting evidence provided by a further 40 TL dates from Lake Urana lunettes (Page *et al.*, 1994) and confined valley deposits upstream at Wagga, (Page, 1994), all within the Murrumbidgee catchment, and from lunette, source-bordering dune and palaeochannel deposits in the Murray sector of the Riverine Plain (Page *et al.*, 1991). Large mixed-load laterally migrating streams operated through all four phases, with the first three terminating with an aggradational phase dramatically affecting preserved channel form. It appears that this terminal aggradational phase is absent in the youngest palaeochannel

phase (the Yanco), possibly as a result of speedy revegetation of the upper catchments following climatic amelioration at the onset of the Holocene.

Page and Nanson's (1996) interpretation of the climatic significance of palaeochannel forms differed from previous work by others in that they recognized that the link between preserved channel form, and the way in which the channel would have appeared for the majority of its functional life, is not always clear. For example, where channels have slope and discharge characteristics balanced between that of meandering and braided streams (Lanes (1957) 'Intermediate Zone'), they are liable to dramatic shifts in their form following disturbance, such as would be expected to occur in conjunction with significant climate change. For channels so balanced it would appear that the preserved channel form does not necessarily indicate the way the river functioned during most of its active life, but rather the manner in which it ceased to function. This probability was incorporated by Page and Nanson (1996) into their migrational / aggradational model of palaeochannel development (Figure 8.3), thus emphasising the importance of the channel's final stages in determining palaeochannel form. Some palaeochannels of the Riverine Plain underwent an aggradational phase following apparently long periods of migrational activity. For other channels, this aggradational phase was absent, leaving the preserved palaeochannel closer in form to a fully functional channel. Their model differs from earlier work on the Plain by Pels (1964a; 1964b; 1969; 1971) and Schumm (1968) who envisaged that channels simply incised and aggraded throughout some climate driven cycle, much like larger versions of arroyos of the mid-western USA.

Pels' model was superseded by the migration / aggradation model due to newly available stratigraphic evidence which demonstrated the close association of aggradational type channel fill deposits with underlying gravels associated with channel migration. Intriguingly, phases of palaeochannel activity that ended with the onset of glacial conditions (or a brief stadial as in the case of OIS 3 Kerarbury channels) have well-preserved aggradational deposits, whereas the palaeochannels of the Yanco phase, which ended with the onset of the Holocene, do not display any aggradational unit. Morphological groupings of palaeochannels therefore do not necessarily reflect great differences in the way channels functioned, but rather the conditions prevalent during the time of their demise.

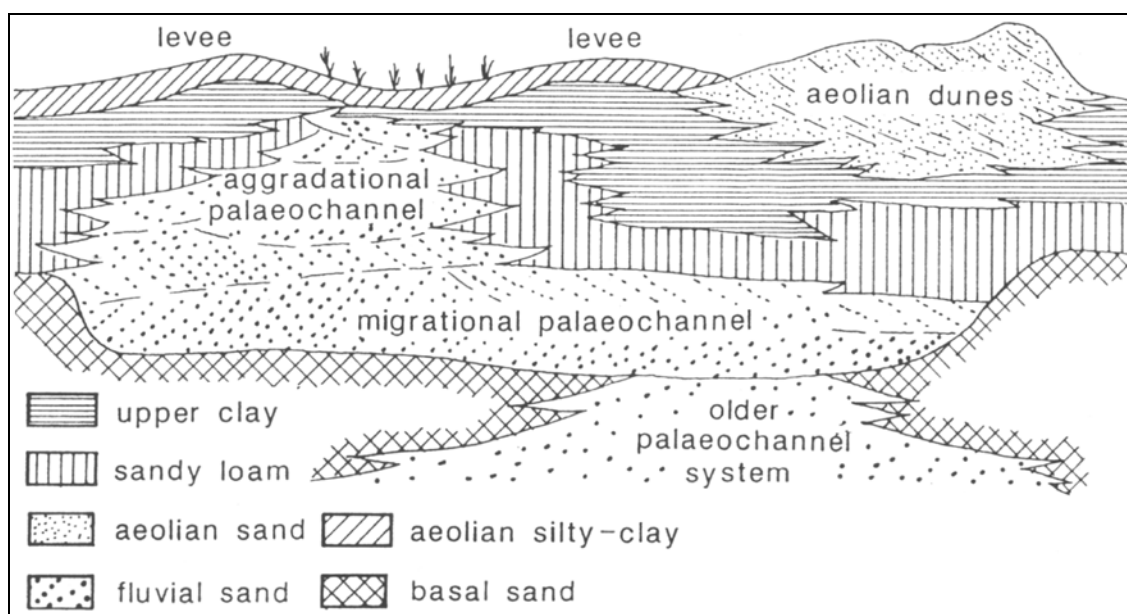


Figure 8.3: *Migrational / Aggradational sedimentological model of Page and Nanson (1996).*

As with all Quaternary studies, the work on the Murrumbidgee sector of the Riverine Plain needs to be assessed for its geochronological integrity. Cognisant of the possibility that TL dates can be inflated by partial bleaching of the luminescence signal prior to deposition, Page *et al.* (1996) present the results of two tests conducted to establish their validity. Firstly, internal consistency within the data set was established by checking that the ages were in correct stratigraphic order. Specifically, source- bordering dunes were shown in every case to be younger than the palaeochannels that supplied them, but perhaps this is to be expected, given that aeolian transport is likely to result in more complete bleaching than fluvial transport. Secondly, ages determined using the difficult to bleach 375°C trap, were shown to be comparable to ages re-determined using the easy to bleach 325°C trap. The authenticity of the fluvial TL dates have since been largely confirmed by Banerjee *et al.* (2002) who redated some of the sites using OSL. The fact that the 375°C trap has been bleached to much the same extent as the 325°C trap (sampled using TL or OSL) highlights the ideal bleaching characteristics of the Riverine Plain environment, providing encouragement for accepting these dates as accurate. It also provides supporting evidence for contentions put forward in Chapter 7 regarding the high probability that Australian fluvial quartz experiences numerous bleaching cycles (ensuring full eviction of the 375°C trap) prior to deposition.

8.5.2 Other Murray-Darling Basin Fluvial Records

Some of the earliest geochronological data for fluvial archives of the Murray-Darling basin were collected from the Goulburn and Murray sectors of the Riverine Plain (Bowler, 1967; Pels, 1969) in the vicinity of the Cadell Fault, which has preserved on its upthrow side palaeochannels which record in their dimensions the pre-faulting hydrology. Although subsequent dating exercises (e.g. Page *et al.*, 1991; Ogden *et al.* 2001) have brought into question the reliability of the radiocarbon dating used by Bowler (1967) and Pels (1969), it is clear that the time prior to the LGM was characterised by rivers much greater in size than their present day manifestations. This is evidenced by two separate formations, the Green Gully – Tallygaroopna formation and the Kotupna formation, which have estimated palaeodischarges in excess of three times the discharge of the contemporary channel (Bowler, 1978) and which have been dated using TL by Page *et al.* (1991) to ~80 – 65 ka and ~ 35 – 25 ka respectively.

To the north of the Murrumbidgee, the Lachlan River provides numerous examples of preserved palaeochannels. These however, have only recently been investigated chronologically (Kemp, 2001). Indeed, much of the fluvial history of the area has hitherto been inferred from the Willandra Lakes and Lake George records mentioned above (e.g. Williams *et al.*, 1986). The now relict Willandra Ck (Figure 8.1) is argued to have ceased operation at about 15 ka, i.e. the end of the Lake Mungo record. Williams *et al.* (1986) argue that this was a time of enhanced discharge in the trunk channel (the proto Lachlan), which caused it to cut down into its clay-mantled floodplain, beheading and pirating flow from the formerly active distributary. From a limited number of sites, Kemp's (2001) work has shown, that, as with the Murrumbidgee, larger discharge channels were present prior to the LGM. Kemp divided palaeochannels of the Lachlan floodplain on the basis of detailed mapping into Culgo (~57 ka), Ulgutherie (35 – 25 ka), Nanima (5-3 ka) and modern (< 2.7 ka) although the reasons for distinguishing Nanima from modern channels is not entirely clear. Kemp assigned ages for these units based on a total of two OSL dates, one TL date and eight ¹⁴C dates from seven separate sites. The apparent absence of a Yanco-aged system (i.e. 20 – 13 ka) is difficult to reconcile with the suggestion of Williams *et al.* (1986) that fluvial activity was

enhanced at about 15 ka and may simply result from the small number of samples Kemp analysed. If there are indeed no large channels dating to the Yanco period, this would suggest that the Lachlan and Murrumbidgee catchments responded very differently to the glacial conditions of OIS 2. Given that the headwaters of the Lachlan are considerably lower than the headwaters of the Murrumbidgee, it is possible that high discharges associated with the spring thaw of a large snow pack were absent in the Lachlan Valley. However, the Murrumbidgee is not alone in having high discharges through the latter part of OIS 2.

To the north of the Lachlan Valley, and with similar elevations in its headwaters, the Macquarie Valley contains extensive palaeochannel features. Watkins and Meakin (1996) have identified two episodes of post - last interglacial palaeochannel activity: The Carrabear Formation (27 – 13 ka) and the stratigraphically superposed Bugwah Formation (undated). The contemporary system, which they have termed the Marra Creek Formation, dates back to ~ 6 ka making the Bugwah Formation somewhere in age between ~13 ka and ~6 ka. Estimations of the relative discharges carried by these systems are not presented by Watkins and Meakin (1996). However, diagrammatic representations of channel forms provided by them suggest meander wavelengths of the Carrabear Formation were 5 - 6 times the present, while the Bugwah Formation had meander wavelengths 1.5 - 2 times the present. Assuming the change in meander scale broadly reflects the magnitude of change in discharge, it appears that the Carrabear Formation was equivalent to the Yanco Formation, with high discharge conditions continuing through OIS 2.

The final Murray-Darling basin fluvial archive considered is that developed from a brief investigation of soil-sedimentary units of the Darling River floodplain near Tilpa by Bowler *et al.* (1978) who tentatively identified three separate units. The oldest dated to ~36 ka (uncalibrated), close to the then limit of radiocarbon dating. No channel dimensions are provided for this unit. More securely dated (uncalibrated radiocarbon dates of 19.2 ± 0.4 ka, 16.8 ± 0.4 ka and 11.2 ± 0.2 ka) are the channel migration deposits of the Acres Billabong palaeochannel, with meander wavelengths and channel radii of curvature values approximately twice those of the contemporary Darling River. These dates and palaeochannel dimensions clearly indicate the equivalence of the Acres Billabong palaeochannel with the Yanco palaeochannels of the Murrumbidgee sector of

the Riverine Plain. Bowler *et al.* (1978) propose that the development of the contemporary Darling River occurred soon after 11 ka; however, no chronological or stratigraphical data is presented in support of this assertion.

8.5.3 Discussion of Murray-Darling Basin Fluvial History

Figure 8.4 illustrates the diversity of fluvial history within the Murray-Darling basin (see Appendix F: table of published dates used to construct Figures 8.4 and 8.5). Unfortunately, most of the records from the Murray-Darling basin suffer due to sampling strategies that are restricted either in number or spatial distribution. The records from the Darling and Goulburn-Murray, even though both have reasonable numbers of dates, are based on very small sampling areas. In contrast, the records from the Lachlan, Macquarie and Namoi are built using very few dates spread across large study areas. Only the Murrumbidgee and Gwydir studies have attempted to comprehensively sample all exposed palaeochannel systems. Mindful of these difficulties, comment is restricted to a number of general observations.

Firstly, all systems record a decline in channel scale since OIS 3. Where the record extends to earlier than OIS 3, channels appear to have been marginally smaller (Page *et al.*, 1996). The latter part of OIS 2 was apparently a time of greatly enhanced discharge for all systems except the Goulburn-Murray. For the three southern most systems, the latter part of OIS 3 was also a time of enhanced fluvial activity. This does not seem to be the case for the systems in the north of the Murray-Darling basin. The absence of a large palaeochannel system between the Culgo (~57 ka) and Ulgutherie (35 – 25 ka) in the Lachlan is puzzling, given that this was a time of high lake levels at both ends of the Lachlan system (see Figure 8.3). Given that temperatures throughout this phase were intermediate between the conditions of the LGM and the LIG, the high lake levels can not be attributed to a major decline in evaporation. Higher precipitation therefore seems likely. The most probable, though somewhat unsatisfying, explanation for the absence of a large palaeochannel system dated to this period is the small number of dates collected from the Lachlan floodplain.

In consideration of Figure 8.4, the LGM as dated by Barrows *et al.*, (2001; 2002) to 17-20 ka does not obviously stand out as a time of palaeochannel inactivity, however, this may have as much to do with the lack of precision of the dating techniques used, as to any genuine LGM fluvial activity. Many previous studies have placed the LGM prior to 20 ka (e.g. Colhoun and Fitzsimmons, 1990; Colhoun *et al.*, 1996; Hope *et al.*, 2000), which accords better with the fluvial evidence presented here. The possibility that the short interval of the LGM itself was a relatively dry phase within a generally 'wetter' OIS 2 can not be excluded. Furthermore, Page *et al.* (1996) record the Gum Creek and Yanco as quite separate channel systems with no LGM palaeochannel system to connect them in time.

The final observation concerns the onset of conditions approximating the present. There appears to be a large range in the age of first appearance of 'modern' channels, from about 12 ka in the Murrumbidgee, to less than 3 ka for the Lachlan and Gwydir. However, some studies (e.g. Page *et al.*, 1996) have taken the youngest palaeochannel date as the limit of modern activity, while other studies (e.g. Young *et al.*, 2002; this study) have taken the oldest date obtained from the modern system as providing a limit on the age of the modern system. These different approaches may appear to explain the apparently wide range in ages for 'modern' channels, and focus attention on the period that Nanson *et al.* (2003) termed the Nambucca Phase (12-3 ka) when discharges were higher but alluviation largely absent.

Histograms of luminescence ages have been used to interpret possible periods of fluvial activity. This approach is based on the assumption that the probability of a field worker sampling alluvium of a particular age is related to the degree of fluvial activity occurring at that time and therefore the extent of alluvium likely to be available for (random) sampling (Nanson *et al.*, 1992). However, this approach has its limitations because it neither accounts for uncertainties on individual dates, nor the variation in the scale of discharge of the features to which the dates refer. A possible alternative means of presenting the data is provided in Figure 8.5. In this case a probability density function is produced by considering the precision of each date, along with the scale of the feature to which it refers. Each published date in Appendix F, along with each date presented in Chapter 7, is translated into a Gaussian distribution of mean and standard

deviation equal to the value and uncertainty of the date, and with an area under the curve equal to the ratio of the palaeochannel discharge to the contemporary discharge.

The resulting distributions from all dates are summed to produce the distribution in Figure 8.5, with peaks representative of palaeochannel systems of either broad spatial extent (resulting in multiple samplings) and/or large estimated discharge. Weighting the data so is thus considered a slight improvement on the standard histogram approach previously employed (e.g. Nanson *et al.* 1992). Objections to this type of data presentation exist (e.g. Galbraith, 1998), however it is difficult to deny that histograms or probability density functions provide the most intuitively accessible picture of data location, albeit that their construction can not be done in a standardised way. However, it should be appreciated that peaks can result because individual studies may have selectively ‘quarried’ a particularly accessible palaeochannel system. In other words, the selection of samples is often far from random.

Despite these problems, when presented in this way the data strongly suggests a concentration of fluvial activity in the Murray-Darling basin during OIS 3, centred on approximately 35 ka, with a secondary peak somewhere around or just after the LGM. The small peak centred on about 5 ka relates to features judged by workers in the field as being the earliest manifestations of the contemporary system, hence the location of this peak should be taken as marking the beginning of the contemporary fluvial regime. For pre-OIS 3 phases the interpretation of peaks is somewhat equivocal, given the likely dominant influence of channel preservation, or lack thereof. The low peak during mid to late OIS 4 may illustrate the relative scarcity of palaeochannels dating to this era, and/or their small scale relative to the larger channels that followed. The low peaks during OIS 5 can not be an indication that fluvial activity was relatively weak then. Stage 5, or at least periods within it, was clearly a dominant phase of fluvial and lacustrine activity right across Australia (Nanson, *et al.* 1992; 2003; Magee *et al.* 2004), therefore the absence of a peak in this region of the graph is almost certainly due to the difficulties associated with locating increasingly older deposits as compared to the relative ease of sampling ‘young’ systems.

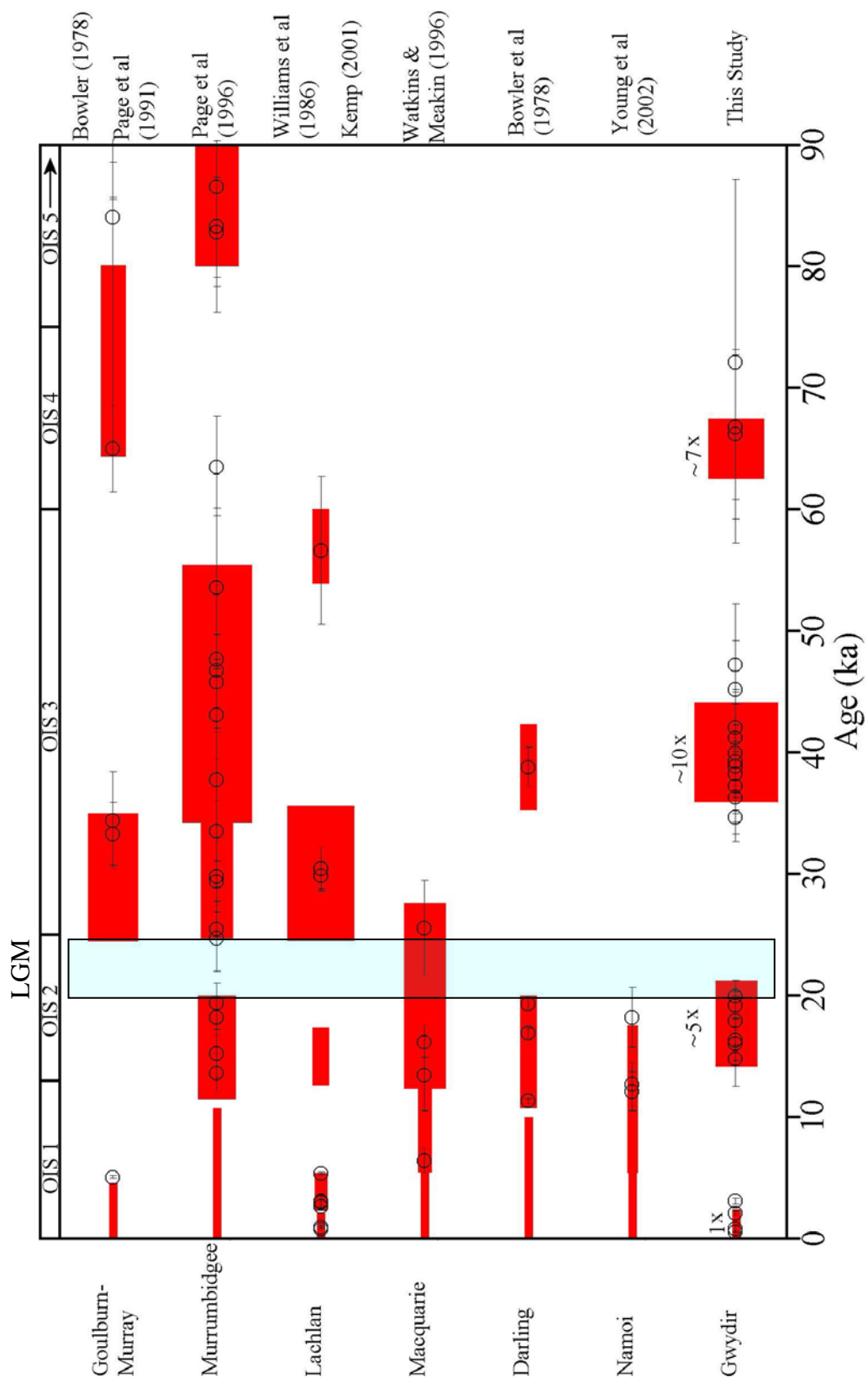


Figure 8.4: Phases of enhanced fluvial activity in the Murray-Darling basin. Thickness of bars indicates approximate discharge of palaeochannels relative to the contemporary system, with multiples printed above Gwydir record indicating scale. Temporal extent of phases includes respective authors judgement of phase length. Circles indicate actual dates.

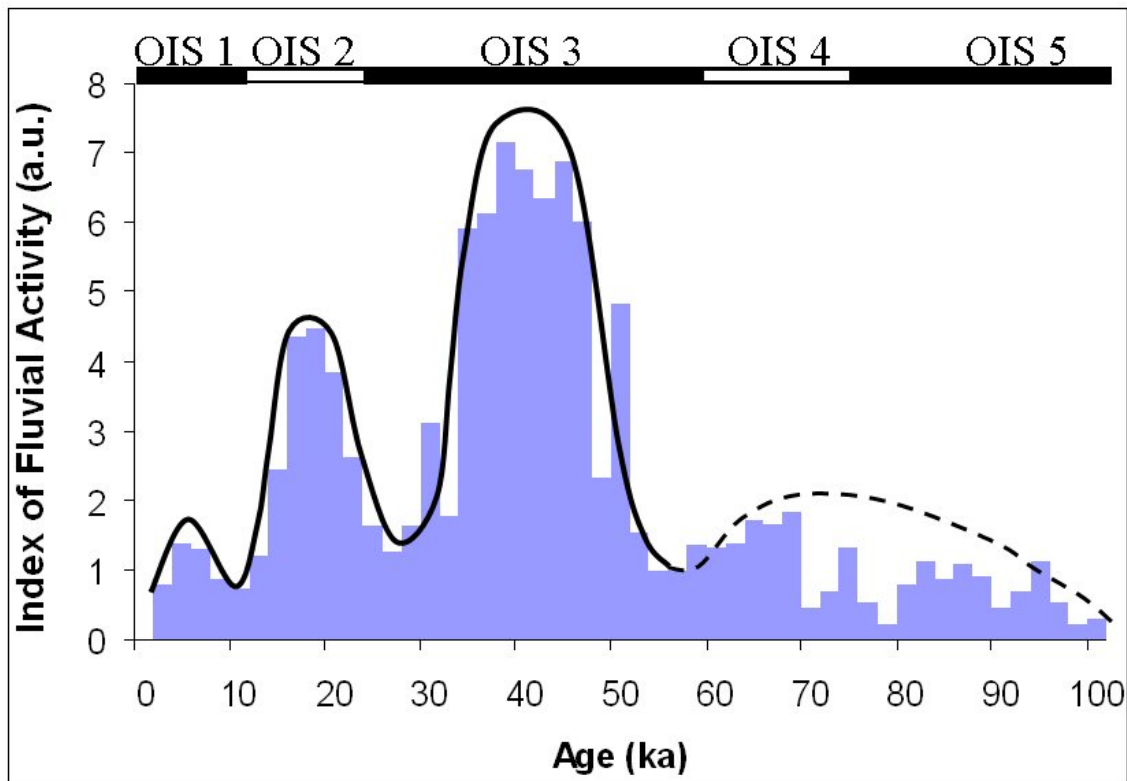


Figure 8.5: *Fluvial activity in the Murray-Darling basin throughout the last glacial cycle. Note broad, indented peak at ~100 - 60 ka and narrow coherent peaks at ~35 - 45 ka; ~17 - 21 ka and ~5 ka. The latter peak probably represents many focused attempts at dating earliest appearance of contemporary channels. See text for details of plot construction.*

8.6 The Gwydir Fan Plain Record

Each of the three phases of enhanced palaeochannel activity that have been identified on the Gwydir fan-plain (Figure 7.11) have equivalents in other valleys in the Murray-Darling basin (Figure 8.4). Additionally, each palaeochannel phase corresponds with episodes of slightly reduced temperatures during the last glacial cycle. A last glacial cycle palaeotemperature curve for the Gwydir Valley is not currently available. However, geomorphological observations, for example the changing height of snowlines and cirque floors (e.g. Galloway, 1965; Peterson and Robinson, 1969), and biogeochemical temperature proxies (e.g. Shakleton and Opdyke, 1973), generally point to a temperature depression during the most intense period of the LGM in the vicinity of 8 - 10°C. When the ages of the Gwydir fan-plain palaeochannels are compared to one of

the better known palaeotemperature curves, the Vostok palaeotemperature curve (Jouzel *et al.* 1987; Petit *et al.* 1990), it is apparent that ambient temperatures were likely to be depressed by about half that experienced at the LGM. Although Galloway (1965) argued that the temperature shifts of the Snowy Mountains region were greater than that experienced in Tasmania, there is in data collected since the suggestion of a negative correlation between magnitude of temperature shifts and latitude (e.g. Crowley, 1991; Broccoli, 2000). It could therefore be supposed that local temperatures during the palaeochannel phases of the Gwydir fan-plain were about 3-4°C less than present. In discussions below, these lower temperatures are incorporated into explanations of higher discharges carried by the palaeochannels, albeit that lower temperatures are argued to affect discharges indirectly via the changes wrought by lower temperatures on atmospheric circulation.

The Gwydir fan-plain is unusual in the Murray-Darling basin in that it apparently has large palaeochannels, termed the Challicum Unit, operative through OIS 4, although it may be noted that these channels have both the poorest surface expression and the poorest age control. Croke *et al.* (1999) have suggested that the 60 – 70 ka period was a time of enhanced monsoonal activity in Australia, which may explain why the Gwydir, the northernmost of the studied streams of the Murray-Darling basin, has recorded a fluvial phase while most other valleys have not. However, the evidence for the presence of an enhanced monsoon during OIS 4 is scant, with global sea levels and temperatures well below the present. Furthermore the southernmost palaeochannels, the Green Gully - Tallygaroopna channels of the Goulburn River, also date from this time (Page *et al.* 1991), indicating that OIS 4 is unlikely to have been a time of enhanced monsoon. The next oldest unit, the Coocalla palaeochannel, dating to ~ 42 ka, corresponds to both high lake levels and high discharges in all but one of the other studied valleys (Figures 8.6; 8.8). It also falls within the ‘OIS 3 Pluvial’ of Nanson *et al.* (1992), a period they identified as exhibiting an Australia-wide increase in fluvial activity. In combination the evidence is strongly suggestive of increased precipitation rather than simply decreased evaporation. Although a slight reduction in evaporation, in line with a modest decline in temperature during OIS 3, could raise lake levels, it could not in itself produce higher peak discharges (see below). Furthermore, the OIS 3 Pluvial of Nanson *et al.* (1992) has been identified in low latitude areas where reduction in evaporation is likely to have been minimal.

The Kamilaroi (~19 ka) and Kookabunna (~16 ka) palaeochannels (Figure 7.1) were emplaced during the speedy climate reversal known as the Termination immediately following the LGM. It may be no coincidence that the Kamilaroi channel, which dates closest to the LGM, is slightly smaller than the later Kookabunna channel (Table 4.5). It could be that in these two channels is a record of climate amelioration following a short dry phase at the height of the LGM (within the generally wetter OIS 2). An end point for this reversal is provided by the sand dunes of the Gwydir fan-plain, which cluster near 4 ka. Though previously referred to in this thesis as source-bordering dunes, they are not truly so, as source-bordering dunes are generally regarded as forming from a regular supply of sand provided from an adjacent seasonally active channel (Williams *et al.*, 1991). This is clearly not the case for the sand dunes of the Gwydir fan plain, which post-date their 'source' channels by tens of thousands of years. These dunes may more properly be termed 'source-limited dunes' as they are likely to form through the aeolian reactivation of deposits from defunct palaeochannels, and thus are limited to their typically low height by the rapid exhaustion of limited material. In this scenario, the time of sand dune emplacement would correspond with P/E minima, as aeolian activation of sandy palaeochannel deposits implies sparse vegetation, and not to periods of seasonally active flow.

8.7 Suggested Mechanism

It appears that colder temperatures have been instrumental in allowing the development of larger peak discharges in the Murray-Darling basin. However, the effect of lower temperatures is not the same across all catchments. Page *et al.* (1996) have discussed the likely effects of increased snowfall and periglacial activity in the headwaters of the Murrumbidgee River which are clearly related to colder phases of the last glacial cycle. Increases in coarse bedload delivered from vegetation-free slopes are inferred, as too are larger peak discharges associated with the spring thaw of a large snowpack. However, such mechanisms can not be operating in the Gwydir catchment. Less than 0.04 % of the catchment above Pallamallawa has an elevation greater than 1400 m, which is considered to be the lower limit of LGM periglacial activity in the region (Galloway, 1965). Although the periods of enhanced fluvial activity in every case in the Gwydir

system appear to coincide with temperatures approximately intermediate between the relatively warm temperatures of the present and the greatly depressed temperatures of the LGM, the effect of snowcover can all but be ruled out. Galloway (1986) has modelled the likely snow conditions present during such 'intermediate' conditions (i.e. temperatures approximately 5°C lower than present), showing that no significant snow cover could develop in the Gwydir catchment. Higher peak discharges can therefore not be due to larger snow packs.

Colder conditions in the Gwydir catchment during the last glacial cycle could have depressed the evaporation potential and therefore increased the catchment's runoff coefficient. However, while this may have increased total flow, it is the peak flows associated with individual hydrological events that largely determine channel size. Larger palaeochannels on the Gwydir fan-plain are therefore indicative of larger rainfall events, not simply an increase in the runoff coefficient. Examination of the present day climate of the Gwydir Valley allows inferences to be drawn as to how this may have occurred.

Storm events in the Gwydir Valley are of three general types: convective, monsoonal and frontal (DLWC, n.d.). Convective storms currently produce high intensity rainfalls; however, due to their localised nature, they make only a limited contribution to stream flow. Increase in the size or frequency of convective storms, especially at a time of depressed global temperatures, are therefore very unlikely to be responsible for the large palaeochannels of the Gwydir fan plain. The greatest peak stream flows on record (e.g. the 1955 flood) are produced by the incursion from the north of monsoonal depressions. However, these events occur in the summer months and, as with convective storms, are very unlikely to have been enhanced when climate was significantly cooler than at present. Most discussions regarding the strength of monsoonal activity (e.g. Johnson *et al.*, 1999; Croke *et al.*, 1999; Wyrwoll and Miller, 2001; Liu *et al.*, 2003) place its greatest effect during intervals of the last glacial cycle only modestly cooler than present. Furthermore, high discharges in the Gwydir catchment are coeval with pluvial features in areas to the south, beyond the reach of the summer monsoon. Thus the most likely cause of increased peak discharge in the Gwydir catchment is an increase in the intensity of winter frontal storms.

Although at present average monthly flows are less during non-summer months, large winter / spring storms can still occur; indeed the largest *daily* total flow recorded at Gravesend was the result of an intense winter storm (Pineena 7). Winter storms in the Gwydir catchment generally result from the passage of westerly cold fronts anchored in the low pressure belt over the Southern Ocean. This process is topographically amplified by the Great Dividing Range in the upper Gwydir catchment, which rises to 1450 metres at a rate in excess of 11 m per kilometre providing a significant orographic intercept. An increase in the intensity and/or frequency of winter - spring frontal storms during cool phases of the last glacial cycle is suggested as the most likely cause of the large size of Gwydir fan-plain palaeochannels.

The largest total flow in a day referred to above was recorded at Gravesend in 1950, at approximately 240 Gl. This equates to $2750 \text{ m}^3 \text{ s}^{-1}$, and a runoff depth of about 22 mm if averaged across the entire upper catchment ($\sim 11\,000 \text{ km}^2$). It is clear that even under the present climatic conditions, when evaporation potential is relatively high and snowpacks are entirely absent, stream flows can be generated which are similar to those suggested by palaeochannel dimensions (see Table 4.5). For rainfall - stream-flow events of the size recorded in 1950, the effect of ambient temperature and vegetation status on runoff coefficients is largely irrelevant. It is difficult to envisage conditions during the Pleistocene which could produce such large flows with anything other than greatly intensified rainfall events.

Event intensity is simply the inverse of event frequency. Westerly frontal storms, such as that which caused the record flow of 1950, presently have a long recurrence interval, though exactly how long is difficult to estimate given the length of record. It is safe to say however, that such events currently are so extreme that they fall outside the range of 'channel-forming' discharges. For flows of such size to be important in determining channel size in the past, they must have been of considerably increased frequency, perhaps occurring once every 2 – 3 years.

At latitudes between $29^\circ - 30^\circ\text{S}$, the upper catchment of the Gwydir River sits right in the middle of the subtropical ridge, the belt of high pressure that forms at the poleward arm of the Hadley cell. The train of high pressure anticyclones that regularly traverse the continent centred on 30°S limit the northern drift of primary and secondary cold

fronts sprouting from the sub-Antarctic trough, the ring of lows following a circumpolar track at around 60°S. The equatorward migration of the subtropical ridge during winter and early spring allows the greater northward penetration of cold fronts. However, it is rare for these to sweep over the Gwydir catchment. Thus, in the Gwydir catchment, at the very northern limit of winter frontal activity, winter storms and the flow events associated with them are comparatively rare. For catchments to the south of the Gwydir, squarely within the path of the mid-latitude westerlies and the cold fronts embedded within them, the hydrology is dominated by flow-events caused by frontal storms. Several authors (e.g. Hesse, 1994; Nanson *et al.*, 1995; Lamy *et al.*, 1999; Hollands *et al.*, *in press*) have suggested that during cooler phases of the last glacial cycle, weather systems were somewhat north of where they are at present. If this were the case, then it could be hypothesised that the influence of winter frontal storms in the Gwydir during cooler phases of the last glacial cycle was analogous to their present day influence in catchments to the south.

An appropriate measure of the latitudinal shift in weather conditions in the Murray-Darling basin is probably found in the shift in position of the Australian continent / Tasman Sea dust path. Hesse (1994) found that the dust carrying winds of the glacials extended some 3° further north than the dust carrying winds of the interglacials. Of particular interest therefore are the conditions in the Lachlan catchment which are at present approximately 3° south of the Gwydir but may have been 3° further north at times during the Late Quaternary. It can be seen in Figure 8.6 that for any large-size winter runoff event, the recurrence interval in the Gwydir catchment is approximately seven times longer than the recurrence interval for the equivalent sized event in the southerly catchments. If this approximate ratio describes the relationship between frequency of large winter storms in the Gwydir at present and large winter storms in the past, then it follows that 'extreme' events (i.e. 20 to 50 yr R.I.) which currently occur too infrequently to directly influence channel size, were in the past within the range of 'channel-forming' events.

This hypothesised northerly migration of weather systems characterised by frontal activity provides a mechanism by which greatly increased formative discharges can be delivered to the head of the fan-plain. Furthermore, larger discharges would more than

likely have been able to maintain single channels further out onto the fan-plain, before breaking down into a distributary system similar to that occurring at present.

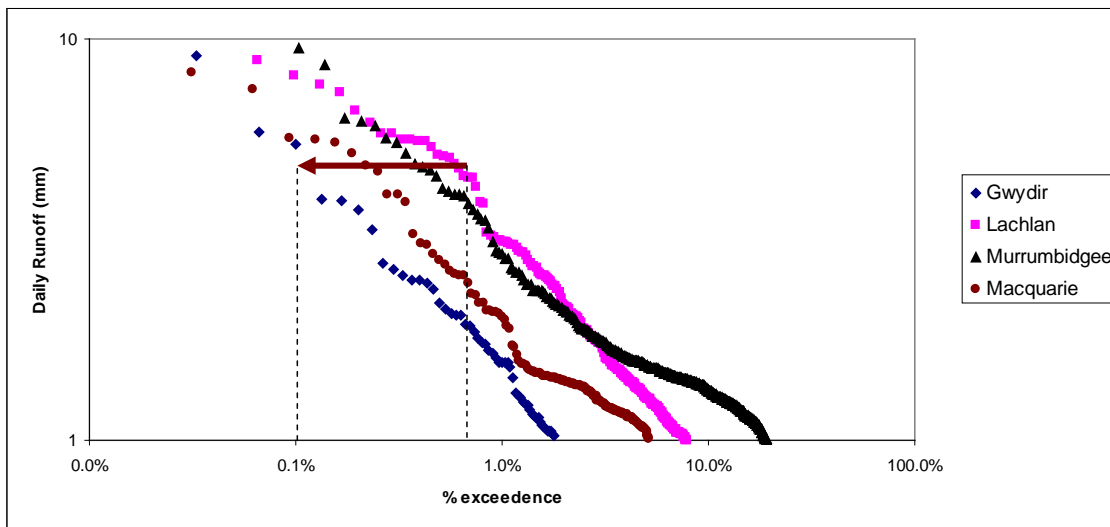


Figure 8.6: Daily runoff event exceedence for four catchments in the Murray-Darling basin, with the offset in % exceedence between the Gwydir and Lachlan traced. Details of data: all curves based on records of greater than 100 years duration. Runoff calculated as discharge / catchment area. All gauging stations in approximately equivalent physiographic settings, i.e. immediately above areas of distributary development. All catchment areas within the range $1 - 5 \times 10^4 \text{ km}^2$. Only events between June and September are included hence 1 % exceedence approximately equivalent to one year recurrence interval. Daily runoff events above 10 mm too infrequent in the Gwydir to plot, hence only values below 10 mm are plotted. It is assumed however, that the approximate ratio of Gwydir values to, for example, Lachlan values continues into more infrequent events.

If, during palaeochannel phases, intense rainfall associated with westerly frontal systems were to dominate, then this may in part explain the apparent change in dominance of the Pilliga Sandstone documented in Chapters Two and Six. The area of the Gwydir Catchment dominated by the Pilliga Sandstone is relatively low elevation ($\sim 450 \text{ m}$) rolling hill country, whereas at higher elevations granites and volcanics on steeper slopes dominate. Relative scarcity of vegetation on isolated high peaks above 1400 m (Galloways [1965] suggested limit of periglacial activity), and perhaps in some sheltered, south facing slopes at lower elevations, due to temperature stress during

glacial periods, combined with occasional intense rainfalls, would result in these areas becoming prolific contributors of coarse bedload (including high potassium material), overwhelming the supply of coarse material from the low-angle, comparatively well-vegetated, sandstone slopes.

8.8 Summary

Palaeoenvironmental records from the Murray-Darling basin and surrounds, including that presented here for the Gwydir fan-plain, provide a complex picture of landscape change in response to climate changes through the last glacial cycle. Neither the precise timing of these changes, nor the specific mechanisms involved, are constant across all catchments within the Murray-Darling basin. However, broadly synchronous periods of widespread increased fluvial activity can be identified when numerous discontinuous records are combined. Furthermore, comparisons between lacustrine and fluvial records, and between fluvial records from diverse catchments, allow inferences to be drawn regarding causal mechanisms and reasons for inter-catchment variability based on considerations of geomorphology and catchment physiography.

Variations in catchment physiography, particularly the height and latitude of the main contributory catchment areas, are in part responsible for the differences in timing and magnitude of fluvial changes within the Murray-Darling basin. Figure 8.4 suggests that the Goulburn-Murray and the Murrumbidgee have apparently seen the most marked decline in channel scale from the Late Pleistocene to the present, possibly because formative discharges during palaeochannel phases were augmented by the spring thaw of large snow packs. Apart from the Gwydir, the more northerly catchments have not seen the same dramatic decline in channel scale as has occurred in the Goulburn-Murray and the Murrumbidgee. It is possible, even likely, that there has been a shift in the drainage network on the Gwydir fan-plain, from a single main channel to division of flow amongst many distributaries, hence the apparent major decline in discharge observed in the Gwydir of magnitude similar to that occurring in the snow-fed catchments of the south.

Determining the significance of high lake levels during previous cooler phases of the last glacial cycle is hindered by the difficulty inherent in distinguishing between the effects of higher precipitation and reduced evaporation. To some extent this difficulty can be overcome by comparing multiple water level records from lakes with different catchment characteristics. The records of Willandra Lakes and Lake George provide a ready example of lakes with very different catchment characteristics responding to climate change in broad synchrony. Fluvial records, on the other hand, allow a more straightforward assessment of the environmental conditions prevailing during their formation. While the detailed climatological significance of larger palaeochannels remains conjectural, it is broadly accepted that larger run-off events lead to larger channels, and that in the Gwydir catchment these could not have been the result of the spring thaw of extensive snow packs nor from minor changes in the vegetation or run-off efficiency of the whole catchment (though it is possible that small areas were denuded during glacial periods and therefore more prolific coarse sediment producers than at present). Only greatly intensified rainfall and associated flood events can be responsible.

In many valleys, the largest palaeochannels and the highest lake levels are found in OIS 3, with 'drier' conditions prevailing immediately before and after. Comparatively low temperatures during the last glacial cycle would have changed the basic hydrological character of catchments, decreasing evaporation and increasing runoff potential. Possible climatological effects of these lower temperatures include a reduction in the latitudinal temperature gradient, enabling greater northerly penetration of westerly frontal systems. Definitive descriptions of palaeoclimatological drivers of channel change remain outside the scope of this thesis, with the focus instead on description of the palaeoenvironmental record as presented in sediments of the Gwydir fan-plain (Figure 8.7). However, the results here provide present the type of evidence that will be necessary if such models are to be developed.

During OIS 4 on the Gwydir fan-plain, palaeochannels of the Chalicum unit were emplaced including extensive gravel deposits signifying large channels comparable in discharge to the Coocalla, Kamilaroi and Kookabunna palaeochannels that followed. Deposits of the Chalicum unit are now almost completely obscured by floodplain accretion associated with subsequent fluvial phases, making it barely detectable in

traditional air photography. In the rest of the Murray-Darling basin deposits coeval with the Chalicum unit have thus far only be found in the Goulburn Murray (the Green Gully – Tallygaroopna system), suggesting OIS 4 was not a period of wide-spread increased fluvial activity (see also Figure 8.5). Alternatively, palaeochannels of other valleys operative during OIS 4 may have been extinguished primarily by channel avulsion, without a long period of channel aggradation. The short climate reversal at the end of OIS 4 may have had an effect mirroring to some extent the effect of the major climate reversal at the end of OIS 2, when there was widespread preservation of channels in their ‘migrational’ state. In this scenario, such features would almost certainly be completely overprinted by subsequent deposits, hence would be very difficult to locate and date. In the Gwydir, palaeochannels younger than OIS 4 have yet to be buried by floodplain clays. In the case of the oldest of these units, the Coocalla, this is because it contains extensive raised deposits resulting from a major phase of channel aggradation prior to final extinction. In the case of the less elevated Kamilaroi and Kookabunna palaeochannels, estimated rates of floodplain aggradation occurring since the onset of the contemporary system (i.e. 0.5 mm a^{-1} for $\sim 3 - 4 \text{ ka}$) have not been sufficient to envelope the channel deposits, hence the Kamilaroi and Kookabunna are still clearly visible on the ground as well as from the air.

The largest palaeochannel on the Gwydir fan-plain, the Coocalla palaeochannel, apparently experienced a period of channel aggradation following an extensive period of channel migration, with the remnants of this final phase present as a subdued ridge of relatively low sinuosity dating to $\sim 39 \text{ ka}$. Across the Murray-Darling basin, mid to late OIS 3 saw extensive fluvial activity and the widespread maintenance of large lakes suggesting that conditions, compared to the present, were genuinely more pluvial rather than just characterised by lower evaporation. Increased precipitation and fluvial activity is also indicated by deposits in coastal valleys to the east of the Murray-Darling basin, with the gravels of the Richmond Unit ($\sim 50 - 40 \text{ ka}$) of the Wollondilly-Nepean River (Nanson *et al.* 2003) being coeval with the Coocalla, while the Rivervale terrace ($\sim 50 - 38 \text{ ka}$) on the Shoalhaven (Nott *et al.* 2002) and the ‘northern terrace’ ($\sim 53 - 36 \text{ ka}$) in the Nambucca Catchment (Nanson *et al.* 2003) provide ages for aggradational phases following major fluvial episodes.

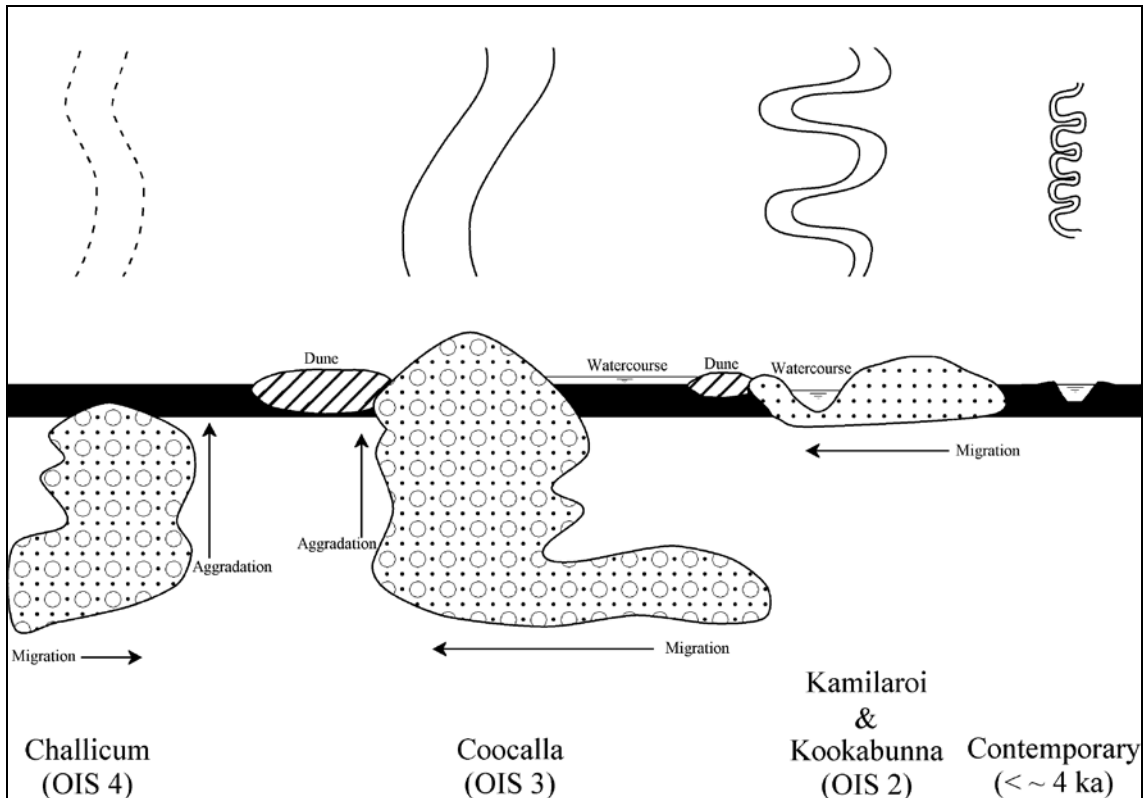


Figure 8.7: Schematic diagram of the age and form of the major depositional features on the Gwydir fan-plain.

In contrast to the relatively straight Coocalla channel, the Kookabunna and Kamilaroi channels preserve distinctly sinuous planforms, and hence were likely to have become abandoned through channel avulsion. It is possible that the Kookabunna and Kamilaroi palaeochannels record in their dimensions the demise of channel discharge associated with the onset of the Holocene, with the late Holocene ‘source limited’ dunes indicating that sands of the palaeochannels were liable to aeolian re-entrainment, possible because of a climatically induced absence of vegetation. The post-LGM record in the Gwydir is closely matched to other fluvial histories across the Murray-Darling basin. Palaeochannels dating to the period immediately following the LGM are common elsewhere (see Figure 8.4), and where systems contain palaeochannels from OIS 3 (e.g. the Murrumbidgee, Page *et al.* [1996] and the Lachlan, Kemp [2001]), these are always larger than the respective OIS 2 palaeochannels.

The final phase of fluvial activity that has been dated in this project is that which includes the present manifestation of the Gwydir distributary system, with its diverse

channel types, watercourses and broad alluvial plains partially mantling the older deposits. Old palaeochannel deposits siphon water from the contemporary system (A. Roberts pers.comm. March, 2001), contributing to the marked downstream decline in discharge and channel capacity. Occasional high flows are now delivered to watercourses which flow in and between palaeochannels. OSL dates obtained in this clay mantle unit provide both an approximate age for the contemporary channels, as well as a rate for floodplain aggradation near Yarraman. The approximate timing of the onset of the contemporary fluvial style corresponds well with ages obtained in the adjacent Namoi, Bellinger and Nambucca Valleys, suggesting that since about 4 – 3 ka, regional precipitation levels have been indistinguishable from those experienced today.

Chapter 9 Summary and Final Remarks

This thesis has examined the controls on channel forms on the Gwydir fan-plain through observation of the spatial and temporal distribution of different channel types. Chapter 2 provided an introduction to the study area with each of the following five chapters concerned with development and application of various quantitative methods for documenting channel diversity. In each case the results of these exercises have allowed inferences to be drawn regarding the mechanisms controlling channel form and change. Data sets have been built, interrogated and compared to data collected elsewhere in order to test previously established models of channel evolution. While many of the conclusions reached remain speculative, new methods of channel analysis have been developed and new lines of enquiry have been identified.

Chapter 2 detailed the close geographic associations between pre-existing landforms and the contemporary fluvial system. Ancient fluvial regimes transported coarse bedload across the entire floodplain, leaving a spatially extensive legacy of sand and gravel deposits which add complexity to the floodplain surface, increasing floodplain storage and complicating flood routing. In contrast, coarse bedload transport by the present regime is restricted to just the upper reaches of the Gwydir River, with the deposition of the contemporary system characterised in the main by a thin veneer of black clay sitting atop the former deposits. Emergent sandy point bars, levees and dunes of ancient systems project through the clay and play a crucial role in directing floodwaters and the sediment suspended therein. Floodplains so built form a highly significant component within the contemporary fluvial system, as the inherent tendency of the channels to breakdown via floodouts to watercourses delivers a large proportion of available water to floodplains. Water discharge as broad sheets of unchannelised flow increases in importance in the lower reaches, with Chapter 3 focusing on the most obvious effect of this on the channels themselves, that is, the overall decline in channel bankfull discharge downstream.

This study presents one of the first detailed investigations of hydraulic geometry in a system where discharge declines downstream, providing relationships well outside the normal range of parameter inter-relationships (Figures 3.6, 3.7). For example, W/D

ratios decrease with increasing discharge in the Mehi, Moomin and Carole tributary streams. The Gwydir alone has a more typical positive relationship between W/D and discharge, achieved through the adoption of an anabranching habit in its low-discharge reaches. The Gwydir fan-plain is unusual in having streams which have low width exponents and high velocity exponents, both primarily a function of the sympathetic downstream decrease in slope and discharge. In contrast to many previously studied streams where downstream decreases in gradient are somewhat offset by downstream decreases in relative boundary roughness associated with discharge increase (e.g. Leopold and Maddock, 1953), streams of the Gwydir fan-plain experience the combined effect of declining gradient and increasing relative boundary roughness (i.e. increasing W/D ratio). Furthermore, the presence of in-stream vegetation greatly adds to flow resistance and directs shear from the bed towards the banks. The variations in in-stream vegetation caused indirectly by the variations in off-take height (Figure 3.13) are argued to have resulted in each channel developing a different bankfull hydraulic geometry. Where channels experience only infrequent flows, for example the Moomin, Carole and downstream reaches of the Mehi, the establishment of in-stream vegetation has caused channels to widen such that they have geometries not consistent with the high material strength of their banks. These differences amongst the hydraulic geometry of the studied streams have been made evident via multivariate hydraulic geometry modelling (Huang and Warner, 1995; Huang and Nanson, 1997; 1998), which has highlighted the differences in apparent bank strength between channels and along individual channels (Table 3.3). Sedimentological investigation of the channels (Figure 3.12) has excluded the possibility that these differences are due to differences in actual material bank strength, hence only a mechanism causing a change in stream hydraulics, specifically the redistribution of stream energy away from the bed towards the bank, can be responsible. The (former) presence of in-stream vegetation is argued to be the most likely mechanism responsible.

Chapter 4 focused on development and application of techniques for the analysis of changes in channelised flow as expressed in planform. In the channels of the Gwydir fan-plain, both meander wavelength and radius of curvature are scaled to depth, velocity, stream power and discharge, but neither appears to directly relate to width (Table 4.3), in apparent contrast to traditional models of meander geometry (e.g. Leopold and Wolman, 1960). Furthermore, sinuosity increases where imposed slope

and stream power decline (Figures 4.11, 4.12), rather than increasing with increasing slope and power as has been generally observed (e.g. Schumm and Khan, 1972). Planform analysis of the contemporary and palaeo- channels of the Gwydir fan-plain has demonstrated the utility of series analysis techniques to objectively identify scale and mode of channels in plan. Planform scale is shown to differ dramatically between palaeochannels and the contemporary channel system, indicating a dramatic decline in bankfull discharge after the palaeochannels formed (Table 4.5). Changes in planform just as dramatic occur within the contemporary system (Figure 4.9). The Gwydir and Mehi appear to have planforms which are adjusted to changes in discharge, with the techniques described in Chapter 4 sensitive enough to measure planform scale changes downstream of individual confluences. In contrast, the Moomin and Carole show limited development in planform scale in response to discharge change. As noted above in discussions of hydraulic geometry, the distributary streams of the Gwydir fan-plain have low width exponents. In fact, the changes in width in the Moomin and Carole are so low as to make their width exponents not significantly different from zero (Table 3.1). The non-responsiveness of width to discharge decline for the Carole and Moomin provides a limit on the decline in scale of meandering in these streams. Although discharge is declining downstream, the scale of meandering is prevented from declining by the 'over-wide' nature of the channels. This produces the observed constancy in downstream planform scale in the Moomin and Carole. It is also likely that the downstream increase in sinuosity observable in the distributary channels (Mehi, Moomin and Carole) is related to this accommodation of the 'over-wide' nature of these channels. To achieve a decline in discharge in the presence of a constant width, slope appears to be declining rapidly through the adoption of a meandering habit. The Gwydir differs from the distributary streams in that by anabranching it is able to maintain relatively narrow channels in its downstream reaches, hence relatively steeper gradients (i.e. lower sinuosity) are needed to transport water and sediment through channels of smaller cross-sectional area. In distributaries where channels have increased their cross-sectional area through widening, lower gradient, highly sinuous reaches persist. Observation of the inter-relationships between slope and width provides insight into the response of these channels to declining discharge.

For the Mehi and Moomin, there are observable negative correlations between sinuosity and both apparent bank strength and stream power (Figures 4.11, 4.12). Stream power

understandably becomes lower as streams become more sinuous and less steep, however the relationship between apparent bank strength, as determined using the multivariate hydraulic geometry model of Huang and co-workers, and sinuosity, is less straightforward. Remembering that no detectable difference in bank sedimentology exists, it is argued that both high sinuosity and low *apparent* bank strength are a result of channels being ‘over-wide’ for their specific complement of underlying hydraulic conditions. Presumably the development of high channel sinuosity requires bank retreat, which in the streams of the Gwydir fan-plain is apparently facilitated by the uneven distribution of boundary shear, whereby an unusually large proportion of the available stream power is expended on the banks.

Unfortunately, the available records of vegetation change are not in themselves sufficient to provide conclusive corroborative evidence for the proposed vegetation and channel-form associations outlined in Chapters 3 and 4, however they do provide glimpses of the former state of the Gwydir distributary system. Anecdotal evidence from elderly residents (Section 3.15), in combination with rare documentary (Appendix A) and photographic (Figure 3.15) evidence, points to past in-channel vegetation communities very different from the present. Because of reduced flow frequencies, the downstream reaches of the distributary channels appear most likely to have been heavily vegetated. Channel formation must have been effected by this, with modelling of the multi-variate hydraulic geometry of each the main channels of the Gwydir distributary system providing insights into the hydraulic effects of different densities of in-channel vegetation. Channels are widest and most sinuous where photographic, documentary and anecdotal evidence suggests that the in-channel vegetation was thickest.

In contrast to many previous non-linear meander scale/discharge relationships typically established using the representative reach approach, the scalar descriptors of planform described in Chapter 4 are shown to be *linearly* related to discharge (Figure 4.13). When measurements of the planform scale of four of the better preserved palaeochannel reaches are related to discharge using the relationships established in the contemporary system, it is clear that the hydrological conditions extant during the emplacement of these palaeochannels was very different from that currently prevailing (Table 4.5). The largest palaeochannel, the Coocalla, has a meander scale corresponding to a palaeodischarge of $\sim 2710 \text{ m}^3\text{s}^{-1}$. The Mia Mia Palaeochannel, which was ultimately

determined on the basis of its age to be part of the Coocalla Palaeochannel, had an estimated palaeodischarge of $\sim 2390 \text{ m}^3\text{s}^{-1}$. The Kamilaroi and Kookabunna Palaeochannels had palaeodischarges of $\sim 1310 \text{ m}^3\text{s}^{-1}$ and $1240 \text{ m}^3\text{s}^{-1}$ respectively. Comparing these values with discharges carried by the modern system is not straightforward. The Coocalla Palaeochannel, including the Mia Mia, was clearly very much larger than anything operating today. The Kamilaroi and Kookabunna channels appear to be approximately the same size as the Gwydir River at the very top of the fan-plain, even though they are some $\sim 100 \text{ km}$ west of the embouchure, where the combined total channel capacity of the modern system is less than $200 \text{ m}^3\text{s}^{-1}$. At least part of the explanation for this dramatic decline in channelised discharge is the propensity for the modern system to deliver much of the discharge that arrives at the top of the fan-plain to unchannelised watercourses (Figures 2.6, 2.10, 2.11, 2.13, 2.14, 2.19), leaving but a small proportion of the flow to be transmitted via channels. Whether similar systems operated during the palaeochannel phases is unknown.

Geochronological investigation of the palaeochannels of the Gwydir fan-plain has been hampered by both the lack of suitable material for ^{14}C dating, and the unsuitability of the sampled 'quartz' for traditional luminescence assay. TL and traditional OSL methods were found to be not suitable for dating the feldspar-rich sands of the Gwydir fan-plain palaeochannels (Section 5.7). Feldspar present as either acid-resistant clasts, or inclusions within quartz (Figure 5.7), was found to cause age underestimation (Table 5.3), either because the feldspar had been bleached by laboratory lighting or because it had lost part of its natural signal due to anomalous fading. A SAR protocol developed for the analysis of quartz in the presence of feldspar (Section 5.8, Olley *et al.*, 2004) has allowed single grain OSL analysis using just the signal emitted by quartz. Furthermore, dose rate data derived from thick source alpha counting, neutron activation analysis and especially high resolution gamma spectrometry, and grain size analysis, have been presented which together illustrate the unlikelihood of secular disequilibrium or β dose rate heterogeneity in the samples collected from the Gwydir fan-plain (Figure 5.13). The calculation of ages using the newly developed SAR protocol, and dose rates which are unlikely to be adversely effected by secular disequilibrium or β dose rate heterogeneity, has enabled the building of a temporal framework within which to place geomorphic developments.

The luminescence sensitivity of quartz has been shown in Chapter 6 to increase along streams in a predictable manner (Figure 6.4a), with streams having highly periodic flow yielding quartz with the greatest sensitivity. This provides a potential mechanism to explain the ideal luminescence characteristics of Australian quartz, that is, the episodic downstream transport of material in large ephemeral rivers, such as the Castlereagh, which provides numerous opportunities for cycles of dosing, heating and bleaching. These cycles have been shown in a laboratory setting to increase the sensitivity of quartz (Figure 6.4b).

Monitoring of quartz sensitivity of bedload sediments throughout the upper Gwydir drainage network has indicated the principal source areas of bedload in the contemporary system (Section 6.5.1), highlighting the likely shift in dominant source area for coarse bedload materials of the lower Gwydir since palaeochannel emplacement. Although no definitive causal explanation for this shift is available, it is possible that an increase in the intensity of rainfall events during the phases of palaeochannel activity had their greatest relative impact in small areas of higher gradient, higher elevation upland regions, where vegetation may have become sparse during glacial periods and where the low-feldspar Pilliga Sandstone is absent (Figure 6.5).

Quartz sensitivity monitoring in the Gwydir distributary system has allowed testing of the model of variable flow recurrence amongst the distributary channels. The ordering of channels in terms of their sensitizing effect on quartz conforms with expectations based on the different hydrological regimes operating in the channels (Figure 6.8). Downstream of the embouchure, the Gwydir River is the most efficient sensitizer of quartz, suggesting that its hydrological regime provides the most opportunities for transport and burial. As they have hydrological regimes dominated by low frequency high magnitude events as a consequence of their high off-takes, the Mehi and Moomin have correspondingly less impact on the luminescence sensitivity of their quartz bedload. In principle, this monitoring of downstream changes in quartz sensitivity to ascertain hydrological regime could be extended to the palaeochannel systems, however, this has not been possible for this project. Likewise, downstream changes in the luminescence sensitivity of palaeochannel quartz should follow predictable patterns,

hence sensitivity monitoring should be able to be used to establish connectivity between discontinuous palaeochannels. This has been demonstrated here in a limited way (Figure 6.9), with obvious discontinuities in quartz sensitivity corresponding to major chronological differences between palaeochannels. Also, the approach has demonstrated the similarity in sensitivity between aeolian dunes and nearby palaeochannels, which is highly suggestive of the palaeochannels having been the immediate source for dune sediments.

This thesis has developed a Quaternary history for the Gwydir fan-plain through documenting both the timing and scale of formative discharge decline. Combining the results of the planform analysis, sedimentological descriptions and geochronological analysis, it is clear that there has been a dramatic decline in formative discharge on the Gwydir fan-plain during the last glacial cycle. Phases of palaeochannel activity have been identified at ~ 66 ka, ~ 39 ka, ~ 19 ka and ~ 16 ka (Figure 7.1). The oldest of these, represented by the deposits of the Challicum Unit, could not be assigned a discharge, as it lacked sufficient surface expression due to its burial by floodplain accretion associated with subsequent fluvial phases. However, extensive gravely bar deposits at depth near sites GF-19 and GF-22 suggest that this system had a discharge comparable in magnitude to the palaeochannels that followed. The largest ($Q_{bf} \approx 2550 \text{ m}^3\text{s}^{-1}$) well preserved palaeochannel, the Coocalla, extends from south of the current head of the fan-plain in a north-westerly direction, with extensive sand and gravel deposition in the vicinity of Moree. In total, 10 OSL dates have been collected from this unit, securely dating it to ~ 39 ka. The next oldest palaeochannel, the Kookabunna dated at three sites to ~ 19 ka, clearly dissects the deposits of the Challicum Unit. The Kookabunna palaeochannel had an estimated Q_{bf} of $\sim 1240 \text{ m}^3\text{s}^{-1}$, which is slightly less than that of the marginally larger ($Q_{bf} \approx 1310 \text{ m}^3\text{s}^{-1}$) Kamilaroi palaeochannel that post-dates it (~ 16 ka). A period of apparent aeolian reactivation of palaeochannel deposits is identified at ~ 4 ka, with floodplain and channel deposits of the contemporary system (total combined channel capacity mid-fan $\approx 200 \text{ m}^3\text{s}^{-1}$) appearing soon after (~ 2.7 ka). Estimates of surface aggradation vary across the fan-plain surface from about 0.02 mma^{-1} in the vicinity of the Challicum palaeochannel, to about 0.5 mma^{-1} near Yarraman (Figure 7.10).

The deposits of the Coocalla palaeochannel, and to a lesser extent the Challicum Unit, appear to be examples of aggradational palaeochannels (*sensu* Page and Nanson, 1996), whereby channel aggradation succeeds an extensive period of channel migration. The Coocalla remains as a subdued ridge of relatively low sinuosity. In contrast, the Kookabunna and Kamilaroi channels still preserve their distinctly sinuous planforms, as they were likely to have become abandoned through channel avulsions, without an extensive phase of channel aggradation. Floodplain aggradation occurring since the onset of the contemporary system (i.e. 0.5 mma^{-1} for $\sim 3 - 4 \text{ ka}$) has not been sufficient to envelope the channel deposits of the Kamilaroi and Kookabunna, hence they are still clearly visible on the ground as well as from the air.

The history of palaeochannel development on the Gwydir fan-plain is consistent with the wider picture of formative discharge decline across the Murray-Darling basin, and in coastal settings to the east (see Chapter 8). In the Murray-Darling basin, deposits coeval with the Challicum unit ($\sim 66 \text{ ka}$) have thus far only be found in the Goulburn-Murray (the Green Gully – Tallygaroopna system of Bowler [1967, 1978], and Page *et al.* [1991]), suggesting that at the broader scale OIS 4 was not a period of increased fluvial activity (Figure 8.4, 8.5). Mid to late OIS 3 saw extensive fluvial activity in the Murray-Darling basin and in adjoining coastal valleys, including in the Gwydir, along with the widespread maintenance of large lakes (Section 8.5, Appendix G). Where catchments contain palaeochannels from OIS 3 (e.g. the Murrumbidgee, Page *et al.* [1996] and the Lachlan, Kemp [2001]), these are always larger than the respective OIS 2 palaeochannels, just as is found in the Gwydir, with the OIS 3 Coocalla Palaeochannel ($\sim 39 \text{ ka}$) having twice the estimated Q_{bf} of the OIS 2 Kamilaroi and Kookabunna channels ($\sim 19 - 16 \text{ ka}$). The approximate timing of the onset of the contemporary fluvial style in the Gwydir corresponds with ages obtained in the adjacent Namoi (Young *et al.* 2002), Bellinger and Nambucca Valleys (Nanson *et al.* 2003), suggesting that since about $4 - 3 \text{ ka}$ regional precipitation levels have been similar to those experienced today.

On the basis of the results presented in this study several suggestions for further research can be made.

- Most of the west flowing rivers of the Murray-Darling basin break down to distributary systems in their lower reaches, hence exploration of the comparative hydraulic geometry and planform of distributaries could be undertaken on a broader basis than that described here. Distributary systems provide the special circumstance of often diverse channel types in close geographical and environmental proximity, where subtle differences in fundamental controlling variables (slope, discharge, sediment load) are readily identifiable. Hence they are classic experiments 'set in train by nature'.
- Monitoring the luminescence sensitivity of quartz has shown potential to provide new information on both sediment provenance and river process. A more detailed examination of quartz sensitivity under more controlled experimental conditions should enable analysis of palaeochannel deposits, providing an aid to connectivity assessment of disjointed palaeochannel remnants and their associated dunes as well as providing insights into channel behaviour.
- The upper Gwydir remains *terrae incognitae* as far as its Quaternary history is concerned, however the upper catchment contains many terraces which may provide considerable palaeoenvironmental information, filling the gap between the well-studied eastern flank of the great dividing range and the western plains.
- In this study the chronology of the 'modern' system has been described with reasonably low precision. When this study was initiated, routine dating of young materials was still in its embryonic phase. However recent work involving the author (Brooke *et al. in press*. Rustomji and Pietsch *in prep*. Tooth *et al. in prep*) has clearly demonstrated the utility of the single grain OSL method developed in Chapter 5 for dating young (i.e. 50 - 500 years) floodplain and channel deposits. If a dating program were initiated focused on the distribution of ages of channel and floodplain deposits in the modern system, new insights into the relationship between channel characteristics and age could be uncovered. In particular, the unusual architecture of the channel off-takes could be explored to explain why in each case the natural state of the distributaries was to not be directly linked to

their trunk channels, but rather separated by low sections of floodplain that were only rarely breached. Does the trunk channel post-date the distributary, or is the distributary cutting back to the trunk? The other somewhat mysterious channel forms on the Gwydir fan-plain are the tortuous meanders of the Mehi and Moomin. Are these a terminal manifestation of the incipient meanders observable in the Gwydir and Carole, or is the relationship between age and sinuosity entirely random?

References

- Aitken, M.J. (1985) *Thermoluminescence dating*. Academic Press, Orlando.
- Aitken, M.J. (1990) *Science-based dating in archaeology*. Longmans, London.
- Aitken, M.J. (1998) *An introduction to optical dating*. Oxford University Press, Oxford.
- Aitken, M.J. and Smith, B.W. (1988) Optical dating: recuperation after bleaching. *Quaternary Science Reviews*, **7**, 387-393.
- An, Z., Bowler, J.M., Opdyke, N.D., Macumber, P.G. and Firman, J.B. (1986) Palaeomagnetic stratigraphy of Lake Bungunia: Plio-Pleistocene precursor of aridity in the Murray Basin, southeastern Australia. *Palaeogeography, Palaeoclimatology, Palaeoecology*, **54**, 219-239.
- Andersson, M., Jeannin, M., Rendell, H.M., Tardot, A. and Townsend, P.D. (1990) TL spectra of mineral mixtures. Discrimination between different components. *Nuclear Tracks and Radiation Measurements*, **17**, 569-577.
- Andersson, M., Rendell, H.M. and Townsend, P.D. (1991) Low temperature spectra of TL from sedimentary quartz and feldspars. *Nuclear Tracks Radiation Measurements*, **18** (1/2), 41-43.
- Armitage, S.J., Duller, G.A.T. and Wintle, A.G. (2000) Quartz from southern Africa: sensitivity changes as a result of thermal pretreatment. *Radiation Measurements*, **32**, (5-6), 571-577.
- Bailey, R.M. (2000) Circumventing possible inaccuracies of the single aliquot regeneration method for the optical dating of quartz. *Radiation Measurements*, **32** (5-6), 833-840.
- Bailey, R.M. (2001) Towards a general kinetic model for optically stimulated luminescence of quartz. *Radiation Measurements*, **33**, 17-45.
- Bailey, R.M., Smith, B.W. and Rhodes, E.J. (1997) Partial bleaching and the decay form characteristics of quartz OSL. *Radiation Measurements*, **27** (2), 123-136.
- Bailey, S.D., Wintle, A.G., Duller, G.A.T. and Bristow, C.S. (2001) Sand deposition during the last millennium at Aberffraw, Anglesey, North Wales as determined by OSL dating of quartz. *Quaternary Science Reviews*, **20**, 701-704.
- Bailiff, I.K. (1994) The pre-dose technique. *Radiation Measurements*, **23**, 471-479.
- Balescu, S., Packman, S., Wintle, A.G. and Grun, R. (1989) TL dating of Pleistocene raised beaches from NW Europe using Potassium feldspar grains. In: *Workshop on*

Long and Short Range Limits in Luminescence Dating, Oxford. Research Laboratory for Archaeology and the History of Art, Occasional Publication 9.

Banerjee, D. (2001) Supralinearity and sensitivity changes in optically stimulated luminescence of annealed quartz. *Radiation Measurements*, **33** (1), 47-57.

Banerjee, D., Page, K. and Lepper, K. (2002) Optical dating of palaeochannel deposits in the Riverine Plain, southeastern Australia: Testing the reliability of existing thermoluminescence dates. *Radiation Protection Dosimetry*, **101** (1-4), 327-332.

Barnes, H.H., Jr. (1967) Roughness characteristics of natural channels. *United States Geological Survey Water Supply Paper*, **1849**.

Barrows, T.T., Stone, J.O., Field, L.K., Cresswell, R.G. (2001) Late Pleistocene glaciation of the Kosciuszko Massif, Snowy Mountains, Australia. *Quaternary Research*, **55**, 179-189.

Barrows, T.T., Stone, J.O., Field, L.K., Cresswell, R.G. (2002). The timing of the last glacial maximum in Australia. *Quaternary Science Reviews*, **21**, 159-173.

Benny, P.G., Sanjeev, N., Rao, T.K.G. and Bhatt, B.C. (2000) Gamma ray induced sensitization of 110 degrees C TL peak in quartz separated from sand. *Radiation Measurements*, **32** (3), 247-252.

Berger, G.W. (1994) Thermoluminescence dating of sediments older than ~100 ka. *Quaternary Science Reviews*, **13**, 445-455.

Blackburn, W.H., Knight, R.W. and Schuster, J.L. (1982) Saltcedar influence on sedimentation in the Brazos River. *Journal of Soil and Water Conservation*, **37**, 298-301.

Blair, T.C. and McPherson, J.G. (1994) Alluvial fans and their natural distinction from rivers based on morphology, hydraulic processes, sedimentary processes, and facies assemblages. *Journal of Sedimentary Research*, **A64**, 450-489.

Blench, T. (1952) Regime theory for self-formed sediment-bearing channels. *Transactions, ASCE*, **117**, 383-408.

Blench, T. (1957) *Regime Behaviour of Canals and Rivers*. Butterworths Scientific Publications, London.

Blong, R.J. and Gillespie, R. (1978) Fluvially transported charcoal gives erroneous ¹⁴C ages for recent deposits. *Nature*, **271**, 739-741.

Bøtter-Jensen, L., Jungner, H. and Mejdahl, V. (1993) Recent developments of OSL techniques for dating quartz and feldspars. *Radiation Protection Dosimetry*, **47** (1-4), 643-648.

- Bøtter-Jensen, L., Agersnap Larsen, N., Mejdahl, V., Poolton, N.R.J., Morris, M.F. and McKeever, S.W.S. (1995) Luminescence sensitivity changes in quartz as a result of annealing. *Radiation Measurements*, **24**, 535-541.
- Bøtter-Jensen, L., Bulur, E., Duller, G.A.T. and Murray, A.S., (2000) Advances in luminescence instrument systems. *Radiation Measurements*, **32**, 523-528.
- Bowall, L., Frean, R., McKeogh, K.J., Rendell, H.M. and Townsend, P.D. (1987) Sensitivity changes in the TL of quartz and feldspar after bleaching. *Crystal Lattice Defects and Amorphous Materials*, **16**, 37-43.
- Bowler, J.M. (1967) Quaternary chronology of Goulburn Valley sediments and their correlation in south-eastern Australia. *Journal of the Geological Society of Australia*, **14**, 287-292.
- Bowler, J.M. (1976) Aridity in Australia: Age, origins and expression in aeolian landforms and sediments. *Earth Science Reviews*, **12**, 279-310.
- Bowler, J.M. (1978) Quaternary climate and tectonics in the evolution of the Riverine Plain, southeastern Australia. In Davies, J.L. and Williams, M.A.J. (eds). *Landform evolution in Australia*. Australian National University Press, Canberra.
- Bowler, J.M. (1986) Quaternary landform evolution. In Jeans, D.N. (ed) *Australia – A geography, Volume One: The natural environment*, 2nd edn, Sydney University Press, 117-147.
- Bowler, J.M., Stockton, E. and Walker, M.J. (1978) Quaternary stratigraphy of the Darling River near Tilpa, NSW. *Proceedings of the Royal Society of Victoria*, **90**, 79-87.
- Bowler, J.M., Johnston, H., Olley, J.M., Prescott, J.R., Roberts, R.G., Shawcross, W. and Spooner, N.A. (2003) New ages for human occupation and climatic change at Lake Mungo, Australia. *Nature*, **421**, 837-84.
- Broccoli, A.J. (2000) Tropical Cooling at the Last Glacial Maximum: An Atmosphere–Mixed Layer Ocean Model Simulation. *Journal of Climate*, **13**, 951-976.
- Brooke, B., Ryan, D., Radke, L., Pietsch, T., Olley, J., Douglas, G., Flood, P. and Packett, R. (submitted) Records of changes in climate, sea level and landuse over the last 1,500 years preserved in beach deposits at Keppel Bay, Queensland, Australia. *Marine Geology*.
- Bulur, E., Botter-Jensen, L. and Murray, A.S. (2000) Optically stimulated luminescence from quartz measured using the linear modulation technique. *Radiation Measurements*, **32** (5-6), 407-411.
- Bulur, E., Duller, G.A.T., Solongo, S., Botter-Jensen, L. and Murray, A.S. (2002) LM-OSL from single grains of quartz: a preliminary study. *Radiation Measurements*, **35** (1), 79-85.

- Butler, B.E. (1950) A theory of prior streams as a causal factor of soil occurrence in the Riverine Plain of southeastern Australia. *Australian Journal of Agricultural Research*, **1**, 231-252.
- Butler, B.E. (1958) *Depositional systems of the Riverine Plain of south-eastern Australia in relation to soils*. **Soil Publication Number 10**. CSIRO Australia.
- Cattle, S.R., McTainsh, G.H. and Wagner, S. (2002) Aeolian dust contributions to soil of the Namoi Valley, northern NSW, Australia. *Catena*, **47**, 245-264.
- Callen, R.A. Wasson, R.J. and Gillespie, R. (1983) Reliability of radiocarbon dating of pedogenic carbonate in the Australian arid zone. *Sedimentary Geology*, **35**, 1-14.
- Chang, H.H. (1979) Geometry of Rivers in Regime. *Journal of the Hydraulics Division, ASCE*, **107**, 839-851.
- Chappell J. (1991) Late Quaternary environmental changes in eastern and central Australia, and their climatic interpretation. *Quaternary Science Reviews*, **10**, 377-390.
- Chawla, S., Rao, T.K.G. and Singhvi, A.K. (1998) Quartz thermoluminescence: Dose and dose-rate effects and their implications. *Radiation Measurements*, **29** (1), 53-63.
- Chen, X.Y., Bowler, J.M. and Magee, J.W. (1993) Late Cenozoic stratigraphy and hydrologic history of Lake Amadeus, a central Australian playa. *Australian Journal of Earth Sciences*, **40**, 1-14.
- Church, M. (1992) Channel Morphology and Typology. In Calow, P. and Petts, G.E. (eds) *The River's Handbook, Hydrological and Ecological Principles*. Blackwell. 126-143.
- Clark, M.L., Rendell, H.M. and Wintle, A.G. (1999) Quality assurance in luminescence dating. *Geomorphology*, **29**, 173-185.
- Cock, B.J., Williams, M.A.J. and Adamson, D.A. (1999) Pleistocene Lake Brachina: a preliminary stratigraphy and chronology of lacustrine sediments from the central Flinders ranges, South Australia. *Australian Journal of Earth Sciences*, **46**, 61-69.
- Cohen, T.J. (2003) *Late Holocene Floodplain Processes and Post-European Channel Dynamics in South-Eastern Australia*. Unpublished PhD Thesis, University of Wollongong, Australia.
- Cohen, T.J. and Nanson, G.C. (in review) Mind the gap: valley deposits and independent proxy climate data identifying the Holocene hypsithermal period of enhanced flow regime in southeastern Australia. *Holocene*.
- Colhoun, E.A. and Fitzsimmons, S.J. (1990) Late cainozoic glaciation in western Tasmania. *Quaternary Science Reviews*, **9**, 199-216.
- Colhoun, E.A., Hannan, D. and Kiernan, K. (1996) Late Wisconsin glaciation of Tasmania. *Papers and Proceedings of the Royal Society of Tasmania*, **130** (2), 33-45.

- Copeland, C., Schooneveldt-Reid, E. and Neller, S. (2003) *Fish Everywhere: An oral history of fish and their habitats in the Gwydir River*. NSW Fisheries, Ballina, NSW.
- Coventry, R.J. (1973) *Abandoned shorelines and the Late Quaternary history of Lake George, New South Wales*. Unpublished PhD thesis, Australian National University.
- Coventry, R.J. (1976) Abandoned shorelines and the Late Quaternary history of Lake George, New South Wales. *Journal of the Geological Society of Australia*, **23(3)**, 249-273.
- Coventry, R.J. and Walker, P.H. (1977) Geomorphological Significance of Late Quaternary Deposits of the Lake George Area, N.S.W. *Australian Geographer*, **13 (6)**, 369-376.
- Croke, J.C., Magee, J.W. and Wallensky, E.P. (1999) The role of the Australian Monsoon in the western catchment of Lake Eyre, central Australia, during the Last Interglacial. *Quaternary International*, **57-58**, 71-80.
- Crowley, T. J. (1991) Past CO₂ changes and tropical sea surface temperatures. *Paleoceanography*, **6**, 387-394.
- Debenham, N.C. (1985) The use of UV emissions in TL dating of sediments. *Nuclear Tracks and Radiation Measurements*, **10**, 717-724.
- Deer, W.A., Howie, R.A. and Zussman, J. (1966) *An introduction to the rock-forming minerals*. Longman Group Limited, London.
- Doyle, C.J. (2003) *Fluvial Geomorphology of the Nambucca River Catchment: Late Quaternary Change, Post-Settlement Channel Degradation and Proposals for River Rehabilitation*. Unpublished PhD Thesis, University of Wollongong, Australia.
- Duller, G.A.T., Botter-Jensen, L and Murray, A.S. (2000) Optical dating of single sand-sized grains of quartz: sources of variability. *Radiation Measurements*, **32**, 453-457.
- Durrani, S.A., Khazal, K.A.R., McKeever, S.W.S. and Riley, R.J. (1977) Studies of changes in the thermoluminescence sensitivity of quartz induced by proton and gamma irradiations. *Radiation Effects*, **33**, 237-244.
- Dury, G.H. (1973) Palaeohydrologic Implications of Some Pluvial Lakes in Northwestern New South Wales, Australia. *Geological Society of America Bulletin*, **84**, 3663-3676.
- Dury, G.H. (1977) Underfit streams: retrospect, perspect, and prospect. In Gregory, K.G. (ed) *River Channel Changes*. Jon Wiley and Sons, Chichester.
- Fagan, S.D. (2001) *Channel and Floodplain Characteristics of Cooper Creek, Central Australia*. Unpublished PhD Thesis, University of Wollongong, Australia.

- Ferguson, R.I. (1973) Regular Meander Path Models. *Water Resources Research*, **9** (4), 1079-1086.
- Ferguson, R.I. (1976) Disturbed periodic model for river meanders. *Earth Surface Processes*, **1**, 337-347.
- Ferguson, R.I. (1977) Meander sinuosity and direction variance. *Geological Society of America Bulletin*, **88**, 212-214.
- Ferguson, R.I. (1981) Channel form and channel changes. In Lewin, J. (ed), *British Rivers*. Allen and Unwin, London, 90-125
- Ferguson, R.I. (1986) Hydraulics and hydraulic geometry. *Progress in Physical Geography*, **10**, 1-31.
- Ferguson, R.I. (1987) Hydraulic and sedimentary controls of channel pattern. In Richards, K.S. (ed) *River Channels, Environment and Process*, Blackwell, London, 129-158.
- Franklin, A.D., Hornyak, W.F. and Dickerson, W. (1992) TL estimation of paleodose of dune-sand quartz. *Quaternary Science Reviews*, **11**, 75-78.
- Fuchs, M. and Lang, A. (2001) OSL dating of coarse-grain fluvial quartz using single-aliquot protocols on sediments from NE Peloponnese, Greece. *Quaternary Science Reviews*, **20**, 783-787.
- Fuchs, M. and Wagner, G.A. (2003) Recognition of insufficient bleaching by small aliquots of quartz for reconstructing soil erosion in Greece. *Quaternary Science Reviews*, **22**, 1161-1167.
- Galbraith, R.F. (1990) The radial plot: graphical assessment of spread in ages. *Nuclear Tracks and Radiation Measurements*, **17**, 207-214.
- Galbraith, R.F. (1998) The trouble with 'probability density' plots of fission track ages. *Radiation Measurements*, **29** (2), 125-131.
- Galbraith, R.F. and Laslett, G.M. (1993) Statistical models for mixed fission track ages. *Nuclear Tracks and Radiation Measurements*, **21**, 459-470.
- Galbraith, R.F., Roberts, R.G., Laslett, G.M., Yoshida, H. and Olley, J.M., (1999) Optical dating of single and multiple grains of quartz from Jinmium rock shelter, northern Australia: Part I, experimental design and statistical models. *Archaeometry*, **41**, 339-364.
- Gale, S.J. and Haworth, R.J. (2002) Beyond the limits of location: human environmental disturbance prior to official European contact in early colonial Australia. *Archaeology in Oceania*, **37**, 123-136.
- Galloway, R.W. (1965) Late Quaternary climates in Australia. *Journal of Geology*, **73**, 603-618.

Galloway, R.W. (1967) Dating of Shore Features at Lake George, New South Wales. *Australian Journal of Science*, **29**, 477.

Galloway, R.W. (1986) Australian snowfields past and present. In Barlow, B.A. (ed) *Flora and fauna of alpine Australasia, ages and origins*. CSIRO, Melbourne.

Geological Survey of New South Wales (1968) *Moree 1: 250 000 Mapsheet*.

Gillespie, R. (1998) Alternative timescales: a critical review of Willandra Lakes dating. *Archaeology in Oceania*, **33**, 169-182

Godfrey-Smith, D.I., Huntley, D.J. and Chen, W.H. (1988) Optical dating studies of quartz and feldspar sediment extracts. *Quaternary Science Reviews*, **7** (3-4), 373-380.

Graf, W.L. (1978) Fluvial adjustments to the spread of tamarisk in the Colorado Plateau region. *Geological Society of America Bulletin*, **89**, 1491-1501.

Grun, R., Packman, S.C. and Pye, K. (1989) Problems involved in TL-dating of Danish cover sands using K-feldspar. In *Workshop on Long and Short Range Limits in Luminescence Dating*, Oxford. Research Laboratory for Archaeology and the History of Art, Occasional Publication 9.

Hadley, R.F. (1961) Influence of riparian vegetation on channel shape, northeastern Arizona. *United States Geological Survey Professional Paper* **424-C**, 30-31.

Harvey, A.M. (1969) Channel capacity and the adjustment of streams to hydrological regime. *Journal of Hydrology*, **8**, 82-89.

Hashimoto, T., Yokosaka, K., Habuki, H. and Hayashi, Y. (1989) Provenance search of dune sands using thermoluminescence colour images (TLCIs) from quartz grains. *Nuclear Tracks and Radiation Measurements*, **16**(1), 3-10.

Hashimoto, T., Sakaue, S., Aoki, H. and Ichino, M. (1994) Dependence of TL-property changes of natural quartzes on aluminium contents accompanied by thermal annealing treatment. *Radiation Measurements*, **23**, 293-299.

Hashimoto T, Katayama H, Sakaue H., Hase, H., Arimura, A. and Ojima, T. (1997) Dependence of some radiation-induced phenomena from natural quartz on hydroxyl-impurity contents. *Radiation Measurements*, **27** (2), 243-250.

Haworth, R.J., Gale, S.J., Short, S.A. and Heijnis, H. (1999) Land use and lake sedimentation on the New England Tablelands of New South Wales, Australia. *Australian Geographer*, **30** (1), 51-73.

Hesse, P.P. (1994) The record of continental dust from Australia in Tasman Sea Sediments. *Quaternary Science Reviews*, **13**, 257-272.

Hey, R.D. (1976) Geometry of river meanders. *Nature*, **262**, 482-4.

- Hey, R.D. and Thorne, C.R. (1986) Stable channels with mobile gravel beds. *Journal of Hydraulic Engineering*, ASCE, **112**, 671-689.
- Hickin, E.J. (1977) The Analysis of River-Planform Responses to Changes in Discharge. In Gregory, K.G. (ed) *River Channel Changes*. Jon Wiley and Sons, Chichester.
- Hickin, E.J. (1983) River channel changes: retrospect and prospect. In Collinson, J.D. and Lewin, J. (eds) *Modern and Ancient Fluvial Systems. Special Publication of the International Association of Sedimentologists*, **6**, 61-83. Blackwell Scientific Publications, Oxford.
- Hicks, D.M. and Mason, P.D. (1991) *Roughness characteristics of New Zealand rivers*. Wellington: Water Resources Survey.
- Hilgers, A., Murray, A. S., Schlaak, N. and Radtke, U. (2001) Comparison of quartz OSL protocols using lateglacial and Holocene dune sands from Brandenburg, Germany. *Quaternary Science Reviews*, **20(5-9)**, 731-736.
- Hollands, C.B., Nanson, G.C., Jones, B.G., Bristow, C.S., Price, D.M. and Pietsch, T.J. (*in press*) Aeolian-fluvial interaction: Evidence for Late Quaternary channel change and wind-rift linear dune formation in the northwestern Simpson Desert, Australia. *Geomorphology*.
- Hope, J.H., Dare-Edwards, A.J. and McIntyre, M.L. (1983) Middens and megafauna: stratigraphy and dating of Lake Tandou lunette, western New South Wales. *Archaeology in Oceania*, **18**, 45-53.
- Hopf, F.V.L., Colhoun, E.A., Barton, C.B. (2000) Late-glacial and Holocene record of vegetation and climate from Cynthia Bay, Lake St Clair, Tasmania. *Journal of Quaternary Sciences*, **15 (7)**, 725-732.
- Horton, R.E. (1945) Erosional development of streams and their drainage basins: hydrophysical approach to quantitative morphology. *Bulletin of the Geological Survey of America*, **56**, 275-370.
- Huang, H.Q. and Nanson, G.C. (1997) Vegetation and channel variation; a case study of four small streams in southeastern Australia. *Geomorphology*, **18**, 237-249.
- Huang, H.Q. and Nanson, G.C. (1998) The influence of bank strength on channel geometry: an integrated analysis of some observations. *Earth Surface Processes and Landforms*, **23**, 865-876.
- Huang, H.Q. and Nanson, G.C. (2000) Hydraulic geometry and maximum flow efficiency as products of the principle of least action. *Earth Surface Processes and Landforms*, **25**, 1-16.
- Huang, H.Q. and Warner, R.F. (1995) The multivariate controls of hydraulic geometry: a causal investigation in terms of boundary shear distribution. *Earth Surface Processes and Landforms*, **20**, 115-130.

- Huntley, D.J., Godfrey-Smith, D.I. and Thewalt, M.L.W. (1985) Optical dating of sediments. *Nature*, **313**, 105-107.
- Huntley, D.J., Godfrey-Smith, D.I., Thewalt, M.L.W., Prescott, J.R. and Hutton, J.T. (1988) Some quartz thermoluminescence spectra relevant to dating. *Nuclear Tracks and Radiation Measurements*, **14**, 27-33.
- Inglis, C. C. (1949), The behavior and control of rivers and canals: *Central Water Power Irrigation and Navigation Report*, **13 (2)**, Poona Research Station, Poona, India.
- Itoh, N., Stoneham, D. and Stoneham, A.M. (2002) Ionic and electronic processes in quartz: Mechanisms of thermoluminescence and optically stimulated luminescence. *Journal of Applied Physics*, **92 (9)**, 5036-5044.
- Jacobs, Z., Duller, G.A.T. and Wintle, A.G. (2003) Optical dating of dune sand from Blombos Cave, South Africa: II- single grain data. *Journal of Human Evolution*, **44**, 613-625.
- Jacobson, G. and Schuett, A.W. (1979) Water levels, balance, and chemistry of Lake George, New South Wales. *BMR Journal of Australian Geology and Geophysics*, **4**, 25-32.
- Jansen, J.D. and Nanson, G.C. (2004) Anabranching and maximum flow efficiency in Magela Creek, northern Australia. *Water Resources Research*, **40**.
- Johnson, B. J., Miller, G. H. Fogel, M. L. Magee, J. W. Gagan, M. K. and Chivas, A. R. (1999) 65,000 years of vegetation change in central Australia and the Australian summer monsoon. *Science*, **284**, 1150-1153.
- Jouzel, J., Lorius, C., Petit, J.R., Genthon, C., Barkov, N.I., Kotlyakov, V.M. and Petrov, V.M. (1987) Vostok ice core - a continuous isotope temperature record over the last climatic cycle (160,000 years). *Nature*, **329 (6138)**, 403-408.
- Jungner, H. and Botter-Jensen, L. (1994) Study of sensitivity change of OSL signals from quartz and feldspars as a function of preheat temperature. *Radiation Measurements*, **23 (2-3)**, 621-624.
- Kemp, J. (2001) *Palaeohydrology and Geomorphology of the Lachlan Valley, New South Wales*. Unpublished PhD Thesis, Australian National University, Canberra.
- Kilpatrick, F.A. and Barnes, H.H. (1964) Channel geometry of Piedmont streams as related to frequency of floods. *United States Geological Survey, Professional Paper*, **422-E**, 1-10.
- Knight, D.W. (1981) Boundary shear in smooth and rough channels. *Journal of the Hydraulic Division, ASCE*, **107**, 839-851.
- Knight, D.W and Patel, H.S. (1985) Boundary shear in smooth rectangular ducts. *Journal of Hydraulic Engineering*, **111**, 29-47.

Knight, D.W., Demetrian, J.D. and Hamed, M.E. (1984) Boundary shear in smooth rectangular channels. *Journal of Hydraulic Engineering*, **101**, 405-422.

Krbetschek, M.R., Gotze, J., Dietrich, A. and Trautmann, T. (1997) Spectral information from minerals relevant for luminescence dating. *Radiation Measurements*, **27 (5/6)**, 695-748.

Kuhns, C.K., Larsen, N.A. and McKeever, S.W.S. (2000) Characteristics of LM-OSL from several different types of quartz. *Radiation Measurements*, **32 (5-6)**, 413-418.

Lacey, G. (1929-1930) Stable channels in alluvium. *Proceedings of the Institute of Civil Engineers, London*, **229**, 259-292.

Lacey, G. (1946) A general theory of flow in alluvium. *Proceedings of the Institute of Civil Engineers, London*, **27**, 16-47.

Lamy, F., Hebbeln, D. and Wefer, G. (1999) High-resolution marine record of climatic change in mid-latitude Chile during the last 28,000 years based on terrigenous sediment parameters. *Quaternary Research*, **51**, 83-93.

Lane, E.W. (1937) Stable channels in erodible material. *Proceedings of the American Society of Civil Engineers*, **102**, 123-142.

Lane, E.W. (1953) Design of stable channels. *Proceedings of the American Society of Civil Engineers*, **79**, 280.1-280.31.

Lane, E.W. (1957) A Study of the Shape of Channels Formed by Natural Streams Flowing in Erodible Material. *United States Army Engineer Division, Sediment Series No. 9*.

Langbein, W.B. (1964) Geometry of river channels. *Proceedings of the American Society of Civil Engineers, Journal of the Hydraulics Division HY2*, **90**, 301-311.

Langbein, W.B. (1965) Geometry of river channels, closure to discussion. *Proceedings of the American Society of Civil Engineers, Journal of the Hydraulics Division HY2*, **91**, 297-313.

Langbein, W.B. and Leopold, L.B. (1966) River meanders – theory of minimum variance. *U.S. Geological Survey Professional Paper*, **422-H**.

Leopold, L.B. and Langbein, W.B. (1962) The concept of entropy in landscape evolution. *U.S. Geological Survey Professional Paper*, **500-A**.

Leopold, L.B. and Maddock, T., Jr., (1953) The hydraulic geometry of stream channels and some physiographic implications. *U.S. Geological Survey Professional Paper*, **252**.

Leopold, L.B. and Miller, J.P. (1956) Ephemeral streams – hydraulic factors and their relation to the drainage net. *U.S. Geological Survey Professional Paper*, **282-A**.

Leopold, L.B. and Wolman, M.G. (1957) River channel patterns: braided, meandering and straight. *U.S. Geological Survey Professional Paper*, **282-B**.

Leopold, L.B. and Wolman, M.G. (1960) River meanders. *Geological Society of America Bulletin*, **71**, 769-794.

Lepper, K. and McKeever, S.W.S. (2002) An objective methodology for dose distribution analysis. *Radiation Protection Dosimetry*, **101**, 349-352.

Lepper, K., Larsen, N.A. and McKeever, S.W.S. (2000) Equivalent dose distribution analysis of Holocene eolian and fluvial quartz sands from central Oklahoma. *Radiation Measurements*, **32**, 603-608.

Li, S.H. (1994) Optical Dating: Insufficiently Bleached Sediments. *Radiation Measurements*, **23 (2-3)**, 563-567.

Li, S.H., Wintle, A.G. (1991) Sensitivity changes of luminescence signals from colluvial sediments after different bleaching procedures. *Ancient TL*, **9**, 50-54.

Li, S.H., Wintle, A.G. (1992) Luminescence sensitivity change due to bleaching of sediments. *Nuclear Tracks and Radiation Measurements*, **20 (4)**, 567-573.

Lindley, E.S., (1919) Regime channels. *Minutes of Proceedings, Punjab Engineering Congress, Lahore, India*, **7**, 63-74.

Liu, Z., Otto-bliesner, B., Kutzbach, J., Li, L. and Shields, C. (2003) Coupled Climate Simulation of the Evolution of Global Monsoons in the Holocene. *Journal of Climate*, **16**, 2472-2490.

Lowry, D.C. and Jennings, J.N. (1974) The Nullabor karst Australia. *Zeitschrift fur Geomorphologie*, **18**, 35-81.

Mackin, J.H. (1948) Concept of the graded river. *Bulletin of the Geological Society of America*, **59**, 463-512.

Mackin, J.H. (1963) Rational and empirical methods of investigation in geology. In Albritton, C.C. (ed) *The fabric of geology*. 135-163.

Magee, J.W., Miller, G.H., Spooner, N.A. and Questiaux, D. (2004) Continuous 150 ky monsoon record from Lake Eyre, Australia: Insolation-forcing implications and unexpected Holocene failure. *Geology*, **32 (10)**, 885-888.

Mahaffey, K. (1985) *The Watercourse Country*. Moree and District Historical Society.

Makaske, B. (2001) Anastomosing rivers: a review of their classification, origin and sedimentary products. *Earth Science Reviews*, **53**, 149-196.

Maroulis, J.C. and Nanson, G.C. (1996) Bedload transport of aggregated muddy alluvium from Cooper Creek, central Australia: a flume study. *Sedimentology*, **43**, 771-790.

Martin, H.A. (1980) Stratigraphic palynology from shallow bores in the Namoi and Gwydir River Valleys, north-central New South Wales. *Proceedings of the Royal Society of New South Wales*, **113**, 81-87.

Martinson, D.G., Pisias, N.G., Hays, J.D., Imbrie, J., Moore, T.C. and Shakleton, N.J. (1987) Age dating and the orbital theory of the ice ages; development of a high-resolution 0 to 300,000-year chronostratigraphy. *Quaternary Research*, **27**(1), 1-29.

Mejdahl, V. (1979) Thermoluminescence dating: beta-dose attenuation in quartz grains. *Archaeometry*, **21**, 61-72.

McKeever, S.W.S. (1985) *Thermoluminescence of Solids*. Cambridge University Press, Cambridge.

McKeever, S.W.S. (1991) Mechanisms of thermoluminescence production: some problems and a few answers? *Nuclear Tracks and Radiation Measurements*, **18**, 5-12.

McKeever, S.W.S. and Morris, M.F. (1994) Computer simulations of optical bleaching of TL and OSL signals. *Radiation Measurements*, **23** (2-3), 301-306.

McKeever, S.W.S., Larsen, N.A., Botter-Jensen, L., Mejdahl, V. (1997) OSL sensitivity changes during single aliquot procedures: Computer simulations. *Radiation Measurements*, **27** (2), 75-82.

Morris, M.F. and McKeever, S.W.S. (1993) Further developments of a model for describing the optical bleaching of thermoluminescence from quartz as applied to sediment dating. *Radiation Protection Dosimetry*, **47**, 637-641.

Murray, A.S. and Clemmensen, L.B. (2001) Luminescence dating of Holocene aeolian sand movement, Thy, Denmark. *Quaternary Science Reviews*, **20**, 751-754.

Murray, A.S. and Mejdahl, V. (1999) Comparison of regenerative-dose single-aliquot and multiple-aliquot (SARA) protocols using heated quartz from archaeological sites. *Quaternary Science Reviews (Quaternary Geochronology)*, **18**, 223-229.

Murray, A.S. and Olley, J.M. (2002) Precision and accuracy in the optically stimulated luminescence dating of sedimentary quartz: a status review. *Geochronometria*, **21**, 1-16.

Murray, A.S. and Roberts, R.G. (1997) Determining the burial time of single grains of quartz using optically stimulated luminescence. *Earth and Planetary Science Letters*, **152**(1-4), 163-180.

Murray, A.S. and Roberts, R.G. (1998) Measurement of the equivalent dose in quartz using a regenerative-dose single-aliquot protocol. *Radiation Measurements*, **29** (5), 503-515.

Murray, A.S. and Wintle, A.G. (1998) Factors controlling the shape of the OSL decay curve in quartz. *Radiation Measurements*, **29** (1), 65-79.

- Murray, A.S. and Wintle, A.G. (2000) Luminescence dating of quartz using an improved single-aliquot regenerative-dose protocol. *Radiation Measurements*, **32** (1), 57-73.
- Murray, A.S., Marten, R., Johnston, A. and Martin, P. (1987) Analysis for naturally occurring radionuclides at environmental concentrations by gamma spectrometry. *Journal of Radioanalytical and Nuclear Chemistry, Articles*, **115**, 263-288.
- Murray, A.S., Olley, J.M. and Caitcheon, G.C. (1995) Measurement of equivalent doses in quartz from contemporary water-lain sediments using optically stimulated luminescence. *Quaternary Science Reviews*, **14**, 365-371.
- Murray, A.S., Roberts, R.G. and Wintle, A.G. (1997) Equivalent dose measurement using a single aliquot of quartz. *Radiation Measurements*, **27** (2), 171-184.
- McTainsh, G.H. (1989) Quaternary aeolian dust processes and sediments in the Australian region. *Quaternary Science Reviews*, **8**, 235-253.
- Nanson, G.C. and Croke, J.C. (1992) A genetic classification of floodplains. *Geomorphology*, **4**, 459-486.
- Nanson, G.C. and Doyle, C.J. (1999) Landscape stability, Quaternary climate change and European degradation of coastal rivers in southeastern Australia. In Rutherford, I. and Bartley, R (eds) *Proceedings of the Second Australian Stream Management Conference, Cooperative Research Centre for Catchment Hydrology, Melbourne Australia*, 473-480.
- Nanson, G.C. and Gibling, M.R. (2003) Rivers and alluvial fans. In: Middleton, G.V. (ed.), *Encyclopedia of Sediments and Sedimentary Rocks*. Kluwer, Dordrecht, pp. 563-583.
- Nanson, G.C. and Huang, H.Q. (1999) Anabranching rivers: divided efficiency leading to fluvial diversity. In Miller, A.J. and Gupta, A. (eds) *Varieties of Fluvial Form*, 477-494. Wiley, Chichester.
- Nanson, G.C. and Knighton, A.D. (1996) Anabranching rivers: their cause, character, and classification. *Earth Surface Processes and Landforms*, **21**, 217-239.
- Nanson, G.C. and Tooth, S. (2004) Arid-Zone Rivers as Indicators of Climate Change. In Singhvi, A.K. and Derbyshire, E. (eds) *Paleoenvironmental Reconstruction in Arid Lands*, 175-216. Oxford & IBH Publishing Co. New Dehli.
- Nanson, G.C., Price, D.M. and Short, S.A. (1992) Wetting and drying of Australia over the past 300 ka. *Geology*, **20** (9), 791-794.
- Nanson, G.C., Chen, X.Y. and Price, D.M. (1995) Aeolian and fluvial evidence of changing climate and wind patterns during the past 100 ka in the western Simpson Desert, Australia. *Palaeogeography, Palaeoclimatology, Palaeoecology*, **113**, 87-102.

Nanson, G.C., Cohen, T.J., Doyle C.J. and Price P.M. (2003) Alluvial Evidence of Major Late-Quaternary Climate and Flow-regime Changes on the Coastal Rivers of New South Wales, Australia. In Gregory, K.J. and Benito, G. (eds) *Palaeohydrology: Understanding Global Change*, John Wiley and Sons, 233-258.

Nanson, G.C., Jones, B.G., Price, D.M. Pietsch, T.J. (2005) Rivers turned to rock: Late Quaternary alluvial induration influencing the behaviour and morphology of an anabranching river in the Australian monsoon tropics. *Geomorphology*, **70 (3-4)**, 398-420.

New South Wales Department of Water Resources (no date) *Water Resources of the Gwydir Valley*

Nott, J., Price, D. and Nanson, G. (2002) Stream response to Quaternary climate change: evidence from the Shoalhaven River catchment, southeastern highlands, temperate Australia. *Quaternary Science Reviews*, **21 (8-9)**, 965-974.

Ogden, R., Spooner, N., Reid, M. and Head, J. (2001) Sediment dates with implications for the age of the conversion from palaeochannel to modern fluvial activity on the Murray River and tributaries. *Quaternary International*, **83-5**, 195-209

Olley, J.M., Murray, A.S. and Roberts, R.G. (1996) The effects of disequilibria in the uranium and thorium decay chains on burial dose rates in fluvial sediments. *Quaternary Science Reviews (Quaternary Geochronology)*, **15**, 751-760.

Olley, J., Caitcheon, G. and Murray, A. (1998) The distribution of apparent dose as determined by optically stimulated luminescence in small aliquots of fluvial quartz: implications for dating young sediments. *Quaternary Science Reviews (Quaternary Geochronology)*, **17**, 1033-1040.

Olley, J.M., Caitcheon, G.C. and Roberts, R.G. (1999) The origin of dose distributions in fluvial sediments, and the prospect of dating single grains of quartz from fluvial deposits using optically stimulated luminescence. *Radiation Measurements*, **30**, 207-217.

Olley, J.M., Pietsch, T. and Roberts, R.G. (2004a) Optical dating of Holocene sediments from a variety of geomorphic setting using single grains of quartz. *Geomorphology*, **60(3-4)**, 337-358.

Olley, J.M. De Dekker, P., Roberts, R.G., Fifield, L.K. and Hancock, G. (2004b) Optical dating of deep-sea sediments using single grains of quartz: comparison with radiocarbon ages and implications for the marine carbon reservoir. *Sedimentary Geology*, **169(3-4)**, 175-189.

Osterkamp, W.R. (1979) Invariant power functions as applied to fluvial geomorphology, in Rhodes, D.D. and Williams, G.P. (eds) *Adjustments of the Fluvial System*, Kendall/Hunt Publishing Co., Iowa, 33-54.

Packman, S.C. and Grun, R. (1992) TL analysis of loess samples from Achenheim. *Quaternary Science Reviews*, **11**, 103-107.

- Page, K.J. (1994) *Late Quaternary stratigraphy and chronology of the Riverine Plain, southeastern Australia*. Unpublished PhD Thesis, University of Wollongong.
- Page, K.J. and Nanson, G.C. (1996) Stratigraphic architecture resulting from Late Quaternary evolution of the Riverine Plain, south-eastern Australia. *Sedimentology*, **43**, 927-945.
- Page, K.J., Nanson, G.C. and Price, D.M. (1991) Thermoluminescence chronology of Late Quaternary deposition on the Riverine Plain of southeastern Australia. *Australian Geographer*, **22**, 14-23.
- Page, K., Dare-Edwards, A., Nanson, G. and Price, D. (1994) Late Quaternary evolution of Lake Urana, New South Wales, Australia. *Journal of Quaternary Science*, **9**, 47-57.
- Page, K., Nanson, G. and Price, D. (1996) Chronology of Murrumbidgee River palaeochannels on the Riverine Plain, southeastern Australia. *Journal of Quaternary Science*, **11**, 311-326.
- Page, K.J., Nanson, G.C. and Frazier, P.S. (2003) Floodplain formation and sediment stratigraphy resulting from oblique accretion on the Murrumbidgee River, Australia. *Journal of Sedimentary Research*, **73** (1), 5-14.
- Park, C.C. (1977) World-wide variations in hydraulic geometry exponents of stream channels: an analysis and some interpretations. *Journal of Hydrology*, **33**, 133-146.
- Pels, S. (1964a) Quaternary sedimentation by prior streams on the Riverine Plain, south-west of Griffith, N.S.W. *Journal and Proceedings, Royal Society of New South Wales*, **97**, 107-115.
- Pels, S. (1964b) The present and ancestral Murray River system. *Australian Geographical Studies*, **2**, 111-119
- Pels, S. (1966) Late Quaternary chronology of the Riverine Plain of southeastern Australia. *Journal of the Geological Society of Australia*, **13**, 27-40.
- Pels, S. (1969) Radio-carbon datings of ancestral river sediments on the Riverine Plain of southeastern Australia and their interpretation. *Journal and Proceedings, Royal Society of New South Wales*, **102**, 189-195
- Pels, S. (1971) River systems and climatic changes in southeastern Australia. In Mulvaney, D.J. and Golsen, J. (eds) *Aboriginal Man and Environment in Australia*, **38-46**. Australian University Press, Canberra.
- Peterson, J.A. and Robinson, G. (1969) Trend surface mapping of cirque floor levels. *Nature*, **222**, 75-76.
- Petit, J.R., Mounier, L., Jouzel, J., Korotkevich, Y.S., Kotlyakov, V.I. and Lorius, C. (1990) Palaeoclimatological and chronological implications of the Vostok core dust record. *Nature*, **343** (6253), 56-58.

Pickup, G. and Reiger, W.A. (1979) A conceptual model of the relationship between channel characteristics and discharge. *Earth Surface Processes*, **4**, 37-42.

Prescott, J.R. and Hutton, J.T. (1994) Cosmic ray contributions to dose rates for luminescence and ESR dating: large depths and long-term time variations. *Radiation Measurements*, **23**, 497-500.

Prescott, J.R. and Hutton, J.T. (1995) Environmental dose rates and radioactive disequilibrium from some Australian luminescence dating sites. *Quaternary Science Reviews (Quaternary Geochronology)*, **14**, 439-448.

Price (1994) TL signatures of quartz grains of different origin. *Radiation Measurements*, **23 (2-3)**, 413-417.

Radtke, U., Janotta, A., Hilgers, A. and Murray, A.S. (2001) The potential for OSL and TL for dating Lateglacial and Holocene dune sands tested with independent age control of the Laacher See tephra (12 880 a) at the Section 'Mainz-Gonsenheim'. *Quaternary Science Reviews*, **20**, 719-724.

Readhead, M.L. (1984) *Thermoluminescence Dating of Some Australian Sedimentary Deposits*. Unpublished PhD Thesis. Australian National University.

Readhead, M.L. (1988) Thermoluminescence dating study of quartz in aeolian sediments from southeastern Australia. *Quaternary Science Reviews*, **7**, 257-264.

Rendell, H.M. (1992) A comparison of TL age estimates from different mineral fractions of sands. *Quaternary Science Reviews*, **11**, 79-83.

Rendell, H.M. and Wood, R.A. (1994) Quartz sample pretreatments for TL/OSL dating: studies of TL emission spectra. *Radiation Measurements*, **23 (2/3)**, 575-580.

Rendall, H.M., Lancaster, N. and Tchakerian, V.P. (1994) Luminescence dating of Late Quaternary aeolian deposits at Dale Lake and Cronese Mountains, Mojave Desert, California. *Quaternary Science Reviews (Quaternary Geochronology)*, **13**, 417-422.

Rhoads, B.L. (1991) A Continuously Varying Parameter Model of Downstream Hydraulic Geometry. *Water Resources Research*, **27**, 1865-1872.

Rhoads, B.L. and Welford, M.R. (1991) Initiation of river meandering. *Progress in Physical Geography*, **15**, 127-156.

Rhodes, D.D. (1987) The b-f-m diagram for downstream hydraulic geometry. *Geografiska Annaler*, **69A**, 147-161.

Rhodes, E.J. (2000) Observations of thermal transfer OSL signals in glacial quartz. *Radiation Measurements*, **32 (5-6)**, 595-602.

- Rhodes, E.J., Bailey, R.M. (1997) The effect of thermal transfer on the zeroing of the luminescence of quartz from recent glaciofluvial sediments. *Quaternary Science Reviews*, **16** (3-5), 291-298.
- Richards, K. (1977) Channel and flow geometry: a geomorphological perspective. *Progress in Physical Geography*, **1**, 65-102.
- Riley, S.J. (1975a) *The Development of Distributary Channel Systems with Special Reference to Channel Morphology: A Case-Study of the Namoi-Gwydir System*. PhD Thesis (unpublished), University of Sydney.
- Riley, S.J. (1975b) The channel shape-grain size relation in eastern Australia and some palaeohydrologic implications. *Sedimentary Geology*, **14**, 253-258.
- Riley, S.J. and Taylor, G. (1978) The geomorphology of the upper Darling River system with special reference to the present fluvial system. *Proceedings of the Royal Society of Victoria*, **90**, 89-102.
- Roberts, R., Yoshida, H., Galbraith, R., Laslett, G., Jones, R. and Smith, M. (1998) Single-aliquot and single-grain optical dating confirm thermoluminescence age estimates at Malakunanja II rock shelter in northern Australia. *Ancient TL*, **16**, 19-24.
- Roberts, R.G., Galbraith, R.F., Olley, J.M., Yoshida, H. and Laslett, G.M. (1999) Optical dating of single and multiple grains of quartz from Jinmium rock shelter, northern Australia: Part II, Results and implications. *Archaeometry*, **41**, 365-395.
- Robertson, G.B., Prescott, J.R. and Hutton, J.T. (1991) Bleaching of the thermoluminescence of feldspars by sunlight. *Nuclear Tracks and Radiation Measurements*, **18**, 101-107.
- Rustomji, P. and Pietsch, P. (in prep) Floodplain deposition in the Lake Burrogorang catchment since settlement.
- Schumm, S.A. (1960) The shape of alluvial channels in relation to sediment type, erosion and sedimentation in a semiarid environment. *U.S. Geological Survey Professional Paper* **352-B**, 17-30.
- Schumm, S. A. (1968) River adjustment to altered hydrologic regimen – Murrumbidgee River and palaeochannels, Australia. *United States Geological Survey Professional Paper* **598**.
- Schumm, S.A. and Khan, H.R. (1972) Experimental Study of Channel Patterns. *Geological Society of America Bulletin*, **83**, 1755-1770.
- Schumm, S.A. and Lichty, R.W. (1965) Time, space and causality in geomorphology. *American Journal of Science*, **263**, 110-119.
- Schumm, S.A., Khan, H.R., Winkley, B.R. and Robbins, L.G. (1972) Variability of River Patterns. *Nature, Physical Science*, **237**, 75-76.

- Schumm, S.A., Erskine, W.D. and Tilleard, J.W. (1996) Morphology, hydrology and evolution of the anastomosing Ovens and Kings Rivers, Victoria, Australia. *Geological Society of America Bulletin*, **108**, 1212-1224.
- Shackleton, N.J. and Opdyke, N.D. (1973) Oxygen Isotope and Palaeomagnetic Stratigraphy of Equatorial Pacific Core V28-238: Oxygen Isotope Temperatures and Ice Volumes on a 10^5 Year and 10^6 Year Scale. *Quaternary Research*, **3**(1), 39-55.
- Simons, D.B. and Albertson, M.L. (1960) Uniform water conveyance channels in alluvium. *Journal of the Hydraulics Division ASCE*, **86**, 33-71.
- Simons, D.B. and Richardson, E.V. (1966) Resistance to Flow in Alluvial Channels. *U.S. Geological Survey Professional Paper* **422-J**.
- Singh, G. and Geissler, E.A. (1985) Late Cainozoic history of vegetation, fire, lake levels and climate, at Lake George, New South Wales, Australia. *Philosophical Transactions of the Royal Society of London*, **311B**, 379-447.
- Singh, G., Opdyke, N.D. and Bowler, J.M. (1981) Late Cainozoic stratigraphy, palaeomagnetic chronology and vegetational history from Lake George, NSW. *Journal of the Geological Society of Australia*, **28**, 435-452.
- Smith, B.W., Aitken, M.J., Rhodes, E.J., Robinson, P.D. and Geldard, D.M. (1986) Optical dating: methodological aspects. *Radiation Protection Dosimetry*, **17**, 229-233.
- Smith, N.D., Cross, T.A., Dufficy, J.P. and Clough, S.R., (1989) Anatomy of an avulsion. *Sedimentology*, **36**, 1-23.
- Spooner, N.A. (1994) On the optical dating signal from quartz. *Radiation Measurements*, **23** (2/3), 593-600.
- Spooner, N.A., Prescott, J.R. and Hutton, J.T. (1988) The effect of illumination wavelength on the bleaching of the Thermoluminescence (TL) of quartz. *Quaternary Science Reviews*, **7** (3-4), 325-329.
- Stanistreet, I.G. and McCarthy, T.S. (1993) The Okavango fan and the classification of subaerial systems. *Sedimentary Geology*, **85**, 115-133.
- Stokes, S. (1994) The timing of OSL sensitivity changes in natural quartz. *Radiation Measurements*, **23**, 601-606.
- Stokes, S. (1999) Luminescence dating application in geomorphological research. *Geomorphology*, **29**, 153-171.
- Stokes, S., Ingram, S., Aitken, M.J., Sirocko, F., Anderson, R. and Leuschner, D. (2003) Alternative chronologies for Late Quaternary (Last Interglacial – Holocene) deep sea sediment via optical dating of silt-size quartz. *Quaternary Science Reviews*, **22**, 925-941.

- Stoneham D. and Stokes, S. (1991) An investigation of the relationship between the 110°C TL peak and optical stimulated luminescence in sedimentary quartz. *Nuclear Tracks and Radiation Measurements*, **18**, 119-123.
- Sweller, S. and Martin, H.A. (2001) A 40,000 year vegetation history and climatic interpretations of Burruga Swamp, Barrington Tops, New South Wales. *Quaternary International*, **83-85**, 233-244.
- Tadros, N.Z. (1993) The Gunnedah Basin, New South Wales. *Geological Survey of New South Wales, Memoir Geology* **12**, 649p.
- Tooth, S. (1997) *The morphology, dynamics and Late Quaternary sedimentary history of ephemeral drainage systems on the Northern Plains of central Australia*. Unpublished PhD thesis. University of Wollongong.
- Tooth, S. and Nanson, G.C. (1999) Anabranching rivers on the Northern Plains of arid central Australia. *Geomorphology*, **29**, 211-233.
- Tooth, S. and Nanson, G.C. (2000a) The role of vegetation in the formation of anabranching channels in an ephemeral river, Northern plains, arid central Australia. *Hydrological Processes*, **14**, 3099-3117.
- Tooth, S. and Nanson, G.C. (2000b) Equilibrium and non-equilibrium conditions in dryland rivers. *Physical Geography*, **21(2)**, 183-211.
- Tooth, S. and Nanson, G.C. (2004) Forms and processes of two highly contrasting rivers in arid central Australia, and the implications for channel-pattern discrimination and prediction. *Geological Survey of America Bulletin*, **116 (7-8)**, 802-816.
- Tooth, S., Coulthard, T.J., Jansen, J.D., Nanson, G.C and Pietsch, T.J. (in prep) In-channel bar growth in Magela Creek.
- van den Berg, J.H. (1995) Prediction of alluvial channel pattern of perennial rivers. *Geomorphology*, **12**, 259-279.
- Vandenberghe, D., Hossain, S.M., De Corte, F. and Van den haute, P. (2003) Investigations on the origin of the equivalent dose distribution in a Dutch coversand. *Radiation Measurements*, **37**, 433-439.
- van der Touw, J.W., Galbraith, R.F. and Laslett, G.M., (1997). A logistic truncated normal mixture model for overdispersed binomial data. *Journal of Statistical Computation and Simulation*, **59**, 349-373.
- Vartanian, E., Guibert, P., Rogue, C., Bechtel, F., Schvoerer, M. (2000) Changes in OSL properties of quartz by preheating: an interpretation. *Radiation Measurements*, **32 (5-6)**, 647-652.
- Wallinga, J. (2002) Optically stimulated luminescence dating of fluvial deposits: a review. *Boreas*, **31(4)**, 303-322.

- Ward, W.T. (1999) *Soils and Landscapes near Narrabri and Edgeroi, NSW, with Data Analysis using Fuzzy k-means*. Division of Soils, CSIRO, Canberra.
- Warner, R.F. (1970) Radio-carbon dates for some fluvial and colluvial deposits in the Bellinger Valley, New South Wales. *Australian Journal of Science*, **32 (9)**, 368-369.
- Warner, R.F. (1972) River Terrace Types in the coastal valleys of New South Wales. *Australian Geographer*, **12**, 1-22.
- Watkins, J.J. and Meakin, N.S. (1996) *Explanatory Notes Nyngan and Walgett 1:250 000 geological mapsheets*. Geological Survey of New South Wales, Sydney.
- Wende, R. and Nanson, G. C. (1998) Anabranching rivers: ridge-form alluvial channels in tropical northern Australia. *Geomorphology*, **22 (3-4)**, 205-224.
- Wharton, G. (1995) The channel-geometry method: guidelines and applications. *Earth Surface Processes and Landforms*, **20**, 649-660.
- Williams, G.P. (1978) Bankfull discharge of rivers. *Water Resources Research*, **14**, 1141-1158.
- Williams, G.P. (1983) Improper use of regression equations in earth sciences. *Geology*, **11**, 195-197.
- Williams, G.P. (1984) Paleohydrologic Equations for Rivers. In Costa, J.E. and Fleisher, P.J. (eds) *Developments and Applications of Geomorphology*. Springer-Verlag Berlin Heidelberg, 343-367
- Williams, M.A.J. (1994) Some implications of past climatic changes in Australia. *Transactions of the Royal Society of South Australia*, **118 (1)**, 17-25.
- Williams, M. A. J., Adamson, D. A. and Baxter, J. T. (1986) Late Quaternary environment in the Nile and Darling basins. *Australian Geographical Studies*, **24 (1)**, 128-144.
- Williams, M.A.J., De Dekker, P., Adamson, D.A. and Talbot, M.R. (1991) Episodic fluvial, lacustrine and aeolian sedimentation in the late Quaternary desert margin system, central western New South Wales. In Williams, M.A.J., De Dekker, P. and Kershaw, A.P. (eds) *The Cainozoic in Australia; a re-appraisal of the evidence*. Geological Society of Australia, Special Publication 18, 258-287.
- Williams, M., Prescott, J.R., Chappell, J., Adamson, D., Cock, B., Walker, K. and Gell, P. (2001) The enigma of a late Pleistocene wetland in the Flinders Ranges, South Australia. *Quaternary International*, **83-85**, 129-144.
- Wintle, A.G. (1973) Anomalous fading of thermoluminescence in mineral samples. *Nature*, **245**, 143-144.
- Wintle A.G. (1985) Sensitization of TL signal by exposure to light. *Ancient TL*, **3**, 16-21.

- Wintle, A.G. (1993) Luminescence dating of Aeolian sands: an overview. In Pye, K. (ed), *The Dynamics and Environmental Context of Aeolian Sedimentary Systems*, 49-58. Geological Society of London, Special Publication 72.
- Wintle, A.G. (1997) Luminescence dating: laboratory procedures and protocols. *Radiation Measurements*, **27**, 769-817.
- Wintle, A.G. and Murray, A.S. (1997) The relationship between quartz thermoluminescence, photo-transferred thermoluminescence and optically stimulated luminescence. *Radiation Measurements*, **27**, 611-624.
- Wintle, A.G. and Murray, A.S. (1998) Towards the development of a preheat procedure for OSL dating of quartz. *Radiation Measurements*, **29** (1), 81-94.
- Wintle, A.G. and Murray A.S. (1999) Luminescence sensitivity changes in quartz. *Radiation Measurements*, **30**, 107-118.
- Wintle, A.G. and Murray, A.S. (2000) Quartz OSL: Effects of thermal treatment and their relevance to laboratory dating procedures. *Radiation Measurements*, **32**, 387-400.
- Wolman, M.G. (1955) The natural channel of Brandywine Creek, Pennsylvania. *U.S. Geological Survey Professional Paper*, **271**.
- Wolman, M.G. and Gerson, R. (1978) Relative scales of time and effectiveness of climate in watershed geomorphology. *Earth Surface Processes*, **3**, 189-208.
- Wolman, M.G. and Leopold, L.B. (1957) River flood plains: some observations on their formation. *United States Geological Survey Professional Paper*, **282C**, 87-109.
- Wolman, M.G. and Miller, J.P. (1960) Magnitude and frequency of forces in geomorphic processes. *Journal of Geology*, **68**, 54-74.
- Woodyer, K.D. (1968) Bankfull frequency in rivers. *Journal of Hydrology*, **6**, 114-142.
- Wyrwoll, K.H. and G. H. Miller, (2001) Initiation of the Australian summer monsoon 14,000 years ago. *Quaternary International*, **83–85**, 119–128.
- Yoshida, H., Roberts, R.G., Olley, J.M. Laslett, G.M., Galbraith, R.F. (2000) Extending the age range of optical dating using single ‘supergrains’ of quartz. *Radiation Measurements*, **32**, 439-446.
- Young, R.W., Young, A.R.M., Price, D.M., Wray, R.A.L. (2002) Geomorphology of the Namoi alluvial plain, northwestern New South Wales. *Australian Journal of Earth Sciences*, **49**, 509-523.
- Zhang, J.F., Zhou, L.P. and Yue, S.Y. (2003) Dating fluvial sediments by optically stimulated luminescence: selection of equivalent doses for age calculation. *Quaternary Science Reviews*, **22**, 1123-1129.

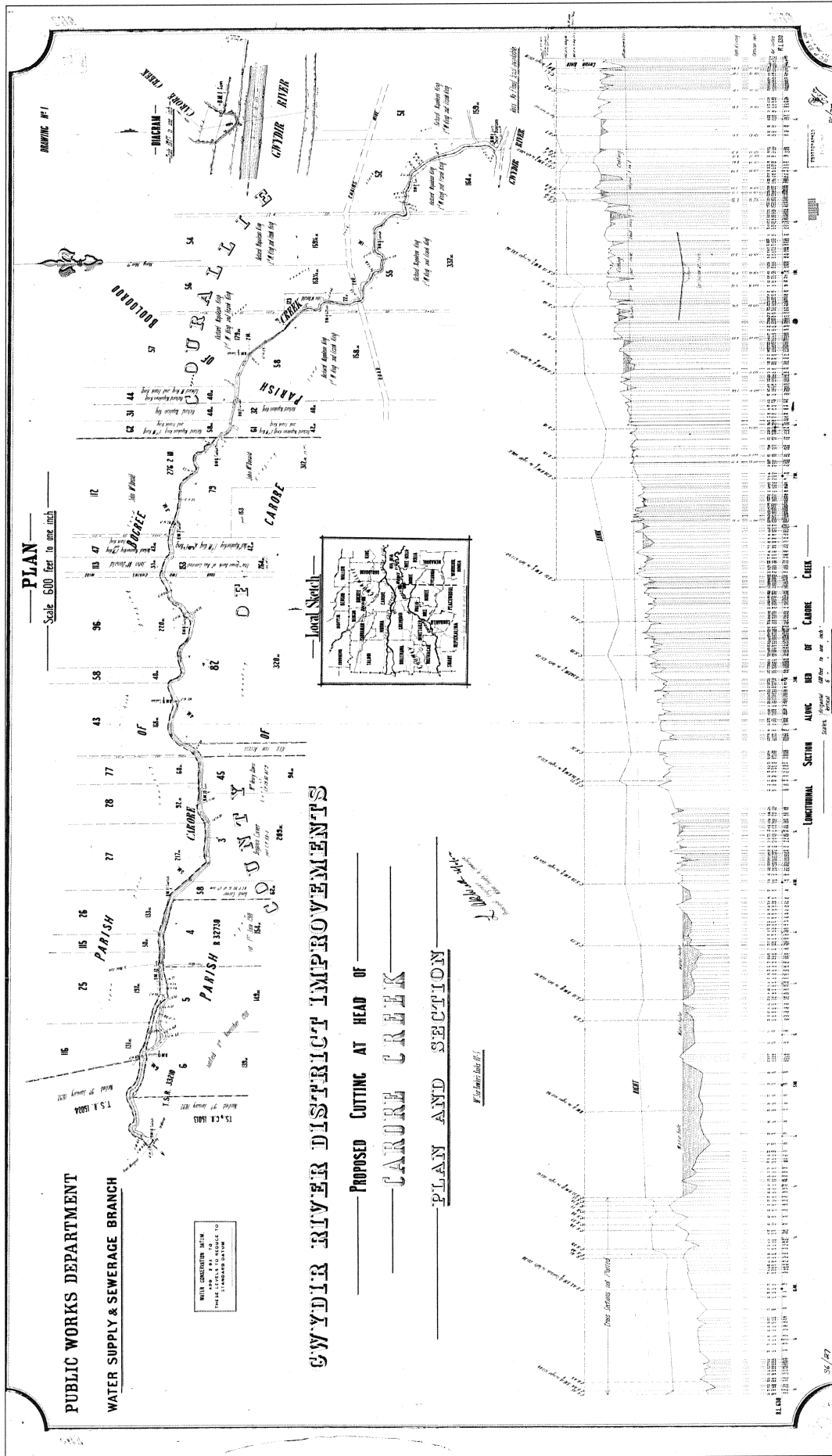
Zhou, L.P. and Wintle, A.G. (1994) Sensitivity change of thermoluminescence signals after laboratory optical bleaching: experiments with loess fine grains. *Quaternary Science Reviews (Quaternary Geochronology)*, **13**, 457-463.

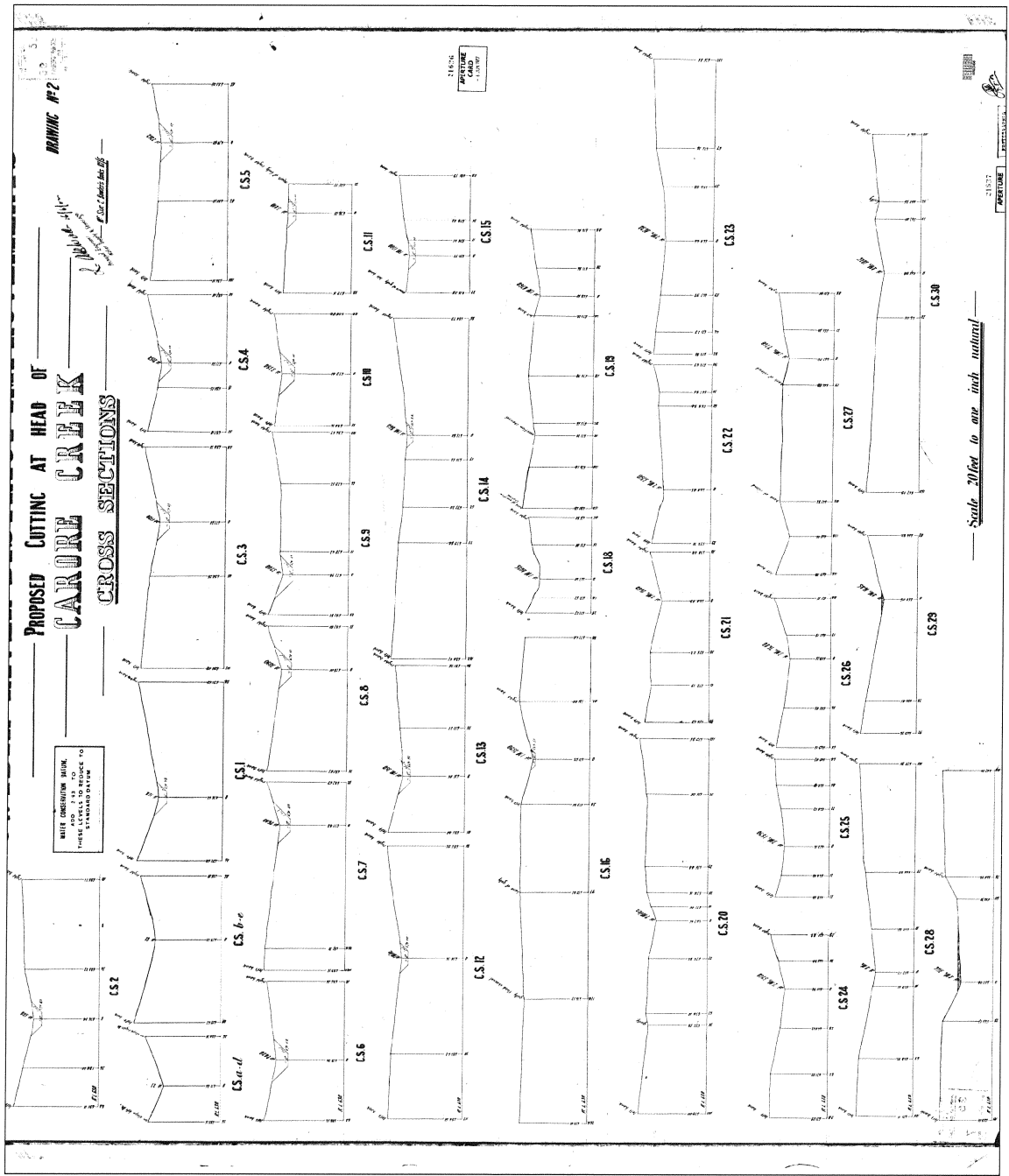
Zimmerman, J. (1971) The radiation-induced increase of the 100°C thermoluminescence sensitivity in fired quartz. *Journal of Physics C: Solid State Physics*, **4**, 3265-3276.

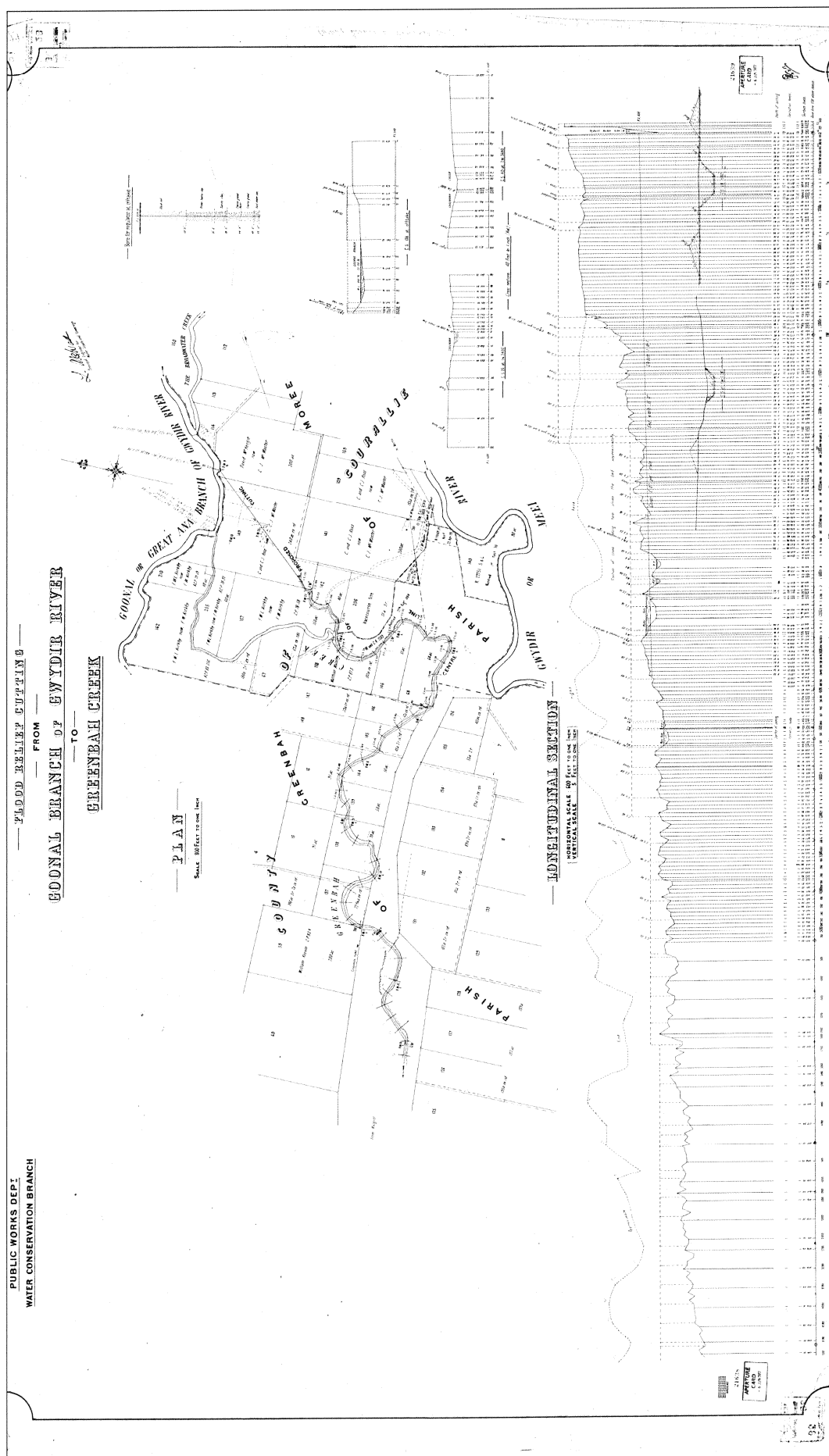
Appendix A: DIPNR survey plans referred to in text.

Table A1: DIPNR survey plans referred to in text.

Plan	Page
36/25	268
36/27	269
36/28	270
36/29	271
36/29	272
36/30	273
36/37	274
36/40	275
36/45	276
36/55	277
36/60	278
36/67	279
36/68	280
36/73	281
36/77	282
36/88	283
36/142	284
36/1205	285
36/1620	286
36/2847	287
36/2952	288
36/2954	289
36/3014_3	290







[illegible]

PUBLIC WORKS DEPARTMENT WATER SUPPLY & SEWERAGE BRANCH

GWYDIR RIVER DISTRICT IMPROVEMENTS LONGITUDINAL SECTIONS

ALONG BEDS OF THE GWYDIR IN BIG RIVER AND MEEHI RIVER

SHOWING RELATIVE FALLS FROM REGULATION

— P. George (Old) / Meehi's New Bed, R/L & R/L

— P. George (New) / Meehi's New Bed, R/L & R/L

— P. George (Old) / Meehi's New Bed, R/L & R/L

— P. George (New) / Meehi's New Bed, R/L & R/L

— P. George (Old) / Meehi's New Bed, R/L & R/L

— P. George (New) / Meehi's New Bed, R/L & R/L

— P. George (Old) / Meehi's New Bed, R/L & R/L

— P. George (New) / Meehi's New Bed, R/L & R/L

— P. George (Old) / Meehi's New Bed, R/L & R/L

— P. George (New) / Meehi's New Bed, R/L & R/L

— P. George (Old) / Meehi's New Bed, R/L & R/L

— P. George (New) / Meehi's New Bed, R/L & R/L

— P. George (Old) / Meehi's New Bed, R/L & R/L

— P. George (New) / Meehi's New Bed, R/L & R/L

— P. George (Old) / Meehi's New Bed, R/L & R/L

— P. George (New) / Meehi's New Bed, R/L & R/L

— P. George (Old) / Meehi's New Bed, R/L & R/L

— P. George (New) / Meehi's New Bed, R/L & R/L

— P. George (Old) / Meehi's New Bed, R/L & R/L

— P. George (New) / Meehi's New Bed, R/L & R/L

— P. George (Old) / Meehi's New Bed, R/L & R/L

— P. George (New) / Meehi's New Bed, R/L & R/L

— P. George (Old) / Meehi's New Bed, R/L & R/L

— P. George (New) / Meehi's New Bed, R/L & R/L

— P. George (Old) / Meehi's New Bed, R/L & R/L

— P. George (New) / Meehi's New Bed, R/L & R/L

— P. George (Old) / Meehi's New Bed, R/L & R/L

— P. George (New) / Meehi's New Bed, R/L & R/L

— P. George (Old) / Meehi's New Bed, R/L & R/L

— P. George (New) / Meehi's New Bed, R/L & R/L

— P. George (Old) / Meehi's New Bed, R/L & R/L

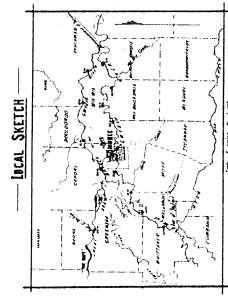
— P. George (New) / Meehi's New Bed, R/L & R/L

— P. George (Old) / Meehi's New Bed, R/L & R/L

— P. George (New) / Meehi's New Bed, R/L & R/L

LONGITUDINAL SECTION ALONG BED OF MEEHI RIVER

LONGITUDINAL SECTION ALONG BED OF GWYDIR OR BIG RIVER



NOTE: — Gwydir River is a source of water supply to the Meehi River. The Meehi River is a dry season.

SCALE: — HORIZONTAL: 1" = 1/2 MI. VERTICAL: 1" = 10 FT.

21413
ENGINEER
C.A.D.
1910

21413
ENGINEER
C.A.D.
1910

34/50

34/50

GWYDIR RIVER DISTRICT IMPROVEMENTS

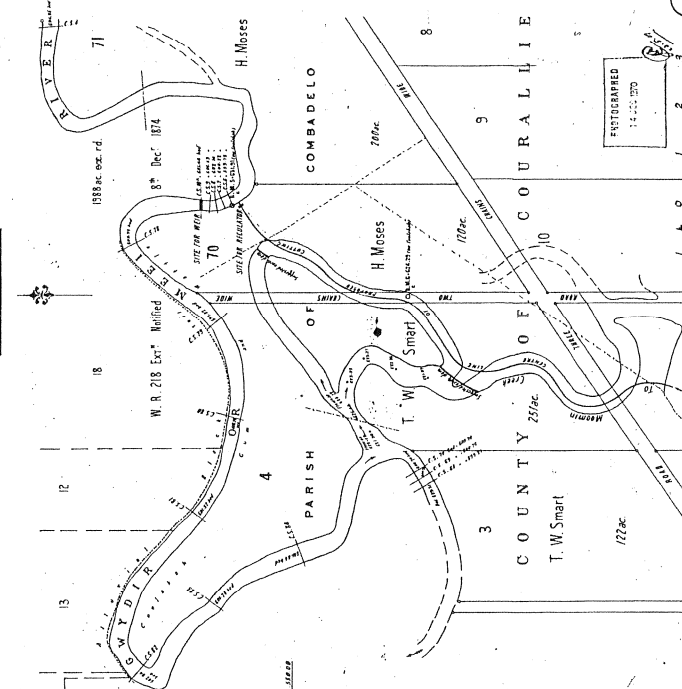
WEIR IN MEEI RIVER AND OFFTAKE TO MOOMIN CREEK

GENERAL PLAN

— SHEWING POSITIONS FOR WEIR AND OFFTAKE —

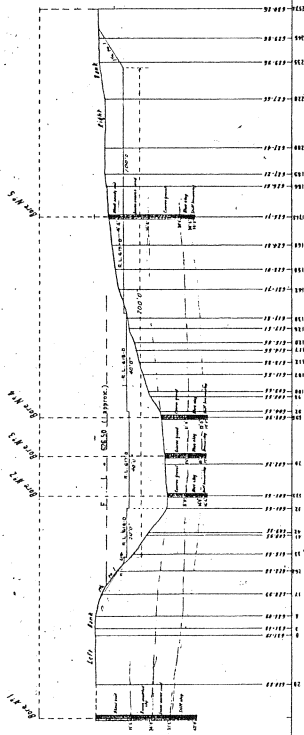
Scale 500 Feet to one Inch

L. M. Smith
 Project Engineer
 U.S. Army Corps of Engineers



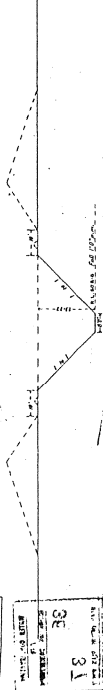
CROSS SECTION 10A (SITE FOR WEIR) KENNY'S

NATURAL SCALE - 20 FEET TO ONE INCH



SECTION OF CUTTING AT SITE FOR REGULATOR

Natural Scale - 20 feet to one inch



21656
 APERTURE
 CARD
 - 6 JUN 1977

21656
 38
 18

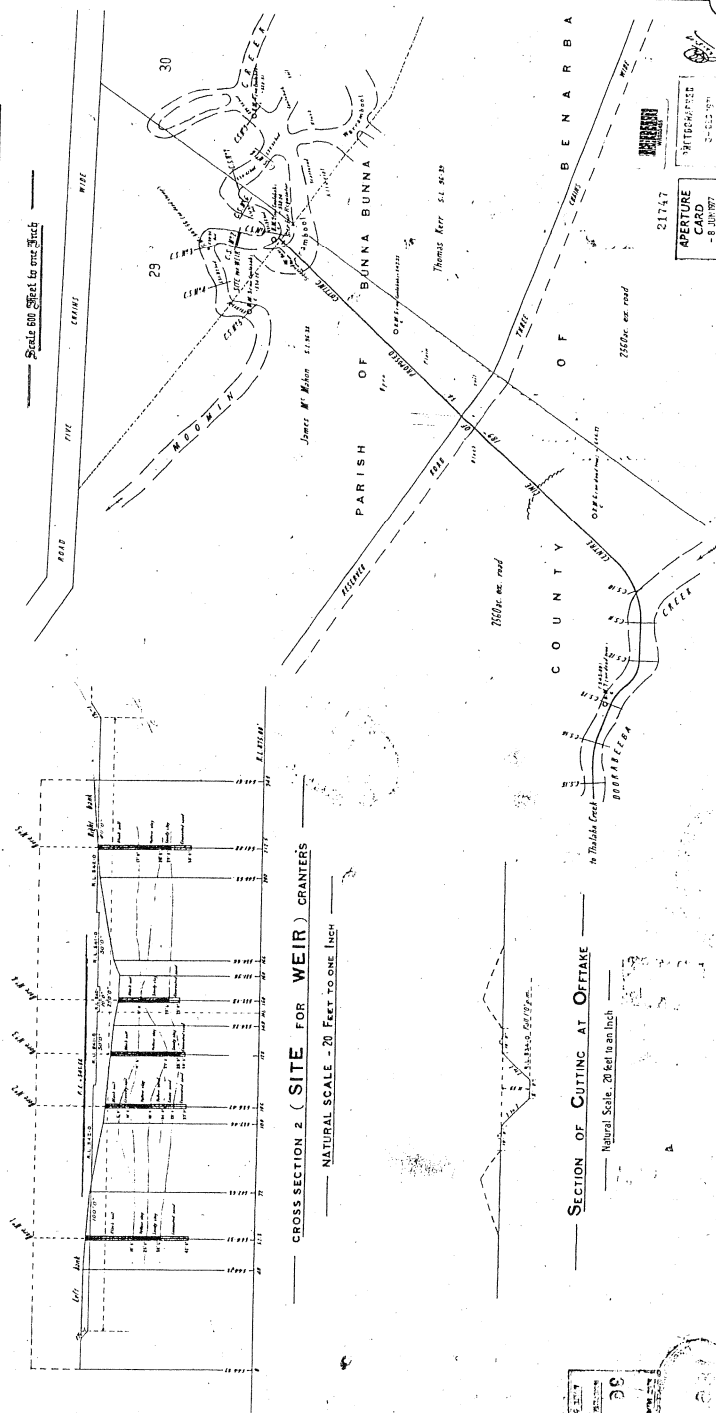
36/37

WEIR IN MOOMIN CREEK AND OFFTAKE TO THALABA CREEK

GENERAL PLAN

SHOWING POSITIONS FOR WEIR AND OFFTAKE

Circle 500 Office to our Office



CROSS SECTION 2 (SITE FOR WEIR) CRANTERS

NATURAL SCALE - 20 FEET TO ONE INCH

SECTION OF CUTTING AT OFFTAKE

— Natural Scale. 20 feet to an Inch

21747

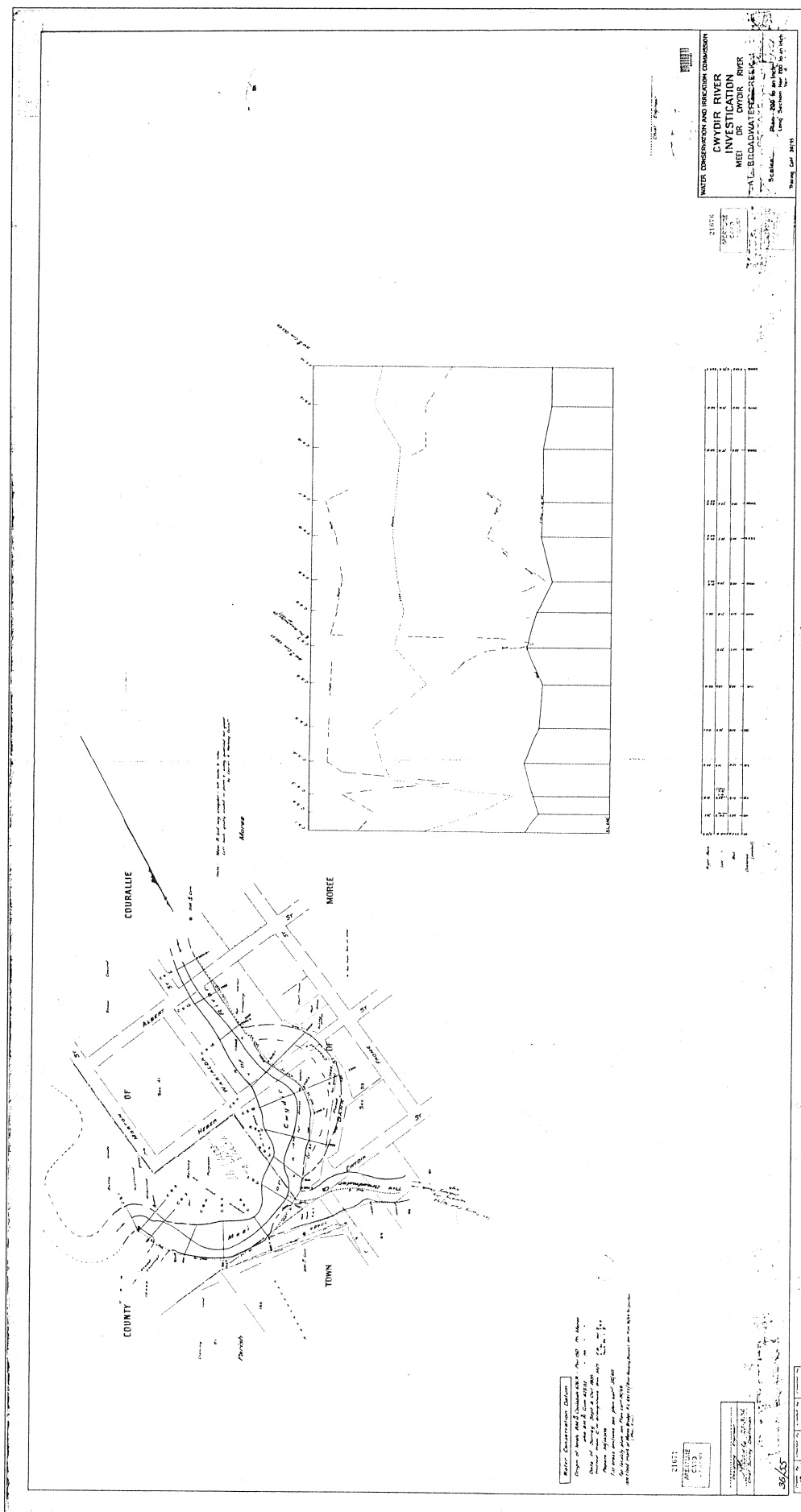
APERTURE
CARD

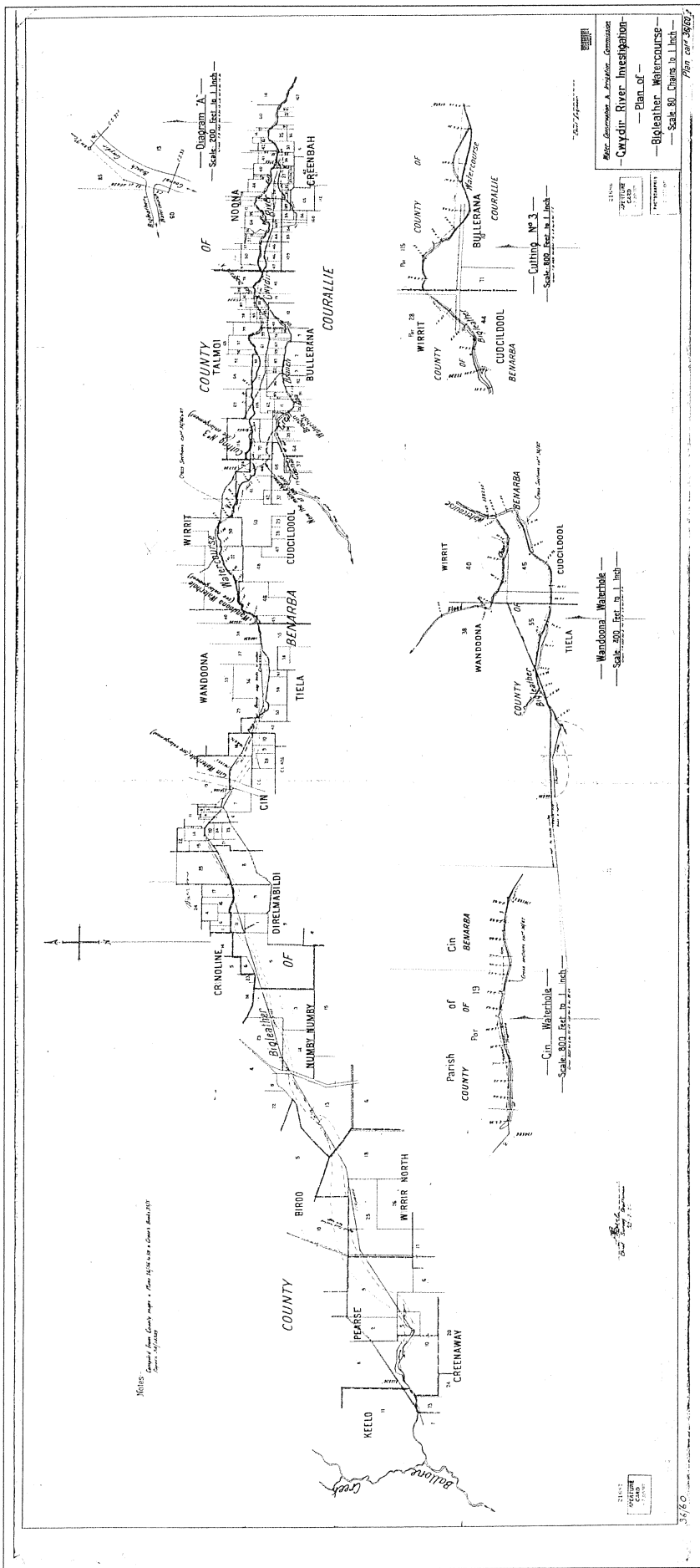
7-63-79

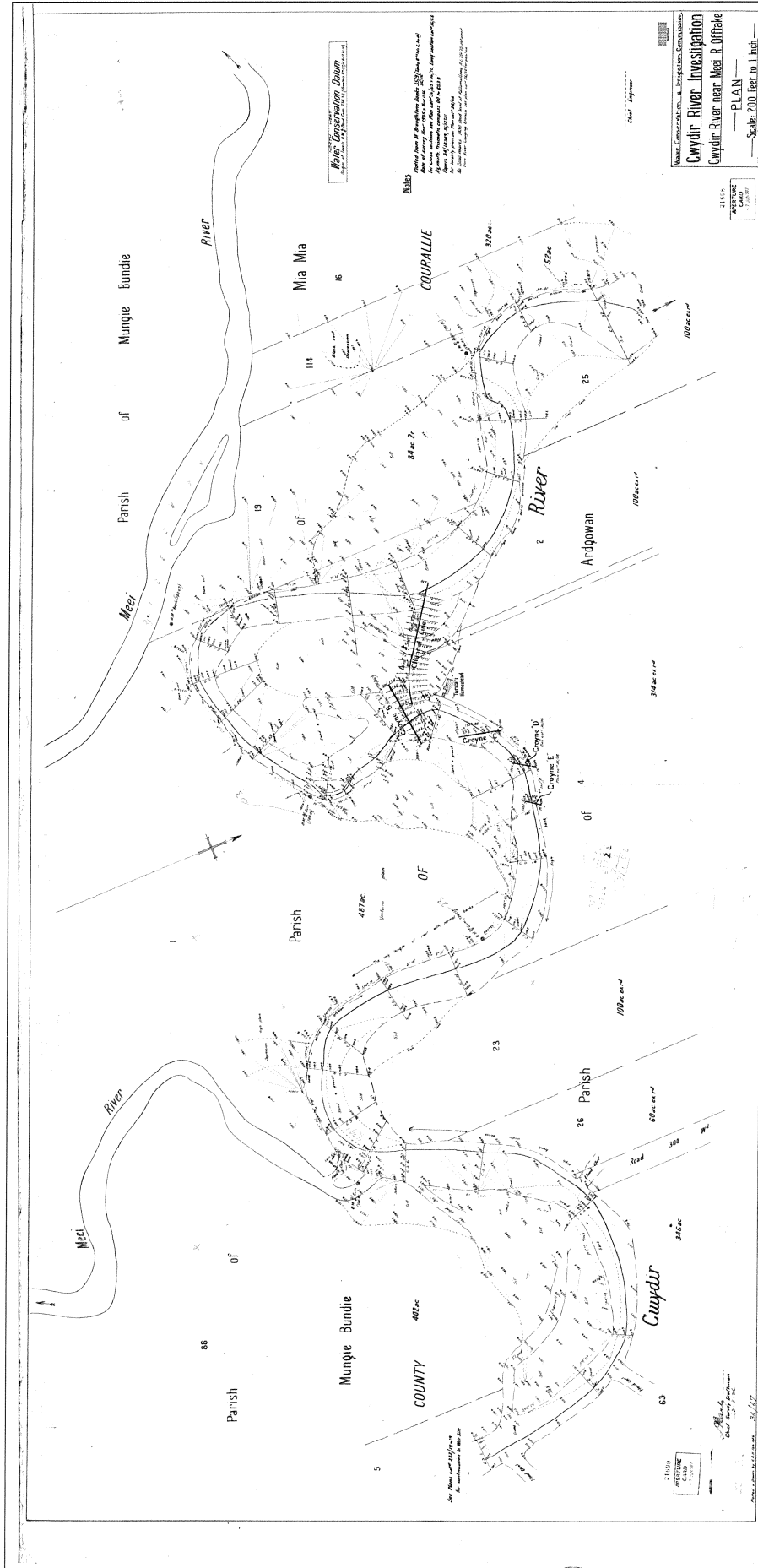
DISCHARGED

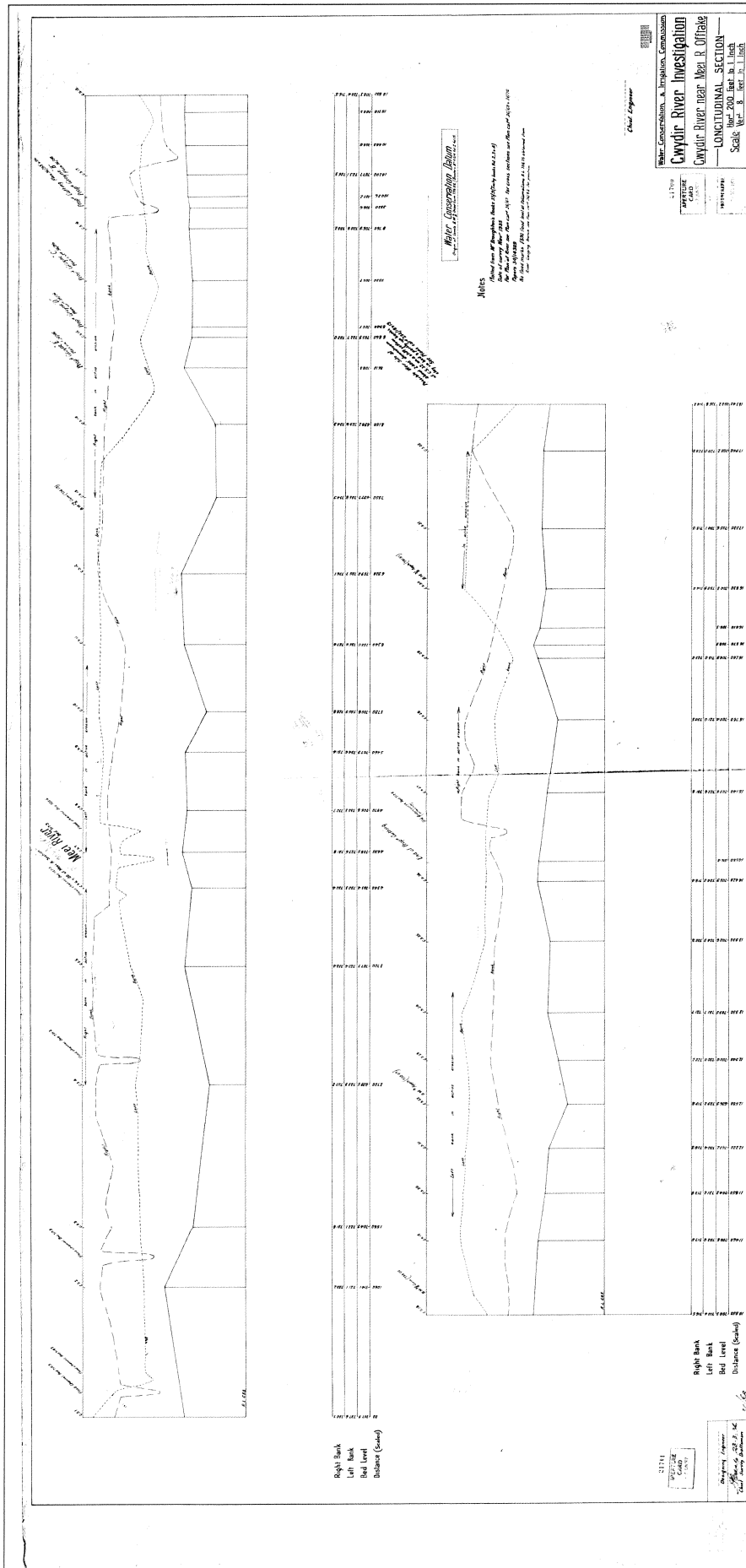
7-63-79

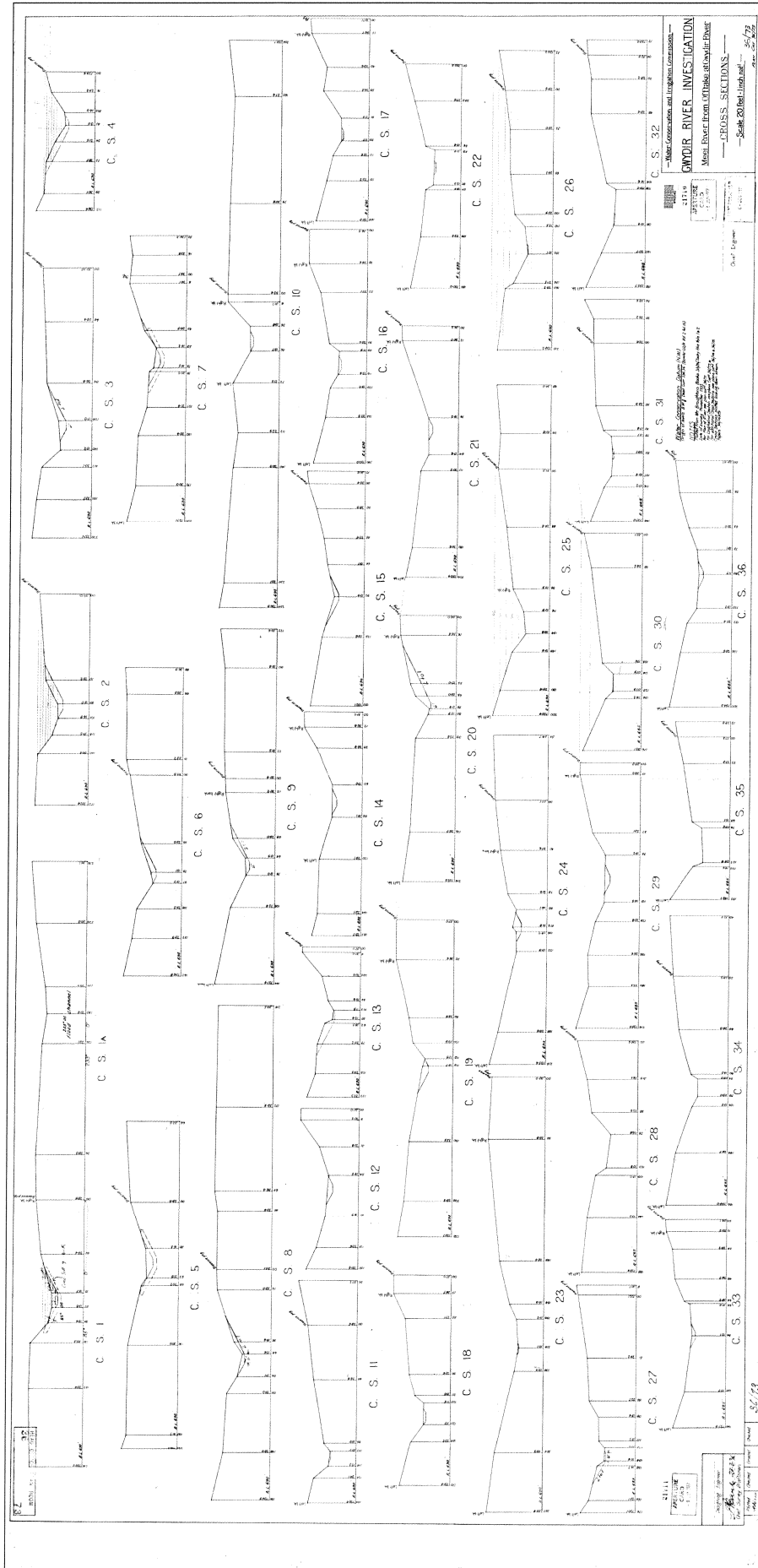
100-443885
TODD, FRED
7-6559

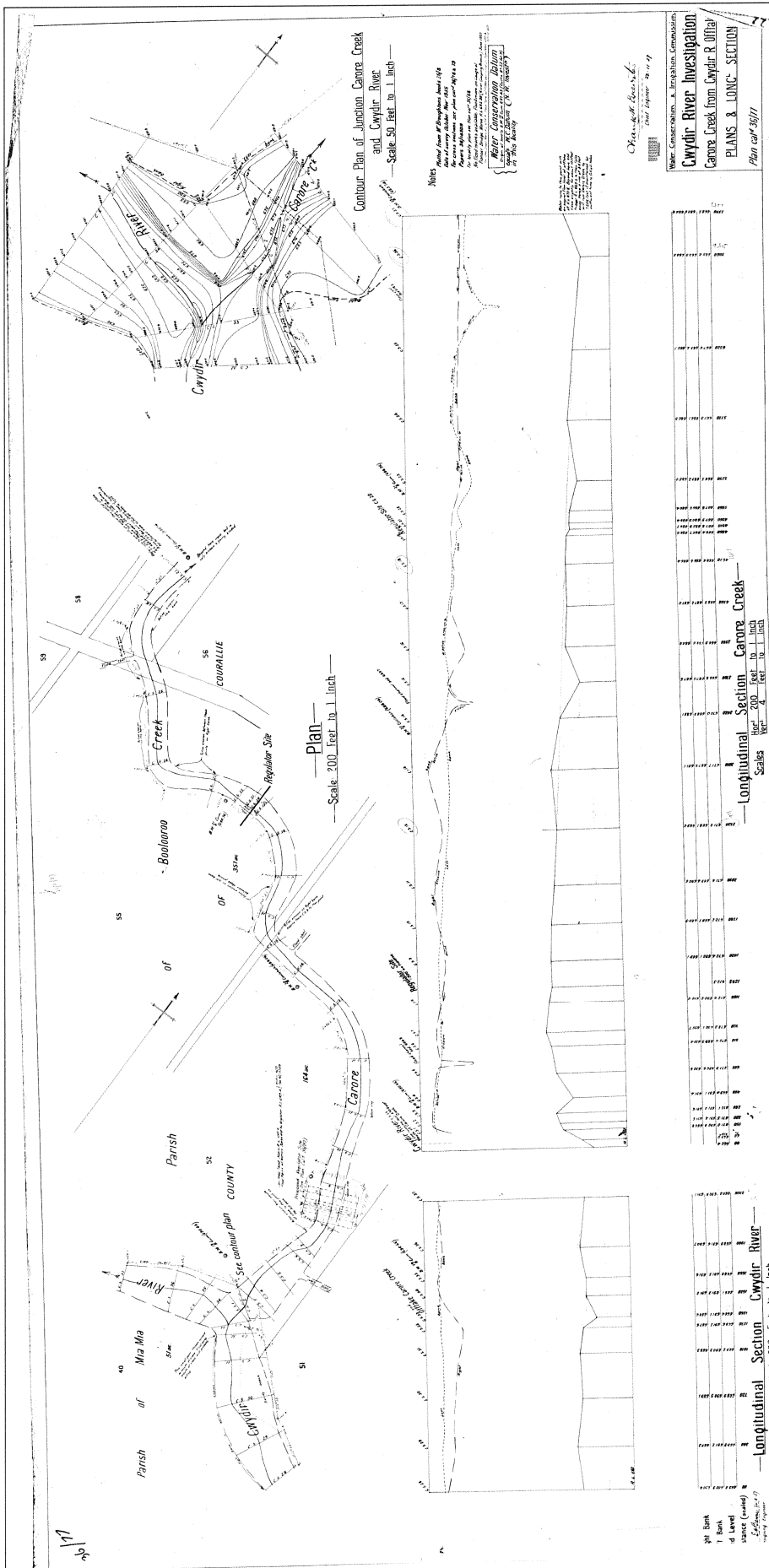


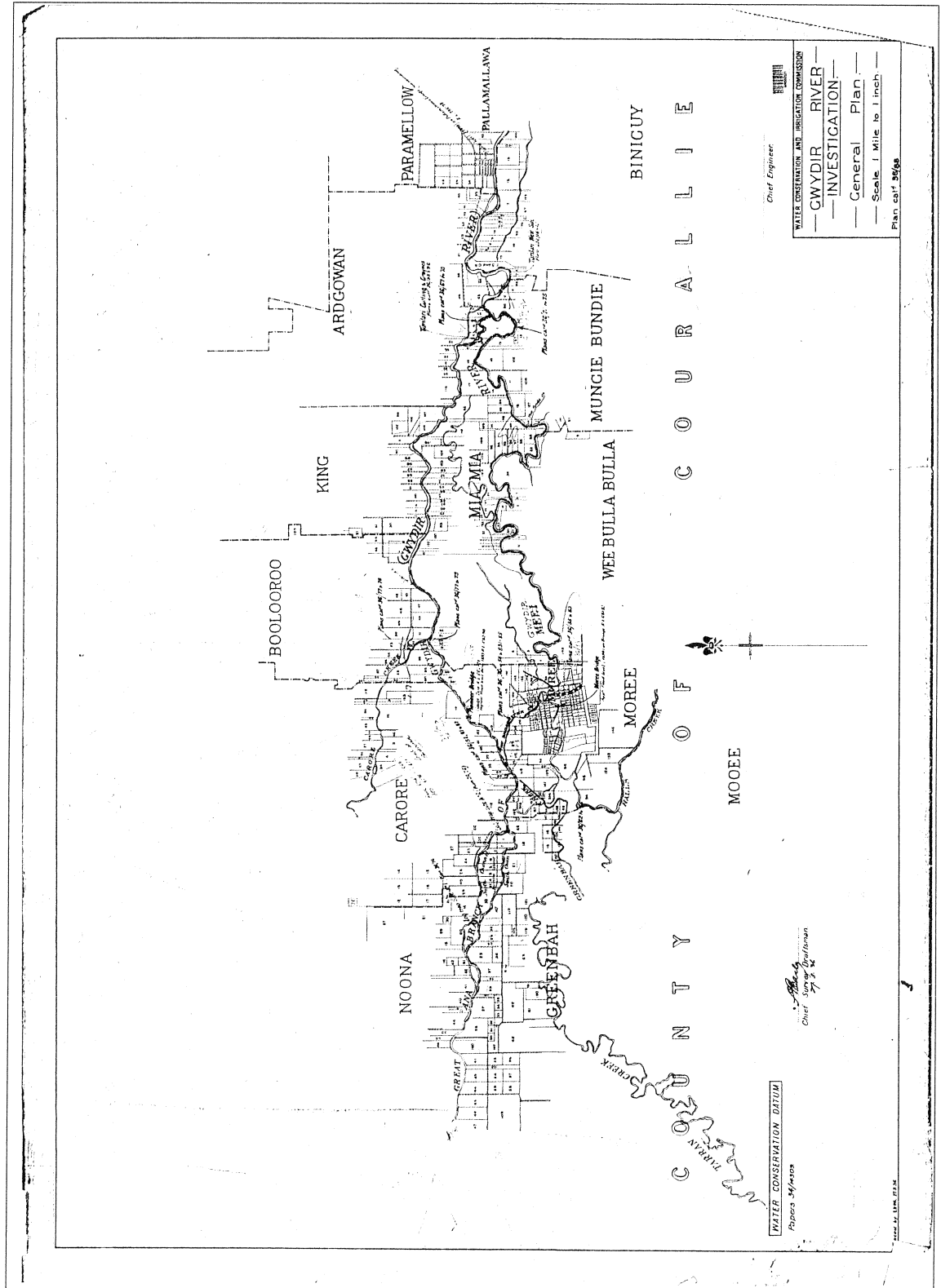




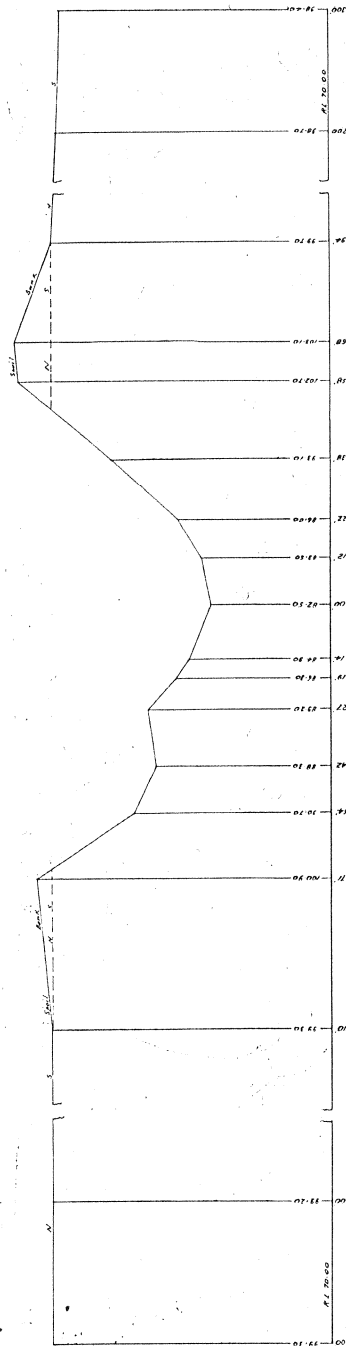
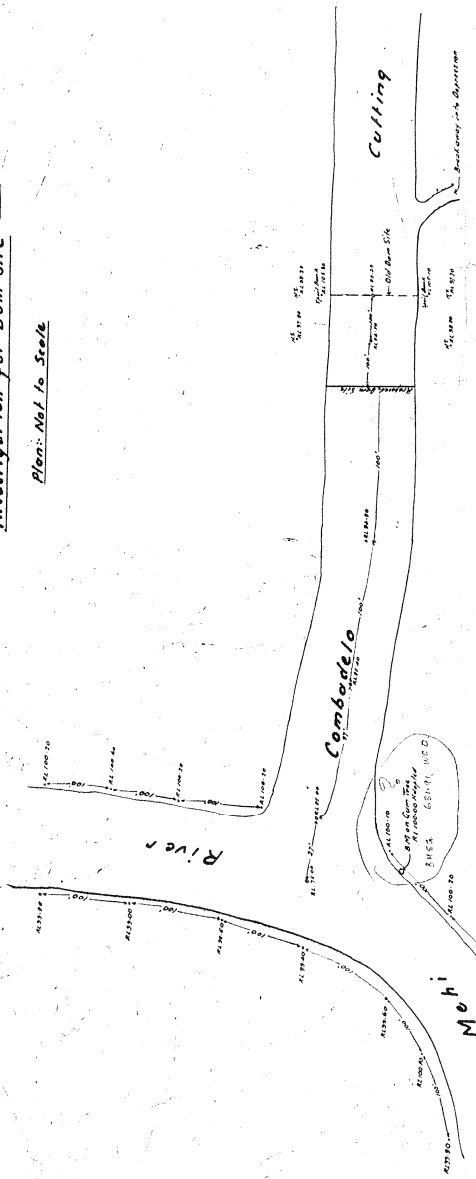








Plan: Not to Scale

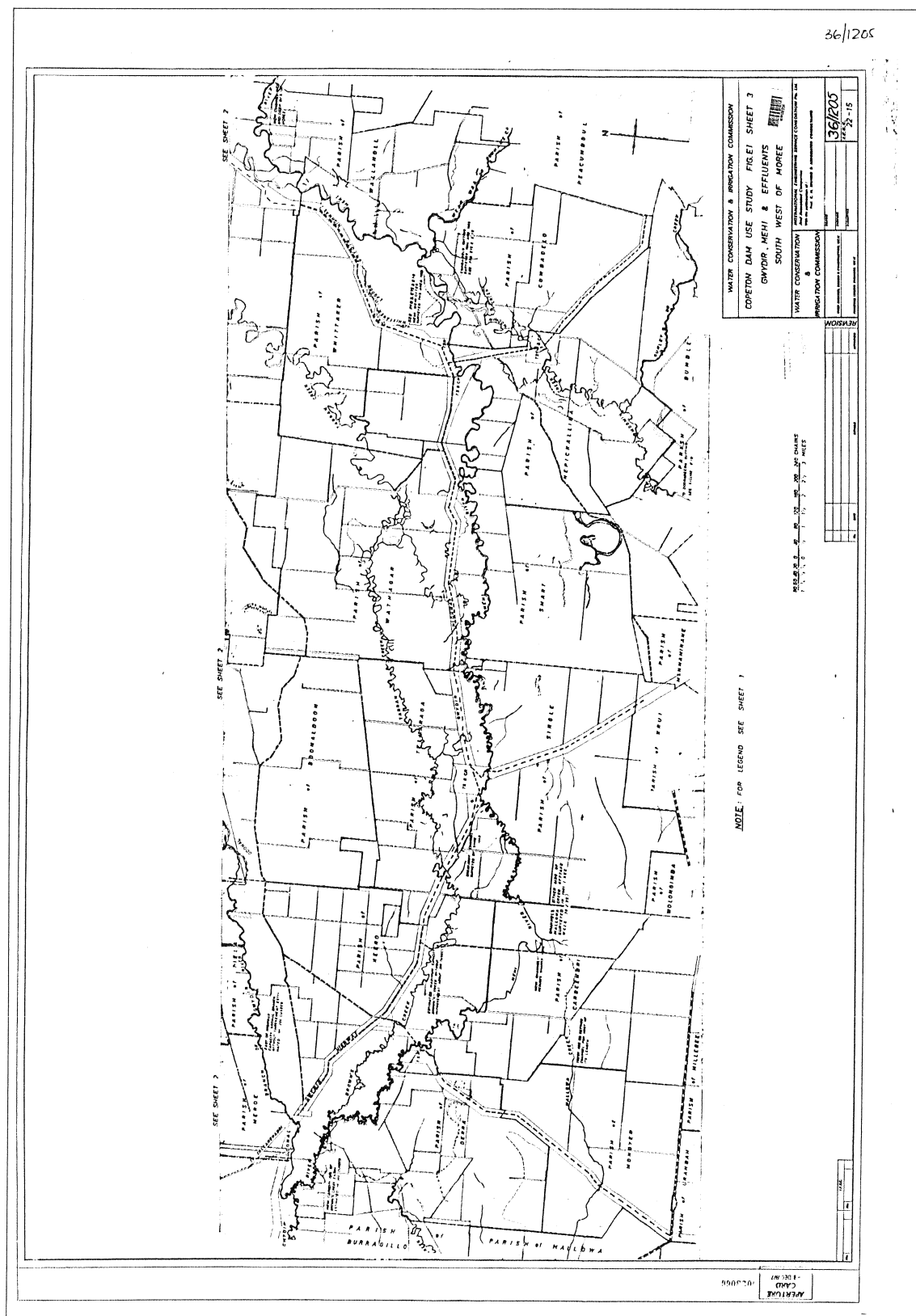


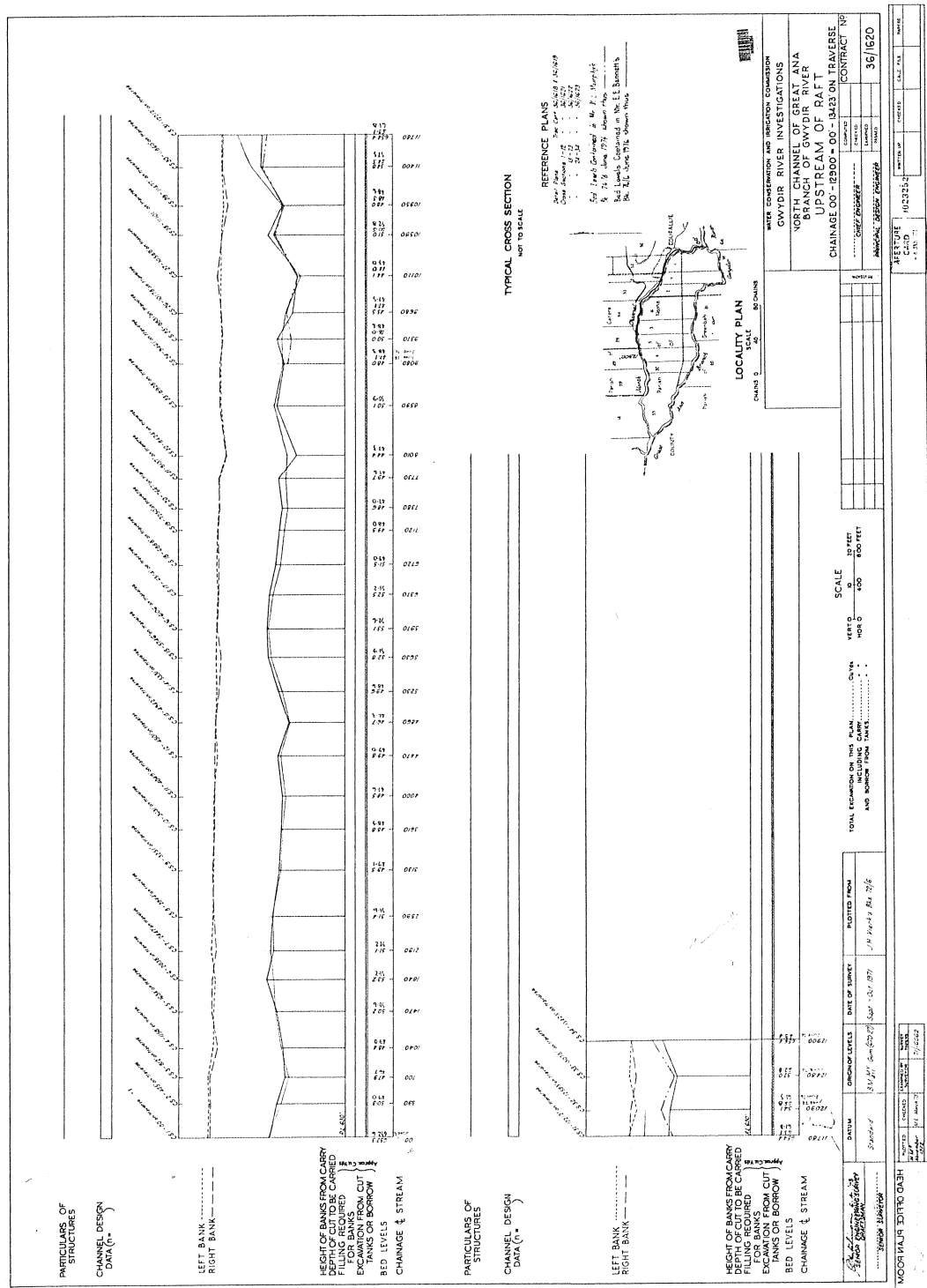
Cross Section

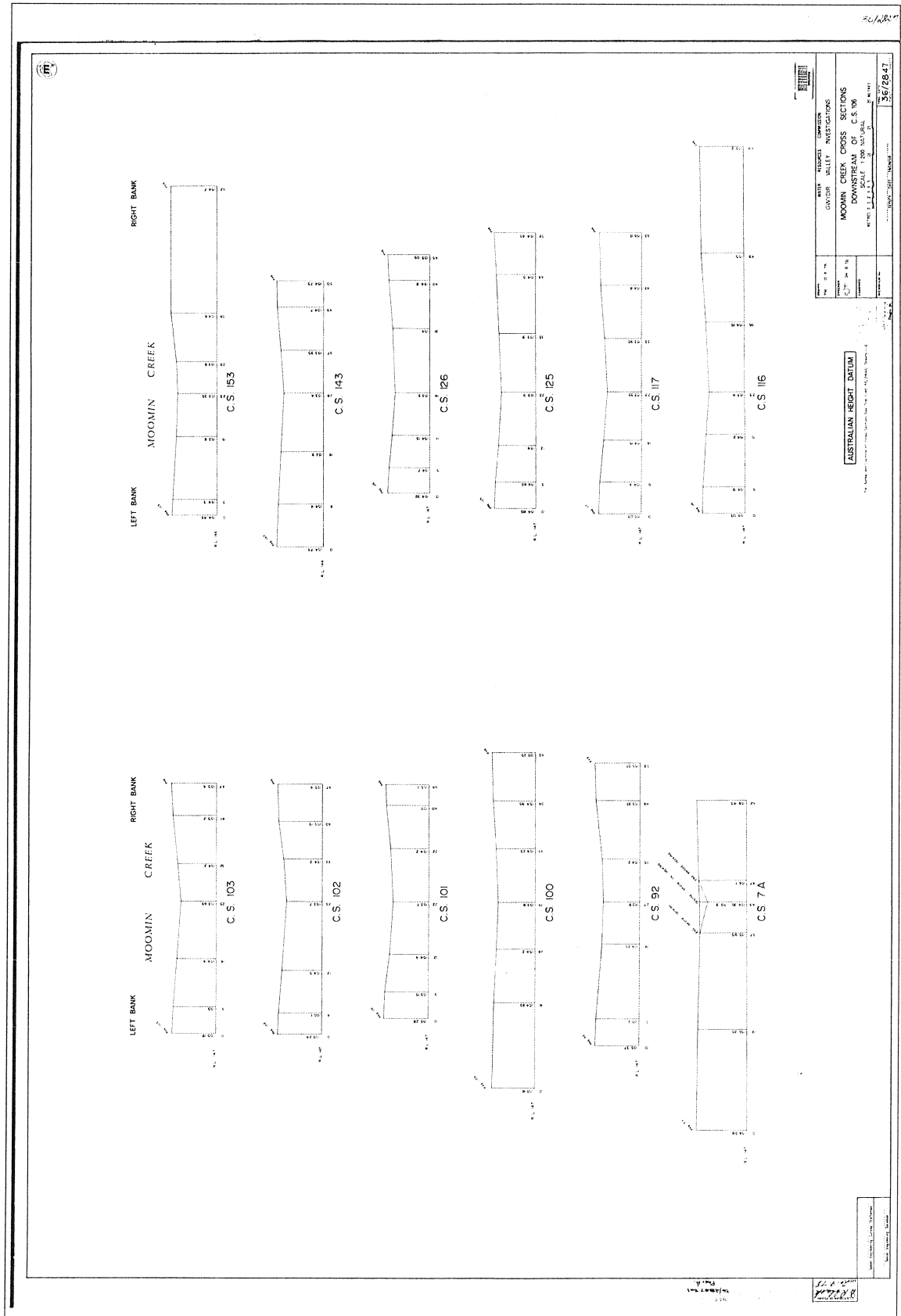
Scale { Hor. 10 ft. = 1 inch.
Ver. 4" = 1 inch.

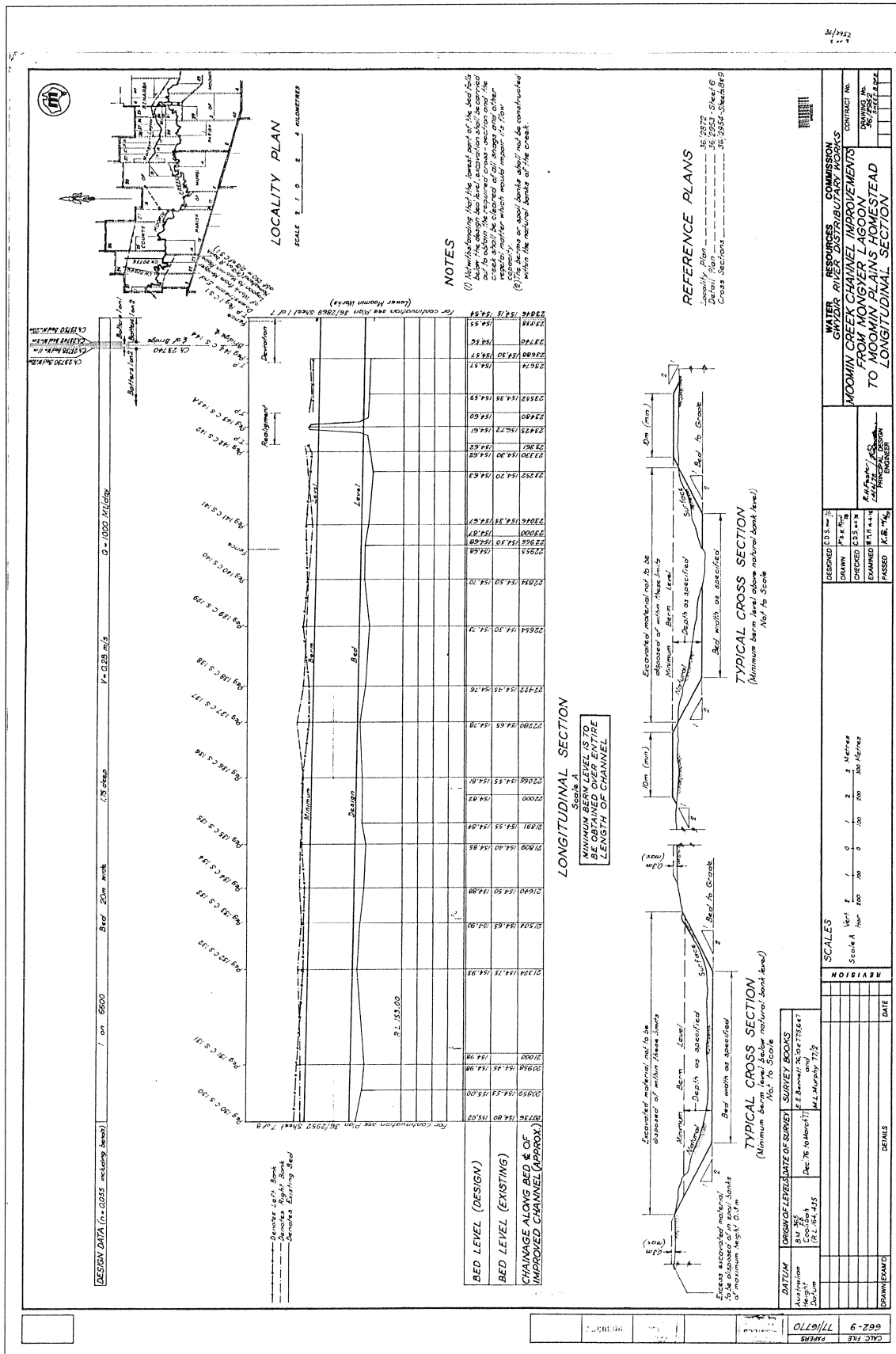
21514
APERTURE
CARD
12 JAN 77

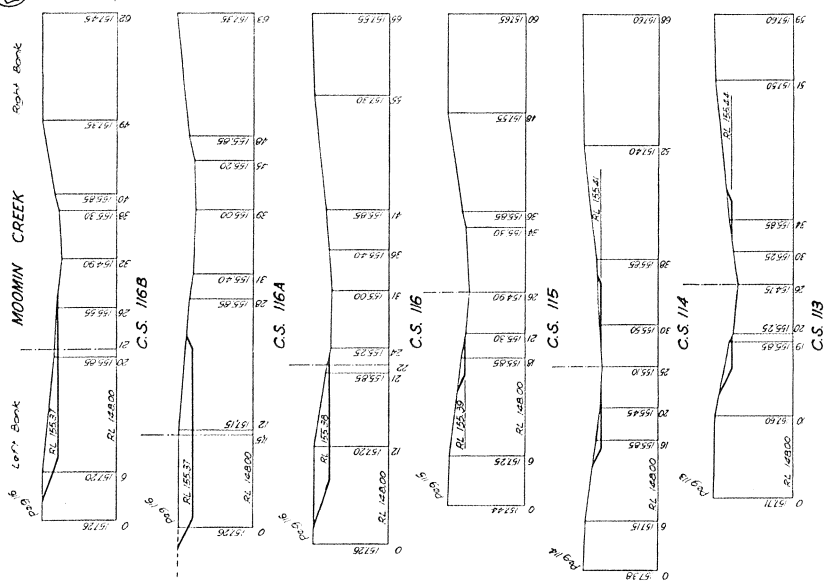
Tracing Cont. 36/42











NOTES

1. All improved channel bed widths on this plan shall be 20m (measured perpendicular to centre-line of improved channel).

2. All improved channel batters shall be long.

3. Survey information obtained from the EE Bennett's Books 777

REFERENCE PLANS

Locality Plan _____ 36/282
Longitudinal Section _____ 36/282 Sheet 687
Detail Plan _____ 36/283 Sheet 586



AUSTRALIAN HEIGHT DATUM

SCALE (Normal)

[illegible]

DESIGNED	COS 404.7
DRAWN	L. J. Thompson April 1974
CHECKED	COS 404.7
EXAMINED	OK 4-1-74
PASSED	

P. M. Foster / P. M. Foster
PRINCIPAL DESIGN
ENGINEER

WATER	RESOURCES	COMMISSION
GWYDIR RIVER	DISTRIBUTUTARY	WORKS
MOOMIN CREEK CHANNEL IMPROVEMENTS		
FROM MONGER LAGOON		
TO MOOMIN PLAINS HOMESTEAD		
CROSS SECTIONS		
<div> <div>CONTRACT NO.</div> <div> <div> <div>REVISION NO.</div> <div>06/2008</div> </div> <div> <div>06/2008</div> <div>06/2008</div> </div> </div> </div>		



Appendix B: Hydraulic geometry data.

Table AB.1: Channel characteristics for representative cross-sections on the Gwydir River.

No.	Eastings	Northings	Distance DS	Q	S	W	D	<i>n</i>	W/D	V
1 _{GS}	803787	6734873	0	1660	0.000562	88	7.4	0.033	11.8	2.6
2	797250	6736570	13	769	0.000535	80	5.1	0.035	15.8	1.9
3	796445	6736345	14.3	820	0.000535	95	4.8	0.035	19.9	1.8
4	795200	6737010	17.2	566	0.000535	89	4.0	0.035	22.6	1.6
5	793720	6738675	20.5	1022	0.000535	135	4.4	0.035	30.9	1.7
6	790890	6741130	25.4	917	0.000535	86	5.5	0.035	15.7	2.0
7	783310	6742985	34.9	868	0.000535	79	5.6	0.035	14.2	2.0
8	779200	6742160	40.3	719	0.000535	47	6.9	0.035	6.8	2.2
9 _{GS}	776125	6741310	44.3	528	0.000535	61	5.0	0.037	12.3	1.7
10 _{GS}	776050	6741240	44.4	519	0.000535	78	4.3	0.039	18.1	1.5
11	771670	6739315	50.4	489	0.000535	89	3.8	0.039	23.3	1.4
12	769570	6740265	53.2	325	0.000535	68	3.6	0.039	19.1	1.4
13	769400	6740335	53.4	357	0.000345	67	4.4	0.039	15.3	1.2
14	769425	6740820	53.9	325	0.000345	62	4.3	0.039	14.5	1.2
15	769505	6741240	54.4	324	0.000345	75	3.8	0.039	19.7	1.1
16	769240	6741320	54.6	249	0.000345	56	3.9	0.039	14.3	1.1
17	768910	6741420	55	193	0.000345	64	3.1	0.039	21.0	1.0
18	768520	6741950	55.7	235	0.000345	50	4.0	0.039	12.4	1.2
19	768255	6742175	56.1	200	0.000345	62	3.2	0.039	19.7	1.0
20	768005	6742180	56.4	180	0.000345	47	3.5	0.039	13.4	1.1
21	767400	6742306	57.1	77	0.000345	47	2.1	0.039	22.3	0.8
22	767030	6742235	57.4	36	0.000345	44	1.4	0.039	32.1	0.6
23	769330	6740185	53.5	78	0.001570	14	3.0	0.039	4.7	1.9
24	768965	6740010	54.1	39	0.001220	17	1.9	0.040	9.0	1.2
25	768540	6740135	55	30	0.000678	22	1.6	0.040	13.2	0.9
26	768412	6740743	55.8	23	0.000513	15	1.9	0.040	7.8	0.8
27	768110	6740830	56.2	17	0.000349	15	1.8	0.040	8.0	0.6
28	766730	6741095	58.1	14	0.000186	18	1.7	0.040	10.9	0.5
29	765860	6741860	59.1	12	0.000159	17	1.7	0.040	10.0	0.4
30	762480	6742285	62.6	40	0.001815	13	2.0	0.040	6.4	1.5
31	761830	6742230	63.3	37	0.001815	19	1.5	0.040	12.8	1.3
32	761700	6742281	63.4	19	0.000406	14	1.9	0.040	7.3	0.7
33	761334	6742472	63.9	32	0.000406	19	2.2	0.040	8.7	0.8
34	760584	6742981	64.9	26	0.000631	24	1.4	0.040	17.4	0.8
35	759800	6743408	65.8	20	0.000856	15	1.5	0.040	10.0	0.9
36	759430	6743433	66.2	24	0.000856	14	1.8	0.040	7.9	1.0
37	758868	6743070	67	55	0.000856	23	2.1	0.040	10.8	1.1
38	758182	6742800	67.8	72	0.000856	25	2.4	0.040	10.6	1.2
39	757866	6742516	68.4	102	0.000856	33	2.5	0.040	13.4	1.3
40	761680	6742195	63.5	24	0.000972	10	2.1	0.040	4.7	1.1
41	761286	6742125	63.9	10	0.000972	22	0.7	0.040	29.9	0.6
42	760521	6742160	64.7	46	0.000972	15	2.4	0.040	6.2	1.3
43	759918	6742365	65.4	64	0.000972	26	2.1	0.040	12.4	1.2
44	759852	6742390	65.4	4	0.001000	8	0.8	0.040	9.7	0.6
45	759703	6742480	65.6	9	0.001000	14	0.9	0.040	15.9	0.7
46	759205	6742456	66.2	12	0.001000	40	0.6	0.040	69.5	0.5
47	758895	6742404	66.5	18	0.001000	13	1.5	0.040	8.5	1.0
48	759640	6742248	65.7	69	0.000867	24	2.4	0.040	10.2	1.2

49	759493	6742241	65.8	80	0.000867	28	2.3	0.040	11.9	1.2
50	758985	6742335	66.4	58	0.000867	25	2.1	0.040	12.0	1.1
51	758779	6742352	66.6	103	0.001263	35	2.1	0.040	16.4	1.4
52	758352	6742371	67.1	142	0.001263	43	2.2	0.040	19.1	1.5
53	757929	6742406	67.6	70	0.001263	26	2.0	0.040	13.3	1.3
54	753755	6745648	74.1	95	0.003070	32	1.6	0.040	19.6	1.8
55	752350	6745905	76.3	244	0.003070	29	3.1	0.040	9.2	2.7
56	757720	6742340	67.8	108	0.000551	58	2.0	0.040	28.7	0.9
57	757040	6742515	68.6	69	0.000551	38	2.0	0.040	19.2	0.9
58	756430	6742620	69.3	85	0.000551	41	2.2	0.040	19.1	0.9
59	753540	6743435	72.8	50	0.000551	35	1.7	0.040	19.8	0.8
60	751310	6744480	76	89	0.000551	30	2.7	0.040	11.3	1.1
61	746475	6747350	83.5	6	0.000484	41	0.5	0.040	91.2	0.3
62	741955	6748475	89.1	9	0.000484	34	0.7	0.040	50.7	0.4
63	741325	6748375	89.8	13	0.000484	26	1.0	0.040	26.5	0.5
64	749375	6744130	78.4	88	0.000446	51	2.1	0.040	24.8	0.8
65	748160	6744725	80.2	67	0.000446	34	2.3	0.040	15.1	0.9
66 _{GS}	746977	6745132	81.5	69	0.000446	33	2.7	0.050	12.5	0.8
67	746140	6745130	82.4	70	0.000446	42	2.3	0.050	18.4	0.7
68	743625	6745915	86.1	46	0.000446	36	2.0	0.050	18.3	0.6
69	743115	6746440	87	93	0.000446	34	3.2	0.050	10.5	0.9
70	740850	6747730	90.8	55	0.000446	33	2.3	0.050	14.2	0.7
71	739930	6748880	92.3	37	0.000314	67	1.3	0.050	51.1	0.4
72	738435	6749925	94.5	32	0.000314	55	1.4	0.050	40.0	0.4
73	736922	6751230	97.1	37	0.000314	25	2.3	0.044	11.2	0.7
74	733310	6750530	101.4	23	0.000500	16	1.9	0.044	8.5	0.7
75	731717	6750380	103.3	16	0.000500	14	1.7	0.044	8.3	0.7
76	731087	6750130	104.1	12	0.000500	12	1.6	0.044	7.2	0.6
77	730724	6749501	104.9	10	0.000500	13	1.3	0.044	10.1	0.6
78	730720	6749480	104.9	11	0.000500	12	1.5	0.044	7.7	0.6
79	730315	6749290	105.4	7	0.000500	12	1.2	0.044	10.5	0.5
80	730119	6749330	105.6	3	0.000500	6	1.0	0.044	6.7	0.4
81	729584	6749370	106.3	2	0.000500	6	0.9	0.044	6.6	0.4

Note: Eastings and Northings are UTM Zone 55 coordinates; Distance DS = stream km from Pallamallawa gauging station, along shortest possible sequence of anabranches; Q = bankfull discharge (m^3s^{-1}) estimated according to the Manning's resistance equation; S = slope (mm^{-1}) of the bankfull water surface; W = bankfull water surface width (m); D = average bankfull channel depth (m); n = Manning's roughness estimated according to Barnes' (1967) procedure and guided by interpolations between calculated n values from gauging stations (indicated by subscript "GS" with site No.) and documented

engineers estimates; V = average flow velocity (ms^{-1}) calculated as $\frac{Q}{A}$ where A = bankfull cross-sectional area (m^2).

Table AB.2: Channel characteristics for representative cross-sections on the Mehi River.

No.	Eastings	Northings	Distance DS	Q	S	W	D	<i>n</i>	W/D	V
1	796415	6736195	0.1	105	0.000388	51	3.0	0.058	17.0	0.7
2	796412	6735534	1.1	128	0.000388	56	3.2	0.058	17.4	0.7
3	795127	6736533	4.3	175	0.000388	60	3.7	0.058	16.2	0.8
4	794672	6737130	5.0	182	0.000388	66	3.6	0.058	18.3	0.8
5	794286	6737341	5.5	148	0.000388	54	3.6	0.058	15.0	0.8
6	776198	6737328	44.8	216	0.000388	67	3.9	0.058	17.0	0.8
7	775832	6737021	45.5	183	0.000388	57	3.9	0.058	14.7	0.8
8 _{GS}	775636	6736465	46.1	575	0.000388	97	5.7	0.058	17.1	1.1
9	766010	6735564	63.1	304	0.000388	62	5.1	0.058	12.1	1.0
10	765239	6735179	64.9	314	0.000388	73	4.7	0.058	15.4	0.9
11	764515	6734904	65.9	310	0.000388	64	5.1	0.058	12.6	1.0
12	764033	6734164	67.0	311	0.000388	57	5.4	0.058	10.5	1.0
13	763351	6732837	69.7	338	0.000388	64	5.3	0.058	12.1	1.0
14	762554	6732606	70.7	269	0.000388	75	4.2	0.058	17.8	0.9
15	760692	6731133	74.8	237	0.000388	49	5.1	0.058	9.5	1.0
16	760380	6729829	76.5	257	0.000388	51	5.2	0.058	9.9	1.0
17	759626	6727825	79.5	152	0.000388	67	3.1	0.058	21.4	0.7
18	758827	6728042	80.8	207	0.000388	52	4.5	0.058	11.4	0.9
19	757300	6726741	83.0	147	0.000388	53	3.6	0.058	14.6	0.8
20	757035	6726952	83.7	215	0.000388	48	4.8	0.058	10.0	0.9
21	756228	6726972	84.6	247	0.000388	65	4.4	0.058	14.8	0.9
22	724694	6724558	162.2	15	0.000229	21	1.8	0.058	11.7	0.4
23	724017	6724400	163.2	4	0.000229	12	1.1	0.058	10.7	0.3
24	723883	6724778	163.5	3	0.000229	10	1.2	0.058	8.7	0.3
25	724333	6725104	164.4	5	0.000229	28	0.8	0.058	35.2	0.2
26 _{GS}	724042	6725734	165.5	35	0.000229	24	2.0	0.031	11.8	0.8
27	723388	6725681	166.3	7	0.000229	15	1.0	0.032	14.4	0.5
28	722233	6726307	168.4	10	0.000229	15	1.3	0.033	12.0	0.5
29	721443	6726626	169.3	18	0.000229	39	1.0	0.034	38.2	0.5
30	721361	6727534	170.3	16	0.000229	29	1.2	0.035	24.6	0.5
31	720629	6728454	172.9	12	0.000229	22	1.2	0.036	18.7	0.5
32	720735	6729478	175.4	12	0.000229	23	1.2	0.037	19.8	0.4
33	720106	6730258	177.0	17	0.000229	24	1.4	0.038	16.9	0.5
34	719405	6730406	178.6	20	0.000229	27	1.5	0.039	18.5	0.5
35	719381	6731544	180.4	22	0.000229	30	1.5	0.040	20.0	0.5
36	718784	6731922	182.3	13	0.000229	22	1.3	0.041	16.2	0.4
37	717732	6732568	185.8	19	0.000229	29	1.4	0.042	20.6	0.4
38	716014	6733592	189.7	24	0.000229	24	1.9	0.043	12.7	0.5
39	716258	6734444	192.1	30	0.000229	33	1.8	0.044	18.3	0.5
40	716330	6735004	193.3	39	0.000229	45	1.8	0.045	25.4	0.5
41 _{GS}	684329	6737467	282.0	35	0.000166	47	1.9	0.050	24.1	0.4
42 _{GS}	684329	6737467	282.0	39	0.000166	77	1.9	0.070	41.4	0.3
43 _{GS}	667034	6733749	329.5	97	0.000141	84	2.7	0.052	31.6	0.4
44 _{GS}	667034	6733749	329.5	57	0.000141	55	2.5	0.052	21.8	0.4
45 _{GS}	667034	6733749	329.5	122	0.000141	60	3.8	0.052	16.0	0.5

Note: All units as for Table 2.1, except Distance DS, which is stream km from channel offtake.

Table AB.3: Channel characteristics for representative cross-sections on Moomin Creek.

No.	Eastings	Northings	Distance DS	Q	S	W	D	<i>n</i>	W/D	V
1	751000	6718465	21.6	36	0.000247	52	2.0	0.075	25.6	0.3
2	750355	6717820	23.7	38	0.000247	82	1.6	0.075	51.4	0.3
3 _{GS}	739845	6712395	53.3	44	0.000247	52	2.4	0.080	21.7	0.3
4 _{GS}	723820	6708746	104.9	45	0.000119	53	2.2	0.048	23.9	0.4
5	715345	6708215	136.0	38	0.000119	66	1.5	0.050	45.0	0.4
6	704270	6716265	177.9	35	0.000119	41	2.3	0.050	17.5	0.4
7	704170	6716240	180.2	13	0.000115	49	1.2	0.051	42.0	0.2
8	703405	6715930	181.4	21	0.000115	63	1.3	0.051	48.5	0.3
9	702070	6715765	184.0	18	0.000115	46	1.6	0.051	29.5	0.3
10	701800	6715960	184.5	14	0.000115	50	1.2	0.052	41.0	0.2
11	701640	6715985	185.0	17	0.000115	59	1.2	0.052	48.6	0.2
12	698675	6716690	192.8	12	0.000115	80	0.8	0.052	96.2	0.2
13	697868	6716200	196.5	15	0.000115	49	1.3	0.053	38.5	0.2
14	697392	6715968	197.6	11	0.000115	62	0.8	0.053	77.3	0.2
15	695872	6716630	203.2	12	0.000115	47	1.2	0.054	40.1	0.2
16	695150	6717455	206.6	16	0.000115	56	1.2	0.054	45.3	0.2
17	694325	6718260	209.6	12	0.000115	43	1.2	0.054	34.9	0.2
18	692586	6718379	214.4	13	0.000115	42	1.3	0.055	31.2	0.2
19	691643	6718600	216.6	14	0.000115	43	1.2	0.055	35.8	0.3
20	688756	6719585	232.0	5	0.000115	39	0.7	0.055	52.1	0.2
21	686990	6720935	238.7	8	0.000115	45	0.9	0.056	49.1	0.2
22	686624	6721377	240.2	5	0.000115	59	0.6	0.056	96.1	0.1
23	686420	6722565	245.5	8	0.000115	57	0.8	0.056	70.3	0.2
24	686217	6723790	249.2	4	0.000115	41	0.7	0.057	58.5	0.1
25	685480	6724640	252.3	7	0.000115	55	0.8	0.057	67.7	0.2
26	685376	6724925	255.3	8	0.000115	42	1.0	0.057	41.7	0.2
27	684357	6725325	258.6	12	0.000115	51	1.2	0.058	44.3	0.2
28	684365	6726980	262.4	10	0.000115	53	1.0	0.058	51.9	0.2
29 _{GS}	683080	6728820	268.5	15	0.000115	57	1.3	0.058	45.3	0.2

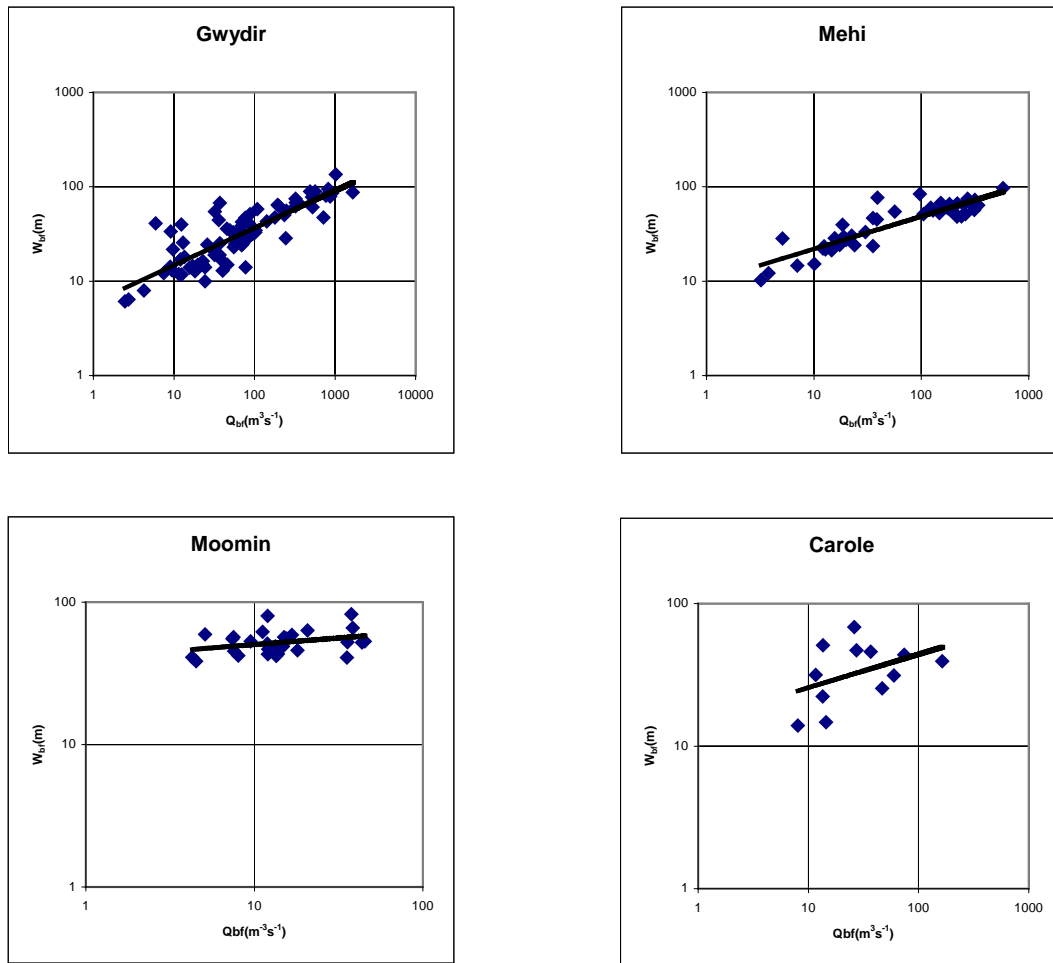
Note: All units as for Table 2.2.

Table AB.4: Channel characteristics for representative cross-sections on Carole Creek.

No.	Eastings	Northings	Distance DS	Q	S	W	D	<i>n</i>	W/D	V
1	780075	6742707	0.0	164	0.001600	39	2.7	0.045	14.8	1.6
2	780200	6743120	0.5	74	0.001600	44	1.5	0.045	28.9	1.1
3	779833	6743563	1.2	13	0.001600	22	0.8	0.045	27.3	0.7
4	776990	6745830	5.8	60	0.001300	31	1.8	0.045	17.8	1.1
5	760510	6763185	44.9	47	0.000440	25	2.4	0.045	10.4	0.8
6	758125	6764998	51.1	15	0.000440	15	1.7	0.045	8.7	0.6
7	757623	6767250	54.7	26	0.000440	69	0.9	0.045	76.7	0.4
8	755070	6768915	58.6	8	0.000440	14	1.2	0.045	11.5	0.5
9	752498	6772119	64.6	27	0.000440	47	1.2	0.045	40.5	0.5
10	750631	6774752	69.4	12	0.000440	32	0.9	0.045	35.5	0.4
11	749662	6775675	71.9	14	0.000440	51	0.7	0.045	70.6	0.4
12 _{GS}	748192	6775244	74.1	37	0.000440	46	1.4	0.045	32.5	0.6

Note: All units as for Table 2.2.

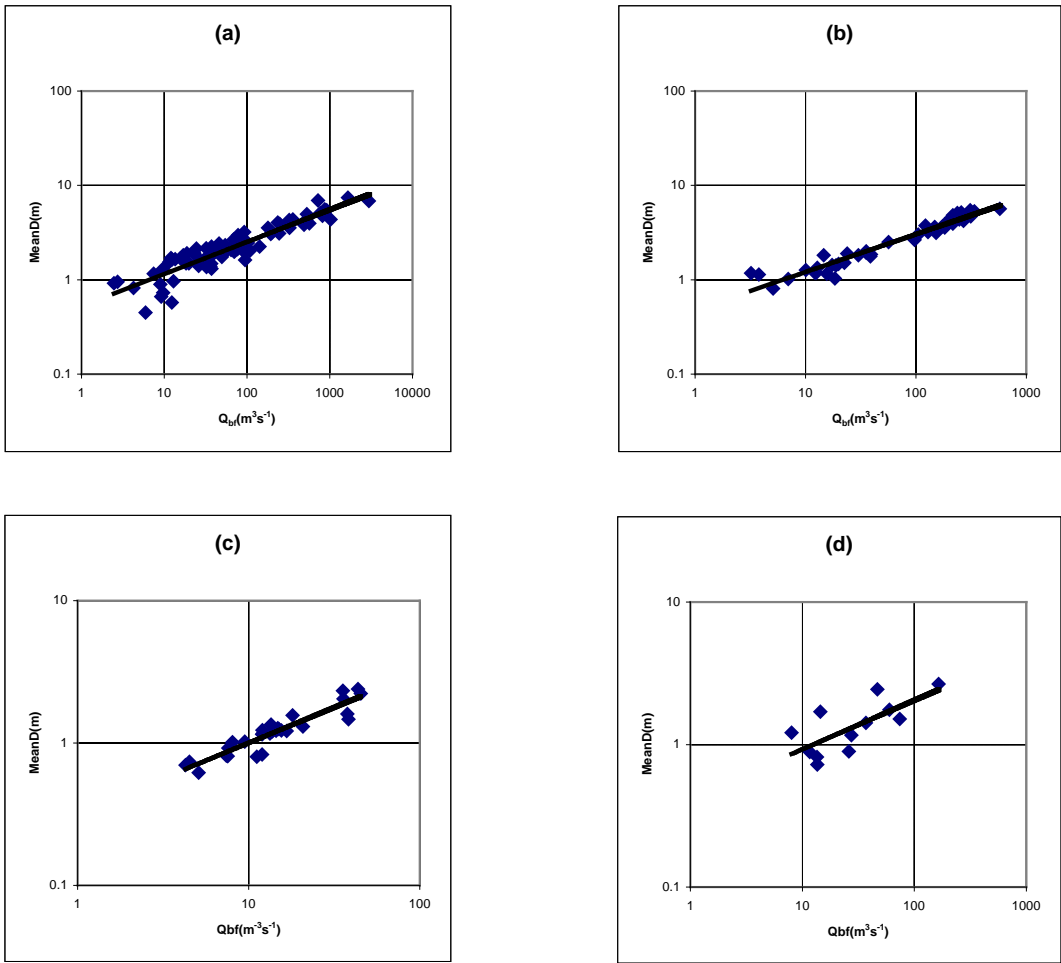
Appendix C: Hydraulic geometry bivariate plots.



Where $W = aQ^b$

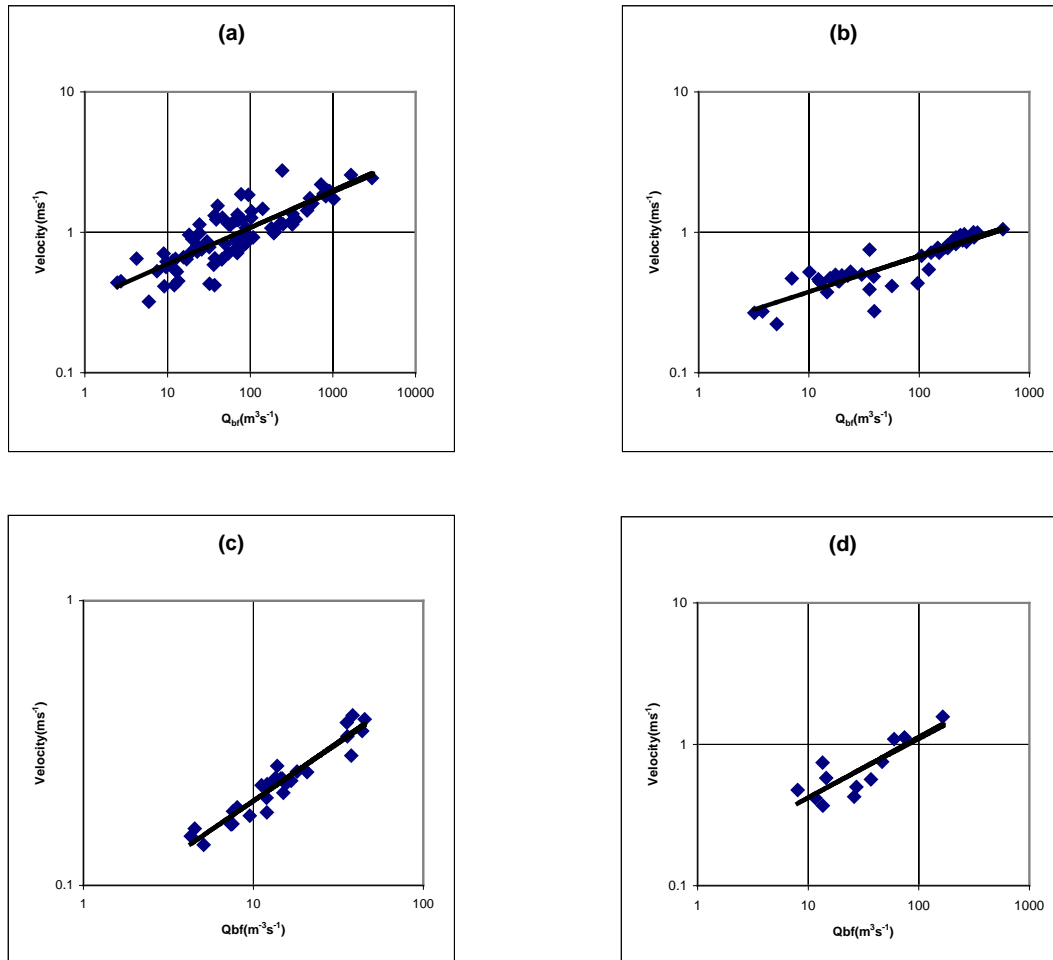
Stream	b	R^2
Gwydir	0.399	0.724
Mehi	0.345	0.798
Moomin	0.092	0.104*
Carole	0.234	0.179*

Figure AC.1: Width vs Discharge Relationships for a) Gwydir River, b) Mehi River, c) Moomin Creek and d) Carole Creek. Table provides calculated values for width exponent, b , with correlation coefficient, R^2 , also shown. * Indicates that exponent is not significantly different from zero at the 95% confidence level.



<i>Where $D = cQ^f$</i>		
Stream	f	R^2
Gwydir	0.341	0.844
Mehi	0.401	0.943
Moomin	0.498	0.859
Carole	0.344	0.529

Figure AC.2: Depth vs Discharge Relationships for a) Gwydir River, b) Mehi River, c) Moomin Creek and d) Carole Creek. Table provides calculated values for depth exponent, f , with correlation coefficient, R^2 , also shown.



Where $V = kQ^m$

Stream	m	R^2
Gwydir	0.259	0.688
Mehi	0.255	0.786
Moomin	0.410	0.911
Carole	0.423	0.691

Figure AC.3: Velocity vs Discharge Relationships for a) Gwydir River, b) Mehi River, c) Moomin Creek and d) Carole Creek. Table provides calculated values for velocity exponent, m , with correlation coefficient, R^2 , also shown.

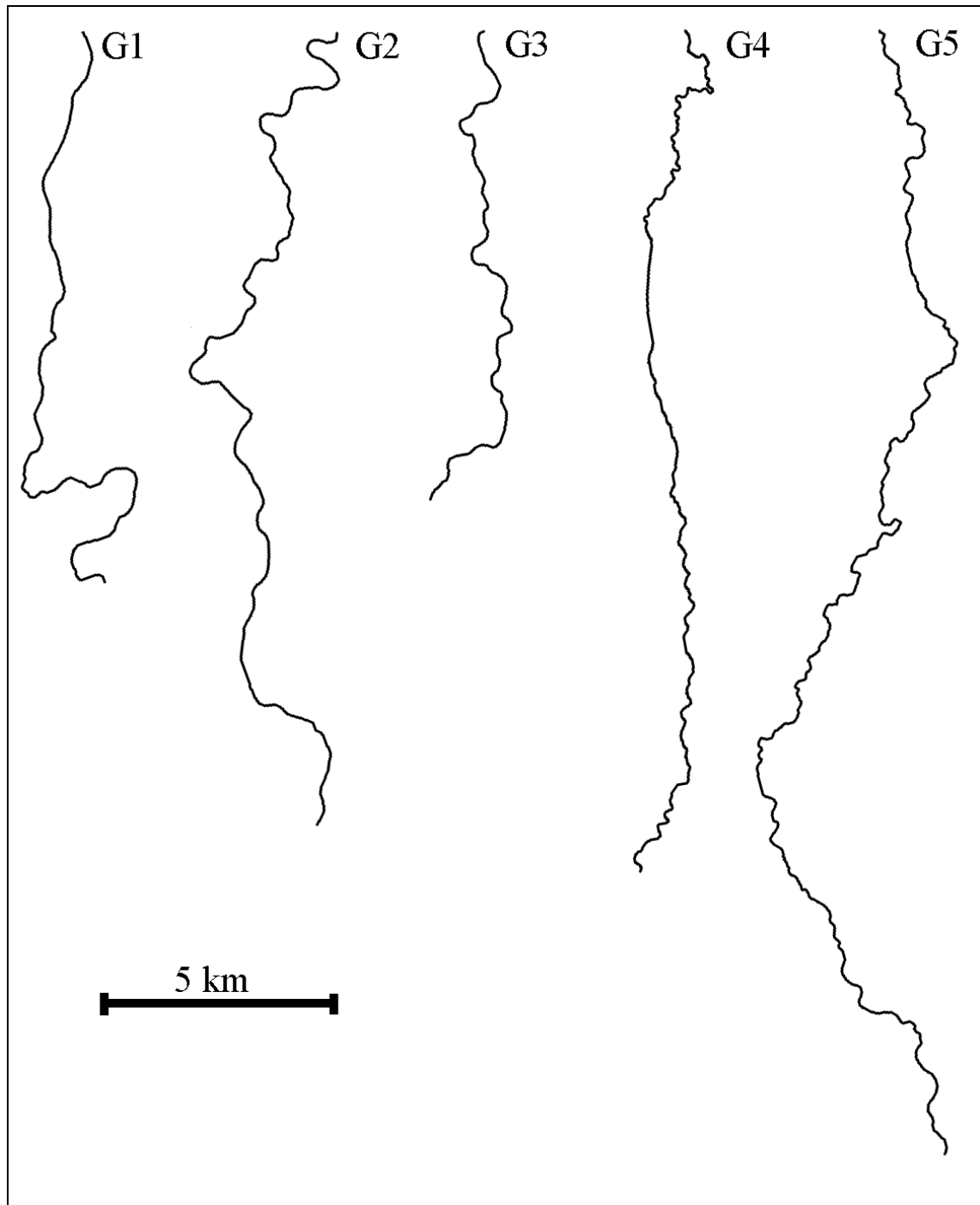
Appendix D: Planform section centrelines.

Figure AD.1: Centrelines for sections of the Gwydir River.

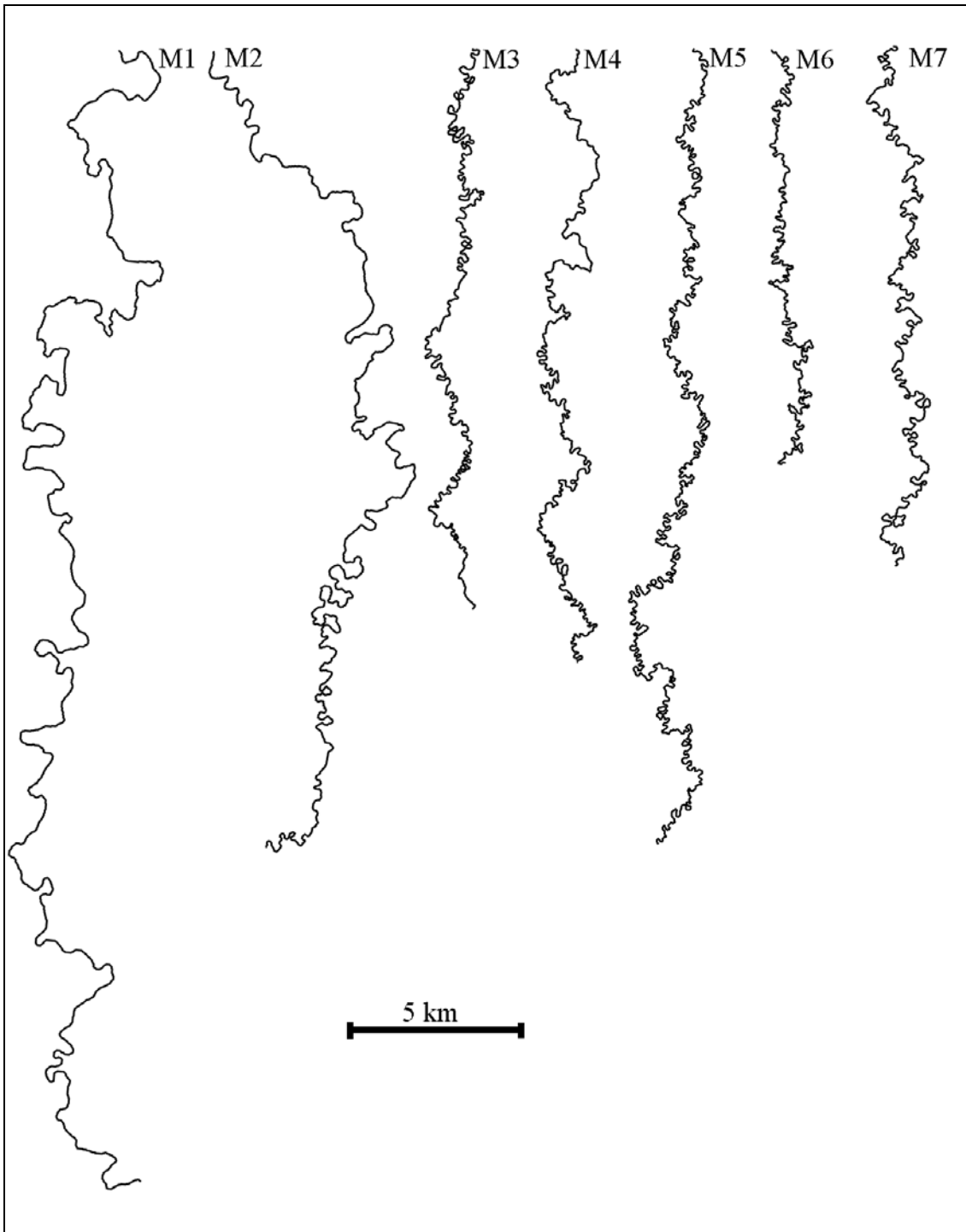


Figure AD.2: Centrelines for sections of the Mehi River.

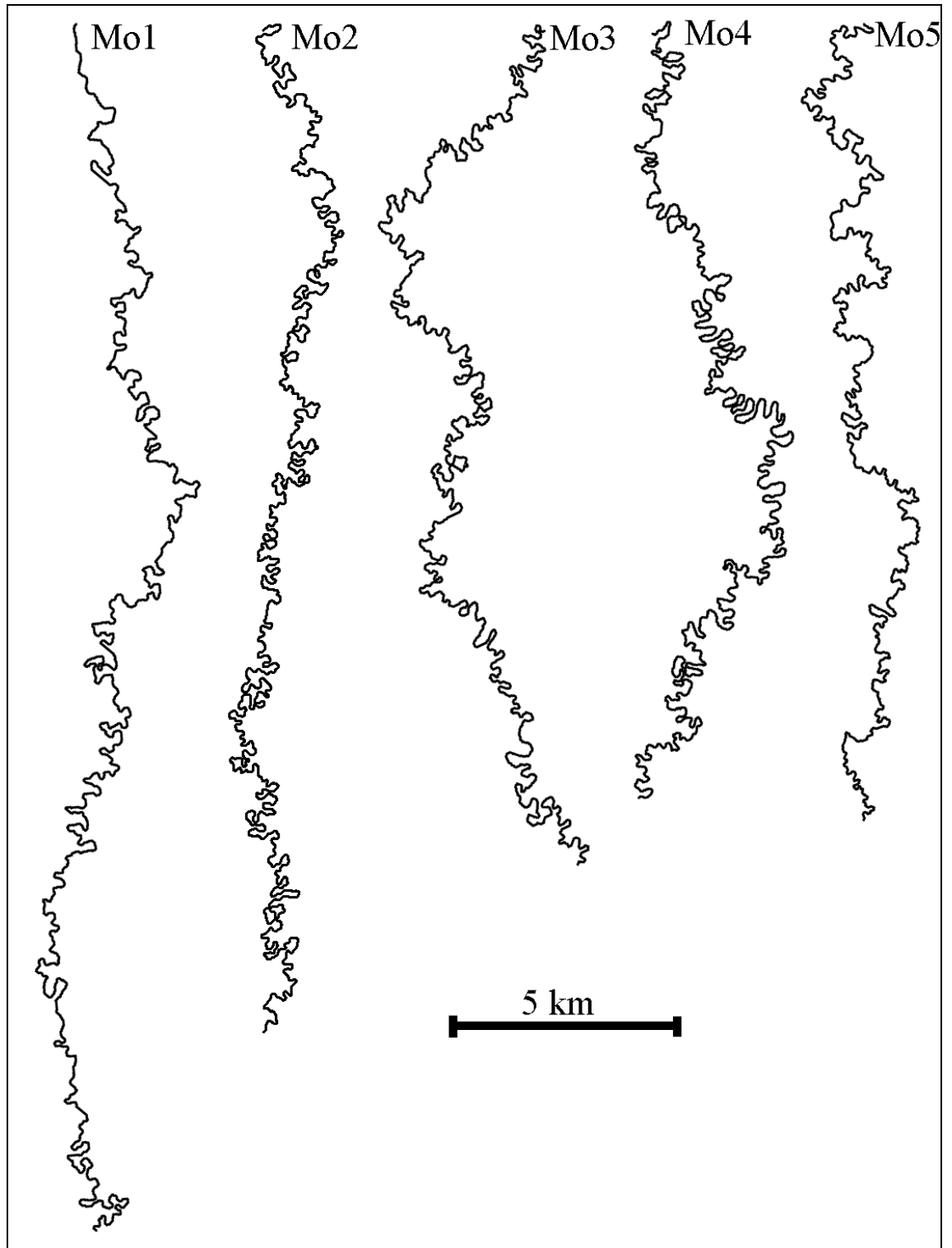


Figure AD.3: Centrelines for sections of Moomin Creek.

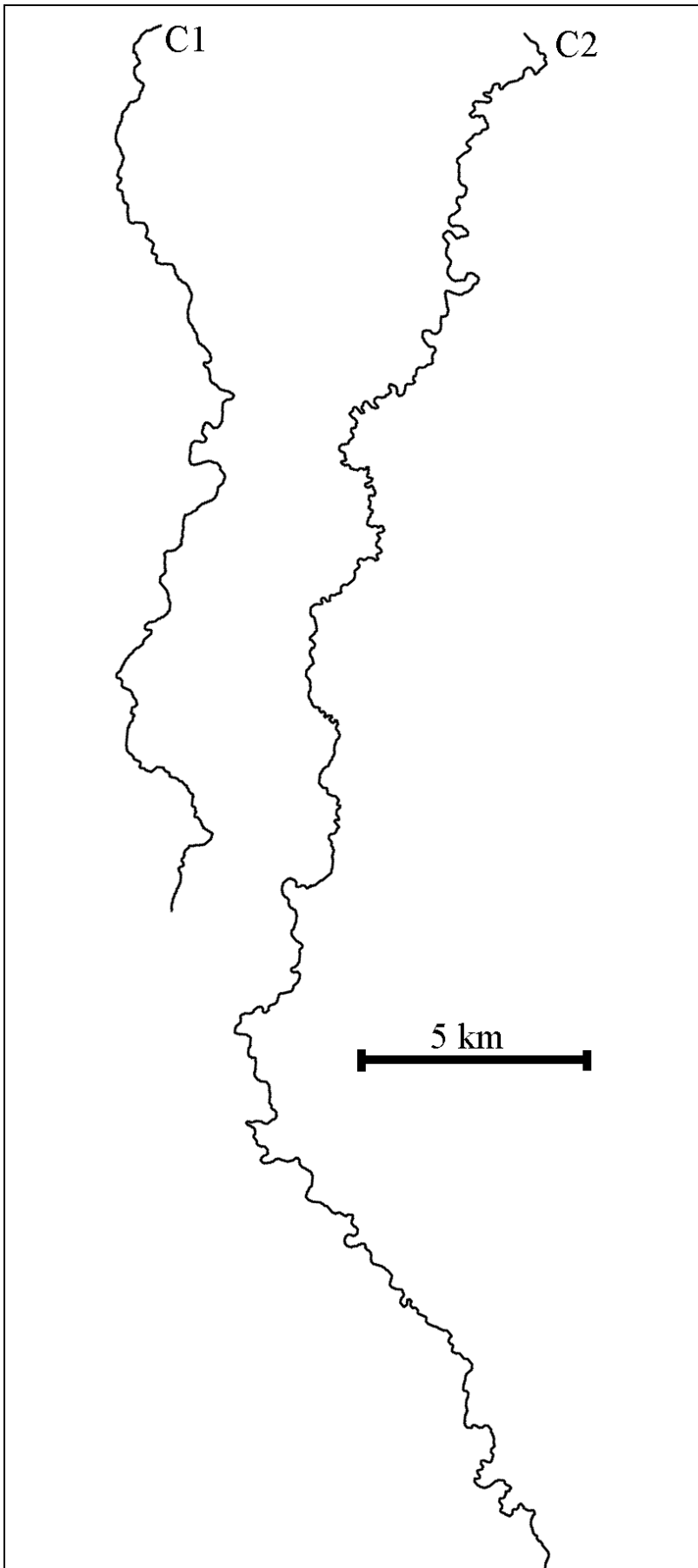
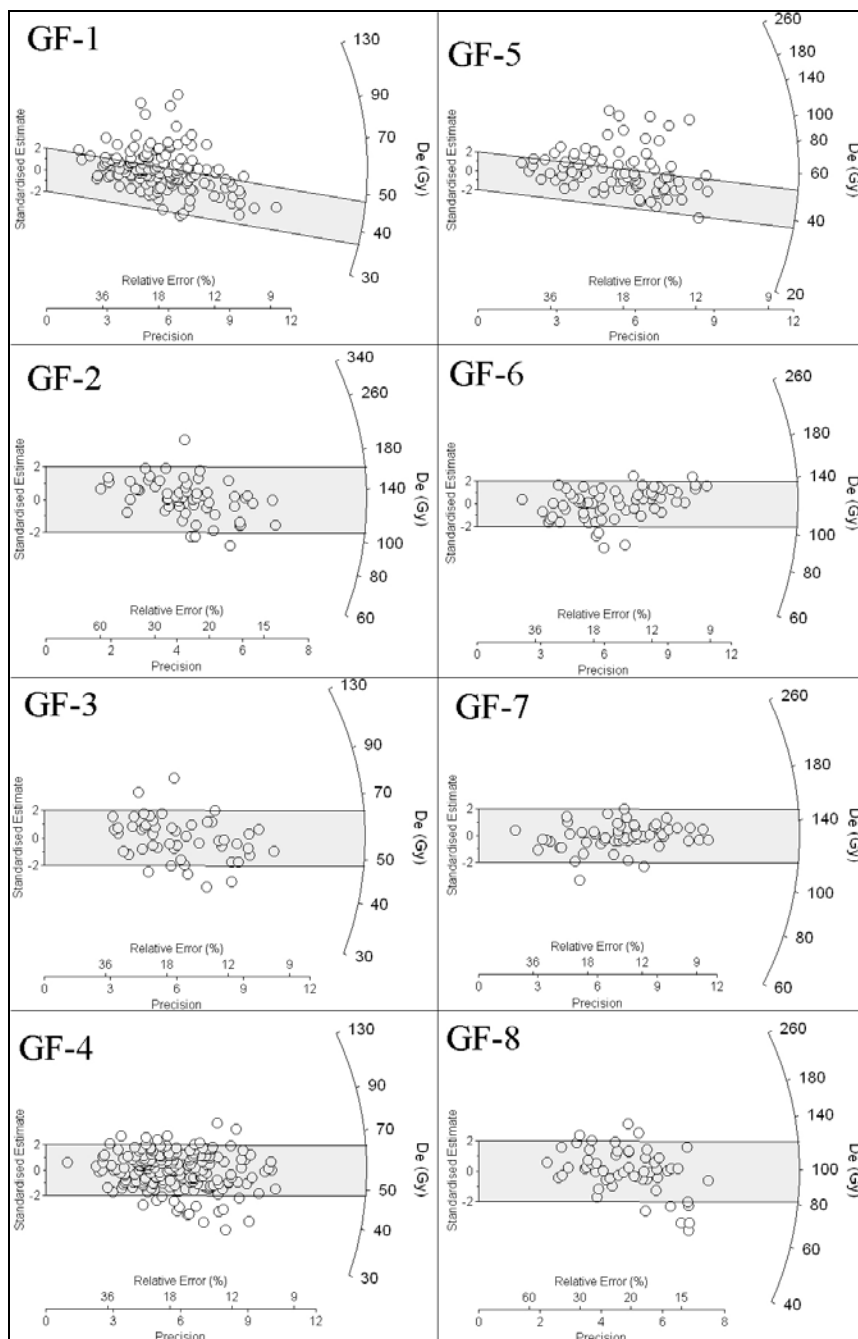
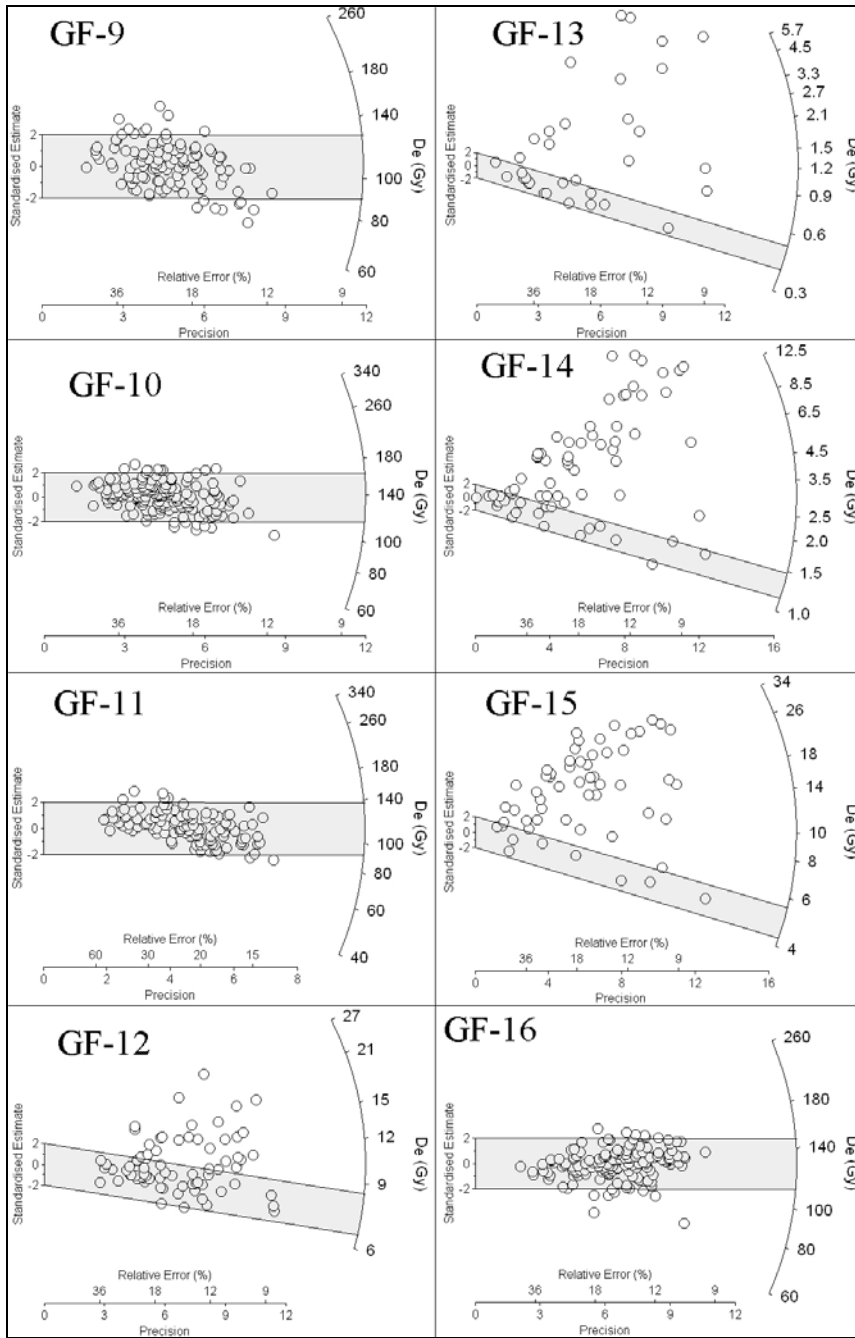
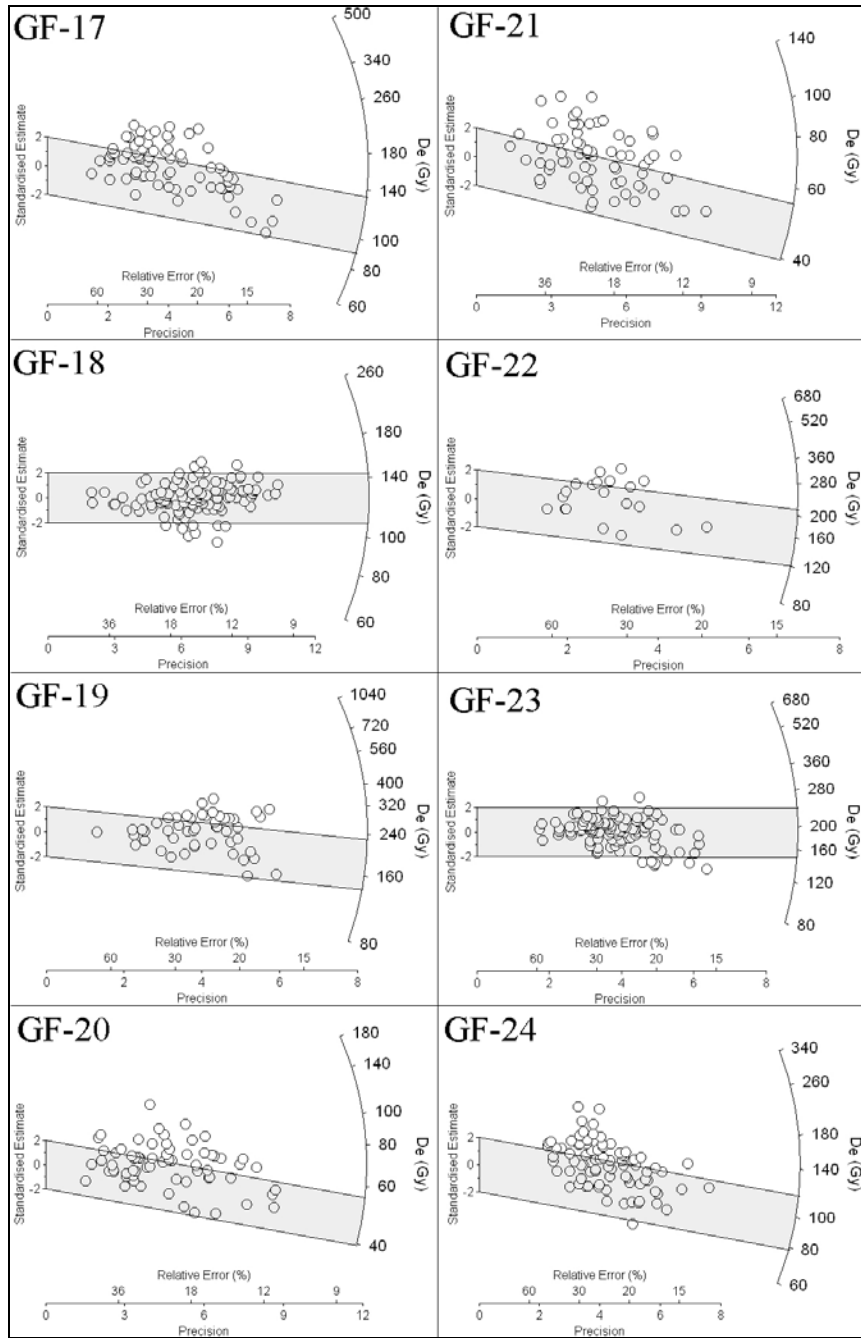


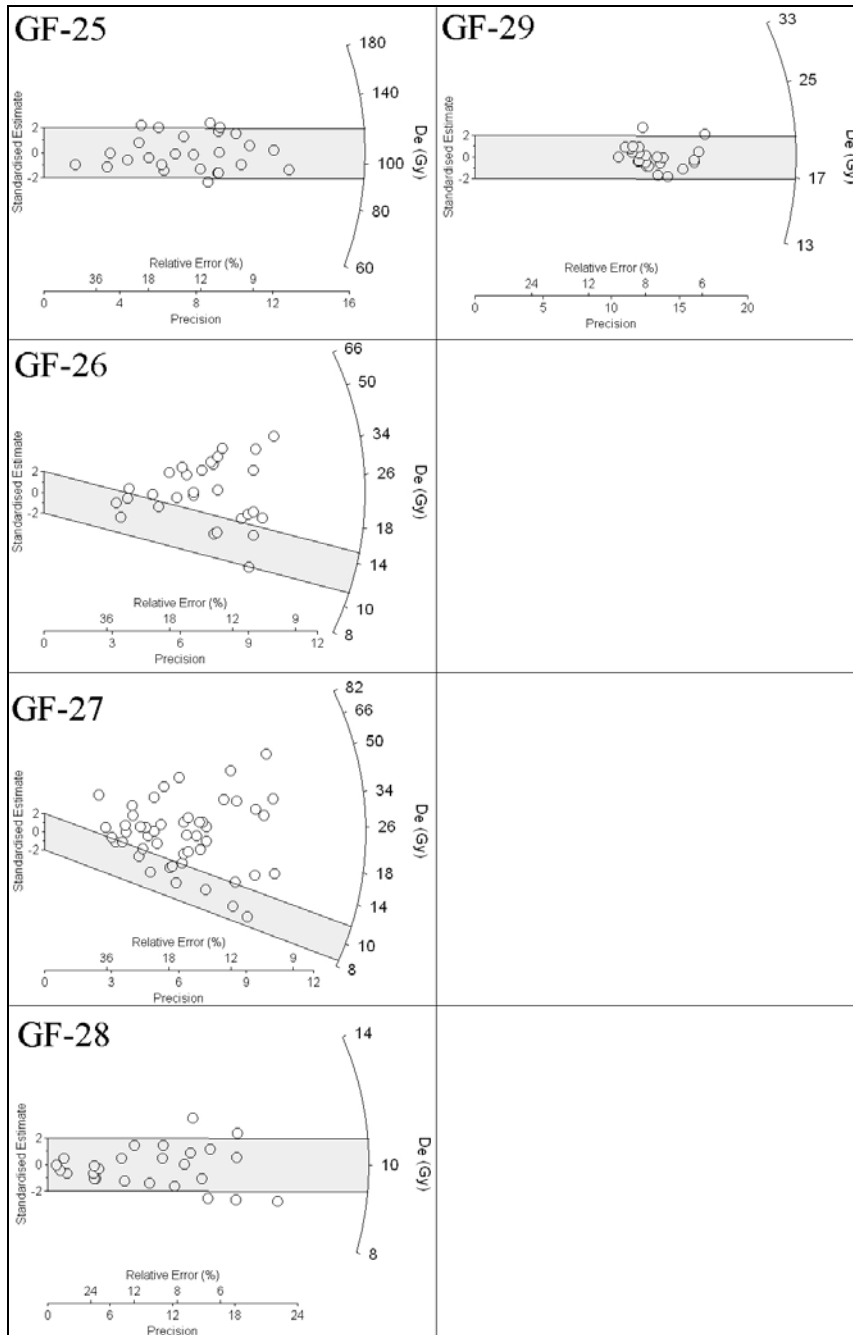
Figure AD.4: Centrelines for sections of Carole Creek.

Appendix E: OSL D_e radial plots.









Appendix F: Published ages for fluvial deposits of the Murray-Darling basin.

Source	System	Valley	Sample	Age (ka)	$\frac{Q_{\text{Palaeo}}}{Q}$ (est.)
Bowler (1978)	Goulburn (Modern)	Murray-Goulburn	Anu-877	8.64 ± 0.55	1
Bowler (1978)	Goulburn (Modern)	Murray-Goulburn	n-302	4.97 ± 0.125	1
Bowler (1978)	Goulburn (Modern)	Murray-Goulburn	n-303	8.09 ± 0.155	1
Bowler <i>et al.</i> (1978)	Acres Billabong	Darling	ANU-1982	11.2 ± 0.2	2
Bowler <i>et al.</i> (1978)	Acres Billabong	Darling	ANU-1984	19.2 ± 0.4	2
Bowler <i>et al.</i> (1978)	Acres Billabong	Darling	ANU-1993	16.8 ± 0.4	2
Kemp (2001)	Modern	Lachlan	ANU-11090	0.85 ± 0.07	1
Kemp (2001)	Modern	Lachlan	ANU-11092	2.6 ± 0.06	1
Kemp (2001)	Nanima	Lachlan	ANU-11093	2.88 ± 0.69	3
Kemp (2001)	Nanima	Lachlan	ANU-11094	3.01 ± 0.07	3
Kemp (2001)	Nanima	Lachlan	ANU-11095	5.29 ± 0.11	3
Kemp (2001)	Modern	Lachlan	ANU-11128	0.72 ± 0.08	1
Kemp (2001)	Ulgutherie	Lachlan	GA1/99	29.86 ± 1.11	6
Kemp (2001)	Ulgutherie	Lachlan	GA2/99	30.4 ± 1.8	6
Kemp (2001)	Culgo	Lachlan	W2168	56.7 ± 6.1	4
Page <i>et al.</i> (1991)	Green Gully - Tallygaroopna	Murray-Goulburn	w747	93.9 ± 5.2	3
Page <i>et al.</i> (1991)	Green Gully - Tallygaroopna	Murray-Goulburn	w748	65.1 ± 3.6	3
Page <i>et al.</i> (1991)	Kotupna	Murray-Goulburn	W750	33.3 ± 2.6	3
Page <i>et al.</i> (1991)	Kotupna	Murray-Goulburn	W751	34.4 ± 4.0	3
Page <i>et al.</i> (1991)	Murray Prior Streams	Murray-Goulburn	w759	94.2 ± 8.5	3
Page <i>et al.</i> (1991)	Green Gully - Tallygaroopna	Murray-Goulburn	w760	84.2 ± 15.5	3
Page <i>et al.</i> (1991)	Murray Prior Streams	Murray-Goulburn	w762	90.1 ± 4.3	3
Page <i>et al.</i> (1996)	Kerarbury	Murrumbidgee	W1360	33.6 ± 2.5	8.3
Page <i>et al.</i> (1996)	Kerarbury	Murrumbidgee	W1361	53.7 ± 6.6	8.3
Page <i>et al.</i> (1996)	Kerarbury	Murrumbidgee	W1362	47.8 ± 6.1	8.3
Page <i>et al.</i> (1996)	Kerarbury	Murrumbidgee	W1363	43.2 ± 3.7	8.3
Page <i>et al.</i> (1996)	Yanco	Murrumbidgee	W1365	19.4 ± 1.6	4.5
Page <i>et al.</i> (1996)	Kerarbury	Murrumbidgee	W1445	63.7 ± 4.1	8.3
Page <i>et al.</i> (1996)	Coleambally	Murrumbidgee	W1446	83 ± 4.5	5.2
Page <i>et al.</i> (1996)	Yanco	Murrumbidgee	W1557	15.2 ± 2.0	4.5
Page <i>et al.</i> (1996)	Yanco	Murrumbidgee	W1558	13.6 ± 1.6	4.5
Page <i>et al.</i> (1996)	Yanco	Murrumbidgee	W1559	18.2 ± 1.5	4.5
Page <i>et al.</i> (1996)	Coleambally	Murrumbidgee	w745	86.8 ± 7.5	5.2
Page <i>et al.</i> (1996)	Kerarbury	Murrumbidgee	w746	46.8 ± 3.0	8.3
Page <i>et al.</i> (1996)	Coleambally	Murrumbidgee	w758	83.5 ± 7.1	5.2
Page <i>et al.</i> (1996)	Coleambally	Murrumbidgee	w904	103.8 ± 8.8	5.2
Page <i>et al.</i> (1996)	Kerarbury	Murrumbidgee	w906	45.9 ± 3.8	8.3
Page <i>et al.</i> (1996)	Kerarbury	Murrumbidgee	W938	37.8 ± 10	8.3
Page <i>et al.</i> (1996)	Gum Creek	Murrumbidgee	W995	25.5 ± 3.5	3.9
Page <i>et al.</i> (1996)	Gum Creek	Murrumbidgee	W996	29.8 ± 2.9	3.9
Page <i>et al.</i> (1996)	Gum Creek	Murrumbidgee	W997	24.7 ± 2.8	3.9

Page <i>et al.</i> (1996)	Gum Creek	Murrumbidgee	W998	29.4 ± 4.6	3.9
This Study	Kamilaroi	Gwydir	GF-1	15.7 ± 1.4	6
This Study	Coocalla	Gwydir	GF-10	45 ± 4	10
This Study	Coocalla	Gwydir	GF-11	36 ± 2	10
This Study	Modern	Gwydir	GF-12	2.71 ± 0.21	1
This Study	Coocalla	Gwydir	GF-16	39 ± 3	10
This Study	Coocalla	Gwydir	GF-17	47 ± 5	10
This Study	Coocalla	Gwydir	GF-18	37 ± 3	10
This Study	Challicum	Gwydir	GF-19	66 ± 7	10
This Study	Coocalla	Gwydir	GF-2	41 ± 4	10
This Study	Kamilaroi	Gwydir	GF-20	15.8 ± 1.7	6
This Study	Kamilaroi	Gwydir	GF-21	17.1 ± 2	6
This Study	Challicum	Gwydir	GF-22	72 ± 15	10
This Study	Challicum	Gwydir	GF-23	66 ± 6	10
This Study	Coocalla	Gwydir	GF-24	39 ± 5	10
This Study	Coocalla	Gwydir	GF25	38 ± 3	10
This Study	Kookabunna	Gwydir	GF-3	19.6 ± 1.3	5
This Study	Kookabunna	Gwydir	GF-4	18.9 ± 1.1	5
This Study	Kookabunna	Gwydir	GF-5	14.5 ± 2.3	5
This Study	Coocalla	Gwydir	GF-6	39 ± 2	10
This Study	Coocalla	Gwydir	GF-7	41 ± 2	10
This Study	Coocalla	Gwydir	GF-8	34 ± 2	10
This Study	Coocalla	Gwydir	GF-9	39 ± 3	10
Watkins and Meakin (1996)	Carrabear	Macquarie	CM37	13.4 ± 2.9	5
Watkins and Meakin (1996)	Carrabear	Macquarie	GG01	16.2 ± 1.3	5
Watkins and Meakin (1996)	Carrabear	Macquarie	WR37	25.6 ± 3.9	5
Watkins and Meakin (1996)	Marra Ck	Macquarie	na	6.4 ± 1	1
Young <i>et al.</i> (2002)	Yarral	Namoi	W2814	18.2 ± 2.8	2
Young <i>et al.</i> (2002)	Pian Ck	Namoi	W2815	12.1 ± 1.6	2
Young <i>et al.</i> (2002)	Pian Ck	Namoi	W2816	12.7 ± 1.8	2

Appendix G: Lake George case study.

This appendix sets out the background and significance of the ‘Winderadeen embankment’ at Lake George in southern NSW. Although not directly related to the present study, this feature has often been referred to as evidence for high lake levels being the result of low evaporation (and by extension, low precipitation) during colder phases of the last glacial cycle. This is contrary to much of the palaeochannel evidence from the Murray-Darling basin, including that provided in the present study. Suspicions were therefore held about the reliability of the chronology established for the Winderadeen embankment. A small OSL dating program was therefore undertaken to test the reliability of the earlier radiocarbon dating program of Coventry (1973; 1976) and Coventry and Walker (1977).

Lakes of the Murray-Darling basin provide environmental records which reflect both broadscale climate change as well as wholly local factors. Former lake levels are determined directly through surveying former beach levels, or indirectly through sedimentological, palaeontological and/or palynological investigation of lake-floor sediments and adjoining aeolian dunes (lunettes). The accuracy of climate records derived from lake level records is dependent entirely on the appropriateness of the models chosen to relate lake level to various climate variables.

Lake George is situated in the centre of a small (932 km²) endorheic catchment that borders the headwaters of the Yass River and Lachlan River catchments to the west and north respectively. Occupying almost twenty percent of its catchment, the majority (~65 %) of inflow is in the form of rainfall directly on the lakes’ surface. Runoff from the surrounding catchment is fed into the lake via universally short streams, increasing the reliability of runoff coefficient estimates (runoff coefficient currently ~12%). Considered to be hydrologically, though not geochemically, sealed (Singh *et al.* 1981), the only significant outflow is in the form of evaporation (Jacobson and Schuett, 1979). The direction of lake level change records the relative intensity of precipitation (inflow) vs. evaporation (outflow), in accordance with standard hydrological budgeting theory (Galloway, 1965). A still-stand in lake levels indicates parity of inflow and outflow. Rainfall, evaporation and lake level records of various forms dating back to the 1820s

demonstrate the close association between lake level change and the ratio of precipitation to evaporation.

Geomorphic evidence for major fluctuations in the water level of Lake George is available in the form of dated (^{14}C) beach / barrier deposits that now sit high above the historic high water mark (Galloway, 1967; Coventry, 1973; 1976; Coventry and Walker, 1977), as well as stratigraphic variations in lake bottom cores which record episodes of deep water deposition, slope wash deposition (onto a dry lake floor) and pedogenesis (Singh *et al.* 1981). Chronological control for the lake bottom cores is via ^{14}C in the upper 2 m with palaeomagnetism and tentative orbital tuning of the palynologically derived palaeotemperature record for greater depths (Singh and Geissler, 1985). Palynological and microfossil records from the lake bottom cores provide indirect evidence of lake level change through their reflection of climate.

The beach/barriers at Lake George were first related to higher lake levels and altered climates by Galloway (1965). However, no chronological control on raised surfaces was available, so the timing of the derived climatic variations was speculative. By assuming a glacial age for one of the higher embankments (at about 30 m above lake bottom), Galloway was able to estimate the runoff and evaporation characteristics likely to have been extant during its emplacement. This left just precipitation as the only 'unknown' in the hydrologic budget equation, thus enabling the calculation of the amount of precipitation necessary to maintain the lake at the beach level. As colder temperatures decrease evaporation, and greater seasonality increases run-off, it was found that precipitation necessary to keep the lake at about 30 m deep, during glacial times, was considerably *less* than Lake George experiences currently. This provided for the first time a model to explain the apparent existence of pluvial features coeval with features signaling greater aridity.

Using a slightly different array of assumptions regarding climate models and catchment behaviour, Coventry (1973; 1976) also calculated glacial precipitation levels to be less than, possibly as low as half of, the present value. With the availability of ^{14}C dating, Coventry (1973; 1976) and Coventry and Walker (1977) were able to establish an environmental history which demonstrates that the latter part of the Quaternary was characterised by falling, though fluctuating, lake levels commensurate with global

temperature rises since the LGM. They also propose that during the 'glacial', the lake was at its highest level, apparently reflecting a dramatic fall in evaporation, outweighing the likely fall in precipitation brought about by lower ocean temperatures.

Approximately 29 ka marks the attainment by Lake George of a still-stand approximately 37 m above lake bottom. Since then all beaches have been formed at lower levels. Since ~17 ka, though Lake George has recorded a number of high water levels, the Willandra Lakes have remained dry, possibly because enhanced fluvial activity in the Lachlan River disconnected Willandra Ck, the feeder channel for Willandra Lakes. Between about 22 ka and 18 ka at Lake George there is an apparent gap in the record of beach deposition that may be due to lake drying accompanying the LGM. However, unpublished OSL dates produced by the ANU (rses.anu.edu.au/environment/eePages/eeCurrentResearch/research_Chappell3.html, data retrieved 01/06/02) suggest that beach deposition continued through this time, though at a level far below the heights recorded at the beginning of the Lake George record (~29 ka) and consistent with the general picture of gradual decline.

Although the relationship between climate change and landform expression at Lake George appears straightforward, it is heavily reliant on an accurate geochronology to enable determination of palaeotemperature. Without an indication of temperature regimes in place, it is not possible to determine whether lake levels changed in response to changes in precipitation or to changes in evaporation. The accuracy of the geochronology then, becomes crucial as it provides the basis for selecting an appropriate temperature for use in the palaeo-hydrological budgeting exercise. The radiocarbon dates produced for Coventry (1973) and subsequently reported in Coventry (1976) and Coventry and Walker (1977), are from fragments of charcoal and 'carbonised' wood, that received only a single acid wash in dilute HCl (Coventry, 1973). Furthermore, no attempt was made to differentiate 'carbonised' wood from charcoal, and it is likely that such material maintained open system behaviour for some time following burial. Considering that non-charcoal samples from Willandra Lakes which received only preliminary acid treatment have been shown to be unreliable by Gillespie (1998), it is likely that the ^{14}C ages for the beach barriers at Lake George are also too young. Sequential ^{14}C dates from the floor of Lake George are also shown to be subject to errors attributable to contamination by younger carbon (Singh *et al.*, 1981;

Singh and Geissler, 1985). These facts alone indicate that considerable care should be exercised when deducing palaeo-precipitation levels from palaeo-lake levels at Lake George. An inaccurate chronology will result in an inaccurate assignation of palaeotemperature and therefore runoff and evaporation.

Perhaps then, the current data on beach levels at Lake George is insufficient to determine palaeo-precipitation levels. The cores collected from the lake floor provide hope for a more accurate climatic signature by combining the geomorphic evidence with the palynological record. Unfortunately, though, there is no simple agreement between the accepted climatic history of the site and the facies analysis of the cores (Sing *et al.*, 1981). Additionally, the ^{14}C dates are from inorganic carbon, and although in this case these are apparently more reliable than dates from diffuse organic carbon, they have been shown in a number of studies elsewhere (Callen *et al.*, 1983; Gillespie, 1998), to require caution rather than ready acceptance. Taken at face value, the record from lake-floor cores indicates that major falls in lake level are recorded during both the intense cold of the glacial maximums as well as during the warm interglacials. It would seem, therefore, that the lake empties in response to both the enhanced evaporation of the interglacials as well as the reduced precipitation of the glacials. It seems that the periods intermediate between glacial and interglacial are characterized by high lake levels, demonstrating that at such times decrease in evaporation relative to the present must have been sufficient to outweigh the likely reduced precipitation caused by lower ocean temperatures.

The composition of the pollen rain through the Quaternary at Lake George appears to be cyclic, in a manner similar to the cyclic oscillations in the marine oxygen isotope record (Singh and Gessler, 1985). However, as with the sedimentological record, there is no simple relationship between lake level fluctuations indicated by the pollen record and glacials and interglacials. Although there are underlying climate drivers represented in the pollen signal, it may be effectively impossible to draw out the effects of all the interplaying environmental factors responsible for the palynology. Recourse therefore, is made simply to the general observations that can be made with confidence, with the intricacies of the story left unaddressed. Restricting the observations to the upper part of the sequence it can be seen that for the most part, cool temperate vegetation predominates, with short intervals of cold climate vegetation, such as that which is

reasonably securely dated at the LGM (~20 ka). Following the LGM there is a rapid replacement of cold and cool temperate climate vegetation with warm temperate species, establishing the present environment.

Returning to the question of chronological uncertainty and the associated problems this creates for inferring climate change, a short field trip to test the accuracy of Coventry (1973; 1976) and Coventry and Walkers's (1977) initial ^{14}C ages was undertaken. As contamination of samples with younger carbon has the greatest effect on older material it was decided to focus efforts on accurately dating the highest (oldest) beach deposit at Lake George. Three samples were collected from the Fernhill Gully site described in Coventry (1973) and Coventry and Walker (1977). A sample was taken from the gravelly beach deposit at ~37 m above lake bottom, originally dated by Coventry and Walker (1977) to 27 ± 1 ka (uncalibrated ^{14}C), as well as from (aeolian?) sand units directly above and below the beach gravel. These were prepared and analysed in the same manner as described for samples from the Gwydir (see Chapter 5) and provided ages of 53 ± 4 ka, 52 ± 4 ka and 47 ± 3 ka respectively. From these (admittedly limited) data, it appears that the lake was at its highest point at around 50 ka, a time of significantly higher temperatures than those used by Coventry (1976) to estimate the evaporation appropriate to the full lake conditions. Clearly, if temperatures were only intermediate between the extreme temperatures of the interglacial and glacial during the emplacement of the Fernhill Gully Beach, then greatly reduced evaporation can not be the reason for the higher lake levels. Along with a higher evaporation commensurate with the higher temperatures of 50 ka, there must have been higher precipitation to maintain the lake at such a high level. Higher precipitation during OIS 3 is exactly the scenario suggested by the large Kerarbury palaeochannels on the Riverine Plain (Page *et al.* 1996), the high terraces of NSW coastal catchments (Nott *et al.* 2002, Nanson *et al.* 2003) and the Wollondilly-Nepean catchment (Nanson *et al.* 2003), as well as the very large Coocalla Palaeochannel of the Gwydir fan-plain.